Delft University of Technology, Faculty of Aerospace Engineering

Thermal Modelling & Analysis

of the Deployable Space Telescope

T.T.D. van Wees

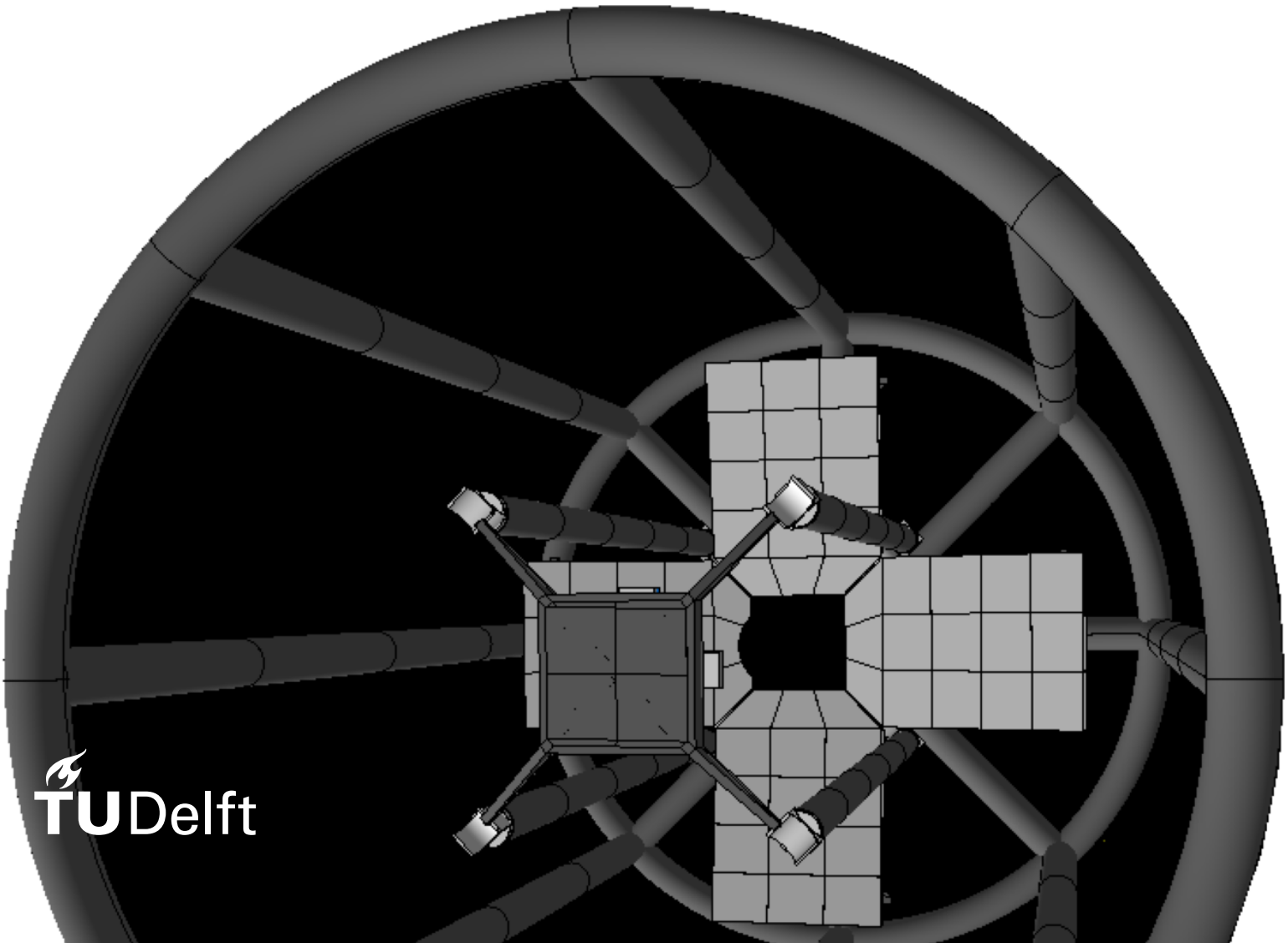

TU Delft

(This page is intentionally left blank.)

Delft University of Technology
Aerospace Engineering Faculty

AE5810: Thesis Space

Thermal Modelling & Analysis of the Deployable Space Telescope

by

T.T.D. van Wees

in partial fulfilment of the requirements for the degree of

Master of Science
in Aerospace Engineering

at Delft University of Technology,
to be defended publicly on Tuesday April 30, 2019 at 11:00.

Student number: 4316177
Thesis duration: August 27, 2018 - April 15, 2019
Thesis committee:

Ir. B.T.C. Zandbergen	TU Delft, SSE, Chair
Dr. Ir. J.M. Kuiper	TU Delft, SSE, Supervisor
Ir. M.C. Naeije	TU Delft, A&SM

(This page is intentionally left blank.)

Summary

The Deployable Space Telescope (DST) project aims at producing a competitive telescope by using segmented deployable light weighted optics which reduces launch volume and mass, and thus launch costs. Due to the criticality of heat management to the performance of the telescope, it is in need of a dedicated thermal analysis. Further, the premature baffle design included in the telescope required this thermal analysis such that recommendations could be given to the baffle designer. To that end, a thermal model has been built in order to determine the expected temperatures throughout the telescope in orbit. The ESATAN Thermal Modelling Suite (ESATAN-TMS) has been the assigned modelling tool for this project.

An initial simplified model has been constructed first, exposed to nominal conditions. These consider the preset conditions as per ESATAN-TMS. The results of these simulations showed that the interior of the baffle absorbs most heat for attitudes during which the Sun can impinge its surface directly. A considerable amount of this heat is radiated towards the top section components of the telescope, which turned out to be most determinant for the experienced temperature variations throughout an orbit.
The simplified model has been updated to a more complex model such that it is fully representative of the DST. The parabolic baffle design has been altered to a cylindrical design and it has been shifted in the telescope to allow for the inclusion of the baffle housing attachment. These baffle changes have affected the spider and the secondary mirror most, since those have experienced an increase in maximum- and overall temperature respectively. The other geometry changes or additions were concluded to have little effect on the initial thermal performance, because their respective thermal resistances and view factors remained similar.

The telescope is designed for worst case scenario Sun Synchronous Orbit (SSO) conditions, for which global-hot and cold thermal cases have been selected. These cases are representative of high- and low thermal input conditions, which in combination with convenient satellite attitudes resulted in extreme node temperatures.

A parametric analysis of the baffle has been performed regarding its shape, blanket position, top closing, dimensions and attitude. The effect of the baffle shape on the telescope temperature is found negligible, with the condition that the opening is small and that the baffle is not made unnecessarily wide. In order to not negatively affect deployability and mass, the MLI blanket should be located externally of the baffle structure. An additional top closing is effective in reducing the temperatures as experienced by the secondary mirror only, while lengthening and narrowing of the baffle is effective for decreasing the experienced temperature variations throughout an orbit. This results from a reduction of the heat flow from space towards the interior of the baffle and the telescope. Further, additional measures should be found for the interior of the baffle since its is known to radiate heat towards the telescope.

The efforts undertaken to improve the model have resulted in a detailed representation of the thermal parameters of the telescope. Further potential improvements to the model have been investigated, such as the desired thermo-optical coatings, a reflective baffle interior and the conductive interfaces. The majority of the Secondary Mirror Support Structure (SMSS) has been modelled black to reduce stray light. A reflective baffle design composed of one vane only proved to be effective in reducing the amount of radiative heat flow from the baffle towards the telescope. However, a major downside of this design is that it features a solid structure which may impact deployability.

The coarse position alignment budgets have been approximated for three designs with; original-, lengthened- and reflective baffle. The calculations considered the largest temperature variations throughout an orbit for the predetermined cold, median and hot conditions. Furthermore, the analysis considered that the system could be aligned at either of the two extreme temperatures. The results have shown that the M2 position budgets in Z will be critical due to deformation of the SMSS booms, which can be partly mitigated by a reflective baffle design. Additionally, the to be designed instrument housing should be given sufficient thickness for it to not become critical for the M1 budgets.
The alignment calculations did not consider the absolute temperatures of the telescope and its components, but rather considered temperature deviations over an orbit. The temperature results showed that the hot case can be critical for alignment depending on average- and extreme ΔT per orbit. The cold case can be critical due to the difference in average temperature (>60°C) with the intended target temperature of 25°C. A thermomechanical model shall determine which is worse.

(This page is intentionally left blank.)

Preface

The report was written as part of a master thesis at the faculty of Aerospace Engineering of Delft University of Technology and details the thermal modelling and analysis for the Deployable Space Telescope. This project is conducted by the Space Systems Engineering Department of TU Delft in cooperation with Airbus Defence and Space Netherlands. The authors work serves to provide an assessment of the expected temperatures encountered by the telescope and its subsystems in operation.

The report aims to inform team members of the DST about the in-orbit temperatures of the system, but can also serve as a guideline for a wider engineering audience on how to approach the assessment of the operational temperature of space systems in general.

The author would like to thank the following people for their valuable contributions and continuous support throughout the project. Hans Kuiper, thesis supervisor, for his input and support throughout the project, as well as his guidance throughout, and in particular in the final project stage. Victor Villalba Corbacho for his swift and crucial contributions that helped to drive the project forwards.
In addition, the author would like to thank his parents and grandparents, and his friends for their ongoing support and inspiration.

van Wees, *T.T.D. 4316177*

Delft, April 2019

(This page is intentionally left blank.)

Contents

(This page is intentionally left blank.)

List of Figures

List of Tables

(This page is intentionally left blank.)

List of Acronyms

ADS	Airbus Defence and Space
AN	Ascending Node
AOCS	Attitude & Orbital Control System
AU	Astronomical Unit
BB	Baffle Blanket
BC	Boundary Condition
BENELUX	Belgium, Netherlands & Luxembourg
BS	Baffle Structure
CATIA	Computer-Aided Three-dimensional Interactive Application
CDHS	Command & Data Handling System
CFRP	Carbon Fiber Reinforced Polymers
COLD	Cold case modelling conditions
CORE	COmpliant Rolling-contact Element
COTS	Commercial Of The Shelf
CTE	Coefficient of Thermal Expansion
DM	Deformable Mirror
DOF	Degrees Of Freedom
DST	Deployable Space Telescope
ECI	Earth Centred Inertial
ECSS	European Cooperation for Space Standardization
EOL	End of Operating Lifetime
ESA	European Space Agency
ESTEC	European Space Research & Technology Centre
FM	Fold Mirror
FSC	Full Sunlit Conditions
GSD	Ground Sampling Distance
HOT	Hot case modelling conditions
ICS	Inertial Coordinate System
IH	Instrument Housing
IPC	In Plane Constraint
IR	InfraRed
LEOP	Launch & Early Orbit Phase
MAIT	Manufacturing Assembly Integration & Testing
MCS	Model Co-ordinate System

MED	Median case simulation conditions
MLI	Multi-Layered Insulation
M1	Primary Mirror
M2	Secondary Mirror
M3	Tertiary Mirror
MSc	Master of Science
NASA	National Aeronautics & Space Administration
NOM	Nominal case simulation conditions
OBC	OnBoard Computer
OLR	Outgoing Longwave Radiation
PET	Polymer Ethylene Terephthalate
PETP	Polyethylene Terephthalate Polyester
PCM	Phase Change Material
PhD	Postgraduate doctoral degree
PMAO	Primary Mirror Active Optics
PMSS	Primary Mirror Support Structure
PSC	Partial Shadow Conditions
RA	Right Ascension
REF	Radiation Exchange Factor
RH	Root Hinge
SE	System Engineering
SiC	Silicon Carbide
SMSS	Secondary Mirror Support Structure
SSE	Space Systems Engineering
SSO	Sun-Synchronous Orbit
TBD	To Be Determined
TCS	Thermal Control System
TMS	Thermal Modelling Suite
TH	Top Hinge
TU Delft	Delft University of Technology
UD	Unidirectional
UJ	Universal Joints
USD	United States Dollars
VDA	Vapour Deposited Aluminium
WB	Without Baffle

List of Symbols

α	Absorptivity	-
α	Right ascension	Degrees
δ	Declination	Degrees
ΔT	Maximum temperature difference	Kelvin or Degrees Celsius
ϵ	Emissivity	-
ϵ	Obliquity of the ecliptic	Degrees
ϵ	local bolometric albedo	-
γ	Vernal equinox	-
Ω	Right ascension of the ascending node	Degrees
ω	Argument of pericenter of periapsis	Degrees
ρ	Reflectivity	-
σ	Stefan Boltzmann constant	W/m^2/m^4
τ	Transmissivity	-
θ	True anomaly	Degrees
Υ	First point of Aries	-
B_{ij}	Gebhart factor	-
d_{S-E}	Mean distance Earth and Sun	Meters
e	Eccentricity	-
E_{IR}	Earth irradiance	W/m^2
F_{ij}	View Factor	-
i_e	Ecliptic obliquity	Degrees
i_{Ss}	Sun synchronous inclination	Degrees
R_S	Sun radius	Meters
S	Spacecraft	-
S_c	Solar constant	W/m^2
T	Orbital period	Seconds
T_E	Earth's temperature	K
T_S	Sun temperature	K
x_E	Sun-Earth axis	-
A	Apocenter or Apoapsis	-
a	Semi-major axis	Meters
F	Focal point	-
G	Greenwich meridian or prime meridian	-
h	Altitude	Meters

i	Inclination	Degrees
k	Thermal Conductivity	Watts/Meters/Kelvin
P	Pericenter or Periapsis	-
Q	Heat	Watts
R	Mean equatorial radius	Meters
r	Radius	Meters
T	Temperature	Kelvin or Degrees Celsius

1 Introduction

Remote sensing is the process of obtaining information about a target from a distance [1]. This approach to sensing is critical in situations where data collection close to, or on the surface of a target is not possible, or in cases where a wider viewpoint from higher elevation is required to gather a larger amount of information. Nowadays, remote sensing is often used in space applications, for example for the purpose of Earth observation. Remote sensing of Earth can provide specific information for, among others, prediction of the weather, severe weather events like volcanic eruptions, tornado's, flooding and dust storms, measuring ocean temperatures and for sea ice tracking, and for natural resource management like monitoring how land is utilised and how it affects the environment [2]. Remote sensing provides mankind with information about our environments status and about the way it is changing. This can be used for commercial and scientific purposes, but can also serve governments and other entities as source of information to take appropriate steps for example against climate change.

Society has a constantly increasing need for high spatio-temporal resolution imagery to provide more accurate insights. To fulfil this need, satellites require large mirrors which generally result in large, heavy and thus costly missions, which in turn drives the development of light-weight mission architectures with competitive performance. In order to address these challenges, the Delft University of Technology (TU Delft) has presented a deployable light-weighted space telescope which reduces mass and launch volume. The design features deployable mirrors, for which the primary is segmented.

This thesis report presents the global thermal model of the current DST design. It includes an initial simplified thermal model, which is adjusted such that it is fully representative of the deployed telescope. This model is subjected to the relevant thermal conditions from which the system temperatures are calculated. These results are used for approximating the coarse position- and thermal budgets.

This report is divided into three parts. The first part introduces and defines the thermal system considered in this report. The second part includes the thermal modelling and temperature assessments results. The third part presents the final thermal results for the entire system, together with conclusions and recommendations for future work.

Firstly, the DST mission is introduced to the reader, which describes the need and objectives of the project, the relevance of this work, the team structure, and finally the objective and deliverables of this thesis (Ch.2). Necessary thermal system aspects are determined, which are used to define thermal system requirements. The top-level system- and thermal requirements are evaluated to provide the necessary constraints and boundary conditions of the thermal model (Ch.3). The existing telescope systems are studied, which allows the researcher to get an impression of the current designs but also to understand the design choices which have been made (Ch.4).

The geometric thermal model is produced in the Workbench of ESATAN TMS, which allows to set the desired environmental and system conditions (Ch.5). An initial simplified thermal model is produced to give an initial impression of the thermal performance (Ch.6). Afterwards, this respective model is updated to a more sophisticated model until it is considered representative of the DST (Ch.7). The updated model is exposed to several sets of worst case scenarios, from which a specific cold and hot case are chosen for further assessment (Ch.8). A parametric analysis of the baffle is chosen to determine the desired and undesired baffle properties (Ch.9). The telescope itself is investigated for further thermal improvements. Afterwards, the considered thermal system designs are presented and their thermal budgets are approximated (Ch.10). Finally, the thermal model performance is discussed (Ch.11).

All the aforementioned research and research outcomes shape the final design of the space telescope (Ch.12). The presentation of the final design is followed by the final conclusions (Ch.13). The report finishes with recommendations for future work. This includes the focus of future work related to the thermal- model and system (Ch.14).

(This page is intentionally left blank.)

I

Thermal System Definition

(This page is intentionally left blank.)

2 DST Mission Overview

The need for the DST mission has been described by means of a mission need- and goal statement (2.1). This two statements have been used as guideline for formulating the mission- objectives and requirements (2.2). The DST mission is thought to be a competitive design by producing a deployable light weighted space telescope with excellent spatial resolution (2.3). The DST project is composed of the two main system branches which have known many past team members as well as current team members (2.4). The DST mission is thought to be composed of several phases in which the process from concept exploration up to end of life will be elaborated (2.5). The thermal system is thought to be composed of three main branches, of which one of them will be considered as deliverable of this thesis (2.6). After the status of the current works have been globally explored, one can define the objective of this thesis (2.7).

2.1 Mission Need & Goal Statement

The mission need- and goal statement have been initially formulated in the work of B. van Marrewijk ([3]) and have been adopted in the DST SE document [4]. The Need Statement is a short description of the operational need, functional deficiency or business opportunity of this project [5]. The Mission Statement is an 'one-liner' that tells what this mission is about and how it can satisfy the need [5].

Mission Need Statement

There is a need for a dramatic decrease in launch cost of high-resolution Earth observation telescopes to provide data with a higher temporal resolution and at a lower price than is currently available [4].

High-resolution Earth observation data is getting more and more important due to a constantly increasing demand of the society. This requires space telescopes with diffraction limited performance featuring large apertures, which drives launch volume and thus launch costs. Therefore, there is a need for cheaper space telescopes featuring similar Ground Sampling Distance (GSD) but with increased temporal resolution. The need for high-resolution data will assure that the data has sufficient quality, while the need for increased temporal resolution will cover the increasing demand of society. Finally, for the design to be competitive it should be made cheaper than its competition.

Mission Goal Statement

The goal of this project is to design and develop a Deployable Space Telescope (DST) that is capable of achieving the same GSD as state-of-the-art Earth Observation satellites for a fraction of the costs, by making it able to achieve a relatively very low stowed volume and mass [4].

The aforementioned need shall be met by designing a space telescope with similar GSD to those of its competitors. In order to reduce launch costs, its aperture shall be made deployable and the total mass should be minimised, hence the suggestion for a deployable light weighted space telescope design with a relatively very low stowed volume.

2.2 Mission Objectives & Requirements

From the aforementioned need and goal statement, two objective statements have been formulated by the project supervisor J.M. Kuiper, as depicted in Table 2.1. These objectives are depicted here since they are considered important for the project, and will be required for indicating traceability.

"Mission requirements should express the stakeholders' needs in a simple, concise, verifiable, and understandable format. We should state them in terms of operational and mission outcomes, rather than implementation and solution concepts" [6]. Thus, the requirements arise from the stakeholder needs and shall be formulated in clear manner, but without specifying how they will be reached. The missions requirements and top level system requirements for the DST project as shown in Appendix A *Mission Requirements*, have been formulated in accordance to the aforementioned criteria.

The identifiers of the last three missions requirements have been changed into top-level system requirements because those are not considered to be functional requirements, but rather properties of the system which it

ID	Description	Parent
MIS-OBJ-01	The Ground Sample Distance of the DST shall be no larger than the state of the art in commercial visual spectrum Earth Observation imaging platforms. As of 2017 this is DigitalGlobe's WorldView-4 satellite with a Ground Sample Distance of 0.31 m in the panchromatic band.	N/A
MIS-OBJ-02	The lifetime cost of the DST shall be less than the state of the art in commercial visual spectrum Earth Observation imaging platforms. As of 2017 this is DigitalGlobe's WorldView-4 satellite with an estimated cost of USD $850 million including ground network upgrades.	N/A

Table 2.1: DST Mission Objectives.

should have. This is the reason for them to be shown in this report, since the proposed system requirements as presented in the next chapter are considered to be top-level system requirements too.

2.3 Project Overview

The initial optical and mechanical design has been presented by D. Dolkens in [7], with the following characteristics: a GSD of 25 cm, operating in a sun-synchronous orbit at an altitude of 500 km, with a stowed volume of 0.363 m^3 and a telescope mass of 74.8 kg (excluding the spacecraft body and baffle).

In the prior conducted literature study [8], a comparison has been made with current state-of-the-art space telescopes, in which it was shown that the DST features similar or even superior GSD (very high resolution), at a fraction of the stowed volume and mass. The DST has an expected- stowed volume of 0.363 m^3 and total mass of ∼150 kg, compared to 18-28 m^3 and 1015-2800 kg respectively of the analogous space telescopes, and is therefore considered significantly smaller and lighter. The reduction in stowed volume will be achieved by incorporating deployable support structures and segmented mirrors. Because of this respective reduction it is thought that dedicated launchers are no necessity and therefore one can consider options, among others, like ride sharing or piggyback launch, which feature lower launch costs.

Another comparison, regarding the temporal resolution, has been made with the WorldView-4 space telescope. The revisit time, or the time it takes to revisit a certain location on Earth, is a function of the orbital period and the swath width. Where a shorter orbital period decreases the revisit time, while a smaller swath width increases the revisit time. The DST has a lower orbital height, 500 km compared to 617 km, and has therefore a shorter orbital period. The WorldView-4 has a larger swath width, 13.1 km compared to 5 km, of which the latter is already assuming the upper bound of the DST swath width. The final analysis of this comparison showed that by using a constellation of at least three DST's with equal longitudinal separation, one can surpass the revisit time of the WorldView-4 telescope, assuming the maximum swath width for the DST of 5 km.

Thus, in the end it has been concluded that the DST could in theory be launched for a fraction of the conventional launch cost. The DST will feature very high spatial resolution, which even surpasses the high spatial resolution need, but can most likely not meet the need for higher temporal resolution with just one or two satellites. Therefore, the focus of the the DST project should be let on producing a space telescopes which outperforms its competitors based on GSD and costs.

2.4 DST Team

Since the initial work of D. Dolkens as presented in 2014, several preceding MSc students have continued the work. Most works have been dedicated to detailed mechanical designs of the deployment mechanisms and others on refinements of the optical system. The DST project is managed and supervised by Dr. Ir. J.M. Kuiper, and supported by two PhD'ers, both with their own specialisation, as shown in Figure 2.1.

The entire project is divided into two main branches, namely: the optical design and the thermomechanical design, supervised by their own dedicated PhD'er. The status of each work (indicated in the orange boxes) has been indicated with remarks from 1 to 3, where (^{1}) indicates a finished work, (^{2}) an ongoing work and (^{3}) the preceding literature study. As aforementioned, most finished works have been dedicated to the mechanical designs of the deployment mechanisms after the initial optical design. Therefore, the decision was made to dedicate the current or subsequent works mainly to testing and thermal designs. Future works will be based on the maturity of the finished designs and their additional recommendations. The last year, the main focus of the project was led on testing of the COmpliant Rolling-contact Element (CORE) hinges, delivering a thermal model, and managing of the systems engineering document.

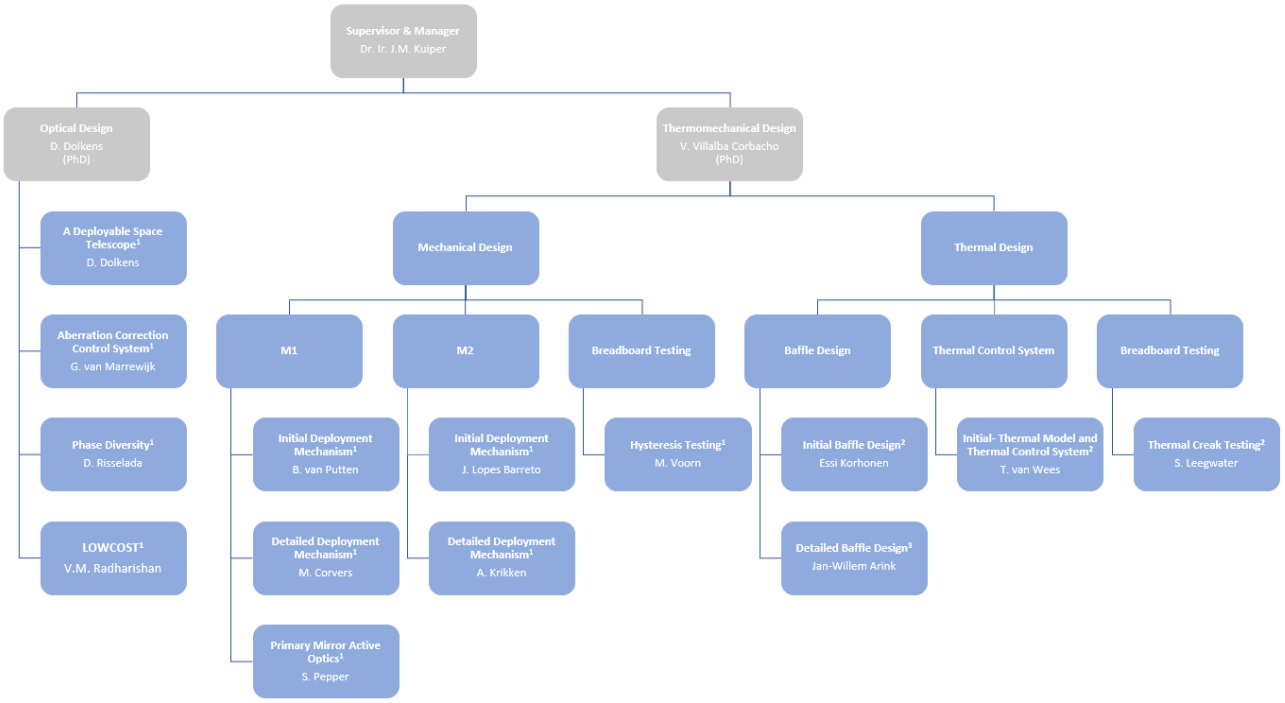

Figure 2.1: DST team overview of past and current members, including their work topics and status as per March 2019.

2.5 DST Mission Phases

The DST mission phases are considered as the main phases of the mission during which certain mission & system aspects will be defined or take place. The DST is considered to have the following mission stages: Pre-Design, Design, MAIT, Pre-launch, Launch, In orbit and EOL. The content of these mission stages will be elaborated below, and have been depicted in Figure 2.2. The mission phases are not necessarily purely chronological, and therefore the pre-design, design and MAIT phase are assumed to be intertwined or part of an iterative process, as indicated by the blue dotted arrows.

The DST mission phases are defined here because it is thought to describe the relationship of this work with respect to the entire project duration, as well as the need for different thermal model configurations and thermal modes, as will be elaborated in Chapter 3.

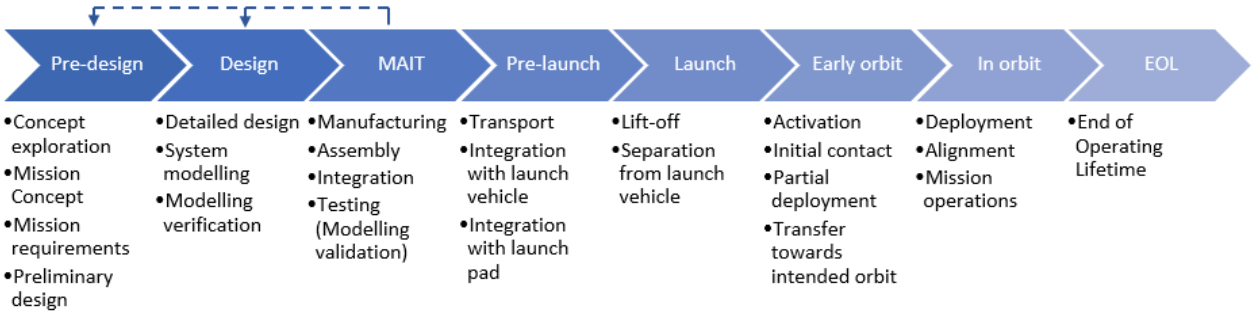

Figure 2.2: DST mission phases.

Pre-Design Phase

The pre-design stage is the phase during which the researcher tries to find a concept which is thought to be mission worthy, after which a mission concept and mission requirements are formulated. It should be mentioned that this reasoning is based on this respective project, while for other projects the mission concept and requirements could originate from the customer needs. The concept exploration, mission concepts and the mission requirements have already been explored and established by former DST team members, which let to several preliminary and detailed designs. The content of this thesis will include the exploration of the preliminary design of the thermal system, by means of a thermal system analysis. This can be used as foundation

for a future DST thermal system design.

Design Phase

The design stage is the phase during which the system will be designed in detail. This phase includes system modelling and modelling verification. For space telescopes, it is common practice to create optical, mechanical and thermal models of the system required for approximating its performance. The majority of the mechanical- and optical models have been designed in detail while the models of the thermal system have lacked behind. Therefore, efforts need to be made for designing these models after which the separate models could ideally be integrated into one model. This will allow the user to approximate performance based on thermal deformations. The output of these models can be used as input for designing the preliminary- and detailed thermal system. The focus of this thesis will therefore be let on producing a thermal model which can be considered representative of the DST.

MAIT Phase

The Manufacturing, Assembly, Integration & Testing (MAIT) stage is the phase during which individual systems are manufactured and assembled, after which they are integrated and/or tested. These tests are primarily conducted for it to check the accuracy of the model with the actual system. Thus, assuming all models are verified before testing, the models can still be inaccurate which basically would mean that incorrect models are applied. The DST project is at this moment mainly within its design process, apart from the CORE hinges for which some initial manufacturing, assembly and testing has taken place during the period of this thesis.

Pre-launch-, Launch-, Early Orbit-, In orbit- and EOL Phase

The pre-launch phase includes the transport of the satellite, the integration with the launch vehicle and integration with the launch pad. At this moment no specifics are determined for this phase yet, except for some system requirements which could be related to this phase. The launch phase includes lift-off from the launch pad and separation from the launch vehicle. After the satellite is separated from the launcher, the system shall be activated, partly deployed for it to generate power and initial contact shall most likely be made with the ground station. Further attitude adjustments are thought to be necessary for it to end up in its intended orbit. The in orbit phase considers the satellite to be in its intended orbit during which it should deploy, align and perform mission operations. The End of Operating Lifetime phase shall be the stage where the satellite will most likely be turned off and re-enter the Earth's atmosphere.

2.6 Potential Thesis Deliverables

The thermal system design is thought to be composed of three main branches, namely: the thermal model (I), the thermomechanical model (II) and the Thermal Control System (TCS) design (III). These three aspects are considered to be potential thesis deliverables. The thermal control system will be the system which actually controls system temperature, while the thermal- and thermomechanical models are tools used for estimating the system- temperatures and mechanical deformations respectively. The general thermal system architecture is shown in Figure 2.3, including the functions which are considered to be relevant for the thermal system.

The thermal model shall be representative of the DST, otherwise it would not be relevant to determine the expected system temperatures. The main function of the thermal model will be to determine temperature, while those are most relevant for the expected worst case scenarios. The thermomechanical model shall convert the aforementioned calculated temperatures into mechanical deformations, and shall be compatible with the optical model for it to allow prediction of the actual optical performance.

As part of designing the thermal control system it is thought that the system functions, the system requirements, the spacecraft modes, the thermal modes, the thermal budgets and the thermal margins shall be determined. All these system aspects, including the thermal model, are thought to be necessary for providing the preliminary thermal control system design. Some aspects will be further elaborated in Chapter 3 .

2.7 Thesis Objective

In the previous sections, it has been explained what the needs and objectives are for the DST project in general, how the DST team is structured, what work has been done, what the relation of this work will be regarding the entire project and which potential thesis deliverables have been considered. The detailed designs of the primary- and secondary mirror deployment and support structures, had reached a satisfactory level of detail

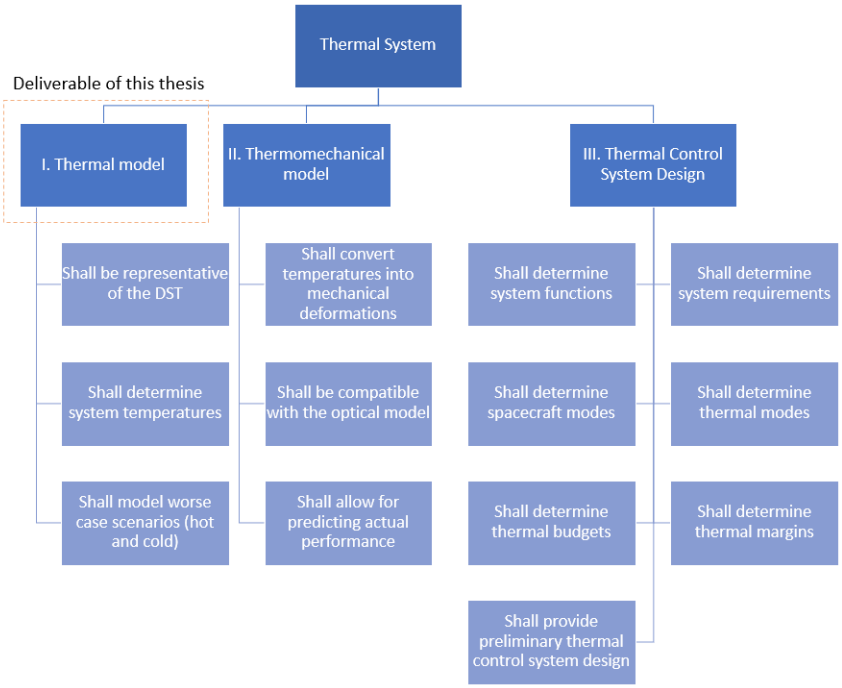

Figure 2.3: Thermal system design architecture.

at the time this work has commenced. The performance of these mechanisms are closely related to their thermal environment and therefore it has been decided that some of the succeeding work should be dedicated to producing a thermal system, hence the necessity of this respective work.

In consultation with the DST supervisor it has been agreed that the focus will be let on producing a thermal model for the DST (I), since the thermomechanical model (II) and the TCS design (III) as shown in Figure 2.3, are simply not part of this thesis. The thermal model shall be representative of the DST and it shall be able to determine the system temperatures for the expected worst case scenarios. This work shall be supplemented with a temperature analysis, due to which recommendations can be given to the DST team. Besides, the thermal model shall be made such for it to be easily adaptable by a future successor, such that it can be improved and used for the thermomechanical model.

The fully representative thermal model of the DST will give the team insights about the expected thermal conditions, which are necessary for it to provide an indication of the to be expected optical performance. The researcher is asked to built a simplified thermal model first, considered as the initial model, which will give the researcher insight about the general behaviour of the model. This will also be useful to get acquainted with the ESATAN TMS Workbench, which is allocated as the dedicated thermal modelling design tool during this project. The thermal model will be added more complexity gradually, until the model can be considered to be fully representative of the DST. The objective of this research thesis is therefore:

To make recommendations to the Deployable Space Telescope team about the expected thermal conditions and critical systems, by designing a thermal model representative of the Deployable Space Telescope with the expected thermal environmental conditions, and by giving an overview of the critical system parameters.

From this research objective, the main research question can be derived:

How can the critical systems of the Deployable Space Telescope be designed such for it to meet the thermal- and/or optical budgets?

This thesis project will be conducted such for it to answer this respective research question.

2.8 Chapter Summary

The mission need- & goal statement, mission objectives and mission requirements have been elaborated. This was thought to be necessary for providing the required traceability in the following Chapters.
The mission characteristics have been compared to current state-of-the-art telescopes from which it was shown that the DST can be considered significantly lighter, smaller and cheaper to launch, when compared to its competition.
The DST team has known several previous team members for which the focus was led on the optical and

mechanical system. The current focus of the project is led on testing of the CORE hinges, delivering a thermal model and management of the systems engineering document.

The DST mission phases have been determined for which it has been determined that the DST project is currently within its (pre)-design and MAIT mission phase.
Potential thesis deliverables have been explored, for which it has been decided that this thesis shall include a fully representative thermal model design of the DST. This model can potentially be used as input for the thermomechanical model and thus the detailed thermal control system design.
The thermal model shall be supplemented with a temperature analysis such that critical systems can be identified, and valuable recommendations regarding these systems can be given to the DST team.

3 Thermal System Aspects & Requirements

The thermal system is thought to include certain system aspects which require elaboration (3.1). The need for a thermal system and its main boundary conditions are thought to be defined by the top-level system requirements (3.2). The thermal system is expected to control temperatures under a given set of constraints, which are considered to be defined by the thermal requirements (3.3).

3.1 Thermal System Aspects

The thermal system aspects are considered as the conditions for the constraints of the thermal model. Therefore one needs to define: the DST configurations (3.1.1), the DST modes (3.1.2), the thermal margins (3.1.3) and the thermal budgets (3.1.4).

3.1.1 Spacecraft Configurations

The DST mission phases have been explored in the previous Chapter including its relation to this report. The thermal system itself will be relevant for all mission phases since its needs to be defined, designed, manufactured, assembled, integrated, tested, launched and finally made operational until EOL. The thermal model, as part of the thermal system, will model the mission phases which are relevant for modelling. Thus when the system is considered to be subjected to thermal loads. These are thought to be the launch-, early orbit-, in orbit- and the EOL phase, as depicted in Figure 3.1. The Launch & Early Orbit Phase (LEOP) have been depicted separately because they are thought to include different satellite configurations. The thermal modelling phases are considered to depict the configuration which is expected to dominate that respective phase.

During the entire launch phase, the DST is expected to be in its stowed position while it is considered to be fully deployed during the in orbit phase. The early launch configuration has not been determined yet. Nevertheless, it is likely that some spacecraft bus systems will be deployed to allow for, among others, communication and power generation. The fully deployed configuration, without the spacecraft bus, has been defined and can therefore be modelled. The stowed configuration is not entirely determined, since among others, the folding of the baffle is still to be determined. This is expected to play an important role in terms of worse case conditions. Besides, the required lock- and hold interfaces have not been determined yet which are thought to result into several essential conductive couplings. The spacecraft bus has not been designed either. Therefore, the partially deployed or stowed configuration cannot be modelled yet, due to which the focus of this thesis will be let on producing a fully deployed thermal model as highlighted in Figure 3.1.

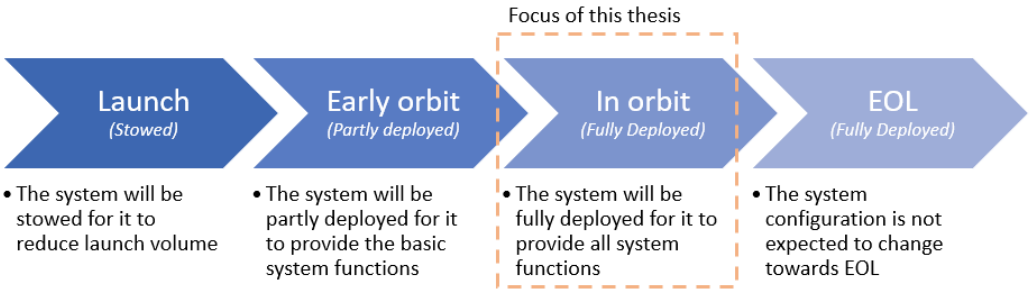

Figure 3.1: DST thermal modelling configurations.

3.1.2 Spacecraft Modes

The mission phases have been mentioned in the second chapter while the thermal modelling phases and their relevance to this thesis have been mentioned in the previous section. The spacecraft itself is considered to feature several modes in which it can be set, namely: off mode, launch mode, survival mode, deployment mode and operational mode. The spacecraft modes have been coupled to certain mission phases as depicted in Figure

3.2. For each of the aforementioned mission phases it has been indicated which spacecraft modes are relevant for the respective mission phase. The pre-design-, design- and MAIT phases are excluded here but are expected to include dedicated test modes.

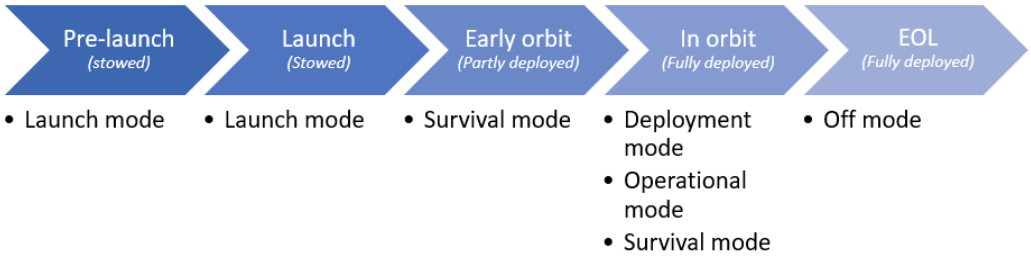

Figure 3.2: Considered spacecraft modes per mission phase.

During pre-launch, the spacecraft is expected to be turned off during transport, while it will be set into launch mode just before or during integration with the launch vehicle. During launch it will remain into launch mode until the spacecraft will be separated from the launcher. Generally, all spacecraft systems are switched off during this phase while the separation detection device is armed, which will be used for safe separation from the launch vehicle. Once the launch mode is terminated, the spacecraft should autonomously be set into survival mode during which the necessary systems like for example the solar panels will be deployed, while power consumption will be minimised. The system should provide sufficient power, thermal control and other operational conditions required for, among others, communications and manoeuvring. Besides, this mode can be used in respond to a major anomaly or in eclipse when no power can be generated, thus as safe mode.

After the spacecraft has been put into its intended orbit it is considered to be set into the deployment mode, during which it will deploy the telescope systems like the baffle and the primary- and secondary mirrors. This is considered to be a separate mode because the state of the system should be set such for it to allow deployment. This could also include deployment of the remainder of the spacecraft bus systems, in case applicable. After the spacecraft has been fully deployed it can be set in the operational mode during which it can perform all operational required tasks like, among others, alignment of the system and producing images.

When entering eclipse it is thought that the spacecraft can be set in survival mode again for it to safe power, or into an eclipse operational mode. During the sunlit part the spacecraft is expected to heat up, during which it is considered to align and be set operational. Towards the eclipse it is expected that the operational loop will be repeated during each subsequent orbit, assuming normal operations. At EOL, the spacecraft can be turned off after which it will probably burn up in the atmosphere.

3.1.3 Thermal Margins

The system designers are expected to take margins on top of the predicted temperature ranges for each thermal mode, to account for unpredictable thermal events. These margins have two functions, first as a safety factor and second as predefined ranges used for testing. The European Cooperation for Space Standardization (ECSS), a cooperative effort of the European Space Agency (ESA), national space agencies and European industry associations, have formulated common standards in the form of general requirements and nomenclature. The ECSS-E-ST-31C document [9], a space engineering document produced by the ECSS regarding general thermal control requirements, is considered as the most recent European common standard. This document provides guidance for: the general requirements architecture, commonly used nomenclature, and testing. The applicable thermal margins architecture have been depicted in Figure 3.3. The general architecture has been taken from [9], while the respective temperature scales have been adopted from [10].

The calculated temperature range shall be obtained by analysis using the thermal model, based on the nominal worst case scenario conditions. These conditions are considered as a certain combination of external fluxes, attitude and unit dissipation modes, excluding failure hence nominal. These conditions are basically representative of the hot and cold conditions. The calculated temperature range plus modelling uncertainties shall be specified as the predicted temperature range, and be limited to the specified design temperature range.

The qualification temperature range is a specified temperature range for each thermal mode, for which the unit is guaranteed to fulfil all specified requirements. The qualification margin is an extra safety margin to account for unexpected events, while the acceptance margin is taken to account for unpredictable events, both to be approved by the system authority. The acceptance temperature range is considered as the extreme temperature range that a system can reach, but shall never exceed, during all mission phases, based on the worst case scenario conditions. The design temperature range is thus allocated as the thermal system design activity

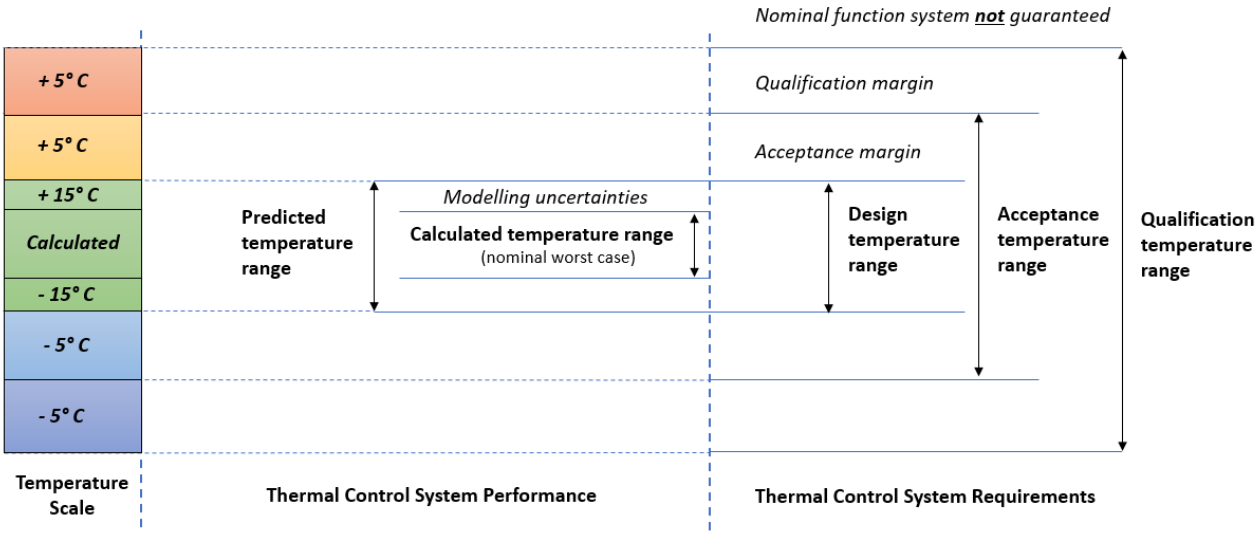

Figure 3.3: Thermal margins architecture for the thermal control system.

range, while the acceptance- and qualification margins are there to account for unpredictable and unexpected events respectively, for which the system is still guaranteed its nominal function.

To conclude, the thermal control system shall be designed such for it to stay within the design temperature ranges during nominal worst case scenario, without system failures. The total margin requires the calculated temperature to be within ±25°C of the qualification temperature range.

3.1.4 Thermal Budgets

The calculated temperature ranges as provided by the thermal model are considered to remain within budget when included with the aforementioned margins. These budgets describe the relation between the predicted temperature range and the design temperature, where the difference between the two is considered as thermal budget. The thermal budgets are considered to be a function of the spacecraft- configuration and modes, specified by the respective thermal requirements.

The top-down system budgets or optical alignment budgets have been formulated in the work of D. Dolkens in [7]. These respective budgets should eventually be translated into thermal requirements, which will be most relevant for the operational spacecraft modes. Sadly, this conversion is not easy since the majority of the telescope components are expected to include complex thermal deformations. In order to determine these deformations completely one requires a thermomechanical model, which is considered to be outside the scope of this project. Therefore, the thermal requirements shall be adopted from other system designers, as will be shown in the next section.

3.2 Top-level System Requirements

The formulated mission requirements as described in the DST SE Document [4] are mainly focused on the optical performance of the system, while no specific attention has been given yet to a system like the thermal control system. In order to create a need for a thermal system it was required to define additional top-level system requirement. This thermal systems, as well as several other systems are considered to be designed such for them to be operational in any expected conditions including uncertainties, as defined by the worst case scenario.

Therefore, two new system requirements required to be formulated, as depicted in Table 3.1. These requirements have been taken from the MarcoPolo-R Mission Requirements Document [11]. The nomenclature used in these requirements have been elaborated in the previous sections. The rationale of these mission requirements will be elaborated below.

SYS-REQ-04

The DST mission is composed of various mission phases during which certain sets of functionalities shall be specified per spacecraft mode and spacecraft configuration. The spacecraft modes are considered to be coupled to

a certain set of system functionalities, constraint by the spacecraft configuration. This because, among others, the telescope is not considered to produce images when not fully deployed. The totality of the spacecraft systems and their functions, shall therefore provide the optical system performance as described in the first mission objective.

SYS-REQ-05

The space segment consists of the space telescope and the launch vehicle, used to deliver the space telescope into space. With most demanding scenario is meant, among others, worst case- ΔV, launch mass and thermal environment. The latter should comprise the extreme range of thermal conditions up to EOL. This scenario shall be documented for each relevant mission phase in a To Be Determined (TBD) Document, such that the designers can choose proper boundary conditions for their designs. The worst case scenario is expected to include any additional safety factors or margins, which are taken to account for unpredictable events, unexpected events and modelling uncertainties.

ID	Description	Parent
SYS-REQ-04	The deployable space telescope systems shall provide the necessary functions during the various mission phases, as a function of the spacecraft configurations and spacecraft modes.	MIS-OBJ-01
SYS-REQ-05	The space segment shall be designed for the mission scenario which is most demanding, considered as the worst case scenario, as defined in the TBD document.	MIS-OBJ-01

Table 3.1: Additional top-level system requirements.

3.3 Thermal System Requirements

The thermal system requirements as considered in this thesis are considered to consist of the main thermal system requirement (3.3.1), and the thermal requirements as flown down from other system designers (3.3.2).

3.3.1 Main Thermal System Requirement

The main thermal system requirement is considered to describe the general function of the thermal control system, as presented in Table 3.2. The thermal system shall regulate the temperatures of the TBD systems, at any mission phase as a function of the spacecraft configurations and spacecraft modes. The mission phases are considered as specific parts of the thermal environment, during which certain thermal conditions can be expected. It is considered to be a function of the spacecraft configuration because it will decisive for the respective thermal interfaces, while the spacecraft modes are determinant for the respective temperature ranges.

ID	Description	Config.	S/C Mode	Parent
THE-SYS-01	The spacecraft thermal system shall cope with the thermal needs of the TBD spacecraft systems, at any mission phase as a function of the spacecraft configurations and spacecraft modes.	Any	Any	SYS-REQ-04

Table 3.2: Main thermal system requirement.

3.3.2 Flow Down Thermal System Requirements

Some of the DST system designers, those of the SMSS and the Primary Mirror Active Optics (PMAO) system, have formulated thermal requirements for their system. The majority of these requirements have been adopted in this study and shown in Table 3.3. This Table has been included with a constraint column in which the component temperature constraint has been described in degrees Celsius, assuming 273°C equals 0 Kelvin. Temperature margins are excluded here. In the previous section it has been explained that the thermal needs of a system are considered to be a function of the spacecraft- configuration and mode. Therefore, an additional column regarding the considered spacecraft mode(s) has been added to the list.

Table 3.3: Flow down thermal system requirements.

ID	Description	Configuration	S/C Mode	Reference: Comment	Constraint(s)
Component Bulk Temperature Limits					
M2-THE-01	The bulk temperature of the booms shall not exceed 373K during stowage.	Stowed	Survival	[12]: Page 50, creep	$T_c \leq 100°C$
M2-THE-02	The bulk temperature of the booms shall not exceed 473K when deployed.	Deployed	Any	[12]: Page 50, creep	$T_c \leq 200°C$
PMAO-THE-01	The bulk temperature of the universal joints shall not deviate more than 2285 K from the assembly temperature (nominally 298 K).	Any	Any	[13]: Table 9.5, buckling	$T_c \leq 2310°C$
PMAO-THE-02	The bulk temperature of the in-plane constraint wire flexures shall not deviate more than 318 K from the assembly temperature (nominally 298 K).	Any	Any	[13]: Table 9.5, buckling	$T_c \leq 343°C$
PMAO-THE-03	The bulk temperature of the moving frame plate shall not deviate more than 442 K from the assembly temperature (nominally 298 K).	Any	Any	[13]: Table 9.5, universal joint yield	$T_c \leq 467°C$
Instrumentation Limits					
PMAO-THE-06	The maximum gradient between the actuators in a push/ pull pair (actuators A,C and B,D) shall not exceed 0.01 K.	Any	Any	[13]: Wheatstone circuit is immune to transients.	$\Delta T < 0.01°C$
PMAO-THE-07	The bulk temperature of the actuators in non-operational phases shall not exceed the range 288 K to 373 K.	Stowed	Survival	[13]: Analogy, Rosetta SPICE	$15°C \leq T_c \leq 100°C$
PMAO-THE-08	The bulk temperature of the actuators in operational phases shall not exceed the range 288 K to 298 K.	Deployed	Operational	[13]: PPA40XL data sheet	$15°C \leq T_c \leq 25°C$

The recommendations of the SMSS designer as described in [12], have been translated into two requirements (M2-THE-01 and M2-THE-02) towards the thermal system. These requirements are there to prevent creep, which refers to permanent deformation due to mechanical stresses. The requirements of the PMAO system have been adopted from [13]. The component steady state heat flow limits have been excluded here since the steady state heat flow charts of the PMAO will not be included within this report.

3.4 Chapter Summary

Several thermal system nomenclature have been described in this Chapter, considered as thermal system aspects. The DST is considered to feature a stowed, partly deployed and fully deployed configuration which are related to certain mission phases. Further, the DST is considered to have at least a launch-, survival-, deployment and operational mode. Each of these system states are considered to define particular system functions.
The calculated temperatures will be determined for the nominal worst case scenario, where nominal refers to no failure. The total margin on the calculated temperature is set to ± 25 °C.
The difference between the predicted temperature range as calculated by the thermal model, with the design temperature range as specified by the thermal requirements, can be considered as thermal budget.

The thermal system is considered to control temperature under a given set of conditions and constraints as defined by the thermal requirements. In order to create a need and constraints for the thermal system at top system level, two additional top-level system requirements were thought to be required.
The thermal system requirements are thought to be a function of the spacecraft configurations and the spacecraft modes. The majority of the flow down thermal system requirements have been adopted in this study, apart from the component steady state flow limits since those results have not been generated.

4 Detailed Design of the DST

The DST is composed of several components and mechanisms which have been designed by other DST team members since the project has been initiated back in 2014. The thermal model of the DST and the subsequent analysis is only relevant for the most recent structural model. A schematic of the DST physical architecture has been shown in Figure 4.1. The components and mechanisms will be elaborated in the following order; the primary mirror segments (4.1), the secondary mirror (4.2), the Primary Mirror Support Structure (PMSS) (4.3) and the SMSS (4.4), the baffle (4.5), and finally the instrument housing (4.6) and the spacecraft bus (4.7).

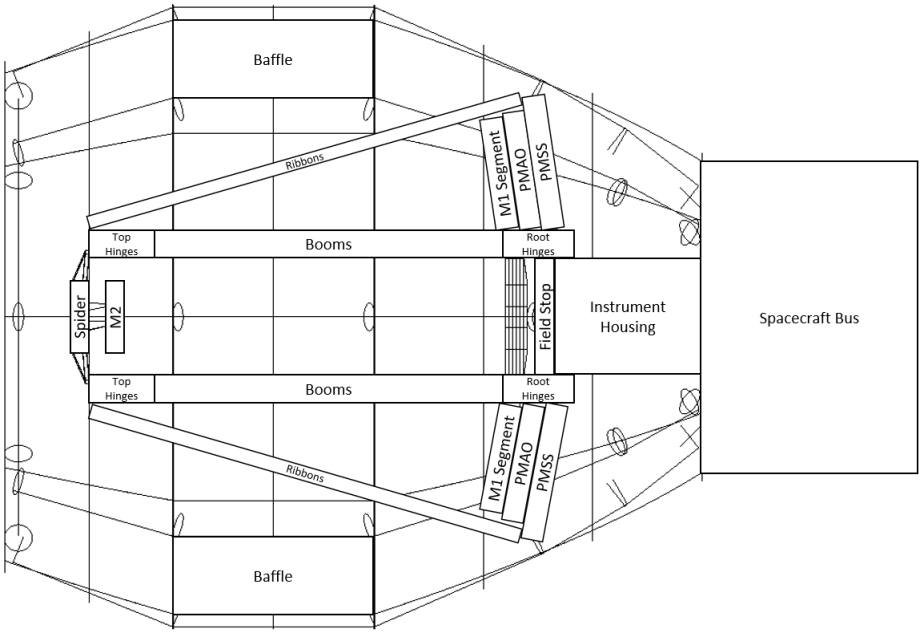

Figure 4.1: Schematic of the Deployable Space Telescope physical architecture, with initial parabolic baffle design.

4.1 Primary Mirror Design

The initial primary mirror (M1) segments characteristics in terms of the mirror material (Silicon Carbide = SiC) and the parabolic shape, were given by D. Dolkens in [7]. Another MSc student, B. van Putten in [14], has produced an initial structural primary mirror segment design which will be adopted in this study. The average angle of the parabolic mirror with the horizon was determined to be around 8 degrees. In order to create a mirror which is lightweight and stiff, the mirror was included with cutouts and made thick respectively.

In [12] by A. Krikken, a clear overview has been given about the dimensions of the deployed and stowed configuration of the primary mirror segments, shown in Figure 4.2a and 4.2b respectively. From this Figure it can be seen that two of its corners feature 45° triangular cut offs with a base of 100mm. These triangular cut offs enable the segments to fit nicely together. Besides, the geometry of the spacecraft bus is clearly indicated with outer sides of 410mm and cut offs of 113.1mm in length. These cut offs are there to account for the secondary deployment structure.

4.2 Secondary Mirror Design

The monolithic secondary mirror (M2) has initially been designed by D. Dolkens in [7] for a three mirror segmented primary mirror. The mirror is not round or circular but adjusted to the shape of the entrance pupil, which safes mass and reduces potential stray light issues [7]. The current secondary mirror design is shown in Figure 4.3a, and it will be made of some type of SiC. The mirror is monolithic, which means that it consists of one piece of material, without any cut-outs as seen for the primary mirror segments.

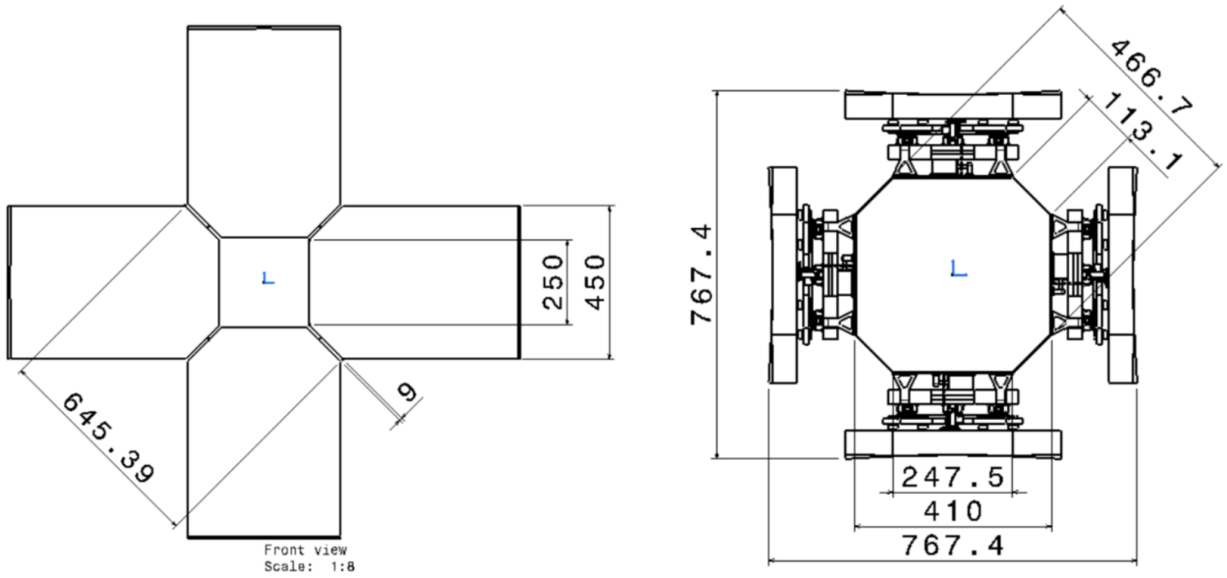

(a) Deployed configuration

(b) Stowed configuration

Figure 4.2: Assembled deployed- and stowed configuration of the primary mirror segments in [mm], taken from [12].

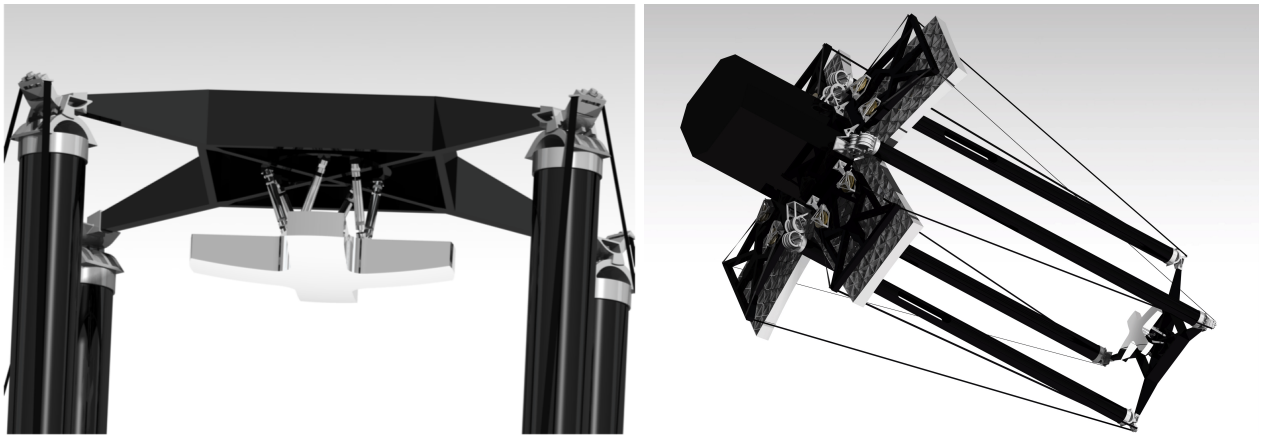

(a) Most recent design of the secondary mirror, taken from [12]

(b) Most recent design with winches and ribbons, taken from [15]

Figure 4.3: Most recent monolithic secondary mirror designs.

4.3 Primary Mirror Support Structure

The initial design for the PMSS has been worked out in [14]. This design included an A-frame support frame with a mid hinged strut, where the cutout in the A-frame was there to fit in the strut for the stowed configuration. During the work of M. Corvers in [15], it was found that the actual working of the self-latching hinge design is completely different as was assumed. Therefore, the deployment mechanism concept trade-off had to be conducted all over again.

With this new concept trade-off the team got help from Prof. Dr. Ir. Just Herder, professor of Interactive Mechanisms and Mechatronics at Delft University of Technology. In parallel to this another MSc student, A. Krikken, who was working on the secondary mirror deployment mechanism, struggled with achieving sufficient stifness in combination with acceptable repeatability and vibration resistance. Therefore, a preloaded ribbon concept deployment mechanism has been proposed, beneficial for both deployment mechanisms. There are still some concerns for this design, but at this moment it is the most recent design. Therefore, the ribbons, the athermalization components and the winches will not be considered in this study.

The deployment mechanism consists of several components each of which should be modelled within ESATAN TMS for it to represent the actual- structure and conditions. This mechanism consists of: the support hinges (Figure 4.4a and 4.4b) and the support frame (Figure 4.4c).

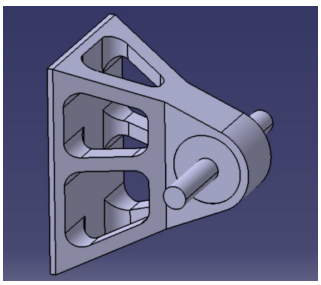

(a) Support hinge, taken from [14]

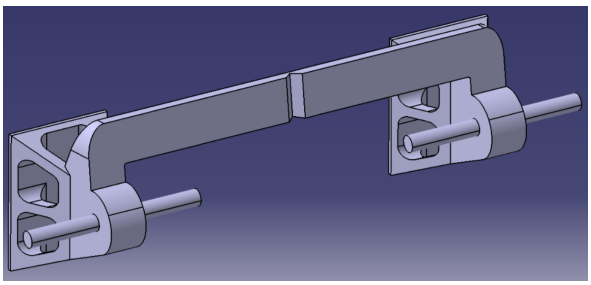

(b) Paired support hinges with connecting bridge and V-groove, taken from [15]

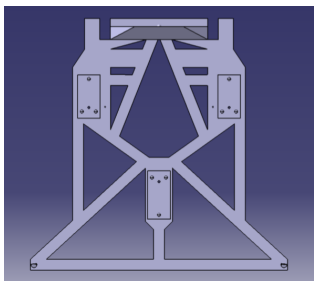

(c) Most recent support frame, taken from [15]

Figure 4.4: Primary Mirror Support Structure components.

4.4 The Secondary Mirror Support Structure

The initial design of the SMSS was made by D. Dolkens in [7], in which three booms were used to connect M2 with the spacecraft bus. This design has been given more detail by L. Barreto in [16], which included four articulated booms used to connect the spacecraft bus and the spider, of which the latter supports M2. The design included four booms because the telescope design had changed from three to four M1 segments, which meant that a three boom design would obstruct the incoming light. A downside of it having an extra boom, is that it becomes overconstrained and therefore it introduces unpredictability with deployment. Further analysis had to be done regarding the M2 deployment budgets and thus its mechanisms which let to the current design.

In the work of A. krikken in [12], one had switched again to a three boom concept because the concept with four booms was overconstrained. It also let to a lighter, yet less stiff system and therefore it was mentioned that this decision should be re-evaluated in a later stage of the project. As aforementioned, this design eventually struggled with achieving sufficient stiffness in combination with acceptable repeatability and vibration resistance. To account for this, ribbons were spanned between the top hinges of the SMSS and the support structure of the primary mirror. But because there are three booms and four M1 segments, two M1 segments will be loaded on one side by the ribbon and therefore the structure will be twisted due to the uneven loading. To account for this, four booms were reintroduced again as shown in Figure 4.3b. This design favours structural stiffness and symmetric loading over an exact constrained design [12].

Some of the design considerations like the spider (4.4.1), the mirror interface (4.4.2), the top- and bottom hinges (4.4.3), the boom and the (integrated) mid hinge (4.4.4) will be further elaborated below.

4.4.1 The SMSS Spider

The spider is used as the connecting interface between the booms and M2. Since it was initially chosen to use three booms instead of four, the initial design by L. Barreto in [16] had to be discarded, and thus a new concept had to be designed. Eventually, it was decided to go for the preloaded ribbon concept deployment mechanism, with four booms, hence the symmetric shape and thus the current design of the spider, as shown in Figure 4.5a.

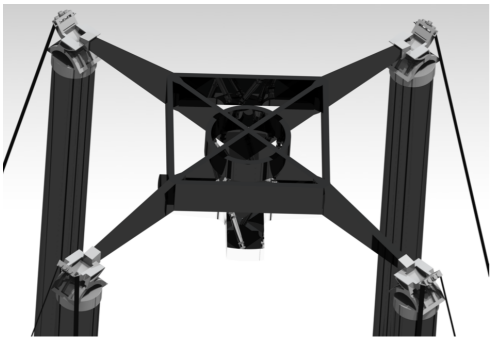

(a) Current design of the spider for four booms.

(b) Current design of the secondary mirror interface.

Figure 4.5: Secondary Mirror Support Structure components, taken from [12].

4.4.2 The SMSS Mirror Interface

The secondary mirror is attached to the spider by means of a mirror interface for which several concepts have been generated by A. Krikken in [12]. The most favourable concept was found to be the flexure based mirror mount in hexapod configuration, made of Aluminium 7075-T6. This is because this concept can be made athermal and therefore its performance can be made independent of bulk temperature changes. The current mirror interface design is shown in Figure 4.5b.

4.4.3 The SMSS Top and Bottom Hinge

The top hinges connect the booms with the spider, and include a Kelvin kinematic mounting interface, which in its totality restrict motion in all three Degrees Of Freedom (DOF). Several top hinge concepts have been created of which the most favourable concept consists of a simple hinge and a flexure, to account for deflections and rotations respectively.

In a later stage of the project it was found that the booms themselves would provide the required degrees of freedom, and therefore the flexure in the top hinge concept turned out to be useless. New concepts were created of which the CORE hinge turned out to be the best option for the top hinge as well as the bottom hinge. This is mainly because of its low hysteresis which means that the process of energy dissipation through deformation or displacement is low [12].

Their final designs are shown in Figure 4.6. In Figure 4.6a it can be seen how the top hinge connects with the top of the boom, the outer parts of the spider, and the ribbons. In Figure 4.6b it can be seen how the bottom hinge connects with the bottom of the boom and the instrument housing. The ribbons are guided through the outer ends of the primary mirror support structure to the winches as designed by M. Corvers in [15], although those will not be considered within this report.

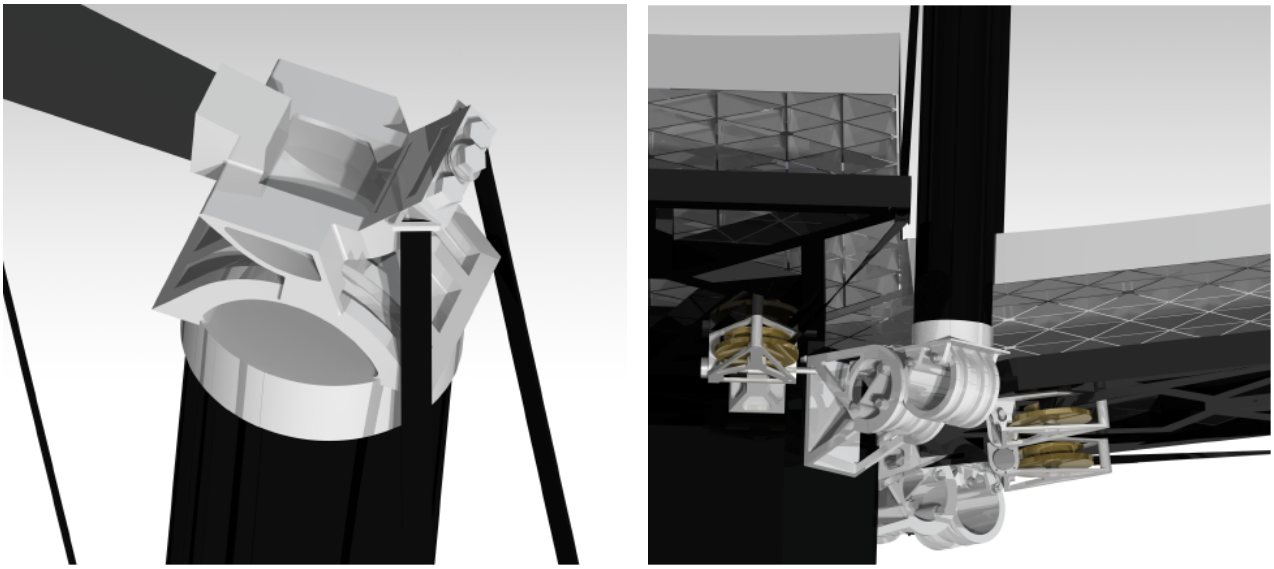

(a) Top hinge (b) Root hinge

Figure 4.6: Current designs of installed top- and bottom hinges, taken from [12].

4.4.4 The SMSS Booms

The secondary mirror needs to be deployed initially from its stowed position for which one has chosen for a mid hinged concept. The strain energy hinge was found to be most promising which is based on the elastic deformation principle, as described in [12]. A tube is initially bent and therefore contains stored energy, when released it releases the stored energy which drives the deployment to its initial state. An integral slotted hinge utilises this concept of which an example is shown in Figure 4.7. This example contains a Carbon Fiber Reinforced Polymers (CFRP) tube with two symmetrical cut-outs (Figure 4.7a), which allows bending of the tube over this area [12] (Figure 4.7b).

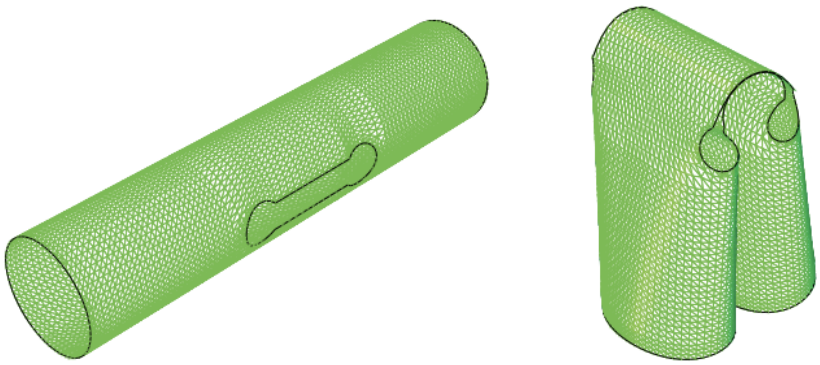

(a) Initial state (deployed) (b) Folded state (stowed)

Figure 4.7: Integral slotted hinge concept, taken from [12].

4.5 The Baffle

The (deployable) baffle will be fitted around the telescope components. In prior research projects it was found that a baffle was required for it to control the amount of stray light and thermal flux from exterior sources. Therefore, E. Korhonen has made an initial design which is shown in Figure 4.8. It must be mentioned that this is just an initial design and thus subject to change throughout the duration of this project.

The baffle structure is visualised in Figure 4.8a which is supposed to be made of some kind of aluminium alloy. The sides are parabolic shaped of which the dimensions are shown in Figure 4.8b. A circular ring structure has been added on top on which the sides are mounted. There is no additional structure at the bottom, probably to safe mass or because it will be mounted to the instrument housing around this area. At this point in time it has not been decided how the baffle will be connected to the rest of the telescope.

The baffle has an opening on top and bottom, as shown in Figure 4.8c. The sides will be covered with MLI for it reflect most of the thermal flux originating from the sides, and thus restricting heat flow as much as possible. The baffle is tightly fitted around the spacecraft bus on the bottom for it to reduce thermal flux entering the baffle from this side. Therefore, it is likely that most of the thermal flux will be entering the baffle from above. A larger opening needs to be present on top for it to supply sufficient amount of light for the telescope while also keeping stray light within acceptable bounds.

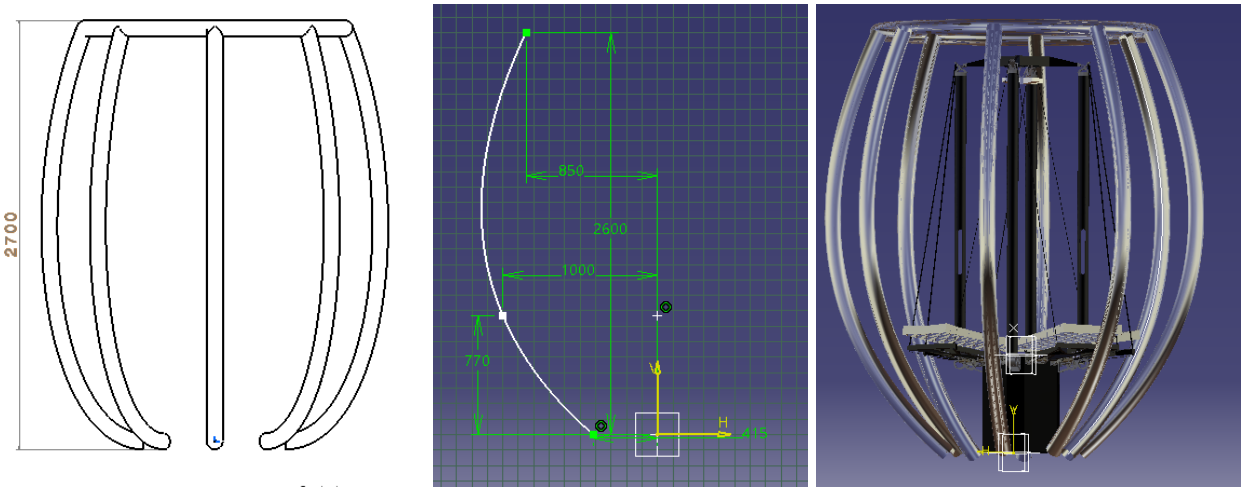

(a) Visualization of the baffle structure (b) Sketch of a parabolic sides of the baffle structure (c) Render of the baffle structure

Figure 4.8: Current baffle structure design as produced by E. Korhonen (26th of July 2018).

4.6 The Instrument Housing

The Instrument Housing (IH) includes the remainder of the optical elements. It has not been worked out in detail yet by other students, because it is thought to be less critical than the aforementioned deployable components, as mentioned by D. Dolkens in [7]. A schematic of the physical telescope architecture is shown in

Figure 4.9, as produced by S. Pepper. It must be mentioned that this Figure includes previous PMSS, SMSS and baffle designs.

The depicted IH includes the tertiary mirror (M3), the Deformable Mirror (DM), the Fold Mirror (FM), and the main detectors. The field stop and the piston cam are permanently mounted to the housing, of which the latter is used to detect misalignment of the primary mirror segments [10]. Other systems, like the PMSS, the SMSS and the baffle, are mounted to the exterior of the housing.

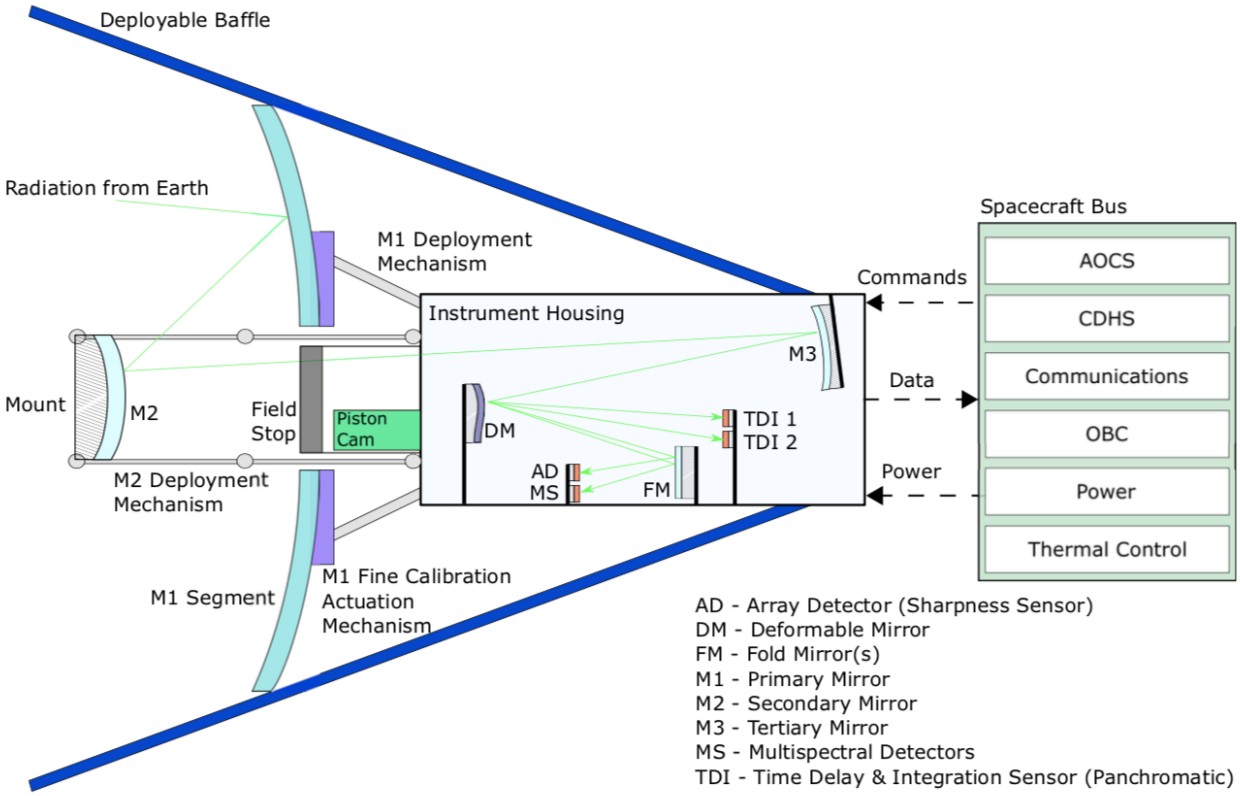

Figure 4.9: Schematic of the physical architecture of the DST, taken from [10].

4.7 The Spacecraft Bus

The spacecraft bus, which includes all other systems, apart from the optical system, is an essential system for the telescope to be fully functional. Examples of these systems are, among others, the Attitude & Orbital Control System (AOCS), the Command & Data Handling System (CDHS), the communication system, the OnBoard Computer (OBC) and the power system. First, it was thought that the spacecraft bus would be designed by Airbus Defence & Space (ADS) since they offer standardised spacecraft busses for payloads. Later, it has been brought to attention that such a standardised spacecraft bus would drive costs drastically and therefore it would be better if it would be designed by a student in the future. At the moment there are no details available about the required performance and therefore it will not be considered within this project.

4.8 Chapter Summary

All relevant design characteristics as determined by other DST team members have been touched in this Chapter. The telescope features four deployable segmented primary mirror segments and one monolithic secondary mirror, included with detailed designs of their support structures. The baffle features a parabolic shape initially.
The remainder of the geometries like the instrument housing and the spacecraft bus, are still to be designed in detail. Where applicable, dimensions have been indicated, and for for the majority of the components renders have been shown for it to give an impression of the DST appearance and its components.

II

Thermal Modelling & Analysis

(This page is intentionally left blank.)

5 ESATAN-TMS Workbench

ESATAN TMS is a dedicated thermal modelling software tool which can predict the temperature distribution in engineering structures and its components by using the thermal network theory. It allows the user to specify thermal network quantities in terms of nodes, conductances and material properties, from which the tool can calculate the steady-state or transient temperature distributions. ESATAN-TMS includes a graphical user interface, referred to as the ESATAN-TMS Workbench, which provides a user friendly interface in which the user can built extensive 3D geometries including pre- and post-processing capabilities. This interface makes the tool easy to use without requiring the user for having detailed knowledge of the language ESATAN-TMS is built on.

The ESATAN-TMS Workbench graphical user interface has been given a clear operating structure in which a subsequent sequence of steps should be followed for the tool to produce the intended thermal results. The tool requires the user to define the following:

- Generation of the geometry model including the material- and thermo-optical properties.
- Defining and running the radiative case.
- Defining boundary condition.
- Defining and running the analysis case.
- Visualisation of the thermal results.

In the following subsections it will be explained what these action comprise and how these relate to the modelling process.

5.1 Generation of the Geometry

The geometry entitles the structure of the spacecraft with all of its components, including its material- and thermo-optical properties. The geometric model requires the user to define: the bulk materials (5.1.1), the thermo-optical material properties (5.1.2), the thermal model components (5.1.3), the properties of the components (5.1.4), geometry combinations (5.1.5), non geometric thermal nodes (5.1.6), fixed and moving geometries (5.1.7), the model assignment (5.1.8), the conductive interfaces (5.1.9) and the user defined conductors (5.1.10).

5.1.1 Geometry Bulk Materials

The components of the structure are made of a certain type of materials with their own unique properties in terms of their density (kg/m^3), specific heat (J/Kg·K) and thermal conductivity (W/m·K). These respective thermal material properties, in combination with the thermo-optical properties of their surfaces, are required for the thermal calculations. The bulk materials describe what the majority of the components are made of considering homogeneous properties.

5.1.2 Geometry Thermo-optical Material Properties

The structural (or bulk) materials of a spacecraft are usually chosen on basis of their mechanical properties and/or mass, while thermal control coatings or paints are usually chosen on basis of their thermo-optical properties. These materials are for example excellent insulators or emitters, or have the ability of absorbing a minimum amount of solar radiation while being efficient InfraRed (IR) emitters. Besides these features, it can also be used to protect their bulk material from degradation effects, although those properties will not be considered in this thesis.

The bulk materials of the designed systems have been determined by their respective designers, which will be adopted in this study. Some of these materials are chosen on basis of their low Coefficient of Thermal Expansion (CTE), which describes the expansion or shrinkage of a material as a function of temperature. The optical material properties are relevant for determining the radiative properties, which have not been fixed yet. Together with the conductive properties, convection not considered, it describes how much heat is rejected or

absorbed. This can be related to a temperature increment, either positive or negative, and thus the amount of expansion or shrinkage of the respective component or system. The optical properties of a material, surface coating or paint, are conserved. This means that energy cannot be lost and thus it must be either absorbed, emitted or gone through. The energy conservation law is as follows:

$$\epsilon_{IR} + \rho^d_{IR} + \rho^s_{IR} + \tau_{IR} = 1 \tag{5.1}$$

$$\alpha_S + \rho^d_S + \rho^s_S + \tau_S = 1 \tag{5.2}$$

With ϵ being the emissivity, α being the absorptivity, ρ the reflectivity, and τ the transmissivity. The subscripts IR refers to the IR spectrum, while S refers to the Solar spectrum. The superscripts for the reflectivity refer to the diffuse (d) and specular (s) reflection. Reflection of smooth surfaces is known as specular reflection, in which the light reflects in a predictable manner, while for diffuse reflection the reflecting is unpredictable. The Workbench of ESATAN TMS considered diffuse reflection only, unless the user specifies the specular reflection too, which reduces the diffuse reflection in equal amount.

Transmissivity

Normally, when thermal control coatings or paints are tested, it is assumed that the tested samples are opaque ($\tau = 0$), which means that the coatings have sufficient thickness for it to prevent interference from the substrate [17]. When considering the application of coatings one should keep in mind that surface preparation, manufacturing techniques, thickness, and application procedures can and will effect the solar absorptance and emittance of the respective coating [17]. Throughout this thesis it will be assumed that all coatings are opaque, thus $\tau = 0$.

Solar Absorptivity

The solar absorptivity can be estimated by measuring the reflectance as a function of wavelength, where the reflected specular and diffuse components are collected together to obtain the total reflectance versus wavelength. The method as described in [17], measures the reflectance of the electromagnetic spectrum from wavelengths 0.3 to 2.4 μm. This relative small portion of the spectrum is considered to contain 95% of the Sun's energy, and therefore one can calculate the solar absorptance as a function of total reflectance and angle of incidence (θ), as shown in equation (5.3).

$$\alpha(\theta) = 1 - \rho(\theta) \tag{5.3}$$

Emissivity

Emissivity is defined as the ratio of the radiant energy emitted by a surface to that emitted by a black body at the same temperature. Generally, one measures the emittance within a certain wavelength band for which the emittance is strong (90% within 5-35 μm for a 300K black body [17]), and compares this to the emittance of a black body at the same temperature, which will result into a value between zero to one. Several types of measurement equipment are available these days, each with their own cons and benefits, and the properties of the coatings themselves are a function of many variables. Therefore, it is recommended to either determine the factors themselves based on several measurements, or to outsource the manufacturing as well as the application of the coatings to specialists.

5.1.3 Geometry Components

After the bulk materials and the thermo-optical coatings have been generated, one can start building the actual geometry. Within the workbench of ESATAN TMS one can define a geometry, which can be considered as a part or component of the DST. In order to create a component one must define the following aspects:

Geometry Name

The name assigned to the respective component must be different from the previous generated components. All sub-components should be named such that it is clear to which main components those are part of. The main components of the DST as will be considered in the initial thermal model are: the baffle, the booms, the instrument housing, the primary mirror, the secondary mirror, the primary mirror deployment structure, the root hinges, the top hinges, and the spider.

Geometry Shape

The geometry shapes which are going to be generally used for the initial thermal model are: a cylinder, a paraboloid, a quadrilateral, a rectangle, and a triangle.

Geometry Type

The geometry type can be either selected as a shell or a solid. Shells still have a thickness although it is visualised as a thin shell in the geometric model. Another difference is found for the allocation of the type of material. A solid is made of one type of material with a certain thickness and one optical set, while a shell can be composed of two types of materials (or just one) with a different optical set at both sides. The downside of selecting a shell is however that its sides will not participate in the view factor determination.

Geometry definition

The respective component can be defined by parameters, points or directions, of which the latter will not be considered here. The definition by parameters and points differs for each shape, for which guidance can be sought in the respective geometry diagram. When defining the parameters one must indicate the measurements of the respective shape, while for points one can use existing geometry nodes or user defined coordinates. The latter function can be useful in case the coordinates are previously available for the user.

Geometry Translations

This function becomes handy when components need to be rotated (°) or translated (m) with respect to a certain reference point. Besides, it can be used to position repetitive components which speeds up the building process. However, one should be aware how the sides are oriented.

5.1.4 Geometry Material Properties

After the geometric composition has been established one can assign the material properties, which as mentioned before is different for shells opposed to solids. The following properties, among others which have not been applied throughout this project, can be assigned to the respective geometry:

Meshing

The meshing of the geometry can be controlled by defining the amount of faces per direction, for which the solid type has an additional direction throughout the thickness. Besides, one can define a mesh ratio which can be useful to allow more nodes to be placed towards the outer ends or the interior. The meshing determines the amount of thermal nodes per surface and thus more or less the accuracy of the thermal gradients across a geometry or component, but it does also effect the solution speed.

Material- and Surface Properties

A difference between shells or solids can be noticed when visualising the thermal model, since although assigning the shell a thickness it will still look flat opposed to a solid. Another difference is found when defining the material- and surface properties. A solid geometry consists of one type of material with one type of optical coating, applied on all exterior surfaces, of which the thickness is defined within the geometry definition. For a shell however, this differs in the sense that it is not necessarily composed of one type of material. It can be composed of two types of materials with different thicknesses, included with similar or different thermo-optical coatings.

Surface Activity

The shell geometry considers two surfaces, exterior and interior, which can be given different material properties, thicknesses and thermo-optical coatings, of which the thickness is not represented in the visual model. Although it will be used for determining its thermal resistance. Another difference can be found in defining its activity which can be either: active, conductive, inactive or radiative. Active refers to its participation to the thermal environment by means of radiation and conduction, while inactive refers to no participation at all. Besides one can define the conductive properties by either selecting the bulk properties of the material, or as effective for which a specific value in $[W/m^2 \cdot K]$ should be inserted.

5.1.5 Geometry combining

All the generated geometries are considered as individuals while generally those can be considered part of a larger system or subsystem. Therefore, geometries should be combined into a logical system architecture which preferably would be similar to the actual system architecture. Besides, standalone geometries which are not combined into larger geometries are usually not taken into consideration during the analysis. This because the analysis will consider a fixed and moving geometry, apart from which no additional geometries will be included within the analysis. The excluded geometries will automatically be considered as inactive.

5.1.6 Non Geometric Thermal Nodes

Non geometric thermal nodes are not geometrically defined but do contribute to the thermal model. This can for example be representative of a heat dissipation node, by means of an electrical system or a system which is kept at a certain temperature. The non geometrical interface allows the user to specify to which node or geometry the heat is transported, including the heat rate and type of heat transport. These type of thermal nodes will not be considered in this thesis because the respective subsystems or parameters, which can potentially generate heat, have simply not been determined yet.

5.1.7 Fixed Components

The components of the geometry can be either fixed or not. The fixed components are considered to fixed to a certain reference axis, being part of a defined reference system. The remainder of the geometry is not fixed, but expected to be rotated or moving throughout orbit with respect to a certain reference. This can for example be applicable for solar panels which are rotated towards the Sun. Geometries which are not placed in either of these two groups will thus not be included in the thermal analysis.

5.1.8 Model Assignment

This respective modelling step has two main functions. Namely, to assign the geometry which should be used for building the thermal model, and to define the reference axis systems for the moving- and the fixed components. This step is a necessity for using the successive modules in the workbench. By assigning the model one defines which parts are considered to be moving or fixed, how these parts are orientated and what rotations of the moving components are allowed.

5.1.9 Conductive Interfaces

The conductive interfaces can be automatically generated within the ESATAN TMS Workbench, by means of the Auto Generate Conductive Interfaces function. This function fuses neighbouring geometries of equal material to each other, such that those are considered to be of the same geometry. Its conductive interfaces is thus equal to the thermal conductivity of the respective material.

The conductive interfaces consider three options, namely: fused, contact or not connected. Fused means that the respective geometries are considered as one piece of material as aforementioned. For a contact conductive interface one considers for example a mechanical connection or epoxy, for which a contact conductance value in $[W/m^2K]$ should be assigned to the respective interface. Sometimes, it can also be the case that geometries visually overlap, while in reality they do not. This can be caused by geometrical limitations of the Workbench in which certain shapes cannot be modelled correctly or to reality, and therefore those interfaces should be set to not connected.

5.1.10 User Defined Conductors

Definition of the conductive interfaces require the geometries to be closely together, and for them to be defined in the first place. Apart from those conductances, the user can define conductors manually. These consider advective, conductive, convective and radiative conductors. The advective and convective conductors will not be considered in this thesis, while the radiative conductors will be calculated as a function of the radiative case. The latter function could become useful when radiative calculations have been determined by means of testing for example.

The conductive conductors can be useful for defining conductances between certain nodes or surfaces, for which the respective conductive component has not been defined as a geometry in the thermal model. It requires the user to define a source- and destination reference, a definition method and a conductive factor. The reference describes from and to which node the conductive interface shall be present. The method describes how the

interface will be defined which can either be by means of calculation, or by specifying a value in [W/K]. The calculated method requires the user to define a thermal conductivity (W/m·K), a cross sectional area (m^2) and a path length (m). These latter two parameters are considered as the shape factor, which can also be specified as a value in case an interface is composed of several shapes.

5.2 Definition of the Radiative Case

Apart from defining a geometry one needs to define the thermal environment (5.2.1), the orbital parameters (5.2.2) and the pointing direction (5.2.3), after which the Workbench can execute the radiative calculations within the radiative module (5.2.4). These calculations are related to one specific geometry or spacecraft configuration, behaviour definition and orbital conditions [18]. Any changes to the aforementioned parameters will require the user to re-run the radiative calculations.

5.2.1 Thermal Environment

The environment describes the two body system of the celestial body and the Sun. By selection of the respective celestial body, which in our case would be Earth, one defines the Sun-planet system in which parameters like, among others, planet radius and sun planet distance are autonomously depicted. Besides, one can select the required inertial reference system which can be either selected with respect to the Sun, or a vernal equinox point. Besides, one can alternate the position and temperature of the Sun, the temperature and albedo of the celestial body, including the calculation method. The calculation method is currently set at uniform, which means that the celestial body is considered to reflect the sunlight uniformly and that it radiates heat at an uniform temperature, just like a black body. Changing the calculation method can increase the accuracy with respect to the real conditions, but also requires some additional input from the user. During this thesis one will alternate the temperature of the Sun and Earth, including change of the albedo, while the calculation method will remain uniform. This because it is though to be sufficient for this stage of the project.

5.2.2 Orbital Parameters

In order to determine the exact position and velocity of a spacecraft one requires a reference frame with respect to which these are described. The DST is supposed to orbit Earth and by defining its orbital parameters one dictates how it will be positioned with respect to this celestial body.

5.2.2.a Reference Frames

The reference frames considered here are geocentric (rotating) reference frames which were thought to be most useful for describing the motion of the satellite with respect to Earth. This geocentric reference frame considers, among others, the Sun to orbit Earth. For simplicity and explanatory reasons, the Earth is considered to be a perfect sphere. The concepts, nomenclature and Figures within this section are taken from [19].

The Earth is considered to rotate about its rotation axis. This axis runs through the Earth's surface of which the points at the surface are referred to as the North- and South Pole. The great circle halfway between these Poles, on the Earth's surface, is called the equator. A great circle can be considered as an intersection of the Earth's sphere which passes through its centre. The great circles which pass the poles are referred to as meridians. The Greenwich meridian or the prime meridian, indicated by G in Figure 5.1a, is considered as the reference meridian on Earth. These meridians, in combination with other parameters, are used to describe a position on the Earth's surface, although they are not considered relevant here and will therefore not be further elaborated on.

A celestial object can be considered as a natural object located outside of the Earth's atmosphere. In order to denote angular positions of a celestial object with respect to the mass centre of Earth, it is found convenient to use the concept of a fictitious celestial sphere. This concept is shown in Figure 5.1a. The celestial sphere has an infinitely large radius, which is considered to be centred at the mass centre of Earth throughout this thesis. The Earth's rotation axis can be extended up to the celestial sphere. These two intersections are considered as the celestial Poles, with the North and South corresponding to those of Earth. The same holds for the celestial equator which is in line with the Earth's equatorial plane. Great circles passing through the celestial poles, on the celestial surfaces, are referred to as hour circles. These hour circles are only considered for the upper branch, which is considered to be above the Earth's equatorial plane or the northern hemisphere.

The Earth is considered to rotate 360 degrees about its spin axis in one day. Because of this rotation, celestial objects appear to be rotating when seen from Earth. This effect is referred to as diurnal motion. The Sun, when observed from Earth, is thought to possess a second motion due to which it will move eastwards, returning to

its original position on the celestial sphere in one year. The ecliptic, as shown in Figure 5.1b is referred to as the path of the Sun over the celestial sphere, which describes the rotation of the Sun around the Earth's centre, with a rate of about 1° per day. The obliquity of the ecliptic (ϵ) is referred to as the angle between the ecliptic plane and the equatorial plane. This parameter is known to change slowly with time. The intersections of the rotation axis of the ecliptic, taken perpendicular to the ecliptic plane, are considered as the ecliptic Poles.

The line of intersection of the equatorial plane and the ecliptic plane, referred to as the first point of Aries or Υ, both shown in Figure 5.1a and 5.1b, is thought to be fundamental in the definition of reference systems [19]. This point is actually not fixed in space, because of slow movement of the ecliptic and the celestial equator due to gravitational interactions, but will be considered fixed in this thesis.

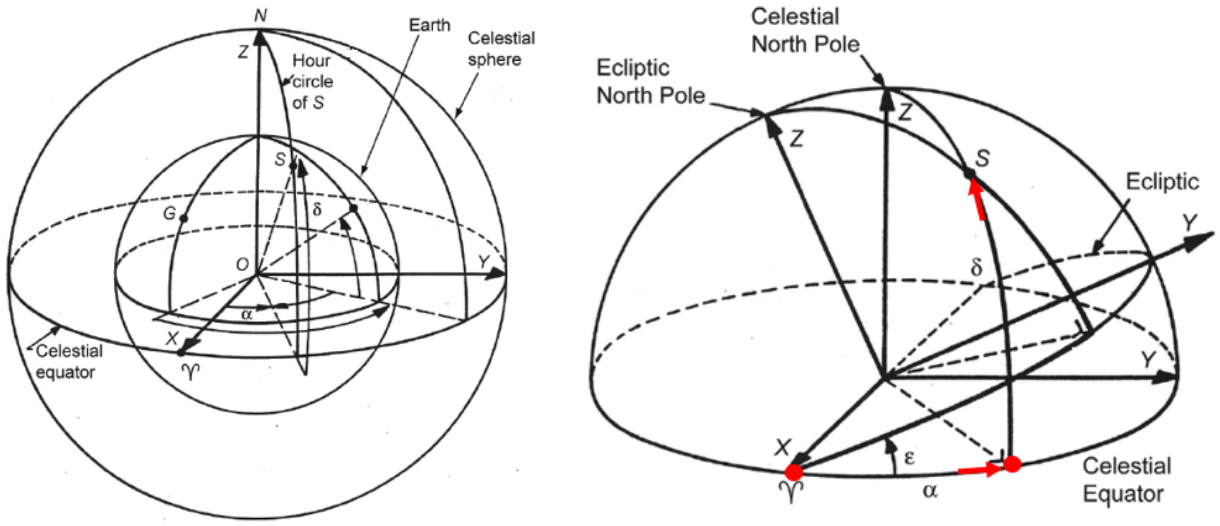

(a) (b)

Figure 5.1: Geocentric celestial (a), and geocentric- equatorial and ecliptic coordinate systems (b), both taken from [19] and partially adjusted for it to represent the relevant parameters.

5.2.2.b Celestial Elements

The angular position of a celestial object in a non-rotating geocentric equatorial reference frame, as indicated by S in Figure 5.1a, is indicated by two parameters: δ and α. The angular measurement has been highlighted in red. The declination, δ, is considered as the geocentric angle measured along the hour circle through a celestial object, while the right ascension, α, is measured along the celestial equator, from the point of Aries up to the aforementioned hour circle. The right ascensions can vary from 0 to 360 °, while the declination varies from -90 to 90 °, for which negative values imply positions south to the equator. If one would include the distance from the celestial object to the Earth's centre, one can describe its position relative to the geocentric equatorial reference frame.

As aforementioned, the ecliptic can be referred to as the path of the Sun over the celestial sphere. Just as for all other celestial objects, its position with respect to the geocentric equatorial reference frame will be expressed in a certain declination, right ascension and distance. The obliquity of the ecliptic is known to change in time, and ESATAN TMS therefore requires the user to define the respective angular positions. The position and orientation of the Sun with respect to Earth is a function of time, although the latter dimension is not necessarily important yet for this project. The DST mission will be sized for the most demanding scenario, as described in SYS-REQ-05, for which certain positional conditions of the Sun with respect to the Earth and the satellite will play a vital role.

The distance between the Sun and Earth can be scaled by means of adjusting the Sun's flux, while its orientation with respect to the Earth and the satellite will be important for the significance of this flux onto the satellite. Or in other words, one should determine a angular position of the Sun with respect to satellite and the Earth, for which its flux significance is largest or smallest. These positions, including certain flux conditions, can be used to determine the hot and cold case for the thermal simulations.

5.2.2.c Orbital Elements

The orbital elements are used to describe the orbit characteristics of a satellite orbiting a celestial body. Some of these characteristics have been determined in previous DST works. A representation of some of these parameters

are depicted in Figure 5.2, of which the relevant ones will be elaborated on below.

Figure 5.2a represents the orbital plane of an elliptical orbit for which the eccentricity (e) and the semi-major axis (a) determine the shape and size of the orbit. The spacecraft (S) orbits the celestial body at a distance r, around its centre of mass or focal point (F). The true anomaly (θ) indicates the position of the spacecraft within its defined orbit. The point of closest approach is called pericenter or periapsis (P), while the point of farthest excursion is called apocenter or apoapsis (A), and for Earth these are respectively apogee and perigee [19]. The distances for these two centres are indicated by r_P and r_A respectively, which as can be seen in the Figure, are a function of the eccentricity and the semi-major axis. From this comparison one can also deduce that for eccentricity equal to zero (e=0), r_P=r_A=a=r, which refers to a circular orbit. This type of orbit will be considered throughout this thesis.

The orientation of the conic section, in case elliptical, is determined by the argument of pericenter or periapsis (ω), depicted in Figure 5.2b, which is considered as the angle between the Ascending Node (AN) and the pericenter in this respective reference system. The right ascension of the ascending node (Ω) is used for describing the orientation of the orbital plane, measured in the reference plane between Υ and the ascending node. The reference plane can be either ecliptic or equatorial, but throughout this thesis one considers the motion of a spacecraft around Earth and therefore the reference plane will be equatorial. The inclination (i) describes the angle between the orbital plane and the reference plane, thus the equatorial plane within this thesis.

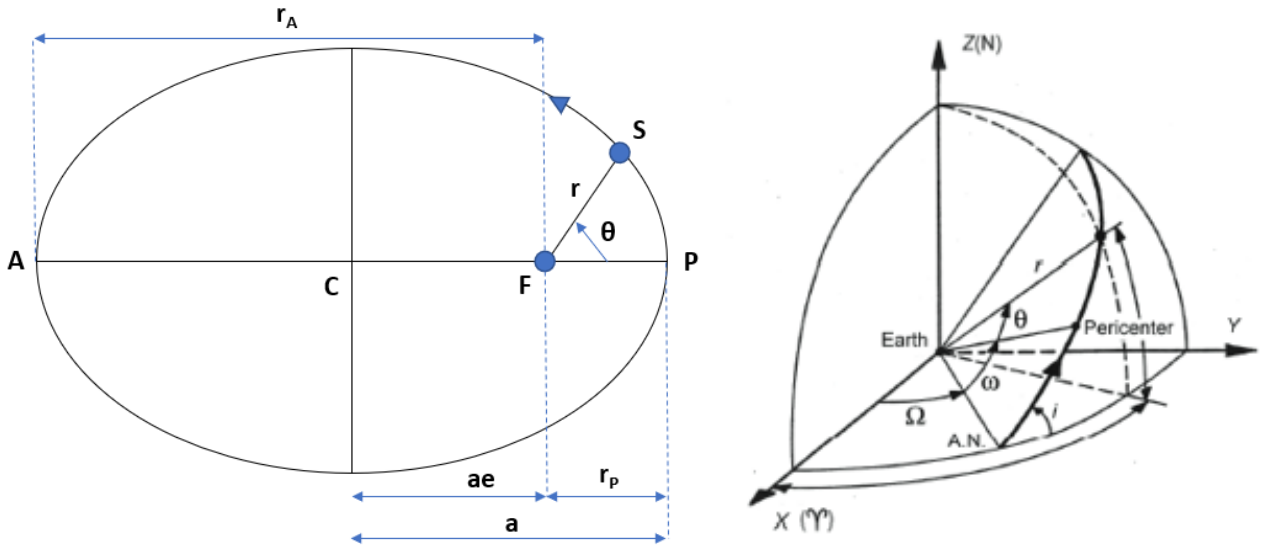

(a) (b)

Figure 5.2: Geometry of an elliptical orbit (a) and definition of the orbital elements (b), both taken from [19] and partially adjusted for it to represent the relevant parameters.

The following inputs are sufficient for ESATAN TMS to define the orbit: eccentricity (-), altitude of perigee or apogee (m), inclination (deg), right ascension (deg) and the argument of periapsis (deg). The altitude of perigee or apogee describes the distance from the surface of the celestial body to the respective point, instead of from the centre. Besides, one can adjust the desired anomaly range and the number of positions which should be calculated.

5.2.3 Pointing Direction

The thermal model is defined with respect to the Model Co-ordinate System (MCS) and should be oriented with respect to the Inertial Coordinate System (ICS). Some of these directions are, among others, the true Sun, Nadir and velocity. This allows the user to define how the satellite or spacecraft should be oriented with respect to the celestial body. Within this thesis one will consider the pointing method by means of pointing- vectors and directions. This requires the user to specify the pointing- vector and direction of the primary- and secondary pointing, where the primary is representative of the fixed frame while the secondary will be representative of the rotating frame.

5.2.4 Case Execution

After the radiative case has been defined one can execute the respective set of conditions. This will calculate the Radiative Exchange Factor (REF) of each node, as a function of its orbital position and thermo-optical properties. ESATAN TMS utilises a Monte Carlo ray tracing method in which it fires a finite numbers of rays from surface i. These rays are traced towards the nodes j, after which the ratio between the total number of rays fired from i is compared to the numbers of rays which impinged the nodes j. This is then converted into a view factor. In combination with the thermo-optical properties it is possible to calculate the Gebhart Factor or REF. The nomenclature, conditions and equations for this exchange have been defined in the preceding literature study [8]. The fully executed radiative case will be stored and available for the thermal analysis.

5.3 Definition of the Boundary Conditions

Boundary conditions are representative of separate thermal interfaces. They can be considered apart from the aforementioned radiative thermal environment and considered as internal heat inputs. These heat inputs can for example be representative of heat dissipating equipment or as thermal control elements applicable for controlling temperatures. The user can select a node, surface, component, geometry or non-geometric node as reference for the Boundary Condition (BC). The Workbench of ESATAN TMS allows the user to consider the following boundary conditions:

Table 5.1: Types of boundary conditions as considered in ESATAN TMS

Type of BC	Description	Units
Initial Temp.	The reference is assigned an initial temperature. This temperature is subject to change due to influences of the thermal environment.	K
Temperature	The reference is assigned a fixed temperature, which is not subject to change during simulation.	K
Heat Load	The reference is assigned a heat load value per unit volume, unit area or unit face, which can be supplemented with a multiplier in case the reference considers several unit volumes, areas or faces. Besides, one can specify the control method which either be selected to always on or to thermostat. For thermostat control, one can define several parameters like; on- and off temperature, and steady state and transient state operational mode.	W/m^3, W/m^2 or W/m
Total Heat Load	A reference can be given a total heat load irrespective of its measurements.	W

5.4 Definition of the Analysis Case

By defining an analysis case one basically defines the thermal network, which is composed, among others, of a radiative case, boundary conditions and a solution routine. The DST as presented in this thesis will not include any types of boundary conditions because those are simply not considered yet. The solution routine describes which part of the orbit should be modelled, in which one specifies a steady state initial point from which the transient analysis will follow. For the transient analysis one will define, among others, the duration of the simulation and the sampling rate.

The resulting solution file will include all requested outputs as a function of the heat inputs, the conductors, the radiative exchange factors and the node heat capacity. The latter property describes how the temperature of the node will change as a function of heat, or in other words its thermal resistance.

5.5 Visualisation of the Thermal Results

The previous section described what is considered to be included in the analysis case. This solution file shall be run after which its intended outputs are stored in the results file. The visualisation function allows the user to depict so called thermal nodes attributes, for single- or orbital results, onto the geometrical structure. Thermal nodes attributes are, among others, temperature, total albedo heat source, total Earth heat source, total internal heat source and total solar heat source. A single result will depict the requested time sample, while orbital results will display the satellite within its orbit for one or more time samples.

Besides, it is possible to define charts of these attributes, including heat- and limit charts. With the use of heat charts one can describe certain types of heat interaction between selected components. By means of limit charts one can determine the extremes of selected attributes without the need to deduct them from the attribute chart

themselves.

5.6 Chapter Summary

The thermal model as part of this project will be constructed in the Workbench of ESATAN TMS. The user is considered to define the bulk material and thermo-optical properties first, after which the geometric model can be constructed and assigned to these properties. Apart from giving it these two properties one should define, among others, the meshing and surface activity. Where the latter property defines to what type of heat transfer the surface will contribute.
The model geometries should be combined into a logical architecture, consisting of fixed- and moving components. This is because the model assignment requires a reference and moving component for defining its orientation with respect to a certain reference system.
The conductive interfaces can be defined automatically within the Workbench of ESATAN TMS, although it requires separate geometries to be closely together. Besides, one can apply user defined advective, conductive, convective and radiative conductors in which one can select a certain reference- and destination node. The latter function does not require the nodes to be neighbouring.

The geometric thermal model shall be exposed to a certain set of thermal environmental and orbital parameters, considered as the radiative case. The thermal environment considers the position of the Sun with respect to Earth and definition of the thermal environmental inputs like the Sun- and Earth temperature, and the planet albedo. The orbital parameters consider how the satellite will orbit the celestial body, or Earth in this project. The thermal model is defined with respect to its MCS and should be oriented as desired with respect to a ICS, or the geocentric equatorial reference frame in this project. By execution of the radiative case one obtains the required REF, which will be used for the subsequent analysis.

Boundary conditions are representative of separate thermal interfaces and can be considered as internal heat inputs, representative of among others, dissipating equipment or thermal control elements. These boundary conditions are considered separately from the REF.
The analysis case can be considered as defining the thermal network, consistent of, among others, the radiative case, the boundary conditions and the solution routine. The solution routine describes how the thermal network shall be solved being a function of, among others, time and sampling rate. The solution outputs can be visualised such for it to represent thermal node attributes onto the thermal model structure or by means of graphs, for selected geometries.

(This page is intentionally left blank.)

6 Initial Thermal Model

This Chapter presents the initial thermal model, visualised in Figure 6.1 and 6.2. It should be mentioned that this model considers false colouring. This model and all successive models are built on the assumptions as listed in Appendix B *Assumption List*. The most current version of the DST geometry is available in CATIA for which the 2.7 version has been used as reference for the thermal models of this project. CATIA features several building tools available for it to create complex geometries. The workbench of ESATAN TMS, used for creating geometries for the subsequent thermal analysis, is limited compared to CATIA and therefore it could be made exactly identical. The sizing of each component, apart from the baffle, could be easily obtained using the measurement function in CATIA.

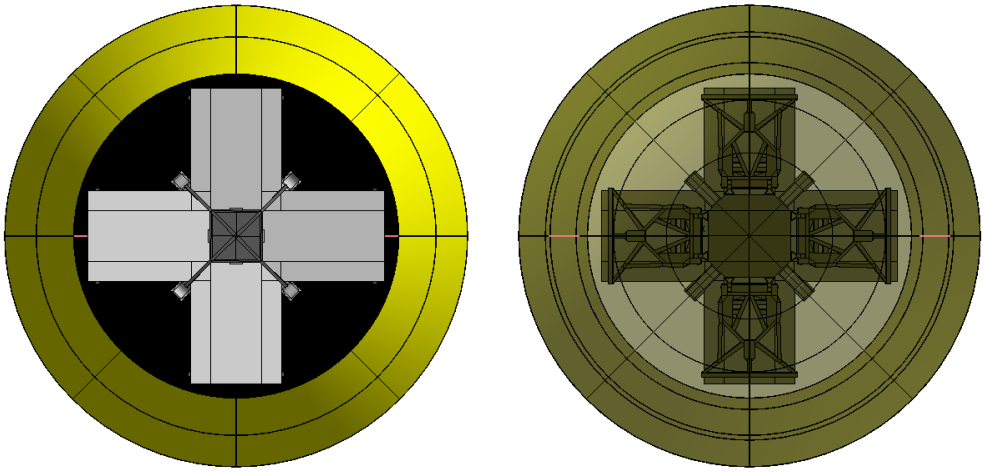

(a) (b)

Figure 6.1: Front view (a) and back view with transparent baffle (b), of the initial thermal model, DST 1.0. As produced in the Workbench of ESATAN TMS.

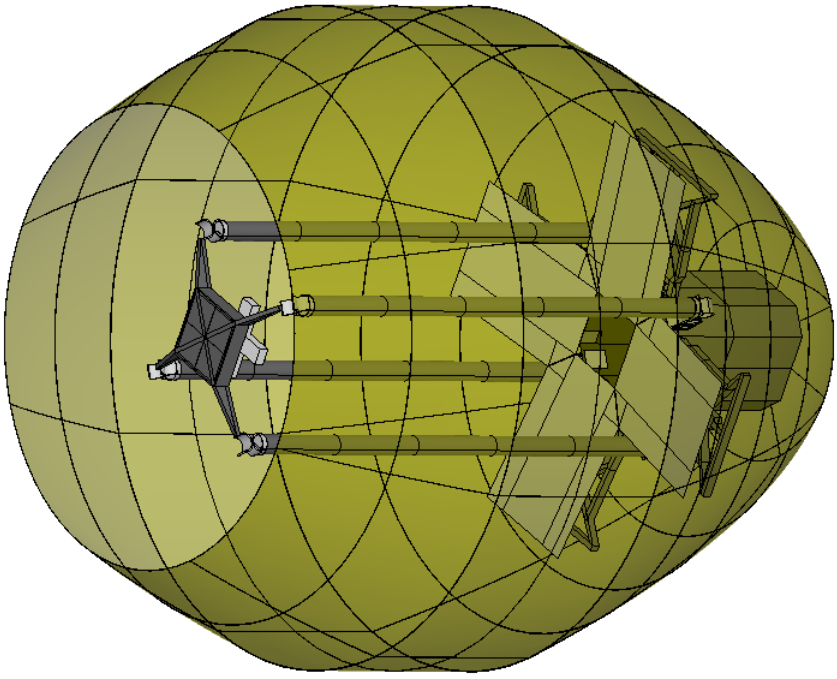

Figure 6.2: Side view of the initial thermal model with transparent baffle, DST 1.0. As produced in the Workbench of ESATAN TMS.

The material and thermo-optical properties of the initial thermal model shall be determined first (6.1). The definition of these properties allows the user to define each geometry of the respective DST components. The initial thermal model geometries are different from the reference geometric CATIA model. Therefore, one needs to elaborate on those differences (6.2). The initial model will be exposed to nominal thermal conditions (6.3). These simulations will consider three types of outer multi-layered insulation blankets from which the most suitable outer layer will be selected for subsequent models (6.4). This will be followed by a global temperature investigation regarding the extreme node temperatures (6.5) and concluded with a temperature distribution investigation (6.6).

6.1 Material & Thermo-Optical Properties

The modelling process steps required for producing a model in ESATAN-TMS workbench have been mentioned in the previous Chapter. These modelling steps will be used to create an initial thermal model with similar characteristics to that of the actual DST model.

6.1.1 Thermal Model Material Properties

The bulk material of a component describes what the majority of the components are made of without potential coatings. Most of the DST bulk materials have been mentioned in the previous chapter. Initially, most of the properties of these materials had been found in various sources, while eventually it has been decided to set a common standard for the DST project. Most material properties are taken from [20], as shown on the last page of the work of S. Pepper in [13]. The properties of these bulk materials, as will be inserted into ESATAN TMS are depicted in Appendix C *Thermal & Thermo-Optical Material Properties*, which are included with their uncoated optical properties. Some of the material properties are further elaborated on, in case assumptions had to be made regarding their specific properties.

CFRP

The specific (thermal) material properties of CFRP depend on factors like: fiber orientation, configuration, volume fraction and temperature [21]. This because the conductivity is different for the fiber direction compared to the through-the-thickness direction, as well as there is a difference for the fibers and the epoxy material. The CFRP material properties depicted in Table C.1 are respective for the unidirectional (UD) tape fiber configuration. This configuration is taken because it features the lowest CTE value, although the CTE value has been taken from [12]. The density value is taken from another sources and therefore it is not necessarily respective for the aforementioned fiber configuration.

PETP

Polyethylene Terephthalate Polyester (PETP) will be used as reference material for the Multi-Layered Insulation (MLI) blanket insulation layers, as will be elaborated on in a later section. The conductivity and density seem to match as those described in [22], and therefore the specific heat value of this material will be used for the MLI insulation layers.

6.1.2 Thermal Model Optical Properties

All components with their bulk material and their applied surface coating, in case applicable, are depicted in Table 6.1. It must be mentioned that the ribbons, the winches and the athermalisation elements have not been considered. For the components of which the optical coating has not been determined yet, the optical properties of the bulk materials themselves are assumed. The primary mirror deployment mechanism is composed of several components used for supporting the mirrors and to enable deployment, of which the majority of the mechanism consist of CFRP.

For the mirror surfaces, other team members, have decided that it should be highly reflective for which the exact properties will be elaborated on below (6.1.2.a). For the baffle it has been determined that the it should be covered with a MLI blanket (6.1.2.b). Further it is thought that it should feature low solar absorptance for it to absorb a minimum amount of heat by the Sun. Minimum solar reflection on the inside would be beneficial for it to keep stray light generation to the minimum, hence the requirement for a suitable thermal control coating (6.1.2.c).

Table 6.1: Summary of the DST component bulk materials.

Component	Bulk Material	Applied Surface Coating
Primary Mirror Segments	BOOSTEC SiC	Protected Silver (front surface)
Secondary Mirror Segment	BOOSTEC SiC	Protected Silver (front surface)
M1 Support Frame	CFRP	Uncoated
M1 Kinematic Interface	CFRP	Uncoated
M1 Support Hinge	CFRP	Uncoated
M1 Winch Mechanism	Ti-6Al-4V	Uncoated
M2 Spider	CFRP	Uncoated
M2 Mirror Interface	Al-7075	Uncoated
M2 Top & Bottom Hinge	Ti-6Al-4V	Uncoated
SMSS Booms	CFRP	Uncoated
Baffle Booms	AL-1100-O	Black Magic coating
Baffle Blanket	MLI	Black Magic coating
Instrument Housing	CFRP	Uncoated

6.1.2.a Reflective Mirror Coating

A silver enhanced coating for the mirror has been selected in [7] with an assumed reflectivity of 97%. From the third system requirement, MIS-REQ-3 [4], the system shall operate in wavelengths varying from 450-692 nm. Potential mirror coatings and their respective enhanced reflectance spectra regions are depicted in Table 6.2. From this Table it can be seen that the enhanced aluminium coating is effective to a wavelength of about 650 nm. Outside this spectral region it features no enhanced reflectance features. It is thought it is therefore not necessarily the best choice for wavelengths $>$ 650 nm, since it will reflect less and thus absorb more. Thus, the wavelength regions as depicted in the Table describes in which waveband the respective coating features its best reflectivity. For the enhanced aluminium coating for example, it only features a reflectivity value of $\sim$0.9 at 700 nm, which is below the average expectation.

Therefore, it is thought that the protected silver coating is a better choice for the intended waveband. The indicated waveband reached from 450 to 2000 nm, for which one should find out what the average reflective properties would be for the operating waveband of 450-692 nm. In [23], a graph is shown for the reflectance with wavelength, with an average value of 96.5% for the aforementioned operating waveband, without considering degradation effects of the space environment, assuming- that the transmissivity is zero, and equal reflectivity for solar and IR.

Table 6.2: Average reflectivity of suitable mirror coatings, taken from [24].

Potential Mirror Coating	Waveband [nm]	Average Reflectivity
DUV (Enhanced) Aluminum	190-600	>0.85
UV (Enhanced) Aluminum	250-700	>0.85
Protected Aluminum	400-700	>0.85
Enhanced Aluminum	450-650	>0.95
Protected Silver	450-2000	>0.98
Protected Gold	700-2000	>0.96

6.1.2.b Multi-layered Insulation

The baffle is made of an aluminium structure entirely covered with MLI. The blanket is composed of several layers, of which the total number of layers is not yet determined. Several possible MLI blanket materials are given in [25]. The outer layer of these blankets are most relevant for the thermal optical properties, while the inner layers generally function as insulation layers.

Insulation Layers

A possible option could be to use aluminium coated (one sided) Polymer Ethylene Terephthalate (PET), featuring low emittance and low absorptance, suitable for a -250° to +150° continuous temperature range. It is one sided because the baffle should be reflective on the outside only. Other options, among others, include aluminium coated polyimide, for low emittance and low solar absorptance, and aluminium coated black Kapton, for high emittance and high solar absorptance.

The isolation sheets sheets as described in [25] are offered with different thicknesses ranging from 0.25-5.0 mil (6-127 μm). From the depicted data it is unknown how the thickness affects the performance other than a larger thickness results into larger typical mass. Therefore, another source has been found, RUAG space insulation [22],

supplier of space insulation materials, including heat transfer data and emissivity as a function of temperature and layering. Besides, they have successfully equipped missions, among others, GAIA and Rosetta.

Outer Layers

As aforementioned, the MLI outer layer should most likely feature low solar absorptance for it to reflect the sunlight impinging at the baffle. Whether it requires low or high emissivity is unknown and therefore three different outer layer options with low absorptivity are given in Table 6.3. This table include the two insulation layer options, of which the 10 layer package is lighter but not suitable for operation above 150 °C. With t being the thickness, α being the absorptivity, ϵ being the emissivity, h being the heat transfer coefficient and $T_{Operation}$ the temperature range in which operation can be guaranteed. The thicknesses as provided for the first two outer layer materials are respective for the FEP layer only. The thickness of the Vapour Deposited Aluminium (VDA) outer layer, of 12.5 μm, is taken from [25], while the thickness of the insulation layers are estimated based on the two possible polyester film thicknesses, of 6 and 12 μm, as provided in [22]. Here it is assumed that the thicker layers are used for the 22 layer package, which in terms of density would make a liable assumption. The exact thickness of each individual layer of the MLI outer layer are not provided and therefore it will be assumed that the VDA, silver and inconed layer will have equal thickness of 12.5 μm.

Table 6.3: Suitable MLI layers, taken from [22].

	t [μm]	ρ [g/m^2]	α [-]	ϵ [-]	**h** [W/m^2 K]	$T_{Operation}$ [°C]
Outer Layer Material						
FEP / VDA	51	-	≤ 0.14	≥ 0.60	-	-
FEP / Silver / Inconel	127	-	≤ 0.09	≥ 0.75	-	-
VDA	12.5	-	≤ 0.14	≤ 0.05	-	-
Insulation layers						
10 layer package	60	150	-	~0.0027	0.0175	-270 to + 150
22 layer package	264	645	-	~0.0023	0.015	-270 to + 350

Modelling Multi-Layered Insulation

The MLI blanket is thus composed of several layers of materials which should be modelled in ESATAN TMS correctly for it to represent the real case closest. A schematic has been made of these layers as shown in Figure 6.3. It be noted that the thicknesses are not representative of those depicted in Table 6.3. The inner layer, as shown in Figure 6.3b, is not described in [22], but is thought to be necessary for the inner coating, the magic black coating, to attach properly, and besides the additional inner layer can provide protection to the insulation layers. In [26], several aluminium and titanium samples were covered with, among others, the magic black coating, and proved to be suitable materials in space conditions. Besides, it is known that a VDA outer layer can be directly applied on the insulation layer, and therefore the inner layer is fixed at 12.5 μm VDA. The material properties of aluminium 7075 are used for the VDA layer. The inner coating, the magic black coating, is also expected to have a certain thickness, but for simplicity reasons its optical properties will be considered only.

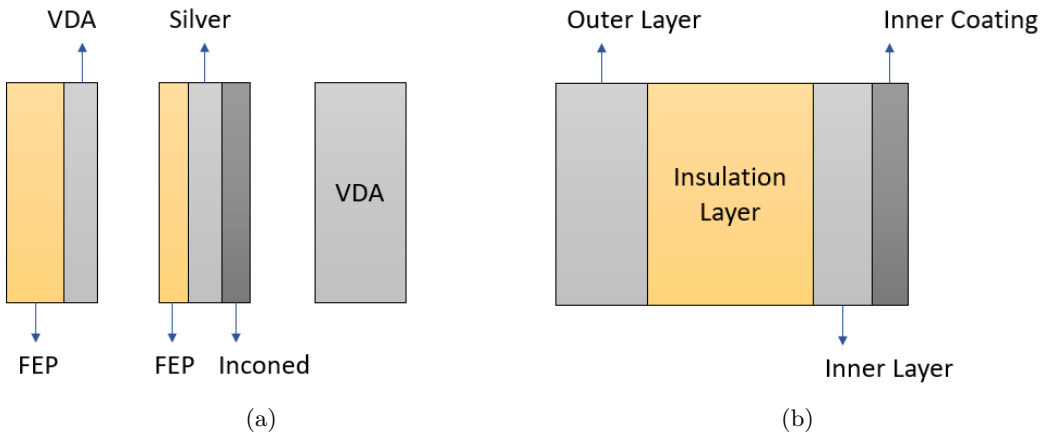

Figure 6.3: Schematic of the top layers (a), and all layers (b) of the MLI blanket.

Modelling MLI is rather complex since it is composed of several layered materials, while a surface in ESATAN TMS can only be composed of two materials maximum. The MLI is essentially composed of a certain top layer, an insulation layer and one coated inner layer. For the insulation layer, both the emissivity and the conductivity are given, thus both the conductive and radiative performance could in theory by used for the thermal model.

The insulation layer itself is composed of several FEP sheets with the given emissivity, while the conductivity of the entire insulation layer is provided. The MLI will be modelled using two separate surface layers, for which the user can select two different materials and thicknesses per surface layer, and select the optical surface and activity per side. Therefore, the MLI can be composed of four different material layer maximum.

Modelling Approach
Three different MLI configurations will be simulated, using the three different outer layers as aforementioned, featuring the same insulation layer and magic black coated inner layer. The MLI blanket will be composed of two surface layers, each composed of two materials with a certain thickness. The surface facing space will feature the optical properties of the outer layer, while the inner surfaces will be set conductive only, and the surface facing the telescope will feature the magic black optical properties. Analysis had shown that the radiative activity of the attached layers is negligible, hence the conductive only activity. Besides, it substantially accelerates the solver since calculation of the view factors for these layers proved to be slow.

6.1.2.c Other thermal Control Coatings

Thermal control coatings are applied for passive thermal control, generally possessing either enhanced absorptivity or emissivity properties. A spacecraft thermal control coatings references guide of NASA [27] has been used for the selection of some potential thermal control coatings. The researcher has picked out one black- and one white coating, one conductive paint and one vapor deposited coating, which are thought to be, among others, typical representatives of general space graded coatings or paints.

It is not known whether the inside of the baffle should necessarily feature high emissivity or not. High emissivity will allow the baffle to radiate more heat towards the telescope, but at this point in time it is unknown whether the telescope structure is too cold or too hot due to the shielding effect of the baffle. Besides, it will be hard to control the heat which will be radiated from the baffle towards the telescope, especially since the baffle will be unevenly illuminated. Another downside will be that a high emissivity will absorb more IR energy from Earth. Nevertheless, as seen in Table 6.4, a good solar absorber is a good emitter. Thus, for low reflectivity one generally requires a good emitter.

The initial baffle designer, E. Korhonen, has proposed another type of black coating, a magic black coating as described in [28]. This coating is optimised for the visual wavelength range, with a large operation temperature range (4 to 653 K). Besides, it has been applied on several space flown satellites. The properties are similar to the Vel-Black coating as described in the thermal control coating reference guide of NASA [27]. Nevertheless, the source is considered more recent and therefore the magic black coating has been selected as the non-reflective coating.

Table 6.4: A small set of potential thermal control coatings.

	Type	α	ϵ	**Reference**
Vel-Black	Black Coating	0.99	0.95	[27]
GSFC White Paint NS43C	White Coating	0.20	0.92	[27]
Aluminium	Vapor Deposited Coating	0.08	0.02	[27]
Electrodag	Conductive Paint	0.90	0.68	[27]
Magic Black	Black	0.99	0.93	[28]

6.1.3 Undetermined Optical Surfaces

The optical control coatings for most components have not been determined yet since it is unknown what properties are required or desired. This is because, no extensive thermal analysis has been conducted before, hence the temperatures and their gradients in orbit are unknown. Therefore, for now it will assumed that these components are uncoated, meaning that these surfaces contain the optical properties of their bulk material. The optical properties of the respective bulk materials are depicted in Table 6.5, mostly applicable at 298K or 25 °C since it is expected to be the baseline reference temperature. The reflectivity of SiC was used for BOOSTEC SiC, the optical properties for unidirectional CFRP have been used for CFRP,

The exact solar reflectivity properties of most materials depend on the surface treatment. When polished the surface will be smooth and most likely be more reflective. Therefore, it is difficult to pre-determine the exact optical properties of the depicted materials. For CFRP and AL-1100-O, specific values have been found and therefore those values can be used directly. For Al-7075, the average values will be used in the subsequent modelling phase. For BOOSTEC SiC, the upper bound value (0.254) of the solar absorptivity will be used since this is considered to be the typical value as described in [29], while the lower bound can be reached after surface preparation. For Ti-6Al-4V, it is mentioned in [30], that the typical finishes, oxidised and tiodised, results into

the upper bound values (0.6), while the polished finish lead to the lower bound value (0.2). For clarity, an extra column has been added to the Table in which it is indicated which values will be used for the thermal model. The chosen values are the most typical finished, but of course these finished should be re-evaluated when the thermal model is more mature.

Table 6.5: Optical properties of non-coated materials.

Material	α	ϵ	**Model input:** α/ϵ	**Reference**
BOOSTEC SiC	0.0005-0.254	0.05	0.254/0.05	[29], [31]
CFRP	0.88	0.88	0.88/0.88	[32]
Ti-6Al-4V	0.2-0.6	0.2-0.6	0.6/0.6	[30]
AL-7075	0.10-0.15	0.05	0.125/0.05	[30]
AL-1100-O	0.14	0.05	0.14/0.05	[33]

6.2 Initial Thermal Model Geometries & Grid

The DST geometry is split in several groups of components. For each of these groups it will be mentioned what the differences are with the structure, which could be either due to simplifications or because of restrictions of the ESATAN TMS Workbench. The grid has been set coarse for most of the components since fast convergence was desired. Some of the larger components like the baffle, the booms and the instrument housing have been given more nodes for it to represent the temperature distribution. The remaining components are relatively small and therefore grid refinement was not necessarily required.

Initial Spider Geometry

The spider connects the secondary mirror with the top hinges, of which the initial thermal model is a close representation compared to the actual geometrical CATIA model as shown in Figure 6.4. The flat plate, which is placed on top of the spider is not designed for the actual geometry yet. This because, it is representative of the mechanical system while the plate is put there for thermal reasons. The thickness of this plate should be determined with a dedicated mechanical analysis, not part of this project. The control coating of the plate will be determined in a later stage of this project.

The spider did feature some weird behaviour regarding sudden steep temperature increments, which could not be solved by changing the size of the grid. After a detailed analysis it was found that the geometry featured some imperfections, which caused extensive heating up too 100 °C, occurring at internal surfaces. The grid itself is set coarse, apart from the top plate which is expected to receive most thermal energy.

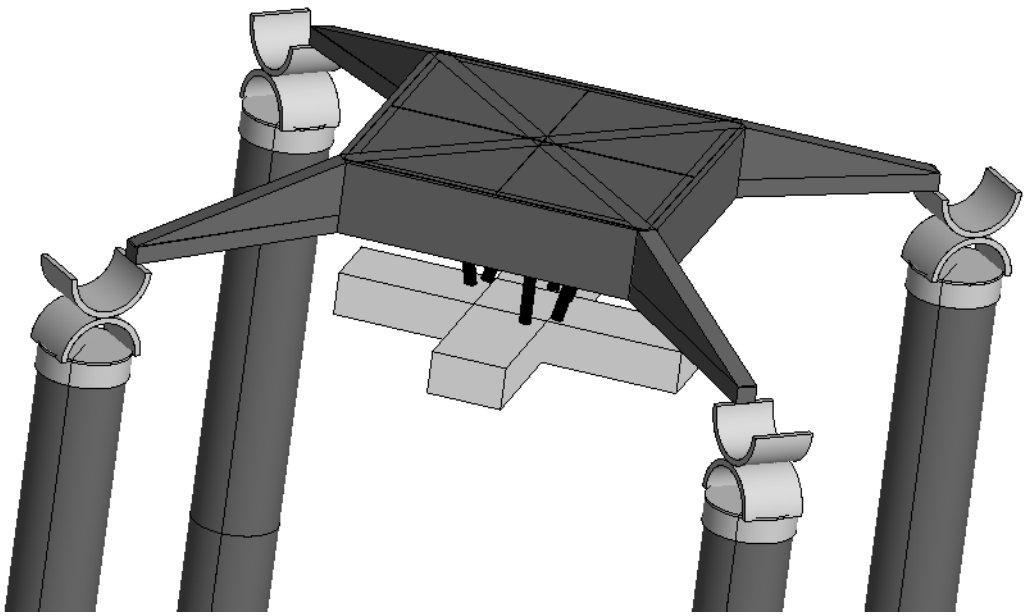

Figure 6.4: Top view of the thermal model telescope, without the baffle. As constructed in the Workbench of ESATAN TMS.

Initial Baffle Geometry

The Initial baffle geometry is composed such that not only the total length will be equal, but also the intended radii of the baffle at the bottom, middle, and top. These radii are respectively: 0.415 m, 1.15 m, and 0.85 m. The actual baffle shape can be seen as being composed of two parabolas, one upper and one lower, of which the lower one is slightly longer (1400 mm) compared to the upper (1200 mm). The bottom parabola has a larger gradient at the bottom because it is longer and features a smaller radius, but it seems that the gradients in between are equal or at least similar. In the Workbench of ESATAN TMS it is not possible to mimic the actual structure, therefore a cylindrical section in the middle is more or less required.

The geometry of the baffle has been completely redefined for which one has started with a back disk placed below the instrument housing, with a radius of 0.415 m. A cylindrical component has been placed in the middle with a radius of 1.15 m, after which two parabolic component has been placed in between and on top. The top parabola has been cut such that it meets the intended top radius of 0.85 m. The height of the middle cylinder has been adjusted such to connect the bottom and the top parabolas. The actual baffle does not have a cylindrical section in the middle, but because the actual shape cannot be mimicked exactly at the bottom it is thought to be a suitable replacement.

The actual baffle design is included with a boom structure consisting of eight legs, covered with MLI and a non-reflecting black coating on the inside. The baffle of the initial thermal model is composed of a MLI blanket only, with three potential outer layers as depicted in Table 6.3. For now, it will be assumed that the thinnest insulation package, thus the 10 inner layer configuration, should be sufficient for the telescope. This also considers that the thicker package is more than four times as heavy, and a lighter configuration would be most desirable. Further analysis should determine how the different outer layer materials effect the thermal results.

The grid for the baffle has been changed many times, this because the baffle suffers the steepest temperature increments and therefore one needed to be sure that this was not caused by the choice of grid. Eventually, it was found that further refinement of the grid did not effect the thermal results significantly.

Initial Booms Geometry

The geometry of the SMSS booms are relatively simple, featuring a long cylinder with integrated mid hinges. The latter is composed of two symmetrical cutouts in the middle of the cylinder as was shown in Figure 4.7. The booms of the initial thermal model do not contain the two cutouts in the middle, nor will any of the subsequent models do. This because it is thought to be relevant for the local analysis, while this project will cover the global analysis. Besides, incorporating such cutouts is not easy. The grid for the booms is chosen such for it to represent the temperature distribution along its length.

Initial Top Hinges Geometry

The actual geometry of the top hinges is complicated, as was shown in Chapter 4. Nevertheless, it was thought that the initial model should feature at least the main characteristics which are considered to be: the boom attachment, two partial cams, and the spider attachment. The resulting structure is shown in Figure 6.4. The conductive couplings between those components and those of the root hinges, have not been determined before but are set to a negligible value. They will not be determined in detail in this report. This because it is thought to be part of a detailed analysis as will be conducted by S. Leegwater. Potential control coatings will be re-evaluated in a later stage of this project.

The grid of top hinges is eventually set coarse, since no direct effect of refining the mesh was seen for the top hinges themselves. During the process, it seems that the choice of grid for the top hinges had substantial effect, up to several tens of degrees in some cases, for: M1, M2, IH, PMSS, SMSS booms, and spider. The current grid choice is most favourable for most of the groups, apart from the IH and the SMSS booms. It is unknown why this is the case, but it is likely this is caused by the shape of the top hinges. These are known to feature sharp corners and could therefore be prone to errors.

Initial Root Hinges Geometry

The following characteristics are considered for the root hinges: boom attachment, two cams and instrument housing attachment. The resulting structure can be seen clearest in Figure 6.5.

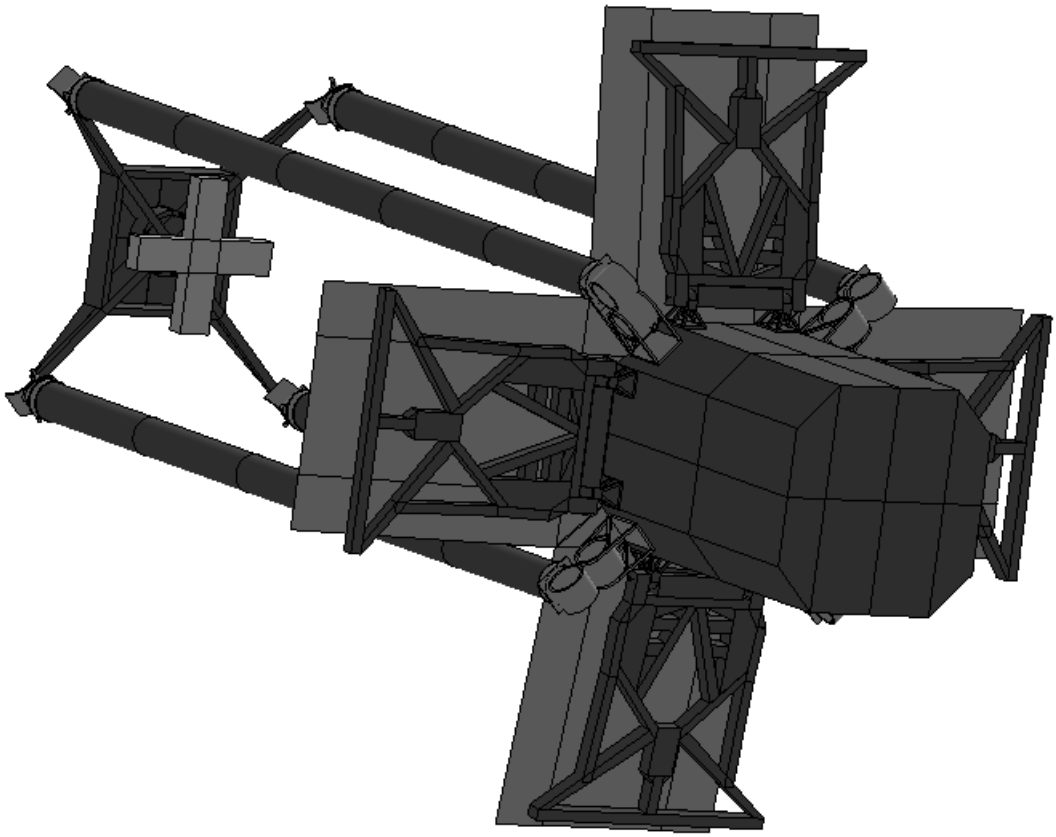

Figure 6.5: Back view of the thermal model telescope, without the baffle. As constructed in the Workbench of ESATAN TMS.

Initial Primary Mirror Geometry

The primary mirror is composed of four concave segments with cutoffs at the inner ends. In the Workbench of ESATAN TMS it is not possible to produce such shape and therefore the segments are modelled straight. The straight segments are placed under an angle of eight degrees, equal to the average angle of the actual concave segments. The thickness of the concave segments vary over the length, but it was found that the average thickness is around 50mm using the measuring tool in CATIA.

The segments are modelled as shells. First it was tried to model them as solids but since they are placed under an angle, there was a lot of intersection between the segments at the cutoffs. Besides, solids can be assigned one thermo-optical coating only, while the actual primary mirror segments are coated with a highly reflective protected silver coating on one side only. The back side of these segments are currently uncoated.

Initial Secondary Mirror Geometry

The secondary mirror is monolithic with smaller thickness and round corners at the ends. In the initial thermal model, this shape is modelled using two solid rectangles as seen in Figure 6.4. This because the rather complex shape cannot be mimicked within the ESATAN TMS Workbench. It is modelled as a solid and therefore it is considered highly reflective on all sides. Further analysis should determine how this affects the thermal solution.

The secondary mirror interface is included in the secondary mirror group, composed of aluminium alloy cylinders without flexures at the top and bottom. Further analysis should determine how the flexures will effect the thermal solution.

Initial Instrument Housing Geometry

The IH has no detailed schematics yet, but the current design can be seen clearest in Figure 6.5. The exterior dimensions were known but the material nor the thermal coating has been determined yet. For the initial thermal model it has been decided to use CFRP as the bulk material, this because it was though to be in line with most of the other components. The thickness is set at 1mm, which is completely arbitrary. For now, the exterior is considered to be uncoated. Further, it is thought that the inside should be non-reflective, for the same reasons as the baffle.

It is likely that the IH will include several heat sources because of, among others, electronics and detectors. Non of these are determined yet and therefore the interior of the IH is set to inactive. This because all heat that is expected to come in, will not come out anymore. The housing material and its thickness, nor the internal heat source are considered to be part of this project. The grid of the instrument housing has been chosen such for it to feature more or less equal nodes in size throughout the structure.

Initial Primary Mirror Support Structure Geometry

The PMSS is a complex structure which was difficult to mimic since it contains lots of angles and cutouts. Besides, each structure consists of a hinge, a kinematic interface, a support structure and the primary mirror actuators. For the initial thermal model it has been tried to mimic the actual hinge, kinematic interface and the support structure as close as possible, as shown in Figure 6.5. The primary mirror actuators have been excluded. This is because the actuators were not designed at the time. Further analysis should determine how this system will effect the thermal solution. The grid of the PMSS is set coarse compared to most of the other groups. Since the PMSS is composed of many small components it was not necessary to apply a finer grid.

6.3 Thermal Environment, Orbital Parameters & Analysis Case

The thermal environment will be decisive for sizing the mission thermally. Besides, the formulated top level system requirement SYS-REQ-05 describes that the spacecraft shall be sized for the mission scenario which is most demanding. A spacecraft orbiting Earth is considered to be thermally effected by direct solar flux, albedo flux, Earth-emitted flux and internal dissipation. The internal dissipation is generated by the spacecraft systems themselves and are generally a function of the spacecraft modes. Since non of the internal systems are defined yet, these will not considered for this project. Further, the thermal environment of the satellite will be a function of the orientation of the Earth with the Sun. In order to determine the required thermal conditions one needs to explore the aforementioned thermal inputs and orientations.

6.3.1 Solar Constant

The solar constant, as experienced by an Earth orbiting spacecraft, is known to vary by the 11-year solar cycle and by the mean distance difference between the Earth and the Sun. This because of the elliptical orbit of the Earth around the Sun [19]. Therefore, two extreme cases can be defined, hot and cold, for which the value of the solar constant can change as depicted in Table 6.6. These fluxes must be converted into temperatures for it to be compatible with ESATAN TMS, which requires equation (6.1):

Table 6.6: Solar constants for hot-, median- and cold case conditions.

	Abbreviation	S_c [W/m^2]	T_S [K]	**Reference**
Hot Case	S_{Hot}	1414	5826	[34]
Median Case	S_{Median}	1367	5778	ESATAN TMS
Cold Case	S_{Cold}	1322	5729	[34]

$$T_S = \left(\frac{S_c \cdot d_{S-E}^2}{R_S^2 \cdot \sigma} \right)^{1/4} \tag{6.1}$$

With T_S being the temperature of the Sun, S_c the solar constant, d_{S-E} the mean distance between the Earth and the Sun, R_S the radius of the Sun and σ the Stefan Boltzmann constant ($5.67{\cdot}10^{-8}$W/m^2/K^4). The mean distance is normalised to one Astronomical Unit (AU) for the aforementioned solar fluxes. The fixed parameters are depicted and elaborated in Appendix D *Thermal Modelling Conditions*.

The maximum-, nominal- and minimum temperatures of the Sun can therefore be considered as a direct function of the solar flux, for which the respective Sun temperatures are depicted in the second last column of Table 6.6. An additional margin of 5 W/m^2 could have been added to the solar constant to account for measurement uncertainties and solar cycle variations, as suggested in [34]. Nevertheless, it is thought to be unnecessary since a margin will be taken on temperature as described in Chapter 3.

6.3.2 Planet Albedo & Temperature

Variations can be taken on the solar albedo factor as well as on the Outgoing Longwave Radiation (OLR) emitted by Earth. The latter source is a combination of radiation emitted by the Earth's surface, radiation by atmospheric gases and cloud tops, of which part is absorbed in the atmosphere [34]. OLR is modelled as planet temperature.

Theory

OLR is not constant over the globe and can be considered as a function of surface temperature and the amount of cloud cover. In general, the largest surface temperatures are found in tropical and desert regions, while the colder regions are found at higher latitudes [34]. Besides the variation in OLR, the albedo factor also varies depending on the surface reflection properties and the cloud cover. More light is reflected with increased cloud cover, just as more light is reflected by ice and snow. In general, continental areas have more albedo than oceanic areas since liquid water is not that reflective. A general trend can be deduced in which lower temperatures, cloud covers, ice and snow are present at higher latitude, which drive albedo. Another trend can be deduced for decreased cloud covers and higher surface temperature for lower latitudes, which drive OLR.

Therefore, it is recommended to apply several combinations of the solar albedo and OLR, as shown by the engineering extreme cases in [34]. Spacecraft components generally feature varying absorbing and emitting properties, thus the worst case scenario can differ per component. For the DST project this is thought to be an overkill of options. Therefore, the most extreme values will be combined and coupled into several sets of worst case scenarios, from which one hot and cold case will be selected accordingly. These worst case scenarios are not only a function of heat input, but also of the orientation of the included bodies.

Application

Earth's temperature can been calculated using equation (6.2) taken from [34], with the assumption that the emissivity equals one (assuming Earth to be a black body radiating with an uniform temperature). E_{IR} represents the Earths irradiance, T_E the Earths temperature and ϵ the local bolometric albedo.

The cases as described in [34] include several combinations of albedo and OLR, from which some of the high inclination cases have been adopted in this thesis. These cases are depicted in Table 6.7, for which the Earth temperature has been calculated using the aforementioned equation. The median case is taken from ESATAN TMS, which is taken here because it is the default setting of the Workbench. The cases as described in the Table consider certain conditions in which less albedo will results into more absorption, and thus a higher Earth temperature. These two parameters are not directly related which is the reason why the highest albedo does not necessarily relates to the lowest OLR.

$$T_E = \left(\frac{E_{IR}}{\sigma \cdot \epsilon} \right)^{1/4} \tag{6.2}$$

Table 6.7: Solar albedo and Earth infrared for hot-, median- and cold case for high inclination orbits.

Case Description	**Albedo** [-]	E_{IR} $[W/m^2]$	T_E [K]	**Reference**
Minimum Albedo	0.06	273.0	263.4	[34]
Minimum OLR	0.40	108.0	208.9	[34]
Maximum Albedo	0.5	180.0	237.4	[34]
Maximum OLR	0.22	332	276.6	[34]
Median	0.306	237.1	254.3	ESATAN TMS

Modelling

The initial thermal model will be useful for understanding the general temperature behaviour of the telescope. This model is simplified and therefore it is thought that it is not necessary to apply worst case conditions yet. For the initial modelling phase it is chosen to use the pre-set thermal conditions of ESATAN TMS, defined by the median conditions in Table 6.7.

6.3.3 Orbital Parameters

The DST is supposed to operate in a SSO. For a satellite to be in such an orbit one requires a certain set of orbital conditions such that it is basically synchronised with the movement of the Sun. In order to explain the required conditions one needs to introduce three sets of additional reference frames, after which the required orbital parameters can be determined.

Additional Reference Frames

The additional required reference frames are depicted in Figure 6.6. The Earth Centred Inertial (ECI) reference frame [γ,τ,N], similar to the aforementioned non-rotating geocentric equatorial reference frame, with γ being the vernal equinox ([19]) and N the axis of Earth's rotation. The Earth's orbit reference frame $[x_E, y_E, z_E]$, has it's $x_E - axis$ aligned with the Sun-Earth direction, with the $Z_E - axis$ representing the Earth's orbit normal, pointing towards the celestial pole. The ecliptic obliquity (i_E) is known to move slowly in time due to gravitational effects of the Sun, the moon and other planets, as described in [19]. However, this effect will not be considered within this project and i_E will therefore be fixed at 23.5° [35] in case necessary. The Earth's orbit reference frame is thus similar to the aforementioned non-rotating geocentric ecliptic reference frame, as introduced in the previous Chapter. The last reference frame, the spacecraft orbit reference frame [x,y,z], has it's x-axis aligned with the Earth-spacecraft direction and the z-axis is the orbit normal.

Sun Synchronous Conditions

"A SSO is defined as the orbit whose normal (z-axis) makes a constant angle with the Sun-Earth direction (x_E-axis)" [35]. Normal is defined as a line or vector that is taken perpendicular to the tangent plane, thus normal to the velocity plane in this case. If this normal line would be kept in line or close to the Sun-Earth direction, one would maintain certain orbital conditions due to which the satellite will not enter Earth's shadow for several months [19].

The angle ϕ as depicted in Figure 6.6b, can be considered to be a function of the true anomaly only since the orbit is circular [19]. As aforementioned in section 5.2.2.c, the true anomaly indicates the position of the spacecraft within its defined orbit. If the inclination (i) of the orbit would be fixed, one obtains a situation for which these SSO conditions would depend on the angle of right ascension of the ascending node (Ω) only.

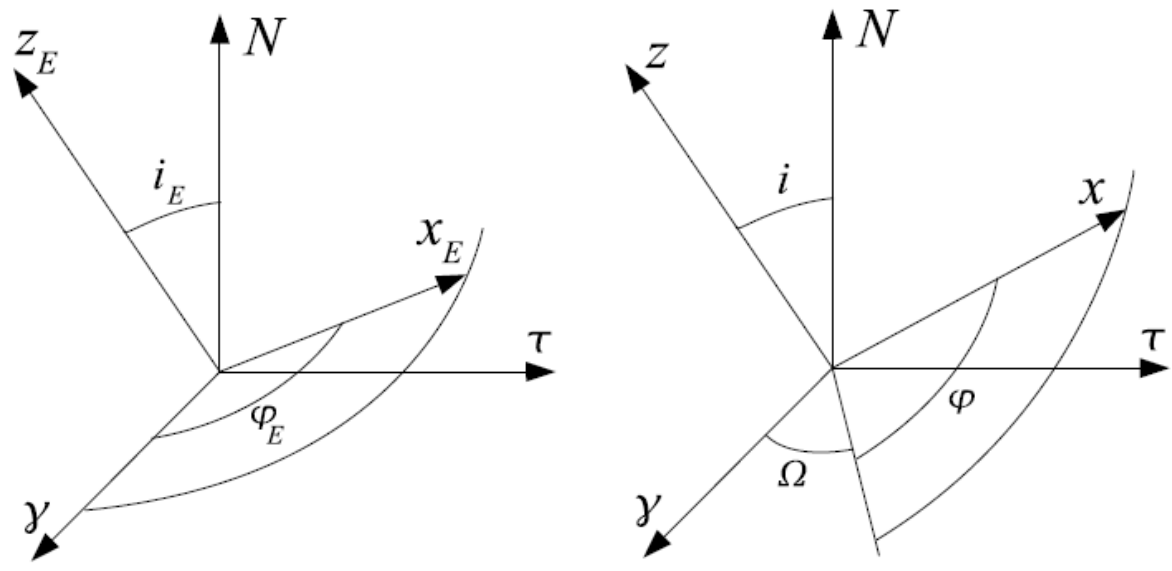

(a) (b)

Figure 6.6: Earth Centred Inertial reference frame [γ,τ,N], Earth orbit reference frame $[x_E, y_E, z_E]$ and Spacecraft orbit reference frame [x,y,z], taken from [35].

Orbital Inclination

The required sun-synchronous inclination (i_{Ss}) can be expressed as being a function of the orbital radius (r) and the mean equatorial radius of Earth (R). This results into Equation (6.3) taken from [19], with a = r due to circular orbit conditions.

$$cos(i_{Ss}) = -0.098916 \left(\frac{r}{R}\right)^{7/2} \tag{6.3}$$

The orbital radius has been determined in the work of [7] and set at 500km, with the mean equatorial radius of Earth being 6378.137km ([36]). Solving equation (6.3) for the provided parameters results into an inclination of 97.4°. For the satellite's normal to be kept in constant angle with the Sun-Earth direction (x_E), one requires the secular rate of change of Ω to be equal to the angular motion of the Sun when viewed from Earth [19]. These parameters will slowly drift in time due to which orbital manoeuvres will be required, although this is not considered relevant throughout this thesis. The considered bodies, apart from the satellite, are therefore considered fixed.

6.3.4 Sun Parameters

The initial thermal model will be useful for exploring the general thermal behaviour for a possible set of orbital conditions. The Sun parameters can be inserted manually into ESATAN TMS or set automatically based on a certain date and time. For the initial thermal model it is thought that it should at least feature the aforementioned eccentricity, orbital height and inclination. The right ascension of the ascending node should then be adjusted such that the normal line of the orbit is kept within a certain angle of the Earth-Sun line. This angle has not been defined before and can be chosen as desired.

The standard Sun/planet system conditions as per ESATAN TMS are depicted in Table 6.8. The planet radius, gravitational acceleration, the orbital precession and the sun radius, are not considered to change throughout this project. The Sun planet distance, the solar declination and the Sun's right ascension provide the position of the Sun with respect to Earth. In a previous section it has been shown that the Sun planet distance varies in time. The solar declination varies from -23.5 to +23.5 ° [19], determined by the ecliptic obliquity. The Sun's right ascension describes the location of the Sun within its defined orbit.

The standard conditions are representative of actual Sun/planet conditions and are thought to be sufficient for the initial model. For the initial model it is thought that it would be interesting to include eclipse too. The angle is therefore set at 15 degrees since it would fly mid-across Europe. Besides, the Sun would be able to impinge the interior of the baffle for certain true anomalies, which could show some interesting behaviour. The remainder of the parameters are chosen such for it to match the SSO conditions.

Table 6.8: Standard Sun/planet system conditions as per ESATAN TMS.

Parameter	Value	Units
Planet Radius	6371	km
Gravitational Acceleration	9.798	m/s^2
Sun Planet Distance	$1.508284754 \cdot 10^{11}$	m
Solar Declination	6.828	deg
Sun's Right Ascension	163.977	deg
Orbital Precession	0.0	deg/s
Sun Radius	$6.958 \cdot 10^{8}$	m

6.3.5 Orbit Visualisation

The aforementioned thermal-, orbital- and Sun/planet conditions are considered as the Nominal (NOM) Case Conditions and are summarised in Appendix D *Thermal Modelling Conditions*. ESATAN TMS provides a function for which the orbit around the Earth with respect to the Sun can be visualised. Sadly, it was found that the respective orientations were unclear and therefore efforts have been made to visualise this by hand. A simplified schematic of the orbit is shown in Figure 6.7, for view a side- and top view have been provided.

Side View

The dotted lines in Figure 6.7a depict the orbital path, while the arrows indicate the direction. The satellite is considered to be rotated such that its constantly pointed to the Earth's surface throughout each orbit. The scaling of the Figures is not correct, since the satellite is considered to be much smaller as well as the Sun is considered to be larger and further away. Nevertheless, the satellite will be in shadow at the depicted true anomaly.

Top View

The orbital path in Figure 6.7b includes some of the time samples which will become relevant in the subsequent analysis. The dotted lines originating from the Sun indicate which areas behind the Earth can be considered to be in shadow. Included with the respective time samples, it is likely that the time samples 1200 and 4400 are still sunlit, while the 800 and 4800 time samples are partly in shadow. Besides it is likely that the Sun will impinge the interior of the baffle at these sunlit samples, while halfway the orbit it will illuminate the back of the baffle mainly.

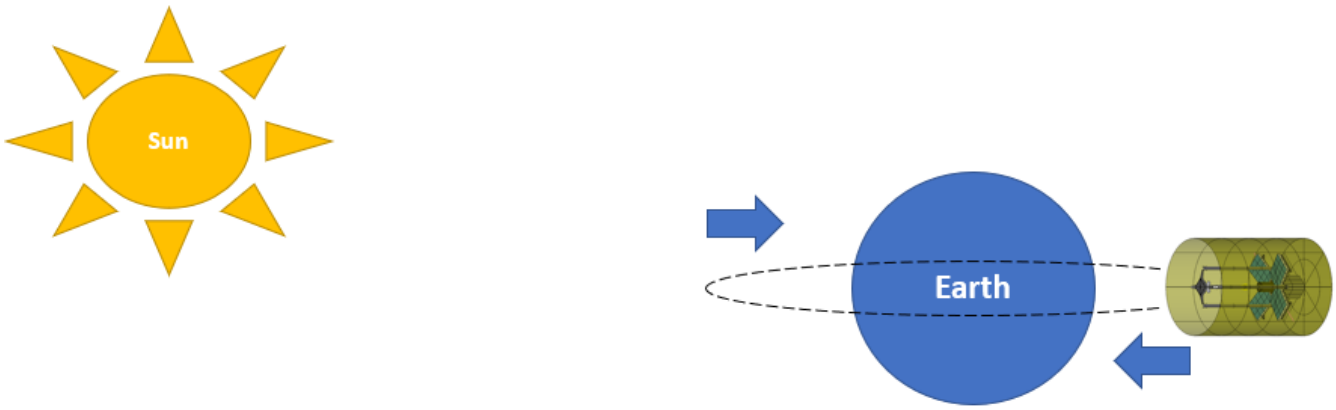

(a) Side view

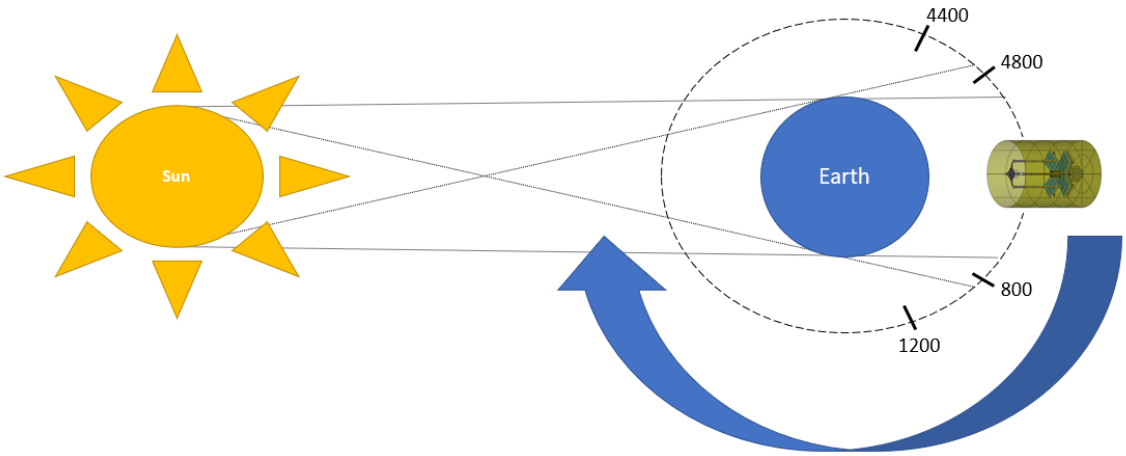

(b) Top view

Figure 6.7: Schematic representation of the nominal Sun/planet and orbital conditions.

6.3.6 Thermal Model Inertial Reference System & Satellite Pointing

The thermal model is considered to be defined within a certain inertial reference system. This system will be used as reference for assembling and pointing the model with respect to a celestial reference system.

6.3.6.a Thermal Model Inertial Reference System

The thermal model of the DST is defined with respect to the MCS, which considers three axis, the x-, y- and z-axis, with respective colours red, green and blue. The thermal model can be considered symmetrical in x and y, but but not in z. The MCS is visualised in Figure 6.8, where the thermal model geometry is set transparent such that the three axis system is clearly visible. This respective MCS is set as standard throughout this project and can be considered as being in line with the aforementioned geometric CATIA model.

Assembling the Model

The geometric thermal model has been defined with respect to the MCS, but should also be oriented with respect to the reference- and moving component frame, by means of assembling the model. ESATAN TMS includes a separate function for this in which one defines the general orientation, the reference- and moving

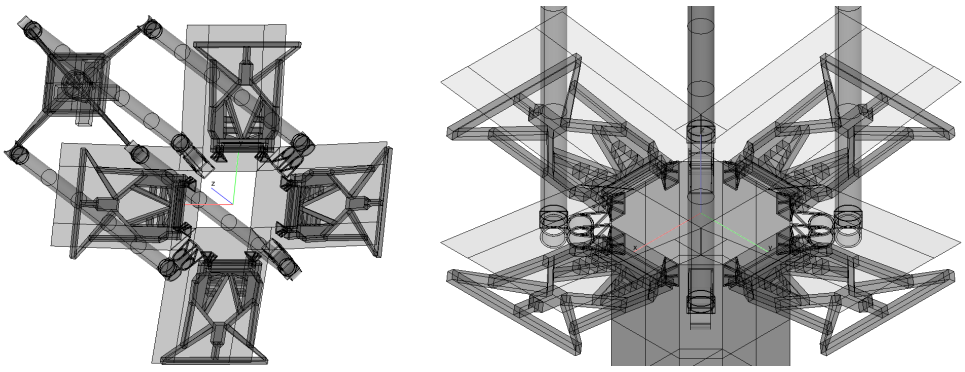

(a) (b)

Figure 6.8: Model Coordinate System visualisation as considered in ESATAN TMS Workbench, with the x- (red), y- (green) and z-axis (blue).

components. The definition of these are mandatory, even when the system is not considered to be moving. Besides, geometries cannot be selected fixed and moving, nor can their axis be taken similar. The orientation is set to True Sun, which will not be relevant for this thesis, although it can become relevant when certain components like the solar panels, are considered to be rotated towards the Sun.

The initial thermal model and all subsequent thermal models, consider the telescope components to be fixed which will be selected as reference, while the baffle is considered to be moving. This is not in line with the actual case, since the baffle is considered to be fixed too, but considering the constraints it is thought inevitable. The x-axis is taken as the rotation axis and the rotation angle is set to 10^{-6} degrees, so by definition the baffle is considered to rotate with a tiny angle, although the model should be assembled differently in the future in case the solar panels will be included. It cannot be set to zero since it will results into strange behaviour. The +z-axis is considered as the pointing vector, which is considered to be parallel to the optical axis.

Pointing the Model

The definition of the reference- and moving reference systems with respect to the MCS, will be used to orient the thermal model with respect to the ECI reference system. This is part of defining the radiative case by means of pointing the model. The pointing function in ESATAN TMS considers primary- and secondary pointing, for which the primary pointing function will consider the reference components, while the secondary considers the moving components. The telescope is considered to image Earth and therefore it should be pointed towards Earth. Nadir is considered as "a single point, or locus of points on the surface of the Earth directly below a sensor as it progresses along its line of flight" [37]. Nadir is therefore considered as the primary pointing direction, which considers the +z-axis of the thermal model MCS. The secondary pointing direction considers the rotating components, which is pointed in the Velocity direction, although the rotating angle is set to zero thus it is not considered to be relevant. The result is shown in Figure 6.9.

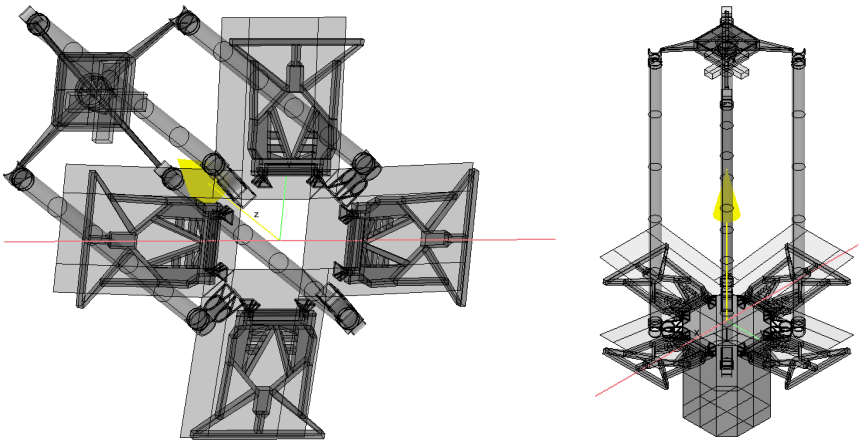

(a) (b)

Figure 6.9: Orientation of the geometric thermal model as considered in ESATAN TMS Workbench, with the yellow arrow being the primary pointing direction (Nadir) and the red line being the secondary pointing direction (Velocity).

6.3.7 Conductive Interfaces

The thermal model considers many small geometries which should be considered as one larger geometry, will others are considered bolted or epoxied to each other. ESATAN TMS includes an Auto Generate Conductive Interfaces in which it automatically determines the fused interfaces, for which it requires the geometries to be adjacent and of equal material. Since all geometries which were considered to be part of one larger geometry were defined such for them to satisfy these two conditions, most of the fused conductive interfaces could be defined automatically. The result of this is shown in Figure 6.10, with the yellow lines being representative of these interfaces.

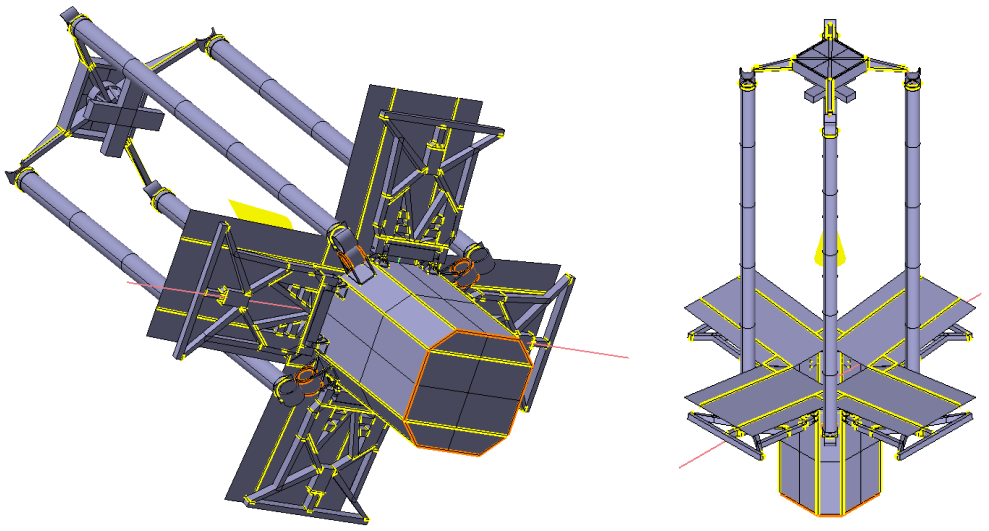

(a) (b)

Figure 6.10: Visualisation of the global telescope conductive interfaces as considered in ESATAN TMS Workbench, with yellow representative of fused interfaces and orange for contact interfaces.

The remainder of the conductive interfaces required manual definition for which a contact conductance had to be set, which are representative of the orange lines. These interfaces can be seen at, among others, the root hinges since the cams are not considered to be fused to each other, and the instrument housing which is assumed to be composed out of two pieces due to assembly reasons. All other components which are considered to be separate are also included with contact conductive interfaces, for which a more detailed representation for the spider and its neighbouring geometries is provided in Figure 6.11. From this Figure it can be seen that, among others, the cams of the top hinges, the top hinges and the spider, and the secondary mirror interfaces and the secondary mirror are considered to be in contact. At this moment it is unknown whether these contact interfaces should be set such for them to encourage or discourage heat flow.

It is therefore thought that the contact conductive interfaces should initially be defined such that it is clear which geometries are considered to be made of one piece, and what geometries are not. The contact interfaces themselves should be set such for them to negligibly interfere with the radiative contributions. The value of the contact conductance is therefore set at 1.0 W/m^2K and should be re-evaluated in a later stage of this project.

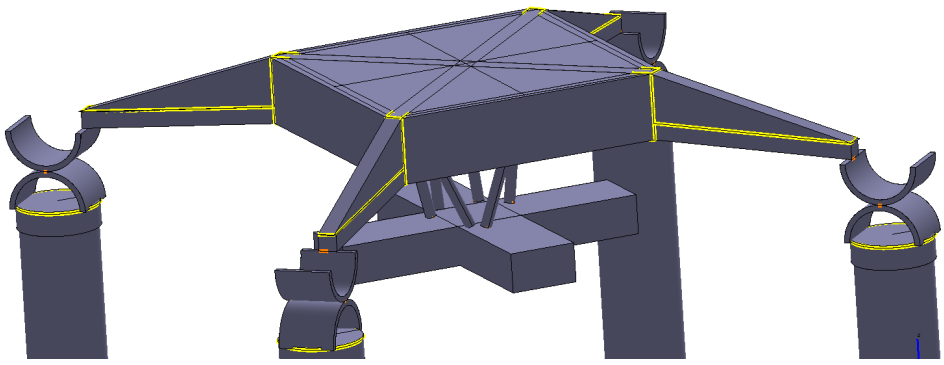

(a)

Figure 6.11: Visualisation of the spider conductive interfaces as considered in ESATAN TMS Workbench, with yellow representative of fused interfaces and orange for contact interfaces.

6.3.8 Analysis Case

After the geometric thermal model has been defined, its conductive interfaces and the radiative case has been run, one can set an analysis case. This analysis can consider one radiative case only, which is considered to be representative of one specific set of; thermal conditions, Sun-Earth and satellite orientation, one geometric thermal model, or one or several radiative cases. The latter option will become useful when considering orbital transfer, by means of a Hohmann transfer for example [18]. For this respective thesis one does not consider transfers, thus single radiative cases will be considered only. The user is required to define, among others, boundary conditions, initial conditions, solution control and output parameters.

Boundary- & Initial Conditions

The initial thermal model does not consider any boundary conditions, nor will the subsequent models in this thesis, since those are simply not defined yet and not considered to be part of this work. Initial conditions can be set in case one wants to define initial temperatures, which can be set from previous analysis. These conditions are not thought to be relevant here, but are thought to become useful when the thermal analysis has gained sufficient progress, or when a specific starting condition will be required.

Solution Control

The considered solution control considers a steady state- and transient solution. A steady state solution will not be required in case certain initial conditions will be chosen. The steady state solution parameters are set automatically by ESATAN TMS which contain the iteration control conditions and the system units. The iteration control conditions include, among others, the maximum number of iterations and the convergence criterion in Kelvin. The system units describe the values for the Stefan-Boltzmann constant and the temperature offset (273K). The latter property defines the offset of the temperature zero in degrees Celsius from the absolute zero temperature in Kelvin. The preset steady state solution is considered to be sufficient throughout this thesis.

Transient Solution
The transient solution requires the user to define, among others, solution start- and end time, and output interval. The start time is set at zero seconds while the solution end time is automatically set to one orbital period. The output interval or frequency specifies at what frequency the output calls will be calculated. The solution outputs are set automatically by ESATAN TMS and consider node- temperature, the four heat sources (Sun, Albedo, Earth and internal), and the conductors. This output set is considered to be sufficient for this project for now.

Steady State Solution
The steady state solution determines the average temperature solution which will be used as initial input. The transient analysis will follow from this average solution, and therefore it requires a certain amount of time for the model to converge around a certain mean average temperature. The total simulation time is therefore determinant for convergence, as well as the output frequency will be determining the temperature behaviour and solving time.

Output Parameters

The selected parameters as defined within the initial thermal model are depicted in Table 6.9. The remainder of the parameters have not been set or altered with respect to the standard ESATAN TMS settings, or have been aforementioned.

Solution End Time
The selected solution end time equals ten orbital periods, for which it was found that most components can be considered sufficiently converged since the mean difference between successive orbits is minimal.

Output Frequency
In Appendix E *Output Frequency* results are shown for the initial thermal model with nominal thermal conditions for two different output frequencies; 400- and 25 seconds. Both frequencies have similar global- and average temperature results, although its total solver time is quite different.

The solver time is about three minutes for the largest considered output frequency, which is considered comfortable to work with. The following solution visualisation procedures take about two minutes each. The smaller frequency does slow down the solver significantly (>10 times) especially when also including the subsequent visualisation of the results, which could take up to an hour.

Discussion
The majority of the analysis will be based on the global maximum-, minimum and average component temperatures. Besides, many simulations and solution graphs are expected to be generated. Therefore, it is thought that a short solver time is most valuable for the majority of this project. An output frequency of 400 seconds is thought to provide sufficient quality data, whole also featuring fast solver time. This output frequency will therefore be used for the remainder for this project, unless specified otherwise.

In case a local analysis or study detailed temperature behaviour is conducted, it is recommended to either define initial conditions such that the solution end time can be shortened or accept that the solver will require a considerable amount of time to solve.

Table 6.9: Selection of the analysis case parameters.

Parameter	Value	Unit
Analysis Case Type	Single Radiative Case	-
Solution End Time	56745.77	[s]
Output Interval	400	[s]
Maximum number of iterations	100	-
Convergence criterion	0.01	-
Initial time step	100	[s]

6.4 Initial MLI Outer Layer Temperature Investigation

As aforementioned, three different MLI outer layers have been considered with equal inner layers or insulation package. Before proceeding to the global temperature results or the updated model in the next Chapter, one should determine a suitable outer layer for the MLI blanket. The initial results of the three top layers are shown in Appendix F *Temperature Results of the MLI Outer Layers*, of which the maximum (T_{max}) and minimum (T_{min}) temperatures are summarised per layer in Table 6.10. Each of the top layers have been exposed to nominal thermal conditions as defined in Appendix D *Thermal Modelling Conditions*.

Table 6.10: Temperature results of the considered MLI outer layers, NOM conditions in degrees Celsius.

	Outer Layer		**Inner Layer**	
FEP/VDA	15	-135	120	-10
FEP/Silver	-15	-155	120	-10
VDA	250	-160	120	-5

Analysis

The three simulated outer layers feature equal inner layer or insulation layers, which is the reason for the inner layers to have similar temperature. The maximum temperature occurs when sunlight impinges the interior of the baffle just after- and before eclipse. The outer layer temperatures are different for each type of outer layer, of which VDA only is most different from the FEP configurations. The maximum temperature of VDA only is substantially higher compared to the FEP configurations. It is thought this is caused by the relatively thin VDA only layer, due to which it is sensitive to large temperature increments when illuminated by the Sun. The two FEP types are similar, while the average temperature is slightly higher for the FEP/VDA configuration.

The temperature of the insulation package needs to stay within -270 to +150°C, as defined by the operational temperature as was shown in Table 6.3. From the results as shown in Table 6.10, this can be considered the case for all outer layer configurations. It is unknown whether this also applies to the VDA only layer, but at least it can be concluded from the numbers that the difference between maximum and minimum is quite substantial ($\sim$ 410°C). The FEP/VDA layer is thinner compared to the FEP/Silver layer, hence it is likely that it will be lighter, also since aluminium has lower density compared to silver. The temperatures of the telescope components are similar for each configuration, although their numbers are not shown here.

Discussion

It is likely that the insulation layers (inner layer) will be most decisive for the telescope components, while the outer layer will be determinant for the experienced temperatures of this layer itself.
The FEP/VDA outer layer is thought most favourable. This because it is considered to be lighter when compared to the FEP/Silver configuration, while also featuring less severe temperature extremes compared to VDA only.

This choice can be re-evaluated in a later stage of the project, but for now the FEP/VDA configuration will be used for the initial- and subsequent models.

6.5 Initial Global Temperature Investigation

The outer layer configuration of the MLI blanket has been determined in the previous section. An initial global temperature investigation regarding the extremes and the behaviour throughout several subsequent orbits is thought to be useful. From this investigation one can determine the follow-up actions regarding improvements of the thermal model geometry or thermal optical surfaces. The results will be presented first (6.5.1), an analyses will follow after (6.5.2), followed by a discussion of this analysis (6.5.3).

6.5.1 Results

The global minimum-, maximum- and average temperatures are depicted in Table 6.11. It must be mentioned that these temperatures are representative for the groups and thus not necessarily for each component of that group, since some of the components can thus be more temperature stable than others. The global temperatures have been rounded to the nearest 2.5 degrees Celsius. This rounding will be maintained throughout this report, unless specified otherwise, such that results are more easily comparable. An asterisk has been added to the primary- and secondary mirrors since those seem to converge after 1,500,000 seconds. Their minimum and maximum temperatures have been taken for the entire interval up to 2,500,000 seconds, while their average temperatures have been taken after convergence. Some of the other components do also require convergence although to a lesser amount and therefore these are not considered yet.

The temperature graphs are shown for all groups in Figure 6.12. This allows for inspection of how the temperatures would change in time, but also when possible to allocate reasons for this. The temperature trend of the secondary mirror is similar to the primary mirror, which is the reason for the temperature graph not being shown here. The results are supplemented with the total heat flow charts from space and the telescope in general, as shown in Figure 6.13.

The Figures are detailed enough to study the general temperature trends, where one orbit equals 5675 seconds. The graphs start in eclipse at 0 seconds, up until 800 seconds. At 1200 seconds, the thermal model has entered the sunlit side up until 4800 seconds, after which it enters the eclipse again. This cycle repeats itself for subsequent orbits.

Table 6.11: Initial thermal model component temperatures, with NOM conditions in degrees Celsius.

	Global Min	**Average Min**	**Mean Average**	**Average ΔT**	**Average Max**	**Global Max**
Baffle	-135.0	-44.7	-28.2	32.2	-12.4	127.5
Spider	2.5	5.9	12.5	13.2	19.1	27.5
Top Hinges	2.5	5.6	11.5	11.7	17.3	25.0
M2*	7.5	14.6	14.8	0.4	15.0	12.5
Booms	5.0	4.9	12.9	11.9	16.8	20.0
Root Hinges	5.0	6.2	10.4	8.3	14.5	15.0
M1*	7.5	13.4	13.5	0.2	13.6	7.5
PMSS	2.5	6.2	10.3	8.1	14.3	32.5
IH	5.0	4.6	10.4	11.7	16.3	17.5

6.5.2 Analysis

The analysis will be split into three segments, each representative of a different visualisation source.

Global Temperature

From Table 6.11, it can be seen that the baffle experiences the largest temperature differences in global and average temperature. Further, it is can be considered coldest in mean average, with largest maximum- and minimum temperatures. The remainder of the telescope components have a mean average temperature of 10.3-14.8 ∘C, with considerably smaller temperature differences in global and average temperature.

The spider and the top hinges feature the largest maximum temperatures, apart from the primary mirror support structure, which can most likely be caused by its position with respect to the baffle opening. The spider, the top hinges, the booms and the instrument housing seem to feature the largest average ΔT. The

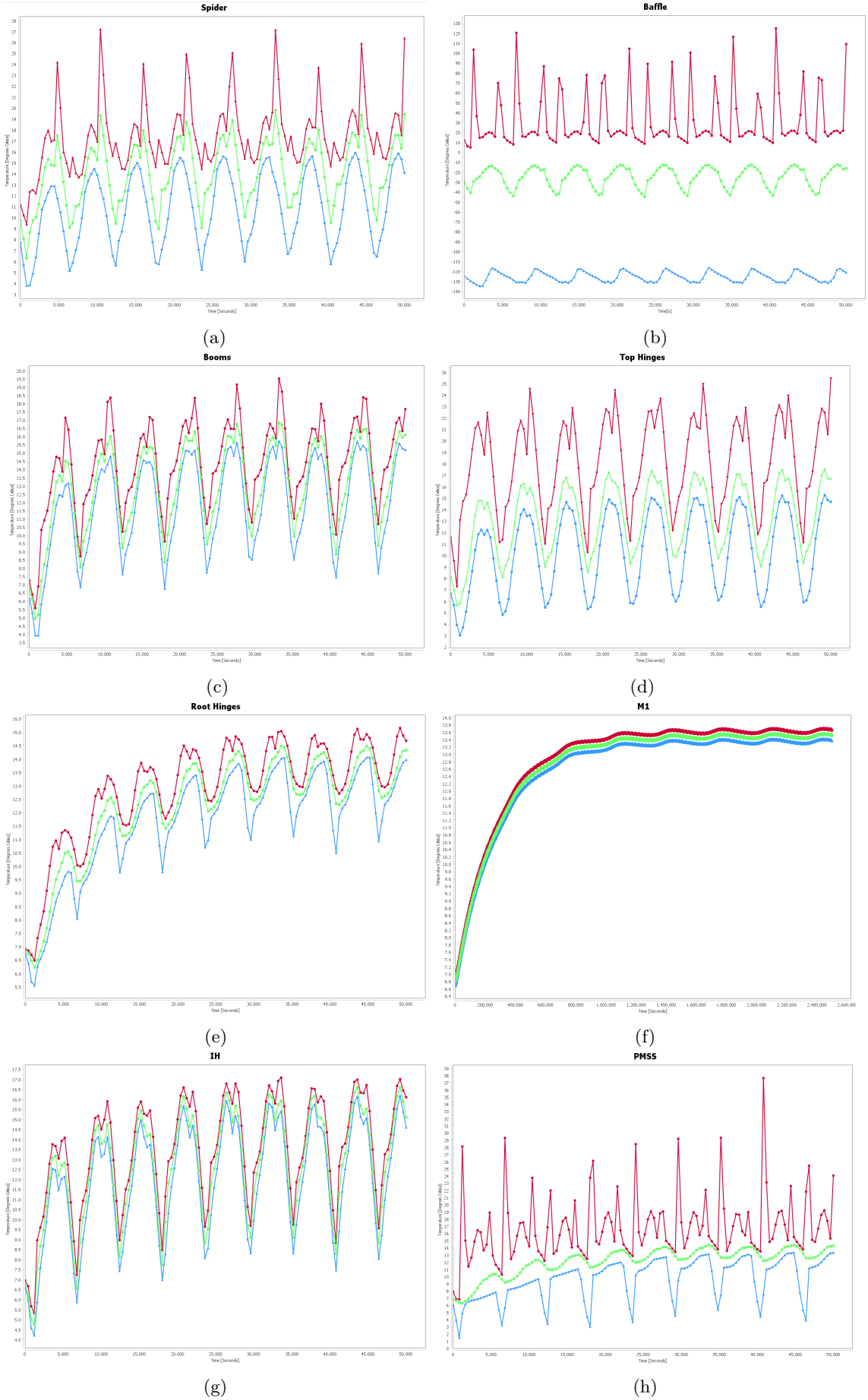

Figure 6.12: Maximum (red), average (green) and minimum (blue) temperature graphs for the spider (a), the baffle (b), the booms (c), the top hinges (d), the root hinges (e), M1 (f), the instrument housing (g), and the PMSS (h). Results visualised using the attribute function in ESATAN TMS.

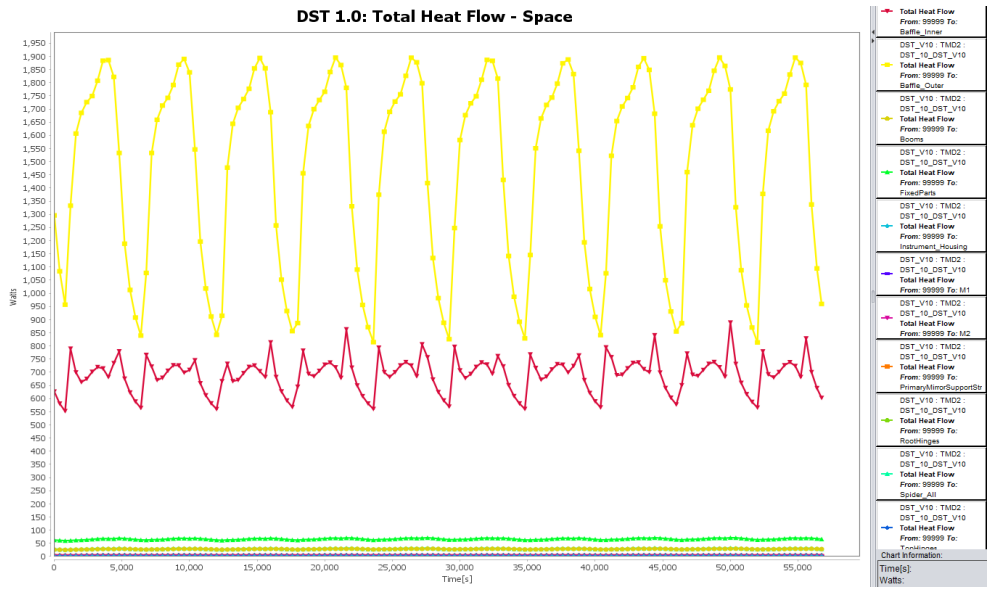

(a) Space to Spacecraft Geometries

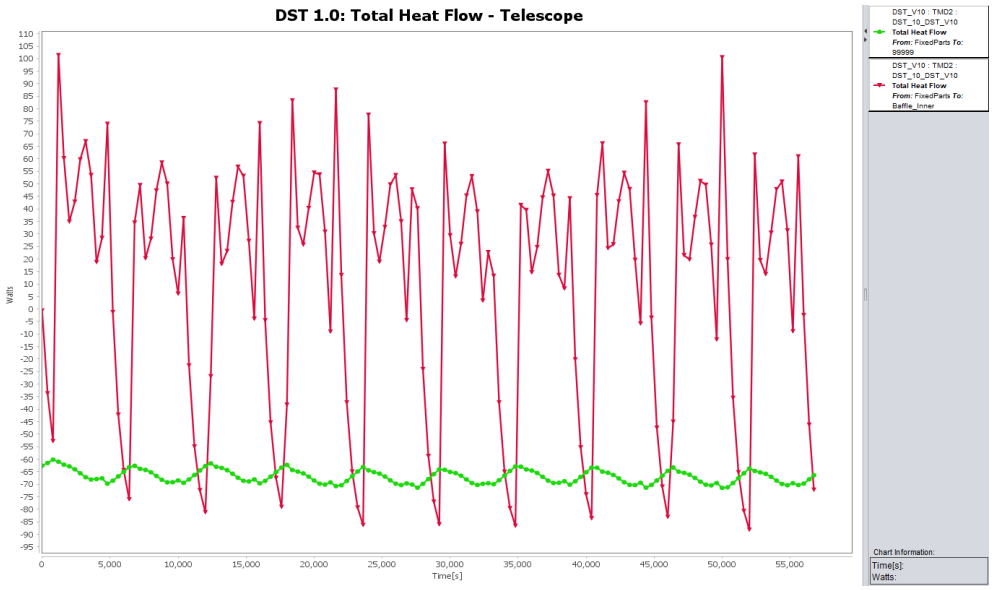

(b) Telescope to Baffle and Space

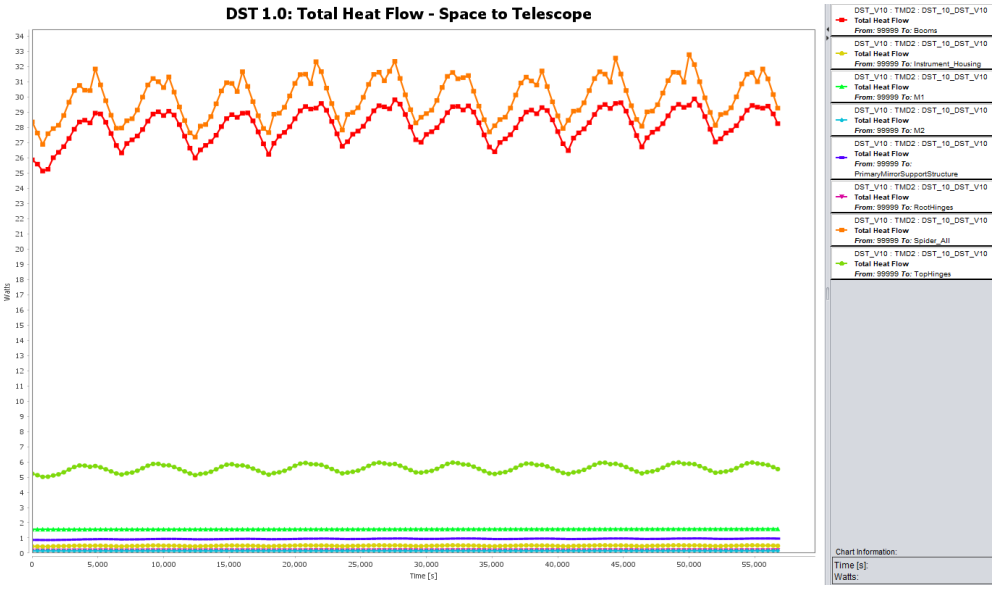

(c) Space to Telescope

Figure 6.13: Total heat flow results for space (a,c) and the telescope (b), for NOM conditions. As visualised using the heat chart function in ESATAN TMS Workbench.

primary- and secondary mirror feature highly reflective coatings thus in theory it does not absorb much heat, which is thought to be the reason for their relatively low average ΔT. The primary mirror support structure has the largest global maximum telescope temperature, although considering the average temperature this can be considered a small volume only.

Temperature Behaviour

The temperature behaviour graphs are shown in 6.12. From these graphs it can be seen that all component groups, apart from the baffle, require a certain amount of orbits for mean convergence. These groups, apart from the primary mirror, can generally be considered mean converged after five orbits. This will become relevant in Chapter 10 for calculating deformations. As aforementioned, the mirrors take even longer to converge.

Most of the components, like the spider, baffle, booms, top hinges and the primary mirror support structure are prone to so called temperature spikes. These events seems to happen just after- and before eclipse. Back in Figure 6.7b it was already shown that the Sun was mostly likely able to impinge the telescope directly at these events. The initial temperature behaviour results show that the suffered spacecraft temperatures are largest during these events, while the temperatures are indeed lowest at end of eclipse.

Total Heat Flow Results

The total heat flow results are shown in Figure 6.13. These heat flow results are representative of radiative heat flow results. From Figure 6.13a it can be seen that majority of the heat flows towards the baffle exterior. The second most amount of heat flows towards the baffle interior, with largest amounts during the aforementioned after- and before eclipse events. The heat flow towards the telescope is much smaller, which could explain the smaller temperature differences.

Figure 6.13b depicts the total heat flow from the telescope (FixedParts) towards the baffle and space. The outer baffle has not been included since there is no heat flow from its exterior towards the telescope, as it should be. It can be seen that there is a constant contribution from space, while the contribution of the baffle is rather fluctuating. The latter seems to be a function of the respective attitude during which it either drains or supplies heat from and to the telescope respectively.

Figure 6.13c is similar to the first shown heat flow chart with the difference that it is excluded from the baffle, such that it can be shown what telescope components receive the largest amount of heat from space. It can be seen that the spider, booms and the top hinges receive most heat in that respective order. This is not necessarily directly related to their respective temperatures since this is also a function of their thermal resistance. Where the thermal resistance determines how much heat will be required to increase temperature of a certain volume.

6.5.3 Discussion

The foreseen temperature results have shown that the baffle seems to be effective in shielding the telescope from the space environment. This because the telescope components feature relative low ΔT, while their average temperatures are within 4.5 °C from each other. The spider, the booms and the top hinges are most effected by space directly.

The telescope itself is significantly effected by the baffle interior since it either drains or supplies heat from and to the telescope. The latter seems to be a function of the satellite attitude with respect to the Sun. This because the baffle supplies heat energy when directly sunlit by the Sun, while it drains heat energy outside these two events. Further research should determine whether this effect should be mitigated or not.

6.6 Initial Temperature Distribution

The global temperatures and their averages, have been investigated in the previous section. In this section it will be visualised how these maxima and minima are distributed along the component groups and the components themselves. The results will be presented first (6.6.1), after which these results are analysed (6.6.2), followed by a discussion of this analysis (6.6.3).

6.6.1 Results

ESATAN TMS allows the user to visualise temperatures onto the structure by means of a colour distribution. The previous section had shown that the extreme temperatures were found around time sample 1200- and 4800 seconds for the first orbit, which correspond to the event of just after- and before eclipse. It is therefore thought

that these two events should be studied in detail, including an intermediate time sample taken at 3200 seconds. The results are shown in Figure 6.14. These time samples are taken because they are most easy to relate to the foreseen orbital visualisation as shown in Figure 6.7b.

It should be mentioned that the colour scaling is different for each time step, since the maximum- and minimum temperatures of the respective time step are different. The shown Figures lay emphasis on the baffle (d up to h) and the rest of the telescope (a up to c).

6.6.2 Analysis

The analysis will be split into three parts considering the three different views.

Telescope Temperature Distribution

Figure 6.14a, 6.14b and 6.14c are representative of the telescope for three different time samples; 1200, 3200 and 4800 seconds respectively. Figure 6.14a relates to the sample just after eclipse from which it can be seen that the temperatures between the depicted components are quite similar. This can be more or less be verified by the temperature graphs as was shown in Figure 6.12, since the difference between the min-, max- and average temperatures are relatively small.

The opposite is true at or around time sample 4800 seconds, since a so called temperature spikes has occurred for the spider (Figure 6.12a), top hinges (Figure 6.12d) and the booms (Figure 6.12c). The same effect is seen in Figure 6.14c where these components have a darker orange colour. The entire telescope increases in temperature when sunlit, for which the components closest to the opening of the baffle have highest temperature. This effect is verified in Figure 6.14b.

Spacecraft Temperature Distribution

Figures 6.14d, 6.14e and 6.14f are representative of the telescope including baffle, for three different time samples; 1200, 3200 and 4800 seconds respectively. From these Figures it can be seen the temperatures of the baffle interior and the telescope are quite similar, while those of the baffle exterior are not.

Baffle Interior Temperature Distribution

Figures 6.14g and 6.14h are targeting the baffle interior including some of the top section components of the telescope, for two different time samples; 1200 and 4800 seconds respectively. From these Figures it can be seen that the baffle interior heats up significantly with respect to the telescope. For the 4800 seconds time sample, the top section of the telescope is heated too. From the heat flow charts, especially Figure 6.13b, it is known that a certain amount of this heat is rejected towards the telescope.

6.6.3 Discussion

The foreseen temperature distribution Figures have showed that the top section components of the telescope are generally hotter compared to the remainder of the telescope. The latter geometries have common temperatures which is thought to be caused by the shielding effect of the baffle. The baffle seems to be less effective in shielding the top section components in certain attitudes for which the Sun can impinge the interior of the baffle and/or these components directly. Assuming that the components need to be around the same temperature for them to align properly, it is thought to be an undesired effect. The baffle interior itself seems to be in close interaction with the telescope, which is thought to be caused by its high emissivity properties. Therefore, when its absorbs heat energy from the Sun for certain attitudes, it will radiate a considerable amount towards the telescope.

This effect could potentially be mitigated by either adjusting the emissivity properties- and/or changing the dimensions of the baffle. Apart from that, it can be said that the baffle should not be rotated towards the Sun as has been the case for these critical events. If the telescope would feature a different angle of right ascension it could be that the aforementioned critical events are less severe. Therefore, the solution can either be sought in attitude prevention or structural improvements.

6.7 Chapter Summary

The majority of the telescope components have remained uncoated since their desired optical properties are yet unknown. The protected silver mirror coating is chosen for the intended operational wavelengths in combination with highest reflectivity properties. The multi-layered insulation properties for the baffle had not been

determined yet, for which several insulation- and outer layers have been explored. A relatively thin insulation package has been chosen for it to safe mass. The exterior layer seems to have small effect on the telescope, although the FEP/VDA outer layer was chosen on basis of its smaller ΔT. The interior of the baffle will be coated with a magic Black coating, for it to reduce stray light.

Each component of the thermal model has been elaborated, for which differences with the actual geometrical model or design have been mentioned. The baffle is not included with a baffle structure and the primary mirror segments are modelled as flat surfaces without curvature. Further, the PMAO and the field stop are not included. The reason for this was to simplify the model, or because components were not designed in detail yet.

The initial thermal environment exploration describes values for the solar constant, planet- albedo and temperature. These parameters are known to vary in time and therefore the minimum-, median- and maximum cases have been determined. The minimum and maximum cases will determine the worst case scenario. Since the initial thermal model is not fully representative of the deployable space telescope it is chosen to apply the median case.

The satellite is supposed to operate in Sun-synchronous conditions, which requires the satellite to be more or less synchronised with the movement of the Sun. The required inclination was determined to be 97.4°. The right ascension of the ascending node is set at 15° such that it passes over the Belgium, Netherlands & Luxembourg (BENELUX). Further, it will include eclipse.
Several Earth centred reference frames have been explored for it to describe the motions of the Sun and the satellite with respect to Earth. The Sun parameters for the initial model have not been altered, since the standard settings of ESATAN TMS were found sufficient. This set of thermal-, orbital- and Sun-planet conditions are referred to as the nominal case conditions.

The initial geometric thermal model is defined with respect to the MCS and it has been described how this model is oriented with respect to ECI reference frame. The telescope itself is considered to be pointed towards the Earth's surface or Nadir direction.
The thermal model has been included with conductive interfaces. Fused geometries are considered to be part one larger geometry, while other neighbouring geometries can be considered to be in contact. Those contact interfaces are set to 1 W/m^2K, such that it is clear that those interfaces are present. It is given a negligible value such that the considered heat flows will consist of radiative heat mainly.
The analysis case defines how the radiative case will be used to generate thermal outputs or results. The solver will be run for the duration of ten orbital periods with a sampling rate of 400 seconds. This is found to be sufficient for identifying the maximum- and minimum temperatures and global temperature behaviour, with descent solver time.

The initial temperature results showed that the baffle can be considered effective in shielding the telescope from the telescope environment. The baffle is less effective for certain attitude for which sunlight can impinge the baffle interior and some of the top section telescope components. Part of the absorbed heat by the baffle is radiated to the telescope. Further research should determine how this effects performance and whether it should be mitigated or not.
Potential improvements can be found for changing the right ascension such that the satellite will not face eclipse, or choose the right ascension of the ascending node such that it will not be pointed towards the Sun. Besides, one could alter the emissivity properties of the baffle interior or the baffle dimensions.

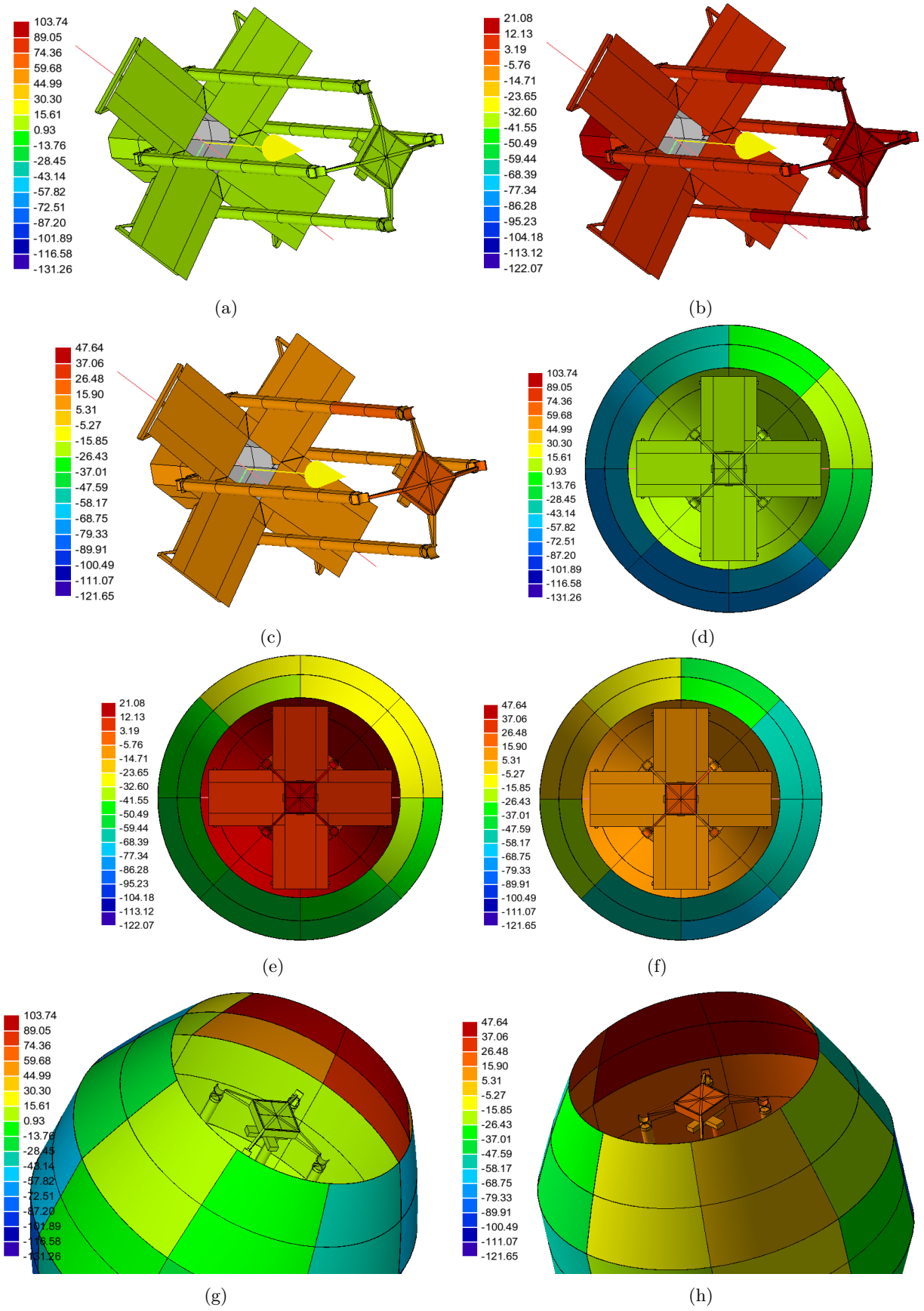

Figure 6.14: Temperature visualisation at the geometry at time step 1200- (a, d & g), 3200- (b & e) and 4800 seconds (c, f & h), produced within the ESATAN TMS Workbench. Sub figures a, b & c are visualisations with hidden baffle. Results presented using the visualisation function in ESATAN TMS.

7 Thermal Model Updates

The initial thermal model has been exposed to nominal conditions and its thermal behaviour has been explored. From the thermal results it became clear that the baffle suffers the largest temperature increments, which is not unexpected since it is used to protect the telescope from the space environment. This initial thermal model has been simplified for it to give an initial impression, which is considered part of the deliverables of this project. Now that these results are generated, one can focus on adding more detail to this initial model in terms of model updates. This is done with the addition of new geometries which were not included before, by adjusting existing geometries which required more detail or simply due to geometry updates by respective system designers.

The initial thermal model (DST 1.0) will be included with: the baffle structure geometry (7.1), the field stop geometry (7.2), a primary mirror segment update (7.3), the primary mirror active optics geometry (7.4), and an updated baffle design (7.5). Some of these additions will be excluded from the thermal model, after which the fully representative DST thermal model will be presented (7.6).

7.1 Initial Baffle Structure Geometry

The baffle structure is composed of eight booms with a torus on top, which has not been modelled before, but will be modelled in this section. This structure is composed of an aluminium and Kapton covered with MLI. The previous thermal models featured the MLI blanket only because of simplicity reasons. Nevertheless, the shape of the MLI blanket had been modelled such for it to represent the actual shape of the baffle structure, and therefore it can be used as guideline for creating the baffle structure.

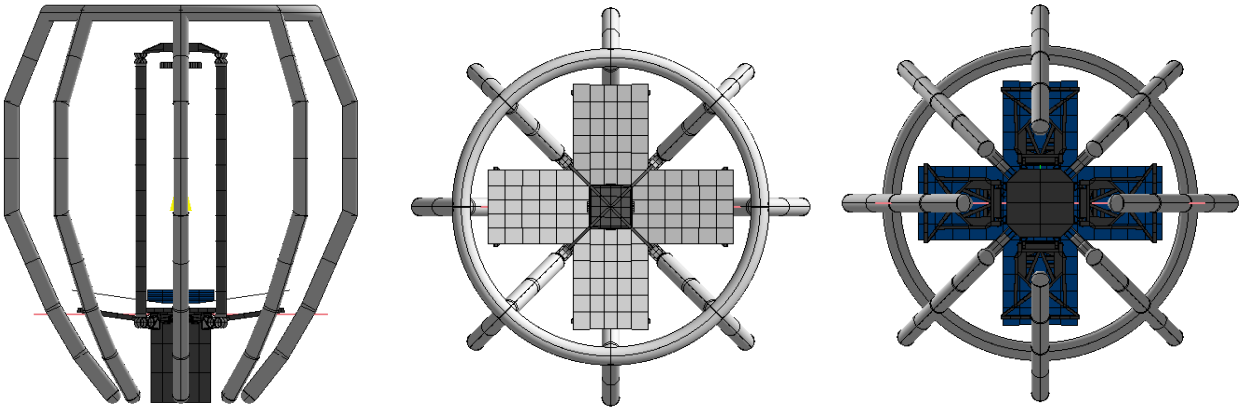

(a) (b) (c)

Figure 7.1: The baffle structure, DST 2.1. As constructed within the Workbench of ESATAN TMS.

Dimensions

The structure of the baffle has been formed using the baffle shell of the initial model as guideline or reference, of which the results are shown in Figure 7.1. The dimensions of the baffle structure and its materials are in line with those of the geometrical model created by E. Korhonen.

Materials

The structure is composed of shell material featuring a Kapton layer (25 μm) covered within Aluminium (25 μm on both sides), with a diameter of 100mm. The total thickness, with adhesive included, will be about 100 μm. Since Kapton has relatively low conductivity (0.12 W/m·K [38]), an purely aluminium boom thickness of 25 μm will be assumed. The choice of the aluminium alloy has been determined by E. Korhonen, chosen to be aluminium 1100-O, of which the relevant thermal optical properties are summarised in Appendix C *Thermal & Thermo-Optical Material Properties*.

Thermo-optical Coatings

The baffle structure will be coated with the magic black coating and the interior of the shell is made conductively active only. The latter is chosen since the interior is not supposed to radiate heat since the excluded Kapton layer would prevent that from happening. The structure is coated black for it to reduce stray light.

7.2 Field Stop Geometry

The instrument housing is at the moment still open on top while actually it should be closed apart from the field stop. For which the latter is used as entrance slit, through which the light can enter the housing. A preliminary design has been rendered in the work of [7], but it is quite to obtain the measurements from it. The field stop will be representative of the intermediate image and will be located off-axis. The exact location of the field stop can be calculated by means of ray tracing but it is thought to be irrelevant here since it is expected to have small effect on the total thermal performance.

Field Stop Housing

From the render as provided on page 85 in [7], it has been estimated that the length of the undetermined part of the instrument housing, referred to as the field stop geometry in the thermal model, should have a length of around 3/5th of the current instrument housing geometry. The length of this geometry has been obtained from the CATIA model and is set at 60 cm, thus the undetermined part has been given a length of 36 cm. The field stop is known as the opening through which the light can enter the instrument housing, but in this work it will be mainly referred to as the geometry for creating this opening.

Field Stop Dimensions

The size of the field stop itself is set at 2 by 15cm in consultation with the system designers. Its long side is taken parallel to the X-axis, which is chosen randomly. The aforementioned render shows that the instrument housing extension, referred to as the part which extends along the telescope axis, is not perfectly cylindrical. Nevertheless, for simplicity reasons it will be modelled cylindrical. The extension will be closed on top, apart from the field stop. The result is shown in Figure 7.2.

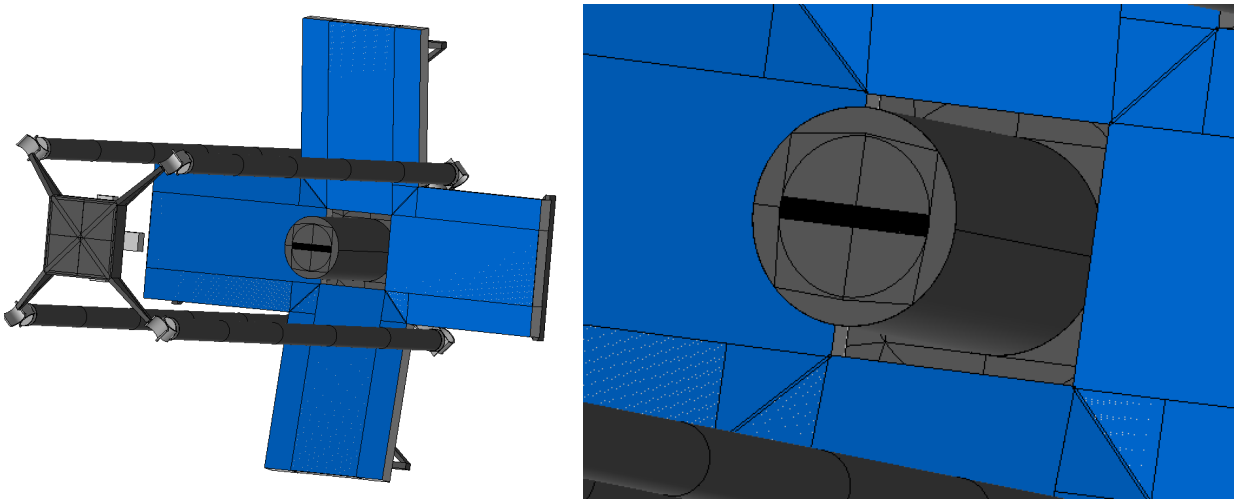

(a) (b)

Figure 7.2: Visualisation of the instrument housing extension which includes the field stop, DST 2.2. As constructed within the Workbench of ESATAN TMS.

7.3 Primary Mirror Segment Update

The primary mirrors were modelled as shells before, as shown in Figure 7.3. This because a shell can be given two different optical surface properties, while this is not possible for solids. The secondary mirror has been modelled as a solid instantly because it imposed no additional difficulties at that time. For the M1 segments this was different since they are concave and put under an angle, which resulted into the segments to overlap each other when modelled as straight solid rectangles. Therefore, the simple approach was taken and shells were chosen initially. Since it is unknown how this effects the actual solution, it has been decided to transform

the M1 geometries into solids.

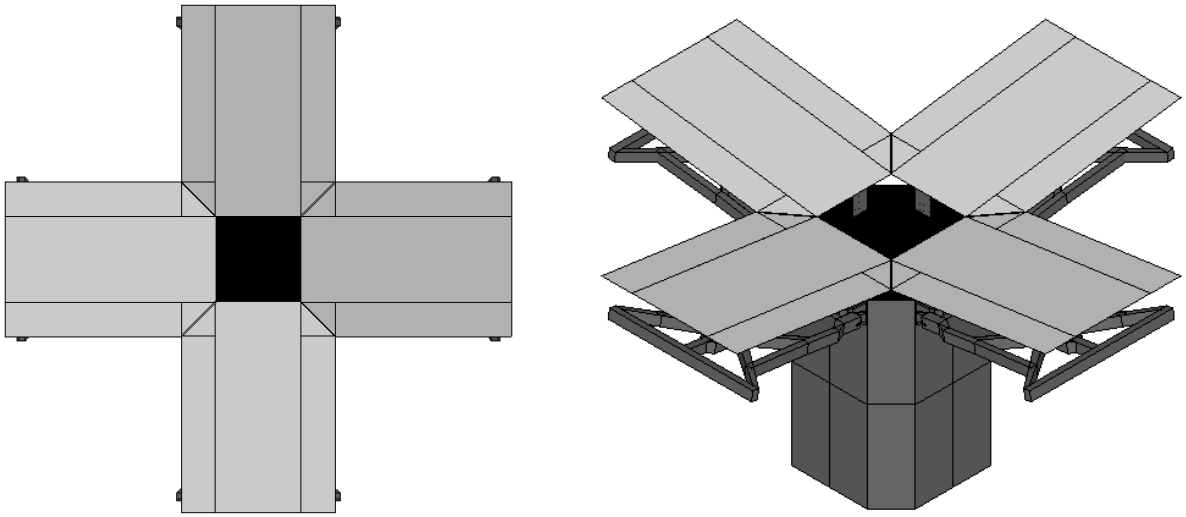

(a) (b)

Figure 7.3: Visualisation of the primary mirror segments as modelled in the initial model, DST 1.0. As constructed within the Workbench of ESATAN TMS.

Main Geometry Adjustments

Straight inclined M1 segments are expected to overlap each other, while in reality those should stay apart by about 5mm. Therefore, the size of the segments had be adjusted a bit for them not to intersect. The length of the segments have therefore been shortened with 2.5mm at the root, while its position with respect to the centre remained unchanged. The triangular cut offs have been enlarged such for it to create sufficient clearance between the segments. The current clearance between the segments is a bit larger than in the CATIA model, but was thought necessary for it to prevent unnecessary temperature spikes.
Besides, each segment is composed of two main solid geometries, while it was composed of five geometries before. This proved to be necessary for it to decrease disturbances, just as sufficient clearance between the segments and some further grid refinement was found required. The adjusted primary mirror segments geometry are shown in Figure 7.4.

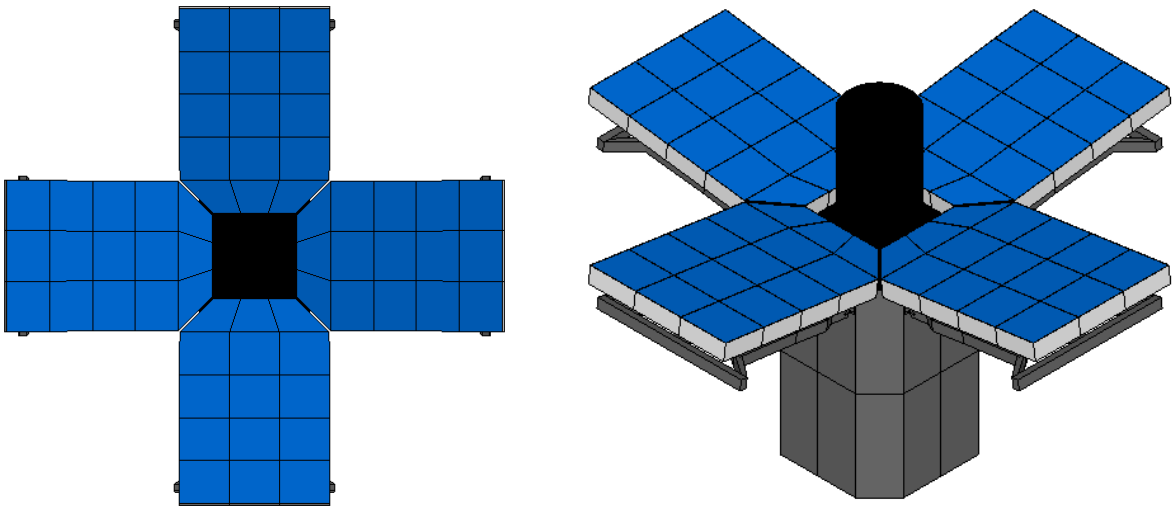

(a) (b)

Figure 7.4: Visualisation of the primary mirror segments as modelled in the updated model, DST 2.3. As constructed within the Workbench of ESATAN TMS.

Mirror Coating Application

The mirror surfaces have been adjusted to solid geometries, indicated in white, included with a separate solid coating on top, indicated in blue. The coating itself is composed of several layers as suggested in [23] for which the actual thicknesses are not provided. Therefore, an assumption needs to be made regarding these thickness and the material properties. The coating will be most important for its thermo-optical properties while its thermal properties are less significant. Therefore, it is chosen to select the material properties of the mirror itself (BOOSTEC SiC), with a thickness of 1 mm. The latter is chosen such for it to be clearly distinguishable in the thermal model, apart from given it another colour. The coating is made solid because solids can be fused to solids and not to shells. This way the coating could be considered part of M1 with different optical properties, as intended in the first place. Another difference is found for the field stop which was not included in Figure 7.3.

7.4 Primary Mirror Active Optics Geometry

The PMOA system will be responsible for the fine actuation of the primary mirror segments. It has not been mentioned in Chapter 4 but will elaborated on in this section. The final design characteristics are presented in the work of S. Pepper in [13] and will be used as main reference. The system will be described first for it to gain an impression of the system (7.4.1). The system geometry parameters will be defined (7.4.2), supplemented with the conductive interfaces (7.4.3), after which results can be generated, followed by a requirement compliance analysis (7.4.4). A final discussion will elaborate on the obtained results (7.4.5).

7.4.1 System Description

The PMAO will be positioned underneath each M1 segment, on top of the support structure of the primary mirror. The PMAO consists of, among others, a fixed structure, a moving frame, actuators, joints, flexures and struts. The final design parameters and its physical representation are shown on page 145 and 146 respectively, in the work of [13]. The detailed design comprises all moving components while its fixed geometry has not been designed in detail yet. For clarity, a 2D schematic of the PMAO has been made shown in Figure 7.5. It must be mentioned that this schematic is made to visualise the conductive connections, for it to be modelled properly in the thermal model, and is not directly representative of the actual design.

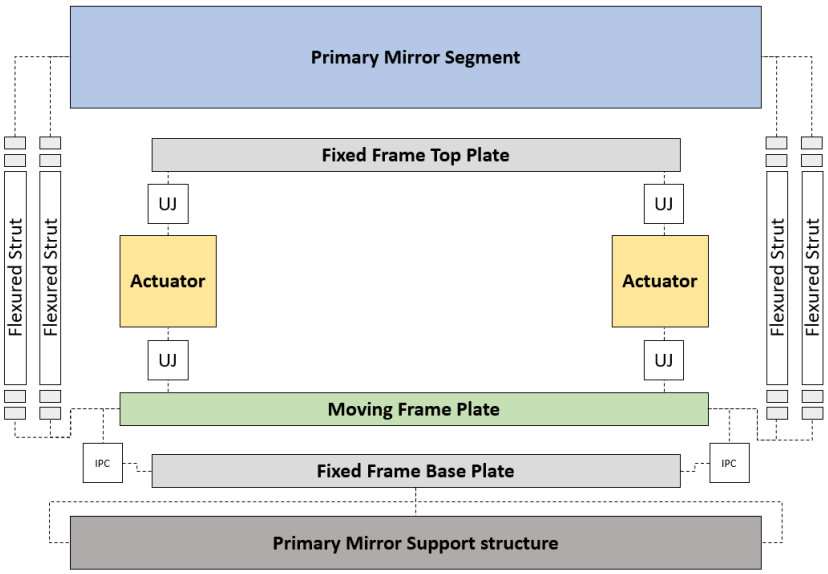

Figure 7.5: 2D Schematic of the Primary Mirror Active Optics.

Figure 7.5 is composed of boxes, representative of the mechanism components, and dotted lines, representative of conductive interfaces. The coloured boxes shall be defined in the thermal model as separate geometries, of which the M1 segments and the PMSS are already present, while the remainder of the boxes shall be defined in terms of their conductive couplings. The fixed top plate is fictional but necessary for the actuators to be connected to the fixed frame. The top- and base plate of the fixed frame shall be connected at some point, since the fixed frame is considered as one frame. The two plates cannot be connected externally since this would interfere with the Bipods, but can for example be connected by means of an internal central cylinder. The latter would also require the moving frame to become ring shaped instead of a disk, as explained by S. Pepper

in person. Thus for now, only the top plate will be included.

The moving frame plate is connected to the M1 segment by means of three Bipods, consisting of two flexured struts each. The actuators are connected to the top plate of the fixed frame and the moving frame plate, by means of flexured Universal Joints (UJ). The fixed frame base plate constraints the moving frame plate by means of in plane constraint (IPC) monolithic wire flexures. The fixed frame base plate is expected to be bolted onto the PMSS for which certain conductive properties shall be estimated, while the top plate of the fixed frame is expected to remain free from the M1 segment.

7.4.2 System Parameters

The PMAO geometry parameters as will be used for the thermal model are depicted in Table 7.1. The moving plate is considered to be separated from the fixed base plate by 2mm, while the total height of the fixed frame is set 52mm, thickness of the top plate not included, since the cylindrical height of 104mm as imposed by the PMAO designer can definitely not be fitted without adjusting the current geometry and/or attitude of the M1 segments and/or the PMSS.

The actuators have been positioned in between the fixed top plate and the moving plate. These actuators are pre-stressed piezoelectric ceramic stacks and are not easy to define by means of one material. Nevertheless, its radius, height and mass (0.085kg) are known, which makes it possible to define an estimate. For simplicity, it will be assumed that actuator is encapsulated in a Ti-6Al-4V hollow case with a certain thickness, which can be calculated with the following equation:

$$m = (2\pi r^2 t + 2\pi r t h) \cdot \rho \tag{7.1}$$

With m being the mass of the actuator, r the actuator radius, t the thickness, h the actuator height and ρ the average density. Solving for the thickness leads to 5.85635mm. These dimensional parameters will be determinative for the thermal resistance of the actuators. The resulting PMAO geometry as constructed in the Workbench of ESATAN TMS is shown in Figure 7.6.

Table 7.1: PMAO geometry parameters for the thermal model.

Geometry	**Shape**	**Radius** [mm]	**Height** [mm]
Fixed Frame Top Plate	Disk	110	5
Actuator	Cylinder	15	20
Moving Frame Plate	Disk	125	5
Fixed Frame Base Plate	Disk	115	5

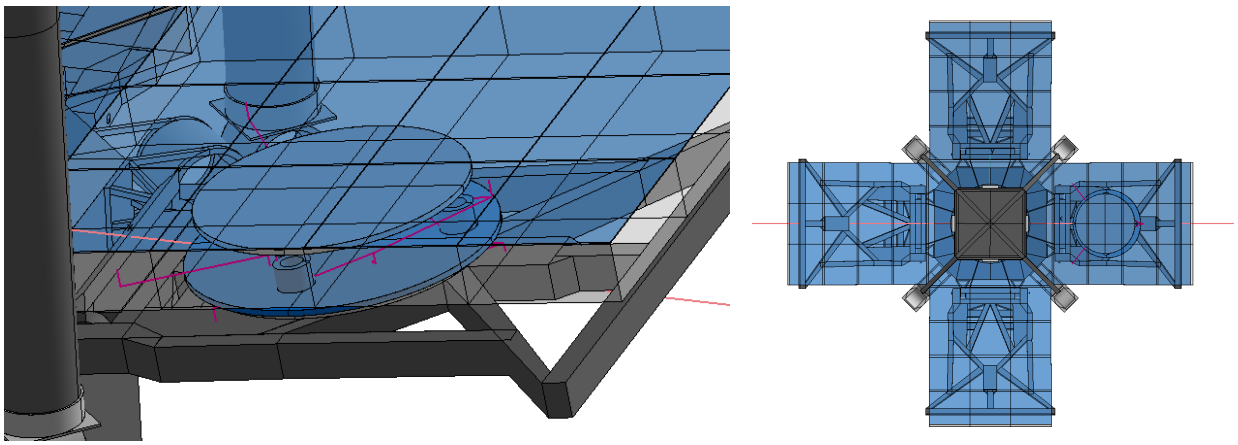

(a) (b)

Figure 7.6: Visualisation of the primary mirror active optics geometry, as constructed within the Workbench of ESATAN TMS.

7.4.3 Conductive Interfaces

The PMAO geometry has been defined but their thermal conductive couplings have not. ESATAN TMS includes a function which can be used to define conductances between two surfaces or nodes, for which the conductance can be calculated as a function of the conductivity, cross sectional area and path length. These values need to

be estimated since most of the respective geometries are composed of several materials and sizes, for which the biggest resistance or the smallest thermal conductance will be most limiting.

Most Limiting Conductance

For the Bipods and the universal joint it was found that their flexure were most limiting, while the in-plane constraints are flexures themselves. The fixed frame base plate is expected to be bolted onto the PMSS, and therefore the shape factor function of ESATAN TMS has been used in which the user can define two surfaces which are expected to touch each other. The latter function has been used to define the conductive interfaces of each quadrant of the base plate, since it is divided into four nodes, with a neighbouring surface of the primary mirror support structure.

Conductive Parameters

The conductive parameters are depicted in Table 7.2. With # referring to the total amount per interface, k the thermal conductivity, A the cross sectional area and L the path length. These conductive interfaces are depicted in Figure 7.7, by means of the purple lines.

Table 7.2: Conductive parameters of the primary mirror active optics, as modelled in the Workbench of ESATAN TMS.

Interface	#	**k** [W/m/K]	**A** [m^2]	**L** [m]	**Comment**	**Reference**
Bipod Strut Flexure	6	10.0	$3.4 \cdot 10^{-5}$	$24 \cdot 10^{-3}$	Four flexures per strut	Figure 8.25 in [13]
Universal Joint Flexure	8	10.0	$5.0 \cdot 10^{-6}$	$12 \cdot 10^{-3}$	One flexure per side of the UJ	Figure 8.5 in [13]
In-Plane Constraint	6	10.0	$1.96 \cdot 10^{-6}$	$45 \cdot 10^{-3}$	-	Figure 8.17 in [13]

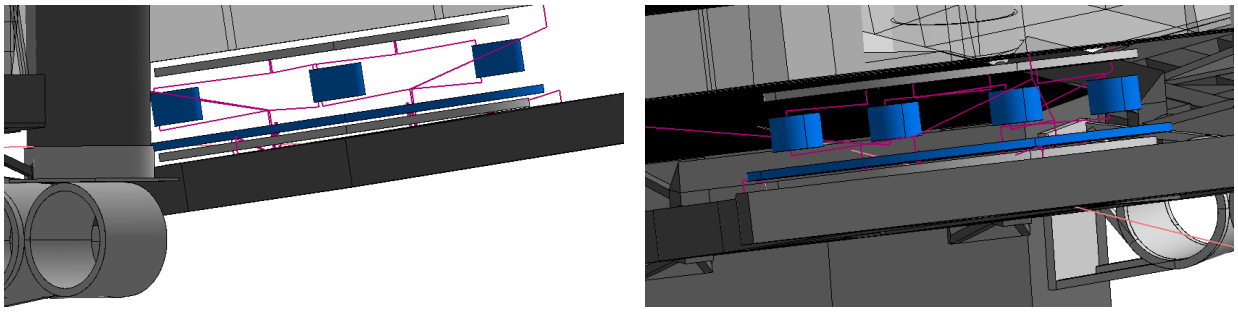

(a) (b)

Figure 7.7: Visualisation of the primary mirror active optics conductive interfaces, as constructed within the Workbench of ESATAN TMS.

7.4.4 Requirement Compliance Analysis

The respective PMAO geometry has been has been exposed to NOM thermal conditions. The shown results consider one geometry only. The temperature behaviour results are depicted in Appendix G *PMAO Results*. These results are representative of the two pairs of actuators as configured by its designer, and the position of the actuators are in accordance with the actual design. The thermal requirements related to the PMAO system have been mentioned in Table 3.3 of Chapter 3. These were formulated in two categories related to material bulk temperature- and instrumentation limits.

The steady state flow limits requirements were not included since there respective components have not been modelled as geometries but as most limiting conductive interface only. The instrumentation limits for stowed configuration could eventually not be addressed either, since this report only considers fully deployed configuration. The remainder of the deployed requirements will be evaluated below. Their compliance verification has been summarised in Table 7.3.

PMAO-THE-01, PMAO-THE-02 and PMAO-THE-03

The bulk temperatures of the components other than the actuators are not represented in the aforementioned results. This is because the actuator requirements were found to be the most limiting and considering the incomplete design it would not be very relevant in the first place. Nevertheless, it is likely that the bulk temperature of the universal joints, the in-plane constraints wire flexures and the moving frame plate are similar to those of the primary mirror support structure and/or the mirror segments.

From the initial thermal results it is known that the average temperatures of these structures are around 10 to 15°C, for the considered nominal conditions. In order to satisfy all three requirements non of their temperatures should exceed 318°C (including margin). It is therefore thought highly unlikely that these requirements will be violated for these conditions in the deployed state. It is more likely that these constraints can become critical in other mission stages during which the DST is still stowed and the baffle undeployed.

PMAO-THE-06

This requirement states that the maximum gradient between the actuators in pairs should not exceed the 0.01°C, and has been assigned as the killer requirement. The deployed actuator temperature results as shown in Figure G.1 indicate that the temperature difference between the pairs is about 0.1°C maximum for pair 1, while it is about 0.4°C maximum for pair 2. The actuator featuring the largest ΔT is the actuator situated closest to the instrument housing, while the other three actuators have similar behaviour. It is therefore likely that this respective temperature budget will not be met for the current system configuration.

PMAO-THE-08

This requirement states that the bulk temperature of the actuators should be situated between 15-25°C. The temperature result show that the average temperatures of the actuators are converging towards 15°C, but do not reach their intended target. It is therefore likely that some type of thermal control will be required for the actuator temperature to stay within budget.

Table 7.3: PMAO Requirement Verification Summary.

	Short description	Compliance	Comment
PMAO-THE-01	The bulk temperature of the universal joints shall not exceed 2310 °C.	Partial	Based on analogy.
PMAO-THE-02	The bulk temperature of the in-plane constraint wire flexures shall not exceed 343 °C.	Partial	Based on analogy. Stowed hot case is considered critical.
PMAO-THE-03	The bulk temperature of the moving frame plate shall not exceed 467 °C.	Partial	Based on analogy. Stowed hot case is considered critical.
PMAO-THE-06	The maximum gradient between the actuator pairs shall not exceed 0.01 °C.	Fail	Needs a physical exterior housing including thermal control.
PMAO-THE-08	The bulk temperature of the operational actuators shall not deviate from 15 to 25 °C.	Fail	Needs thermal control.

7.4.5 Discussion

The results as shown in the previous section indicate that the mentioned requirements will most likely not be met by the current system without the addition of thermal control. The experienced gradients, referring to the temperature differences between the actuators in pairs, are violated by a factor 10 to 100. The bulk temperature budgets of the actuators are violated too, although it is considered to be near target. Besides, it only considers nominal conditions while the mean average temperatures of the majority of the systems are expected to be around -40 °C for COLD conditions, as will be shown in the following Chapter. It is therefore thought that the current system cannot be made operational without any form of thermal control.

The missing exterior housing of the PMAO is thought to be the predominant cause for the actuator gradients. In order to address the gradient requirement properly one should design a fully representative exterior housing such that the actuators are protected by direct influences of the neighbouring geometries. This housing should insulate the actuators from its environment such that heat flow to and from its surrounds is minimised.
Besides, in order to make it a reliable estimate one should update the conductive interfaces such that it represents the entire interfaces instead of the most limiting sections only. Further, one should re-evaluate the thermal

resistance of the actuators such that it is fully representative of the design. These alternations would allow for a better estimate, although *PMAO-THE-06* seems to be an undisputed killer requirement.

7.5 Final Baffle Design

The Baffle design as shown in section 4.5 had to be adjusted eventually due to all the difficulties the elliptical structure was causing in progressing the design. The elliptical shape posed some difficulties for the thermal model too, since the shape could not be mimicked closely. The new baffle design has been made cylindrical. The baffle structure will be octagon, with an equal amount of booms as before. The MLI will be wrapped around it such that it will look cylindrical. First, one will elaborate on the cylindrical structure (7.5.1), after which the baffle housing will be introduced (7.5.2).

7.5.1 Baffle Structure Update

The total length of the baffle has remained unchanged (2700mm), just as the boom diameter (100mm) and the used materials (Al-1100-O and Kapton). The octagon diameter is 2000mm throughout the length. The new design as provided by E. Korhonen is shown in Figure 7.8a, and will be a lot easier to built in the Workbench of ESATAN TMS compared to the previous design. The most current design features straight booms which are placed such for it to form the octagon, connected by a torus on top and at the bottom. The top will remain open, while the bottom is closed and mounted onto the instrument housing, as shown in Figure 7.8b and 7.8c. The actual mounting method or interface was not designed yet at the time, and therefore it was chosen to temporarily mount it onto the instrument housing. The MLI blanket is expected to be deployed around this structure for now, while other MLI configurations will be explored in the next Chapter.

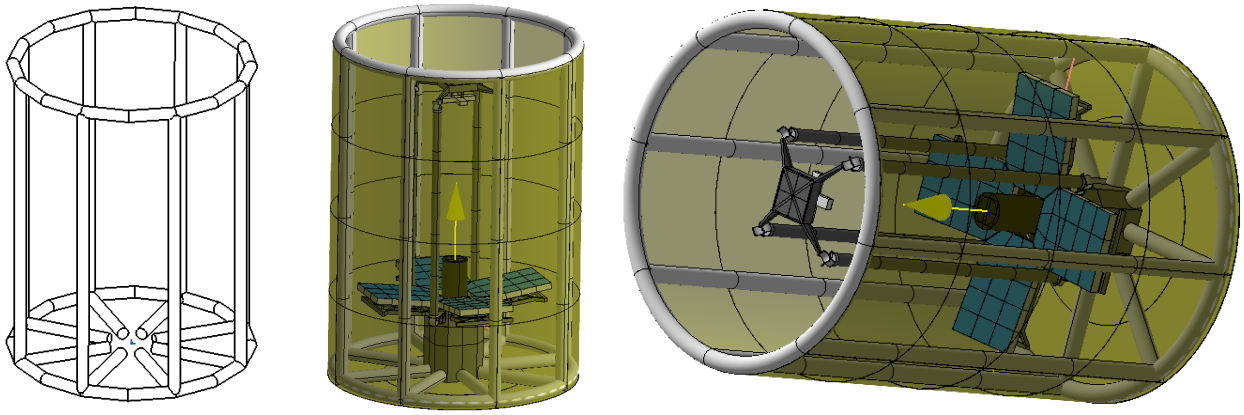

(a) E. Korhonen (b) ESATAN TMS (c) ESATAN TMS

Figure 7.8: Visualisation of the baffle geometry as per December 2018, DST 2.5.

7.5.2 Baffle Housing Geometry

As aforementioned, the exact integration of the baffle structure with the instrument housing or the spacecraft bus has not exactly been determined before. The attachment as shown in Figure 7.8 can be considered as an initial estimate. Apart from the interface used for mounting the baffle onto the spacecraft, it will also function as storage element for to be determined elements. Therefore, this element will be considered as the baffle housing from now on. The instrument housing has been sized such for it to include the remainder of the telescope instruments required for obtaining an image. Besides, this housing should be mechanically and thermally stable for it to provide the required performance. Mounting the baffle structure directly onto the instrument housing would therefore have not been desired, as well as it has not been designed to include any other structural components.

Baffle Housing Design

The preliminary design of the baffle housing as designed by E. Korhonen is considered separated from the instrument housing, where the final sizing depends on the required volume for storage. This decision is made for storage and deployment reasons, but is thought to be sense when considering the aforementioned reasons. The baffle itself will not be extended and therefore be translated a bit compared to the telescope. As aforementioned, the exact dimensions and properties of the baffle housing are still to be determined. The baffle designer has

indicated that it is likely that the entire volume will fit into a similar shape as the instrument housing, with a maximum height of 20cm. The result of including such a baffle housing is shown in Figure 7.9. The temperature results of the baffle housing will be largely dependent on the exact properties of the geometry, which have not been determined yet. Therefore, the baffle housing will be made inactive for now.

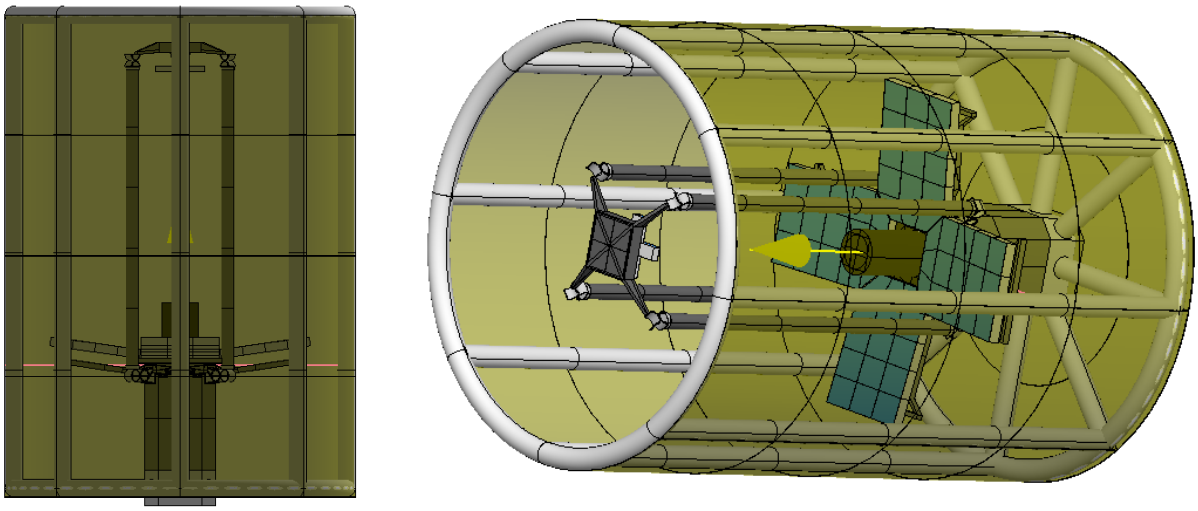

(a) (b)

Figure 7.9: Visualisation of the baffle housing, DST 2.6. As constructed within the Workbench of ESATAN TMS.

Discussion

The reason for including the baffle housing for now is to facilitate the change in relative position of the baffle with the telescope. The top of the telescope will be situated more closely towards the opening and will most likely be effected by this change. Further research shall determine how large this effect will be.

7.6 Fully Representative Thermal Model

The initial thermal model has been updated in the previous sections, such for it to be closely representative of the actual DST geometry. Some of these geometries should however not be in included, since they have not been designed in detail or because they are incomplete. This would lead to irrelevant results. The fully representative thermal model, excluding the PMAO and the baffle housing, will be referred to as the DST 2.7 model as shown in Figure 7.10. The excluded geometries will be elaborated below. Subsequent models will also be excluded from these two systems.

Exclusion of the Primary Mirror Active Optics

A mass estimate has been made for the exterior housing of the PMAO, although the exact design of it has not been designed in detail yet. Because of the complexity of the mechanism it will require a creative solution, which is not considered as part of this thesis. Besides, modelling the mechanism without the exterior housing resulted into an exposed mechanism, from which results have been delivered and recommendations for future work have been formulated. Therefore, it has been decided to exclude the PMAO from the fully respective model.

Exclusion of the Baffle Housing

The baffle housing has been visualised and the position of the baffle itself has been adjusted such that it will be mounted midway the baffle housing. The position of the baffle will not be altered, but the baffle housing itself will be excluded from the fully representative model. This is because its material and thickness have not been determined, which will be leading for the thermal results. Besides, just assuming some properties will effect the thermal performance of the baffle, as also it will interfere with the instrument housing due to which the thermal model has been assembled.

7.7 Thermal Model Performance Comparison

The fully representative thermal model has been presented in the previous section as the DST 2.7 model. As of this moment it is unknown how this has effected the thermal performance in comparison to the initial model, as presented in the previous Chapter. The DST 2.7 model has therefore been exposed to NOM conditions for which the temperature results, including those of the initial model, are depicted in Table 7.4. The heat flow charts have not been included since it is thought that such an extensive analysis will not be required here. The initial thermal model (DST 1.0) has not been included with a baffle structure, which is the reason for the results not being shown here. The results are analysed below.

Baffle

The baffle blanket of the DST 2.7 model features lower global- and average ΔT, which is either thought to be caused by a change in baffle shape or by addition of the baffle structure. The baffle structure itself has higher minimum temperature compared to the baffle, since it is covered by the blanket from cold space, while it is not at maximum temperature occurrence.

Spider, Top Hinges, M2 and Booms

The spider features larger global- and average ΔT, thus it became more sensitive for a change in temperature during an orbit which can be caused by the lowered baffle. The top hinges are a couple of degrees colder overall, with a similar but smaller trend for the booms. The secondary mirror experiences an overall increase in temperature, which can most likely be assigned lowering of the baffle too. The booms are considered most similar.

Root Hinges, M1, PMSS and IH

The root hinges and the primary mirror support structure feature smaller global- and average ΔT, while the primary mirror features larger global ΔT. The latter is thought to be caused by the change in geometry, while the primary mirror support structure could be better insulated from space by the changed baffle. The instrument housing features larger global- and average ΔT, which can be caused by the change of baffle position due to which it is lowered from before.

Discussion

Further research regarding the baffle dimensions and/or positions is thought to be necessary. This because most changes with respect to the initial model are thought to be assigned to the change in baffle design and/or lowering of the baffle.

Table 7.4: Temperature results for the DST- 1.0 and 2.7 model, for NOM conditions in degrees Celsius.

	DST 1.0					**DST 2.7**				
	Glo. Min	Av. Min	Av. ΔT	Av. Max	Glo. Max	Glo. Min	Av. Min	Av. ΔT	Av. Max	Glo. Max
Baffle Bl.	-134.4	-44.7	32.3	-12.4	126.7	-89.8	-36.1	20.5	-15.6	118.4
Baffle Str.	-	-	-	-	-	-25.6	-4.9	30.9	26.0	110.0
Spider	3.5	5.9	13.2	19.1	26.6	1.3	4.2	16.1	20.3	36.8
Top Hinges	2.9	5.6	11.7	17.3	25.6	0.7	3.5	12.3	15.8	21.6
M2	7.1	8.5	1.9	10.4	11.5	29.7	32.9	1.5	34.4	37.6
Booms	3.8	4.9	11.9	16.8	19.2	1.9	4.2	11.2	15.6	19.4
Root Hing.	5.4	2.8	8.2	14.3	15.0	5.0	5.8	6.7	12.5	13.6
M1	6.6	6.7	1.1	7.8	8.0	5.4	7.1	0.5	7.6	10.4
PMSS	1.4	6.2	8.1	14.3	32.7	0.1	6.0	6.3	12.3	18.6
IH	4.1	4.6	11.7	16.3	17.0	-0.5	3.1	12.8	15.9	18.8

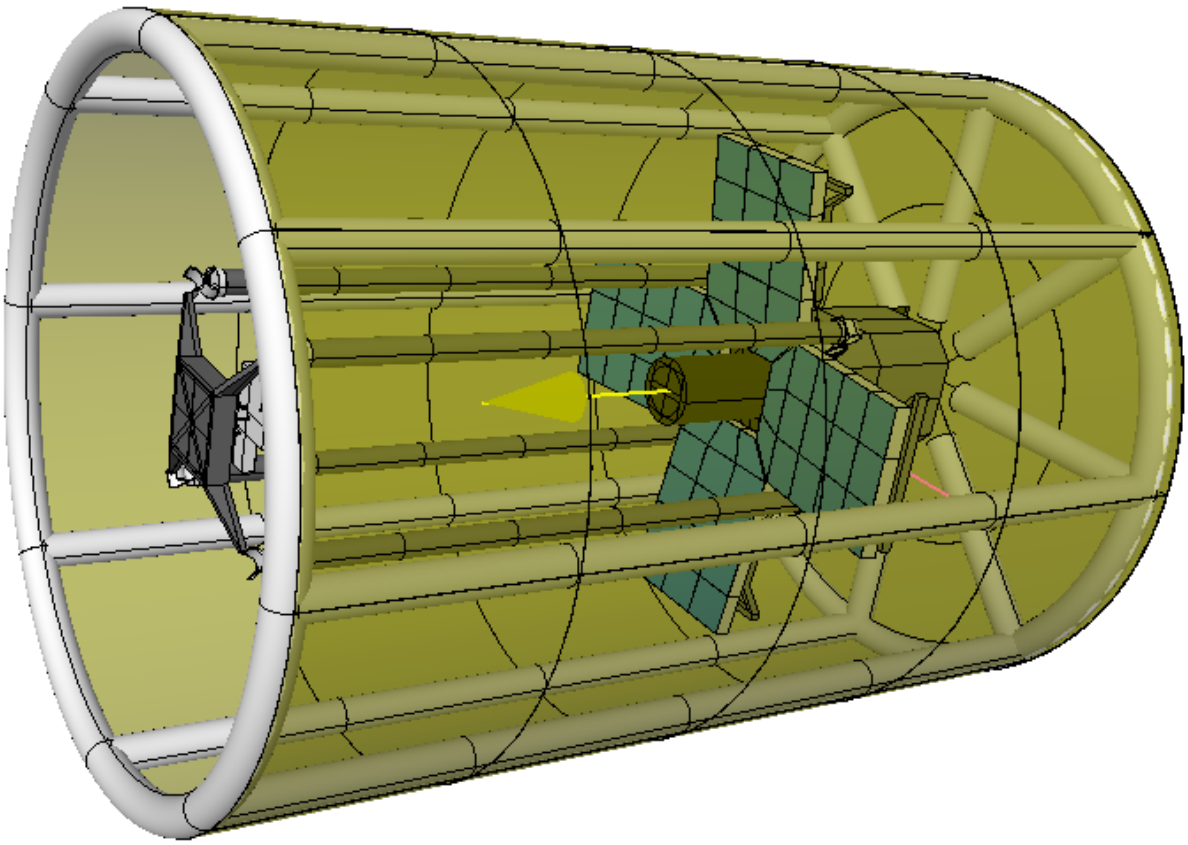

(a)

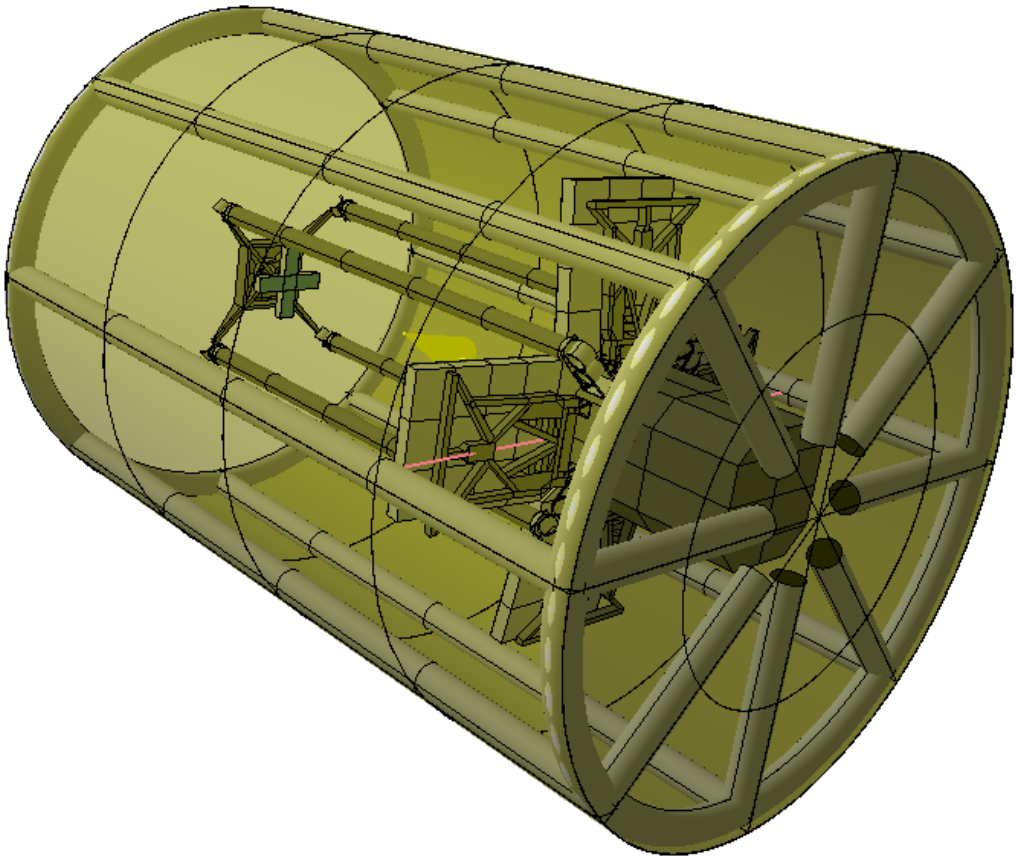

(b)

Figure 7.10: Visualisation of the fully representative thermal model, DST 2.7. As constructed within the Workbench of ESATAN TMS.

7.8 Chapter Summary

The initial thermal model (DST 1.0) has been included with some of the missing systems, while some of the existing systems have been adjusted or updated. The baffle has been included with its structure onto which the MLI blanket shall be deployed. The instrument housing featured a large gap on top before and had to be included with the field stop housing. The size of the field stop has been defined in accordance with the system designers.
The primary mirror segments were modelled as flat surfaces before and had to be adjusted because the segments had overlap at the cut-offs. Besides, it was unsure whether the segments could be modelled properly without it having actual physical nodes on the sides. The cut-offs have been adjusted such for the segments to have sufficient clearance without the occurrence of so called temperature spikes, which cause inexplicable oscillatory ΔT increments.

The PMAO system, not mentioned before because it still had to be designed, has been included to the thermal model. This system has been included with the most limiting thermal resistances and exposed to NOM conditions. The results showed that the system will be in need of thermal control for it to meet some of its instrumentation limit budgets, although the exterior housing should be designed first for it to insulate the actuators from its surroundings.
The baffle structure has been updated to account for the change in design shape, which has been redesigned from elliptical into cylindrical in relation to deployable feasibility. Besides, a baffle housing has been added onto which the baffle structure is expected to be mounted.

The PMAO system is considered to be incomplete without an actual protective design of its exterior housing. Therefore, its interior mechanisms become exposed which makes it sensitive to changes in temperature. Besides, the most critical thermal requirements have been addressed for nominal thermal conditions, which is though to provide sufficient insights for now.
The baffle structure has not been designed in detail either, due to which its thermal resistance cannot be determined. This thermal resistance, representative of how its temperature will change with net heat flow, is determinant for its change in temperature. Therefore, the fully representative model (DST 2.7) will be excluded from the PMAO and the baffle housing.

The thermal performance of the fully representative thermal model has been compared with the initial model. Most of the changes are thought to be caused by either the change in baffle shape, the addition of the baffle structure and/or lowering the baffle with respect to the telescope. It seems that these changes have largest effect on the spider and the secondary mirror, with an increase in maximum- and overall temperature respectively. It is therefore thought that further research regarding the baffle dimensions and/or positions is necessary.

8 Global Thermal Model Results

Requirement *SYS-REQ-05* states that the thermal system shall be designed for the mission scenario which is most demanding. Therefore, one needs to consider certain hot and cold conditions scenarios, for which the hottest and coldest case will be selected as most demanding. The DST 2.7 model shall be exposed to several sets of thermal conditions which can potentially be considered as worst case scenarios (8.1). The thermal model will be exposed to these sets of thermal conditions for which results will be presented and analysed (8.2). These results will be concluded with a discussion from which a hot and cold case will be selected (8.3).

8.1 Scenario Selection

Worst case scenarios consist of a certain combination of minimum and maximum environmental conditions, for which the effect is dependent on the thermo-optical properties of the satellite and its respective orientation with respect to the Sun-Earth system. The cases for maximum-, minimum- and median conditions for the solar flux, OLR and albedo have been specified in Chapter 6. The orientation of the satellite and the Sun-Earth system however have not. Normally, the position of the Sun with respect to Earth, or visa versa, determines the aforementioned thermal conditions.

The position of the Sun with respect to Earth will be fixed within this report, for which the thermal conditions will be varied such for it to represent the minimum- and maximum heat input parameters. The right ascension of the satellite will be fixed such for it to result into the coldest and hottest conditions. The relevant parameters will be elaborated below.

8.1.1 Sun Orientation

The Sun is considered to orbit Earth, for which its path is determined by the ecliptic. This path is a function of the obliquity of the ecliptic, which as aforementioned is assumed to be fixed at 23.5 °. The orbit of the Sun around Earth can be considered elliptical, although it will be considered circular for now. The heat inputs as defined before (Solar flux, albedo and OLR) are normalised to a Sun/Earth distance of 1 AU. The first point of Aries (♈) is known as the intersection plane of the ecliptic and the equatorial plane [19], and is therefore thought to be a suitable starting point from which Earth orbits can easily be defined in terms of its right ascension. The resultant Sun orientation parameters are depicted in Table 8.1.

Table 8.1: Sun Parameters for the worst case scenarios.

Parameter	Value	Units
Sun Planet Distance	$1.5 \cdot 10^{11}$	m
Solar Declination	0	deg
Sun's Right Ascension	0	deg

8.1.2 Satellite Orientation

The position of the Sun with respect to Earth has been fixed to a convenient position at ♈ in the previous section. From the initial thermal model results it became apparent that the satellite should preferably be oriented such that the Sun impinges its baffle interior the least. This is thought to imply that the orbit normal should be more or less in line with the Sun-Earth axis. Apart from that, it should face a relatively long eclipse for coldest conditions. The selected satellite orientations are visualised in Figure 8.1.

Full Sunlit Conditions

Figure 8.1a represents an orbital condition for which the satellite does not enter eclipse. The right ascension is set at 90 degrees for it to have its orbit normal close to the X-axis or ♈. The orbit itself is represented by the green line, where green indicates that it is sunlit. The yellow arrow, highlighted with the small red arrow, points towards the position of the Sun. From the Figure it can be seen that the Sun is situated at ♈. This respective Sun, Earth and satellite orientation will be considered as the 90 degrees Right Ascension (RA) Full Sunlit Conditions (FSC), thus RA90-FSC.

Partial Shadow Conditions

Figure 8.1b represents the orbital conditions for which the satellite is closest to the Sun but also includes a relatively long eclipse. The right ascension is set at zero degrees such that its orbit normal is near the depicted Y-axis. From the orbital path it can be seen that it is partially red too, which indicates that it will be in shadow. Although it will be in shadow, it will also be closest to the Sun. This respective Sun, Earth and satellite orientation will be considered as the Partial Shadow Conditions (PSC). No additional PSC orbits have been considered here since it is thought that eclipses are generally undesired.

Other Sunlit Conditions

It was found by means of trial and error that by applying an offset of ± 20 degrees, the satellite does still not enter eclipse. These conditions will be considered with RA 70 and 110 degrees for FSC, thus RA70-FSC and RA110-FSC, as shown in Figure 8.1c and 8.1d respectively. These orientations have been considered because the Sun will be able to impinge the baffle more easily, compared to RA90-FSC.

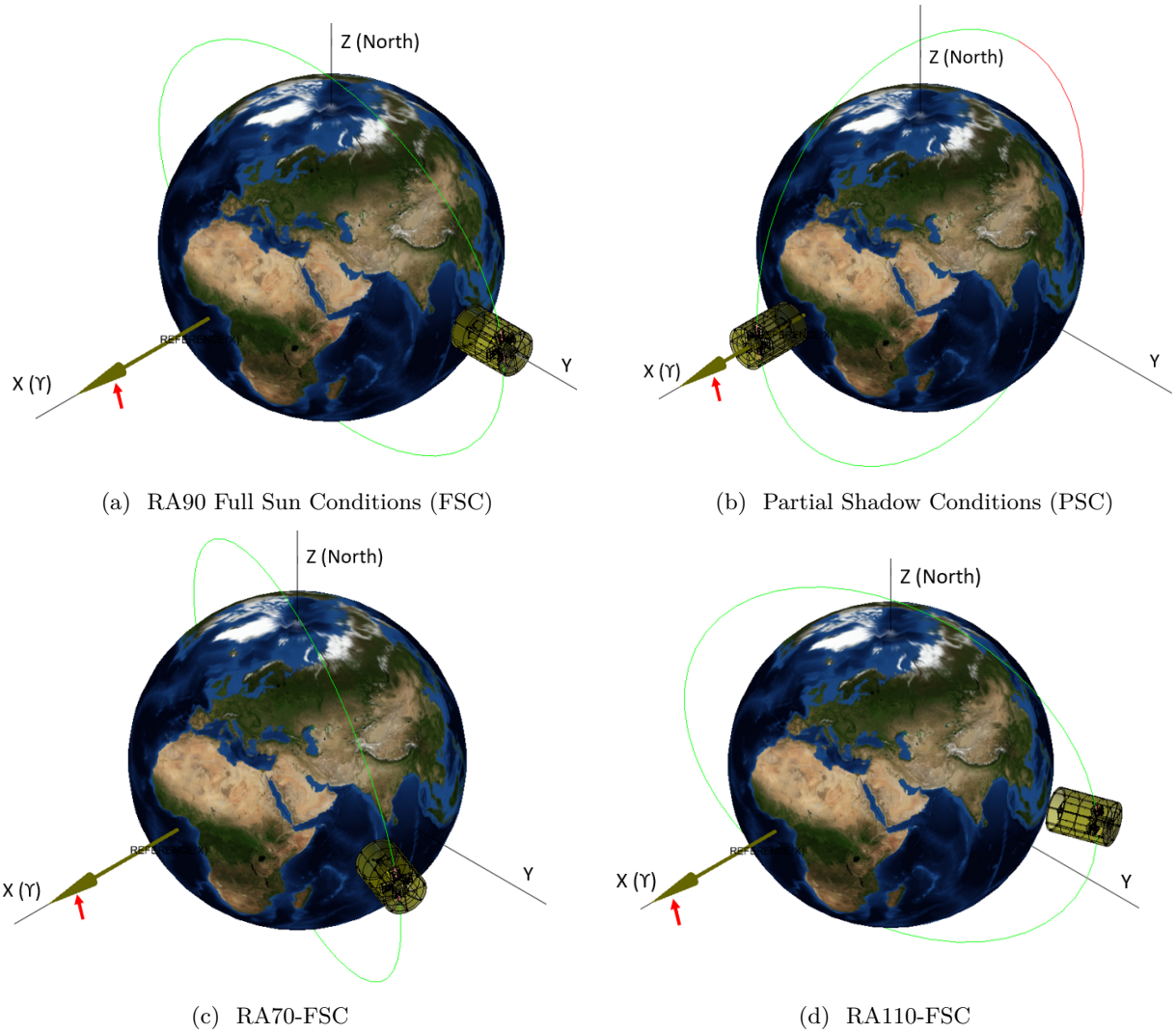

(a) RA90 Full Sun Conditions (FSC)

(b) Partial Shadow Conditions (PSC)

(c) RA70-FSC

(d) RA110-FSC

Figure 8.1: Visualisations of the Sun, Earth and satellite orientation for the considered worst case scenarios. As visualised within the Workbench of ESATAN TMS.

8.1.3 Simulation Cases

The aforementioned thermal conditions are combined in simulation cases. Herewith one considers four satellite orientations (RA70-FSC, RA90-FSC, RA110-FSC and PSC), with several combinations of heat inputs (Solar flux, albedo and Earth temperature). The heat input combinations are depicted in Table 8.2.

Table 8.2: Solar albedo and Earth infrared for hot-, median- and cold case for high inclination orbits.

Case Description	**Abbreviation**	**Solar Flux** $[W/m^2]$	T_{Sun} [K]	**Albedo** [-]	E_{IR} $[W/m^2]$	T_{Earth} [K]
Minimum Solar flux & Albedo	SA-MIN	1322	5729	0.06	273.0	263.4
Minimum Solar flux & OLR	SOLR-MIN	1322	5729	0.40	108.0	208.9
Median Solar flux, Albedo & OLR	SAOLR-MED	1367	5778	0.306	237.1	254.3
Maximum Solar flux & Albedo	SA-MAX	1414	5826	0.5	180.0	237.4
Maximum Solar flux & OLR	SOLR-MAX	1414	5826	0.22	332	276.6

8.2 Results & Analysis

The simulation results are depicted in Tables 8.3 to 8.7. These Tables depict the minimum- and maximum node temperatures, including average ΔT. The node temperatures have been rounded to the nearest 2.5°C. The ΔT as shown in the Tables depict the maximum temperature variation between the minimum- and maximum average temperature. This data is shown because it will be most determinant for the final analysis of this report. The coldest and hottest temperature as suffered per main geometry, are marked in blue and red respectively. The maximum suffered average ΔT's are marked in yellow. Additional temperature data is provided in Table 8.8. This Table includes the mean average temperature.

FSC Simulations

The RA70- and the RA110-FSC simulations, are similar for each set of thermal conditions. This could be explained by the similar conditions of the orbit, which are almost copies from each other when mirrored in the Sun-Earth line or X-axis. Large differences for the maximum baffle temperatures, as well as on the average ΔT, are seen with respect to the RA90-FSC simulations. This is thought to be caused by the orientation of the baffle, for which a larger amount of sunlight can enter the baffle directly.

Driving Thermal Conditions

The SOLR-MIN simulations are colder than the SA-MIN simulations. This could indicate that the OLR contribution is the main driver for telescope temperatures, while the SA contribution is less determinant for low solar flux input. The same can be said for the SOLR-MAX and the SA-MAX simulations, where a maximum OLR is driving most of the telescope component temperatures, apart from PSC-SA-MAX. The latter simulation is thought to be driving the telescope temperatures because of its orientation with respect to the Sun, having maximum power in combination with largest albedo conditions.

Extreme Temperatures

The FSC-SOLR-MIN simulation features the lowest temperatures for all components. This simulation considers full SSO conditions but without eclipse, with minimum solar flux and OLR. The largest temperatures are suffered for the RA70- and RA110-FSC-SOLR-MAX, and the PSC-SA-MAX simulations. The PSC-SA-MAX features the largest ΔT, but not the highest temperatures. This simulation provides useful information about the expected ΔT when the baffle is deployed, when facing a relatively long eclipse while also passing the Sun close by. It must be concluded that this will most likely not be desired.

Table 8.3: Temperature results for minimum solar flux and albedo, in degrees Celsius.

	RA70-FSC-SA-MIN			RA90-FSC-SA-MIN			RA110-FSC-SA-MIN			PSC-SA-MIN		
	Min T	Av. ΔT	Max T	Min T	Av. ΔT	Max T	Min T	Av. ΔT	Max T	Min T	Av. ΔT	Max T
Baffle Blanket	-85.0	9.3	117.5	-85.0	2.9	40.0	-85.0	9.4	117.5	-85.0	16.8	105.0
Baffle Structure	-17.5	28.2	107.5	-22.5	11.4	62.5	-17.5	29.1	107.5	-25.0	23.8	95.0
Spider	7.5	28.6	70.0	-12.5	2.9	-5.0	5.0	30.1	62.5	-7.5	9.3	10.0
Top Hinges	0.0	23.2	55.0	-10.0	3.7	-2.5	0.0	23.7	52.5	-7.5	8.1	7.5
M2	27.5	0.7	30.0	-5.0	0.1	-5.0	30.0	0.7	30.0	7.5	0.6	7.5
Booms	5.0	15.5	35.0	-7.5	4.7	0.0	5.0	16.7	35.0	-5.0	7.9	7.5
Root Hinges	7.5	5.6	15.0	-5.0	1.7	-2.5	7.5	5.5	15.0	-5.0	5.1	2.5
M1	7.5	0.4	15.0	-5.0	0.1	-5.0	7.5	0.3	15.0	-5.0	0.4	0.0
PMSS	5.2	5.2	20.7	-7.5	1.7	-2.5	5.0	5.1	20.0	-5.0	4.9	5.0
IH	5.0	12.8	22.5	-7.5	3.6	-2.5	2.5	13.4	22.5	-7.5	7.7	5.0

Table 8.4: Temperature results for minimum solar flux and OLR, in degrees Celsius.

	RA70-FSC-SOLR-MIN			RA90-FSC-SOLR-MIN			RA110-FSC-SOLR-MIN			PSC-SOLR-MIN		
	Min T	Av. ΔT	Max T	Min T	Av. ΔT	Max T	Min T	Av. ΔT	Max T	Min T	Av. ΔT	Max T
Baffle Blanket	-122.5	7.1	107.5	-122.5	2.3	20.0	-122.5	7.5	107.5	-112.5	26.8	97.5
Baffle Structure	-40.0	24.8	97.5	-57.5	11.5	47.5	-35.0	24.7	97.5	-55.0	40.0	85.0
Spider	-12.5	25.4	55.0	-50.0	1.5	-40.0	-15.0	27.5	47.5	-17.5	19.7	10.0
Top Hinges	-20.0	19.6	37.5	-45.0	2.5	-37.5	-20.0	20.6	32.5	-20.0	19.2	7.5
M2	17.5	0.7	17.5	-35.0	0.0	-35.0	20.0	0.7	20.0	20.0	0.8	22.5
Booms	-12.5	11.3	12.5	-42.5	3.4	-35.0	-15.0	12.5	15.0	-15.0	19.3	10.0
Root Hinges	-12.5	4.1	-7.5	-42.5	1.2	-40.0	-12.5	4.2	-7.5	-10.0	9.6	2.5
M1	-12.5	0.3	-7.5	-40.0	0.0	-40.0	-12.5	0.7	-7.5	-12.5	0.7	0.0
PMSS	-15.0	4.0	-2.5	-42.5	1.2	-40.0	-15.0	4.0	-2.5	-17.5	9.2	10.0
IH	-15.0	9.5	0.0	-42.5	2.5	-37.5	-17.5	9.9	0.0	-22.5	22.9	15.0

Table 8.5: Temperature results for median solar flux, albedo and OLR, in degrees Celsius.

	RA70-FSC-SAOLR-MED			RA90-FSC-SAOLR-MED			RA110-FSC-SAOLR-MED			PSC-SAOLR-MED		
	Min T	Av. ΔT	Max T	Min T	Av. ΔT	Max T	Min T	Av. ΔT	Max T	Min T	Av. ΔT	Max T
Baffle Blanket	-90.0	7.3	117.5	-90.0	2.2	37.5	-90.0	7.6	117.5	-87.5	21.0	110.0
Baffle Structure	-15.0	24.0	107.5	-25.0	10.1	60.0	-12.5	24.1	107.5	-27.5	30.8	97.5
Spider	10.0	26.3	72.5	-15.0	1.8	-7.5	7.5	27.9	65.0	0.0	15.2	25.0
Top Hinges	2.5	20.7	57.5	-12.5	2.6	-7.5	2.5	21.5	52.5	0.0	15.4	22.5
M2	35.0	0.6	35.0	-7.5	0.1	-7.5	35.0	0.6	35.0	30.0	0.5	32.5
Booms	7.5	12.2	35.0	-10.0	3.6	-5.0	7.5	13.5	35.0	2.5	14.8	22.5
Root Hinges	10.0	4.2	17.5	-10.0	1.2	-7.5	10.0	4.2	15.0	7.5	6.1	17.5
M1	10.0	0.3	15.0	-10.0	0.0	-7.5	10.0	0.3	15.0	7.5	0.5	15.0
PMSS	7.5	4.1	20.0	-10.0	1.2	-7.5	7.5	3.9	20.0	2.5	5.8	22.5
IH	7.5	9.9	22.5	-10.0	2.7	-7.5	5.0	10.5	22.5	0.0	15.7	25.0

Table 8.6: Temperature results for maximum solar flux and albedo, in degrees Celsius.

	RA70-FSC-SA-MAX			RA90-FSC-SA-MAX			RA110-FSC-SA-MAX			PSC-SA-MAX		
	Min T	Av. ΔT	Max T	Min T	Av. ΔT	Max T	Min T	Av. ΔT	Max T	Min T	Av. ΔT	Max T
Baffle Blanket	-102.5	6.0	117.5	-102.5	1.8	32.5	-102.5	6.3	117.5	-97.5	28.9	110.0
Baffle Structure	-17.5	21.1	107.5	-35.0	9.4	60.0	-12.5	20.7	107.5	-32.5	46.2	100.0
Spider	7.5	24.8	70.0	-27.5	1.1	-17.5	5.0	26.7	65.0	2.5	25.9	37.5
Top Hinges	0.0	19.1	55.0	-22.5	1.8	-15.0	0.0	19.8	50.0	2.5	25.4	35.0
M2	35.0	0.6	37.5	-12.5	0.0	-12.5	37.5	0.6	37.5	42.5	1.1	45.0
Booms	5.0	9.9	30.0	-20.0	2.8	-12.5	5.0	11.2	30.0	5.0	26.3	35.0
Root Hinges	7.5	2.8	12.5	-17.5	0.8	-17.5	7.5	3.2	12.5	12.5	12.2	30.0
M1	7.5	0.3	12.5	-17.5	0.0	-17.5	7.5	0.3	12.5	10.0	0.9	25.0
PMSS	5.0	2.7	15.0	-20.0	0.8	-17.5	5.0	3.0	15.0	2.5	11.4	40.0
IH	5.0	7.9	17.5	-20.0	2.0	-17.5	2.5	8.4	17.5	0.0	28.5	42.5

Table 8.7: Temperature results for maximum solar flux and OLR, in degrees Celsius.

	RA70-FSC-SOLR-MAX			RA90-FSC-SOLR-MAX			RA110-FSC-SOLR-MAX			PSC-SOLR-MAX		
	Min T	Av. ΔT	Max T	Min T	Av. ΔT	Max T	Min T	Av. ΔT	Max T	Min T	Av. ΔT	Max T
Baffle Blanket	-75.0	7.7	127.5	-75.0	3.3	50.0	-75.0	8.0	127.5	-75.0	18.2	117.5
Baffle Structure	0.0	34.4	115.0	-7.5	9.8	70.0	0.0	24.6	117.5	-10.0	26.7	107.5
Spider	20.0	27.5	85.0	2.5	2.2	10.0	17.5	26.8	77.5	12.5	13.0	32.5
Top Hinges	17.5	22.0	70.0	5.0	3.0	10.0	17.5	21.0	65.0	12.5	12.6	32.5
M2	45.0	0.7	45.0	10.0	0.0	10.0	45.0	0.3	47.5	35.0	0.5	37.5
Booms	20.0	13.6	47.5	5.0	4.0	12.5	20.0	14.9	47.5	12.5	17.9	32.5
Root Hinges	22.5	4.6	30.0	7.5	1.3	10.0	22.5	4.7	30.0	17.5	5.0	25.0
M1	22.5	0.3	30.0	7.5	0.1	10.0	22.5	0.3	30.0	17.5	0.4	22.5
PMSS	20.0	4.3	35.0	7.5	1.2	10.0	20.0	4.2	35.0	15.0	4.8	27.5
IH	20.0	10.7	35.0	7.5	2.9	12.5	20.0	11.4	35.0	12.5	11.7	30.0

Table 8.8: Average temperature results for the potential cold and hot case, in degrees Celsius.

	RA90-FSC-SOLR-MIN Average T	**RA70-FSC-SOLR-MAX** Average T	**RA110-FSC-SOLR-MAX** Average T
Baffle Blanket	-37.2	-2.8	-2.9
Baffle Structure	-35.1	31.2	31.1
Spider	-45.4	38.3	37.1
Top Hinges	- 41.4	34.4	32.4
M2	-35.3	44.7	50.0
Booms	-39.6	30.3	33.7
Root Hinges	-40.5	26.7	26.6
M1	-40.6	25.9	25.7
PMSS	-40.4	26.7	26.5
IH	-40.6	27.4	27.5

8.3 Discussion

The maximum global temperatures of the telescope seems to be driven most by the contribution of the solar flux and OLR, for FSC. However, the maximum fluctuation in average temperature (ΔT) occurs for PSC with maximum solar flux and albedo. Further, the coldest case is not found for an orbit with eclipse. This is thought to be caused by the baffle.

Hot and Cold Case Preselection

The operational window is still to be determined, but it is likely that the operational window will occur when the experienced ΔT are smallest. Further, it is thought that the chosen cold and hot cases should feature the maximum and minimum node temperatures, since other team members are in need of those temperatures specifically. Keeping this two aspects in mind, it is chosen to select a hot case out of the FSC simulations for this project.

Hot and Cold Case Determination

The RA70-FSC-SOLR-MAX simulation is thought to be slightly hotter, when compared to RA110-FSC-SOLR-MAX. This because it has higher global temperatures and larger ΔT for the spider and the top hinges. This is expected to become important for the M2 alignment. Further, the average temperature of those cases are similar. The RA90-FSC-SOLR-MIN simulation is thought to be coldest, with a significant difference ($\pm$70°C) in average temperature from the FSC-SOLR-MAX conditions.

Therefore, the RA90-FSC-SOLR-MIN and RA70-FSC-SOLR-MAX are assigned cold case conditions (COLD) and hot case conditions (HOT) scenario, respectively Their simulation parameters are summarised in Appendix D *Thermal Modelling Conditions*.

8.4 Chapter Summary

The considered thermal conditions include certain values for the solar constant, planet- albedo and temperature. These values were normalised to 1 AU but did not consider the orientation of the Sun yet. Usually, the thermal conditions are a function of the orientation of the Sun and Earth, in combination with the 11-year solar cycle. For this research it was thought convenient to fix the position of the Sun at the first point of Aries (Υ). In combination with the satellites inclination of 97.4 ° (close to 90°), this led to a convenient orientation of the Sun-Earth and satellite. The simulations do not consider movement of the planet or Sun system during simulations.

The potential worst case scenarios consider four types of satellite orbits. The first considers full sun conditions (RA90-FSC), meaning that it will not enter eclipse and that its orbit normal can be considered more or less parallel to the Sun-Earth axis. The second considers partial shadow conditions with a relatively long eclipse (PSC), where its orbit normal can be considered almost orthogonal to the Sun-Earth axis. The third and fourth type are chosen such for it to explore the bounds of the angle of right ascension, for which the satellite does still not enter eclipse (RA70- and RA110-FSC).
Each of these orbits have been subjected to thermal conditions for which either the solar flux and albedo, or the solar flux and planet temperature, are maximum or minimum. An additional median case has been added, similar to the nominal conditions but with equal Sun-Earth orientation as RA90-FSC. The latter will become useful for the coarse position budget analysis.

The temperature results showed that the RA90-FSC-SOLR-MIN featured the lowest minimum temperatures and was therefore considered as the simulation case with coldest conditions and thus assigned COLD. The coldest case was thus not found for an orbit with eclipse, which is thought to be caused by the baffle.
The PSC-SA-MAX simulation case featured the largest average ΔT and highest maximum temperatures for the bottom section of the telescope, while the RA70-FSC-SOLR-MAX featured the highest maximum temperatures for the remainder of the satellite components. A potential operational window was thought to be chosen such for it to feature small average ΔT, while the maximum global temperatures are most relevant for other team members. Therefore, the RA70-FSC-SOLR-MAX was assigned HOT.

The worst case scenario analysis of this Chapter has shown that the composed simulation cases impose varying challenges for the telescope. Therefore, it can be verified that each component has different worst case scenario as mentioned in [34].

(This page is intentionally left blank.)

9 Parametric Analysis of the Baffle

It has been prior been concluded that the baffle can be considered an effective tool in shielding the telescope from the space environment. Further, it is shown that the baffle interior is in close connection with the telescope in a thermal sense. It is therefore thought that a parametric analysis of the baffle can become useful for the determination of the ideal baffle parameters. The temperature results of the fully representative thermal model (DST 2.7) for COLD and HOT conditions are shown in Table 9.1. These will be used as the control set in the subsequent analysis.

The parametric analysis will consider a shape analysis (9.1), a baffle blanket position analysis (9.2), a top closing analysis (9.3), a dimensional analysis for the diameter and length of the baffle (9.4), and an attitude analysis of the baffle and the telescope (9.5).

It must be mentioned that the conductive interfaces between geometries of the different materials have not been determined yet, and thus are defined such for it to have rather small contributions. Therefore, the net total heat flow can be considered to be composed of radiative heat flow mainly. Positive heat flows indicate that heat is rejected while negative heat flows indicate that heat is absorbed.

Table 9.1: DST 2.7 temperature results of the control model for the COLD and HOT case, in degrees Celsius.

	COLD		**HOT**	
	Min T	Mean T	Mean T	Max T
Baffle Blanket	-122.5	-37.3	-2.8	127.5
Baffle Structure	-57.5	-35.1	31.2	115.0
Spider	-50.0	-45.4	38.3	85.0
Top Hinge	-45.0	-41.4	34.4	70.0
M2	-35.0	-35.3	44.8	45.0
Booms	-42.5	-39.6	29.3	47.5
Root Hinge	-42.5	-40.5	26.7	30.0
M1	-40.0	-40.8	25.9	30.0
PMSS	-42.5	-40.5	26.7	35.0
IH	-42.5	-40.6	27.5	35.0

9.1 Shape Analysis

The baffle has been completely modelled and rebuilt again from its initial parabolic shape to its fully cylindrical shape. The actual shape will most likely be chosen based on its deployable and strength factors, rather than its thermal performance. It is therefore thought that it would be interesting to generate some data as a function of the baffle shape.

In order to determine the effect of the baffle shape, several shapes will be tested under equal thermal conditions. The conditions of each shape shall be mentioned first, after which the shape of each model will be elaborated. These are followed by results and concluded with a final discussion.

9.1.1 Baffle Shell Conditions

The goal of this section will be to determine the most effective baffle shape in a thermal sense, but also to distinguish the reasons for their thermal performance differences. In order to make the thermal results of each baffle variation comparable, there are some conditions set which will need to be met by each shape:

Model Grid

The grid of the model determines the amount of nodes in which a certain geometry is divided. If heat impinges on a certain node, the eventual thermal effect will depend on its thermal and thermo-optical properties. This basically described how much heat is absorbed and how this effects its temperature per unit volume. If the entire unit volume would have equal thickness throughout and the geometry would be illuminated evenly, it would not matter in how much nodes it will be defined. This because the amount of heat per unit volume will

be equal throughout.

The node distribution will specifically be important for the interior nodes of the baffle since the top will be exposed to sunlight, while nodes further away from the top will not. One should therefore try to maintain equal node size of the baffle for each shape variation. If the total baffle length of each baffle will be kept the same, one could try to match the grid distribution of the control model more easily, while the difference in width or gradient of the baffle will cause a small difference in respective grid size. As long as the latter difference will be small, the thermal results will be comparable.

Model Dimensions and Orientation

The baffle shape models will differ in shape or will be similar apart from some small differences. Nevertheless, some variables need to be fixed for them to be comparable in terms of their thermal results.

Baffle length
The total length of the baffle, thus the considering the entire geometry is set at 2800mm. The baffle structure is not included here, and for the DST 3.1 model, it will stick 50mm out on top, apart from the MLI blanket. Thus the total length of the MLI blanket is considered to be 2750mm, which is set as the total length for each baffle shape variation (DST 3.x).

Baffle Orientation
Its orientation will be fixed to the telescope, aligned to the optical axis. The baffle shape models are thus not considered to rotate with respect to the remainder of the telescope, or to displace in any direction compared to the control model. The opening and the back of the baffle will thus be situated at equal z distance for each DST 3.x model.

Model Composition

Each DST 3.x model will include the same version of the telescope as defined by the DST 2.7 model. Apart from that they will include a baffle composed of MLI only, consisting of an outer and inner layer with the properties as determined in Chapter 6. All models will have an opening on top, and will be closed at the bottom. The baffle structure is excluded because it will simplify the analysis, as well as it will not be necessary to build a separate structure for each baffle variation.

The baffle housing has been excluded from the analysis too, since it was made inactive before, but because it has overlap with the back of the baffle it made the latter part inactive too. It will be shown in the Figures but excluded from the analysis. The back of the baffle is expected to play a role regarding the minimum temperatures, and since the back of the instrument housing was already made inactive before, excluding or including the baffle housing is not expected to effect the thermal solutions anyways.

Model Differences

The DST 3.x models will be similar for them to be comparable, but also different in order to determine the effect of certain shapes. The control model has an cylindrical shape, while the previous models were parabolic. Some other shapes, like rectangular or spherical, have not been studied yet. Therefore, variations will be taken on known shapes as well as new shapes will be explored.

Model Thermal Environment

The used thermal environmental parameters are in line with those as described in Appendix D *Thermal Modelling Conditions*.

9.1.2 Baffle Shell Geometries

The baffle shell geometry will be simulated for several variations which are based on the initial baffle geometry and the secondary baffle geometry, which are elliptical and cylindrical shaped respectively. Some other variations will be added for it to explore new shapes as mentioned in the previous section. The first model; DST 3.1, shown in Figure 9.1a and 9.2a, can be considered as the control model of the current geometrical model without the baffle structure. The remainder of the models will be elaborated in this section.

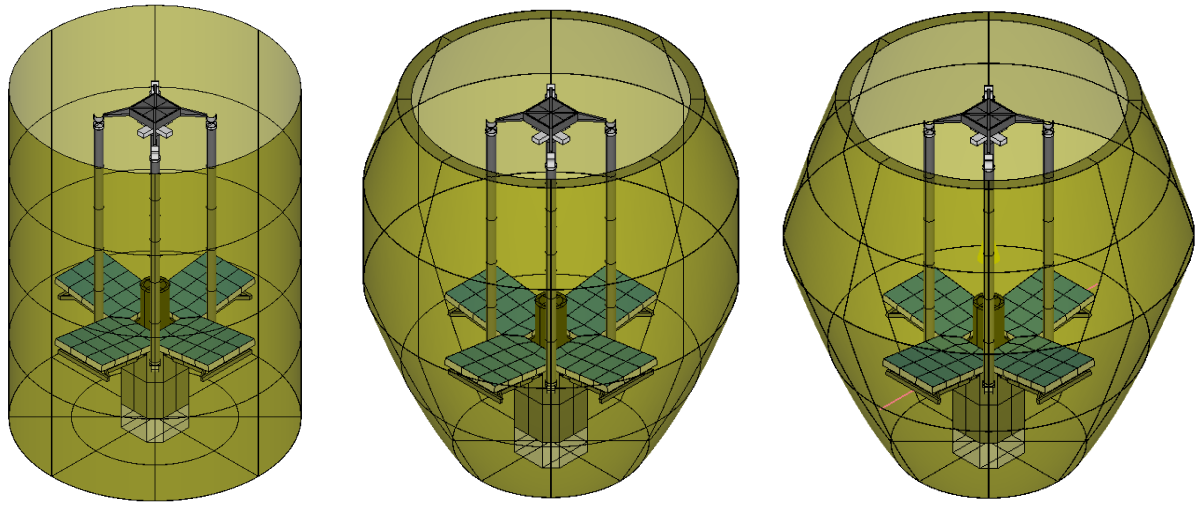

(a) DST 3.1 (Control Model) (b) DST 3.2 (c) DST 3.3

Figure 9.1: Variations of the baffle shell: DST- 3.1, 3.2 and 3.3. Overall view. As constructed within the Workbench of ESATAN TMS.

DST 3.2

DST 3.2, shown in Figure 9.1b and 9.2b, is similar to the initial baffle design without the baffle structure. The initial baffle geometry is composed of cylinders, partial paraboloids and disks. The top disk or ring, was placed there for it to fit nicely to the baffle structure. All the sections together were sized such for it to match the baffle structure closely, without interfering it. Its structural dimensions where sized such for it to meet the length and top-, mid- and bottom- radii as described in the initial baffle design as shown in Chapter 4.

DST 3.3

DST 3.3, shown in Figure 9.1c and 9.2c, is composed of two cones without the cylindrical part in the middle. This model of the baffle is similar to the DST 3.2 model. The cylindrical mid section has been removed, while the top and bottom cones have been extended such for them to meet each other in between. When comparing the models DST 3.1, 3.2 and 3.3, shown in the Figures 9.2a, 9.2b and 9.2c respectively, one could argue that the DST 3.2 model is an intermediate version of the other two. Besides, it is composed of two main sections instead of three which simplifies the model. These were the two reasons for modelling this baffle variation.

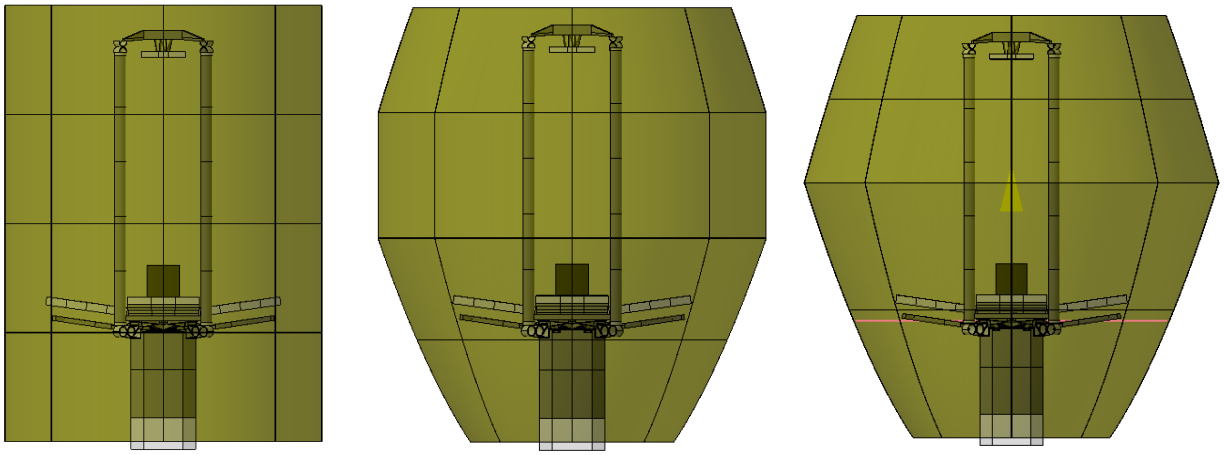

(a) DST 3.1 (b) DST 3.2 (c) DST 3.3

Figure 9.2: Variations of the baffle shell: DST- 3.1, 3.2 and 3.3. Side view. As constructed within the Workbench of ESATAN TMS.

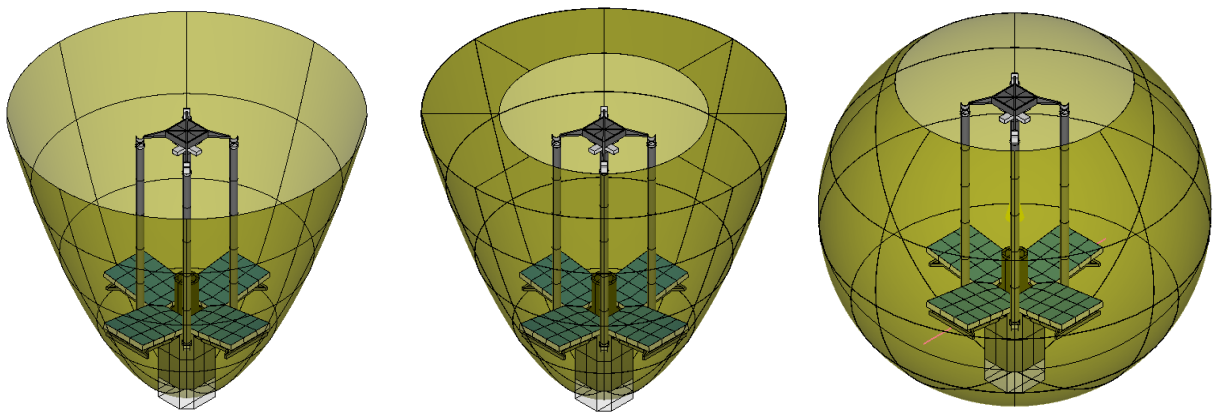

(a) DST 3.4 (b) DST 3.5 (c) DST 3.6

Figure 9.3: Variations of the baffle shell: DST- 3.4, 3.5 and 3.6. Overall view. As constructed within the Workbench of ESATAN TMS.

DST 3.4

DST 3.4, shown in Figure 9.3a and 9.4a, is purely parabolic made such for it to not obstruct the segments with minimal clearance. This model of the baffle has been completely redefined and can be considered as one of the simplest geometries in the sense that it is only composed of one geometry only. A parabolic shape is chosen because the initial baffle shape was parabolic. The parabolic shape has been adjusted such for it to not obstruct the primary mirror segments with minimum clearance. The downside of this shape is the fact that it is completely open at the top, featuring the largest baffle opening of all variations. The DST 3.3 model is composed of two parabolic geometries, with the top one rotated 180 degrees, while this model is composed of only one paraboloid.

DST 3.5

DST 3.5, shown in Figure 9.3b and 9.4a, is a variation on the previous model with a closing disk on top. This model is a variation of DST 3.4, with a ring layer on top with an inner radius of 0.85m. The latter radius is equal in size compared to the top opening of the initial baffle design. This addition is thought to sooth the extremes by means of retaining heat during eclipse and reflecting heat when sunlit, or in short it will be harder for the Sun to impinge on the interior of the baffle.

DST 3.6

The DST 3.6 model shown in Figure 9.3c and 9.4c, is purely spherical. This model is a variation of the initial parabolic geometrical model, made fully spherical with equal total length (2750mm) and equal size of the baffle opening (radius = 0.85m). The radius of the sphere and the opening on top are adjusted such for it to meet the aforementioned parameters. The downside of this geometry is its large mid radius which will drive the size of the MLI blanket.

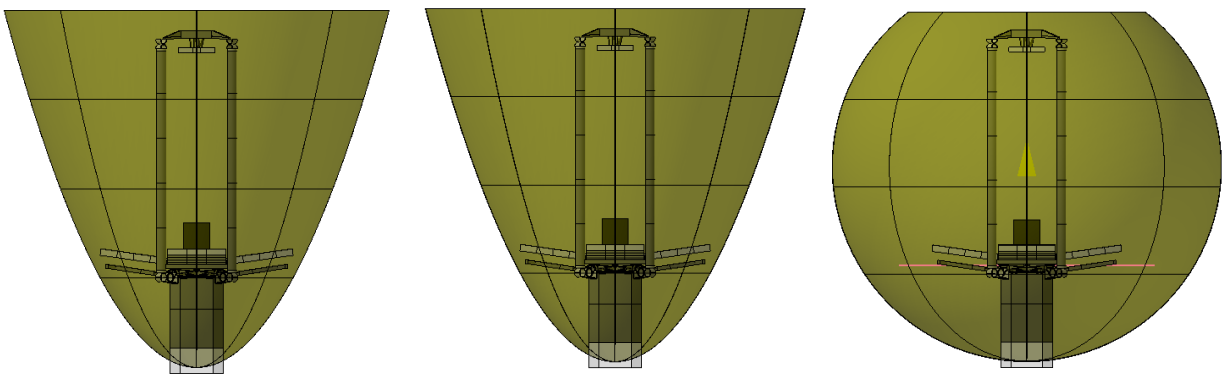

(a) DST 3.4 (b) DST 3.5 (c) DST 3.6

Figure 9.4: Variations of the baffle shell: DST- 3.4, 3.5 and 3.6. Side view. As constructed within the Workbench of ESATAN TMS.

DST 3.7

The DST 3.7 model, shown in Figure 9.5a and 9.5b, is similar to the control model but instead it is made rectangular. This model is a variation of the DST 3.1 model, but instead of it being cylindrical it is made rectangular. The width of this baffle equals the diameter of the cylindrical baffle. This shape has been added since it is quite similar to the actual cylindrical baffle, but then made squared instead of circular.

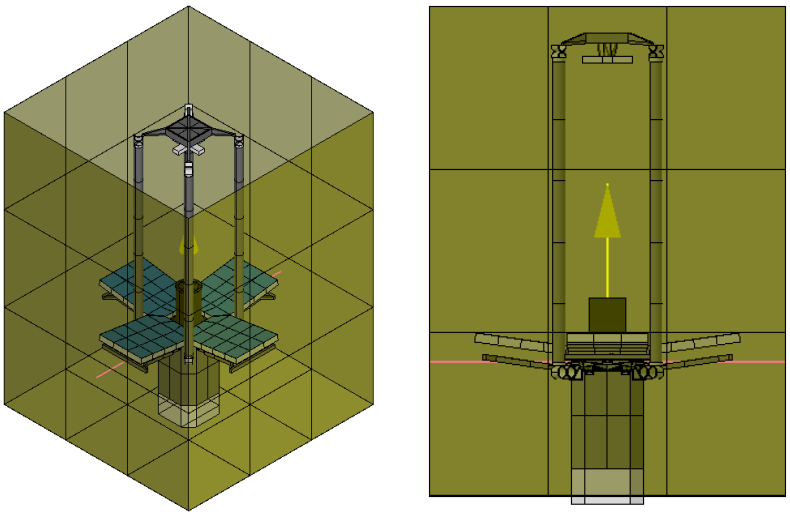

(a) Overall view (b) Side view

Figure 9.5: Variations of the baffle shell: DST 3.7. As constructed within the Workbench of ESATAN TMS.

DST 3.8

The DST 3.8 model, not shown here, is a naked telescope without any baffle. It is included here since the COLD and HOT conditions have not been applied to this model before.

9.1.3 Temperature Results & Analysis

The baffle variations, DST 3.1-3.8, have been subjected to HOT and COLD thermal conditions for the during of ten orbits, for which the temperature results are shown in Table 9.2, 9.3 and 9.4. For each baffle DST 3.x model, the minimum- and the mean average temperature of the COLD case has been depicted, included with the mean average- and the maximum temperature of the HOT case. It is chosen to exclude the maximum- and minimum temperatures of the COLD and HOT conditions respectively, because those are thought to be irrelevant here.

Table 9.2: Temperature results for DST 3.1, 3.2 and 3.3, in degrees Celsius.

	DST 3.1				**DST 3.2**				**DST 3.3**			
	COLD		**HOT**		**COLD**		**HOT**		**COLD**		**HOT**	
	Min	Mean	Mean	Max	Min	Mean	Mean	Max	Min	Mean	Mean	Max
Baffle	-157.5	-70.5	-17.9	135.0	-160.0	-48.3	-1.1	125.0	-155.0	-47.3	0.0	130.0
Spider	-55.0	-48.7	39.6	87.5	-50.0	-46.2	40.9	90.0	-50.0	-46.3	41.0	90.0
TH	-50.0	-44.3	35.5	70.0	-50.0	-43.9	36.7	67.5	-50.0	-44.0	36.9	67.5
M2	-37.5	-38.6	75.1	75.0	-37.5	-37.7	80.8	82.5	-37.5	-37.9	80.9	82.5
Booms	-47.5	-41.9	28.7	55.0	-45.0	-39.8	31.6	52.5	-45.0	-40.2	31.8	52.5
RH	-45.0	-43.3	25.5	30.0	-42.5	-40.2	29.3	35.0	-42.5	-40.7	29.6	35.0
M1	-45.0	-43.3	24.7	30.0	-42.5	-40.7	27.8	32.5	-42.5	-41.1	27.9	35.0
PMSS	-45.0	-43.3	25.4	32.5	-45.0	-40.2	29.3	42.5	-45.0	-40.7	29.6	42.5
IH	-47.5	-43.6	26.3	35.0	-45.0	-40.3	30.3	40.0	-45.0	-40.7	30.6	40.0

The DST 3.1 model functions as the control model from which the temperature differences larger than or equal to 10°C, are marked in green or red. The green coloured boxes indicate an improvement, while a red box indicates a deterioration. The target temperature is here assumed to be 25°C.

Table 9.3: Temperature results for DST 3.4, 3.5 and 3.6, in degrees Celsius.

	DST 3.4				DST 3.5				DST 3.6			
	COLD		HOT		COLD		HOT		COLD		HOT	
	Min	Mean	Mean	Max	Min	Mean	Mean	Max	Min	Mean	Mean	Max
Baffle	-170.0	-68.0	-19.5	147.5	-170.0	-62.3	-9.5	127.5	-190.0	-52.8	6.1	115.0
Spider	-50.0	-44.0	41.1	95.0	-52.5	-46.6	39.1	87.5	-52.5	-48.0	39.9	87.5
TH	-52.5	-48.1	40.7	70.0	-47.5	-42.2	35.1	67.5	-47.5	-43.4	35.4	67.5
M2	-40.0	-40.8	83.2	85.0	-37.5	-36.9	51.5	52.5	-37.5	-37.7	71.5	72.5
Booms	-50.0	-44.9	27.5	62.5	-42.5	-39.0	31.8	47.5	-42.5	-39.0	32.3	50.0
RH	-47.5	-46.7	22.2	25.0	-42.5	-39.4	29.8	35.0	-42.5	-39.2	35.4	40.0
M1	-47.5	-46.4	21.5	27.5	-42.5	-40.6	28.0	35.0	-40.0	-40.0	28.7	37.5
PMSS	-50.0	-46.6	22.1	35.0	-42.5	-39.4	29.8	40.0	-42.5	-39.2	30.7	45.0
IH	-50.0	-46.6	23.1	32.5	-42.5	-39.6	30.5	40.0	-42.5	-39.2	31.9	45.0

Table 9.4: Temperature results for DST 3.7 and 3.8, in degrees Celsius.

	DST 3.7				DST 3.8			
	COLD		HOT		COLD		HOT	
	Min	Mean	Mean	Max	Min	Mean	Mean	Max
Baffle	-122.5	-48.3	-3.6	157.5	-	-	-	-
Spider	-55.0	-49.4	40.3	87.5	-32.5	-6.2	33.8	85.0
Top Hinge	-50.0	-44.8	37.1	70.0	-2.5	19.8	43.1	55.0
M2	-40.0	-39.4	80.2	82.5	102.5	104.6	131.5	132.5
Booms	-47.5	-41.5	29.8	57.5	-20.0	17.6	40.7	67.5
Root Hinge	-45.0	-42.6	26.7	32.5	-92.5	-4.1	8.3	712.5
M1	-45.0	-43.3	25.1	35.0	-62.5	27.2	61.0	217.5
PMSS	-45.0	-42.6	26.6	37.5	-160.0	-29.4	-5.7	7320.0
IH	-47.5	-42.7	8.9	37.5	-127.5	-14.5	8.9	127.5

DST 3.1 & 3.3
As aforementioned, the models DST 3.1-3.3, are similar variations with 3.1 being most straight and 3.3 being most curved. The curvature near the top seems to have a positive effect on the temperatures of the baffle, by means of increasing the average and decreasing the maximum, with little to no effect on the remainder of the telescope.

DST 3.4
The baffle of the DST 3.4 model suffers the most extreme temperature differences, by means of lower minimum and higher maximum temperatures, which is thought to be caused by its relatively large baffle opening. This effect is mostly noticeable for its baffle, followed by the secondary mirror, the spider and the booms.

DST 3.5
The DST 3.5 model has decreased maximum temperatures opposed to the 3.4 model, for the baffle, spider, top hinge, secondary mirror and booms. The maximum temperatures have increased for the root hinges, the primary mirror, the primary mirror support structure and the instrument housing. The same trend is seen for their average temperatures, thus the additional top closing ring layer of the DST 3.5 model is effective in reducing the temperatures of all the components in front of the primary mirror segments, while it is also more effective in insulation the remainder of the telescope.

DST 3.6
The DST 3.6 model has the lowest maximum baffle temperature but also the lowest minimum temperature, featuring the most curvature near the top when compared to the DST- 3.1 and 3.2 model. Thus, it seems that a straight surface is more sensitive for temperature increments, although this should not be interpreted as a fact, since it can also be caused by other factors like grid size for example.

DST 3.7 & 3.8
The average component temperatures of the DST- 3.1-3.7 models do not differ much overall, apart from the baffle and the secondary mirror. The temperatures of the DST 3.8 model are most different, with extreme temperatures for the secondary mirror, the root hinges, primary mirror segments and the primary mirror support structure. Although, it is thought that the latter is rather a modelling error considering that the average temperatures are less effected, which can be caused by sharp edges or imperfect defined geometries.

9.1.4 Heat Flow Results & Analysis

The temperature results as shown in the previous section have indicated some temperature differences which will be elaborated in this section. These difference will be elaborated per component group or several groups.

Secondary Mirror

The heat flow results for the secondary mirror are shown in Figures 9.6a, 9.6b and 9.6c. These Figures depict the heat flow contributions of space (blue) and the baffle interior (red). The heat flow from space towards the secondary mirror is smallest for DST 3.5, while it is largest for DST 3.4. The largest heat flows originate from the baffle interior, although it is smaller during eclipse. This effect is smallest for the DST 3.5 where the baffle is less exposed to space, while it is largest for the DST 3.4 model. These results are in line with the foreseen temperature results.

Booms

The heat flow results for the booms are shown in Figures 9.6d, 9.6e and 9.6f. A similar trend is shown for the booms, although the difference between the DST 3.1 and 3.5 model is smaller. The top closing seems effective in reducing the heat flow from space to the secondary mirror and the booms. However, it is not effective in reducing the heat flow from the baffle to the booms. Therefore, it is not effective in reducing the temperatures for the booms.

Spider

The heat flow results for the spider are shown in Figures 9.6g, 9.6h and 9.6i. The DST 3.4 model has a large baffle opening, which seems to be the reason for the larger heat flow from space and thus the higher temperature. The heat flow from the baffle has not changed. The differences between the DST 3.4 and 3.6 are small, hence the similarity in temperatures.

Instrument Housing, Root Hinges and the Primary Mirror Support Structure

The heat flow results for the baffle are shown in Figures 9.7a and 9.7b. These Figures depict the heat flow contributions of the baffle interior (red), instrument housing (green), root hinges (orange) and the PMSS (yellow). From these results it can be seen that the considered telescope components of the DST 3.1 model have minor heat flow with the baffle, while a similar but stronger trend is seen for the DST 3.6 model.

The heat flow results for space are shown in Figures 9.7c and 9.7d. These results indicate that the considered telescope components receive negligible heat flow from space for both models, while the baffle interior receives larger total heat flow for the DST 3.1 model. The latter would explain the elevated maximum temperature of the baffle. The shown results cannot exclude a specific reason for the increase in temperature for the root hinges, primary mirror support structure or the instrument housing. It could be caused by the difference in behaviour between those component groups and the baffle, although it cannot be said for sure.

9.1.5 Discussion of results

The model with enlarged baffle opening (DST 3.4), features elevated temperatures for most of its SMSS components while featuring reduced temperatures for the remainder of the geometries. This effect is strongest for the secondary mirror. The model with reduced baffle opening (DST 3.5) shows an opposite trend. Further, the fully cylindrical model (DST 3.6) has elevated temperatures for the root hinges, the primary mirror support structures and the instrument housing. Apart from that, the largest effects are seen for the baffle itself. A larger opening causes the baffle interior to absorb larger amounts of heat, which drives temperature. Therefore, the baffle opening should not be enlarged, nor should the bottom be widened.

The total heat flow results have indicated that a potential top closing, as seen for the DST 3.5 model, can be effective in decreasing heat from and to the secondary mirror. A wide baffle with a large opening is not desired since both the baffle and the top section of the telescope become more exposed. The top closing is also effective in decreasing the heat flow from space to, among others, the spider and the booms. Nevertheless, their temperature have not changed much since the heat flow from the baffle is not effected by the top closing.

Thus to conclude, the effect of the baffle shape itself is relatively small, with the condition that the opening is small and that the baffle is not made unnecessary wide. Further, an additional top closing may decrease heat flow from space towards the secondary mirror.

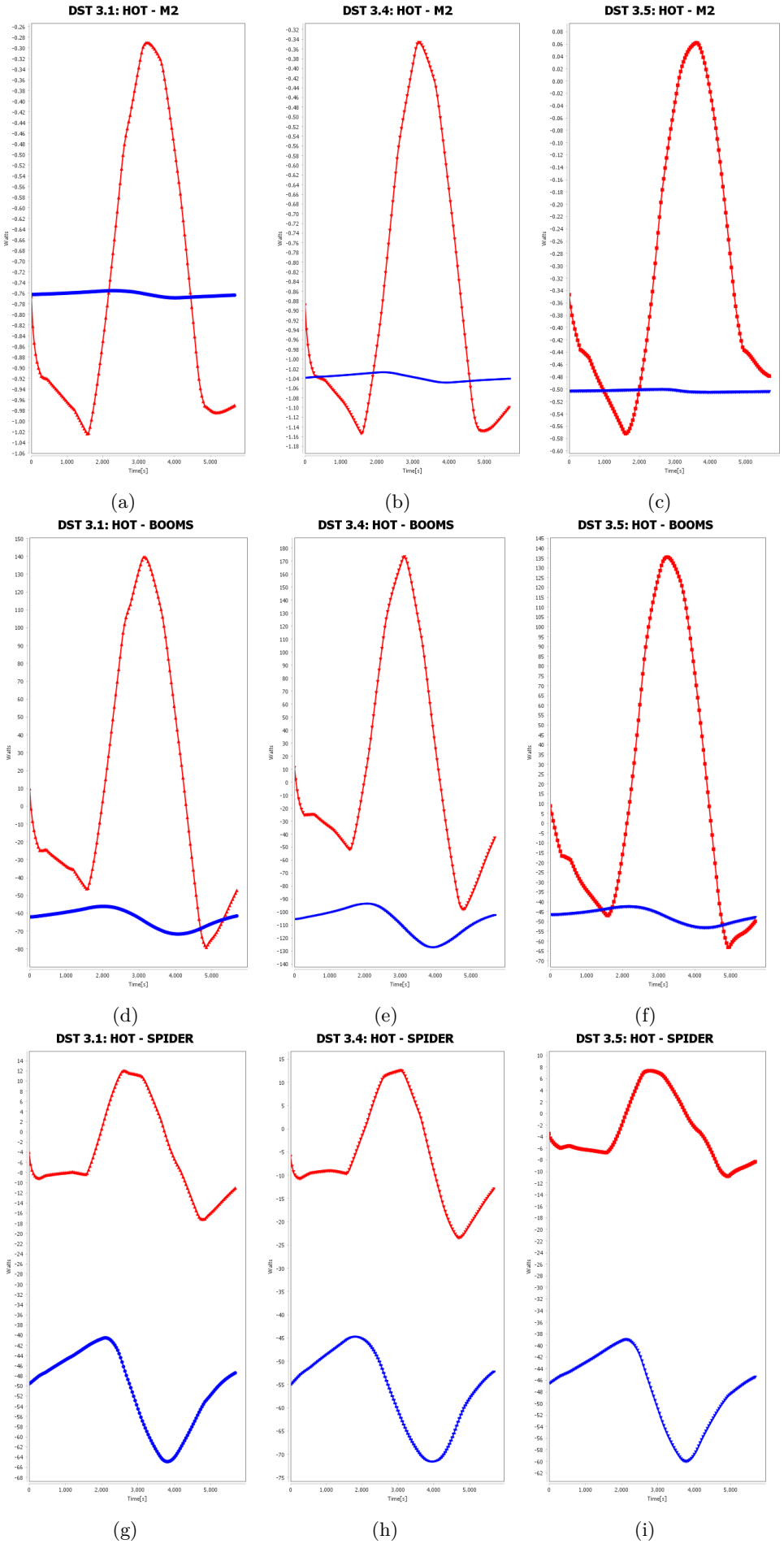

Figure 9.6: Total heat flow results for the secondary mirror (a-c), booms (d-f) and spider (g-i), towards the baffle interior (red) and space (blue). For the duration of one orbital period with 40 second sampling, HOT thermal conditions. As visualised using the heat chart function in ESATAN TMS Workbench.

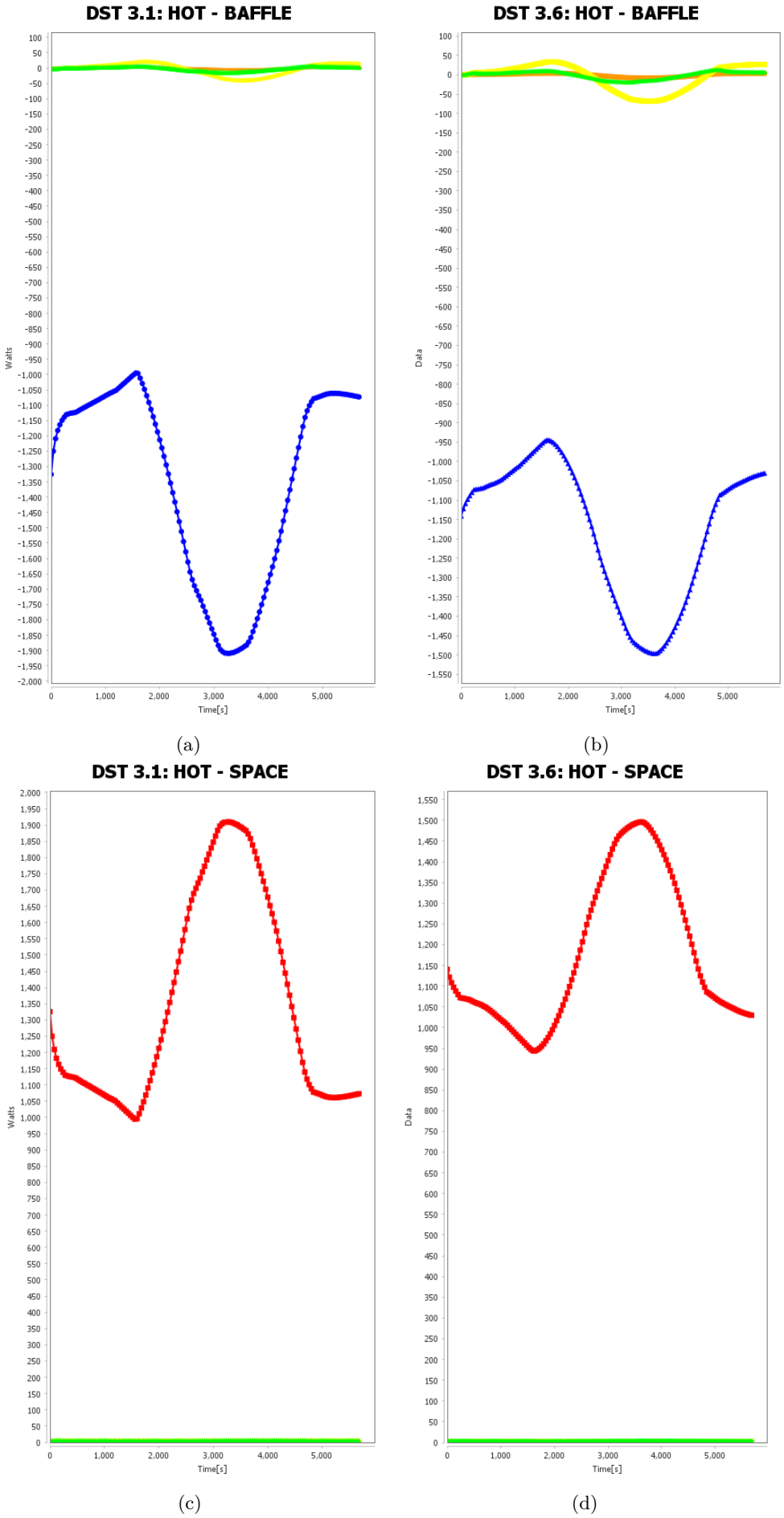

Figure 9.7: Total heat flow results for the baffle interior (a,b) and space (c,d), towards the baffle (red), space (blue), instrument housing (green), root hinges (orange) and the PMSS (yellow). For the duration of one orbital period with 40 second sampling, HOT thermal conditions. As visualised using the heat chart function in ESATAN TMS Workbench.

9.2 Position Analysis of the Baffle Blanket

The position of the MLI blanket with respect to the booms has not been fixed yet and therefore it is thought that it would be interesting to see how the configuration effects the thermal solution. The comparison will include several configurations (9.2.1), results & analysis (9.2.2) and discussion of results (9.2.3).

9.2.1 Configurations

Three different positions of the MLI blanket will be tested, namely: external: DST 2.7 (Figure 9.8a), in between: DST 4.2 (Figure 9.8b), and internal: DST 4.3 (Figure 9.8c). These Figures include a transparent MLI blanket which is made such for it to depict the remainder of the telescope, while in reality it will be opaque. The properties of the MLI blanket remain unchanged while the radii have been adjusted accordingly for them to fit the chosen configuration.

The DST 2.7 model has its baffle structure located internally of the MLI blanket, apart from the top torus, while for DST 4.2 half of the baffle structure is located within and half outside the blanket. The DST 4.3 model has its entire baffle structure located externally from the MLI blanket. Another configuration (DST 4.4), not shown here, has equal MLI configuration as the DST 4.3 model with the only difference that the booms are covered in MLI.

Four different MLI configurations as shown in Figure 9.8, will be tested for their differences. The only difference between these configurations is the position of the MLI blanket with respect to the boom structure, apart from the DST 4.4 which has different thermo-optical properties for its baffle structure.

9.2.2 Results & Analysis

The 4.x models have been exposed under NOM conditions for the duration of ten orbital periods with a sampling rate of 400 seconds. These conditions are chosen because it was thought to be sufficient for allocating the effect of the different MLI configurations. The corresponding results are summarised in Table 9.5 and 9.6. The DST 2.7 model functions as the control model, similar to the DST 3.1 with the only difference that the DST 2.7 includes a baffle structure. Just as in the previous section, differences larger than 10 degrees Celsius in comparison with the control model, have been marked yellow.

First Impression

First of all, it is thought that the baffle blanket is not effected much by its position with respect to the baffle structure, apart from the DST 4.4 which features different thermo-optical properties for its baffle structure. The major differences can be seen for the baffle structure itself, which is thought to be caused by the fact that its more or less exposed to the space environment. Besides, the baffle structure of the DST 2.7, 4.2 and 4.3 models are coated with the magic black coating, which features very high- solar absorptive and emissivity properties. The latter optical property is thought to drive the decrease in temperature when faced to space, with the lowest baffle temperatures seen for the DST 4.3 model.

DST 4.2

The DST 4.2 model features larger global ΔT for the root hinges, primary mirror support structure and instrument housing. This is thought to be caused by the boom structure which retracts heat from the telescope when it cold, but also radiates heat when its hot. Thus, the baffle blanket does not isolate the entire telescope in this situation since heat can be conducted within the baffle structure from the interior to the exterior and vice versa. The latter is in this case undesired behaviour since heat should be retained during eclipse while heat is reflected or rejected when sunlit.

DST 4.3 & 4.4

The DST 4.3 model has the largest baffle structure area facing space, thus it is colder compared to the 2.7 and the 4.2 model. The DST 4.4 baffle structure is encapsulated in FEP/VDA and therefore it received only a relatively tiny amount of heat, which could explain why it is substantially colder. The global temperature differences for the baffle structure are largest for the DST 4.3 model, while they are smallest for the DST 4.4 model. Thus without any additional coatings, an exterior baffle can be considered significantly exposed to space.

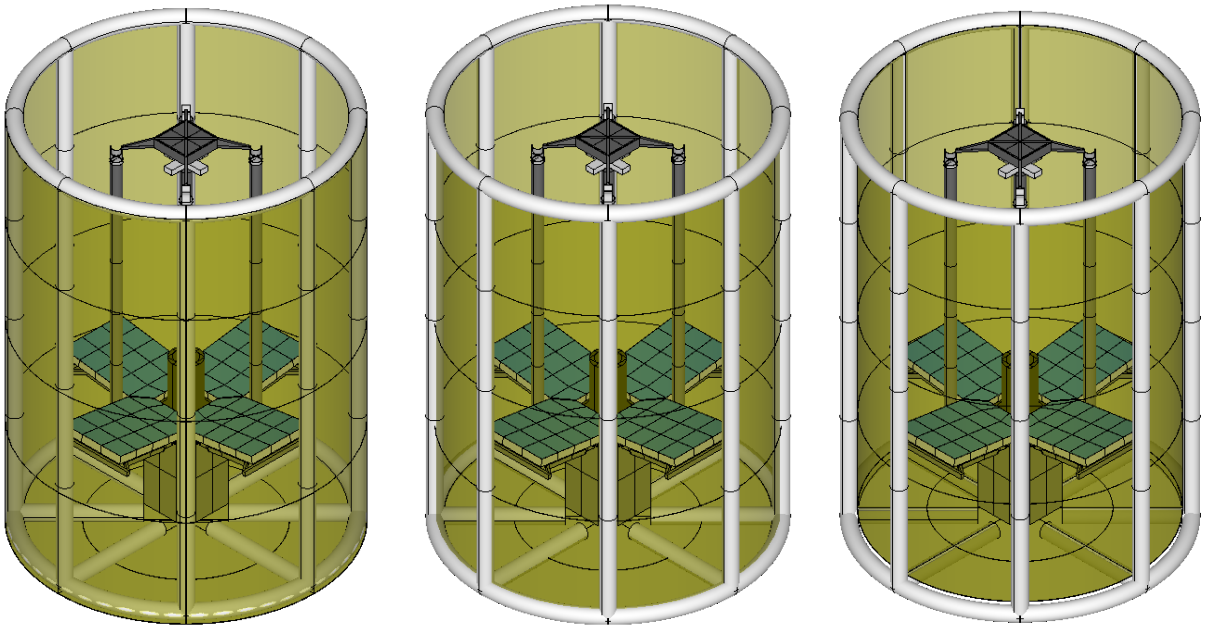

(a) DST 2.7 (b) DST 4.2 (c) DST 4.3 and DST 4.4

Figure 9.8: The different considering MLI configurations (DST 4.x): external (a), in between (b), and internal (c). As constructed in the ESATAN TMS Workbench.

Table 9.5: Temperature results for DST- 2.7 and 4.2, in degrees Celsius.

	DST 2.7			**DST 4.2**		
	Min T	Mean T	Max T	Min T	Mean T	Max T
Baffle Blanket	-90.0	-17.5	122.5	-87.5	-15.0	125.0
Baffle Structure	-25.0	10.0	110.0	-75.0	-10.0	75.0
Spider	2.5	12.5	30.0	-2.5	12.5	32.5
Top Hinges	0.0	10.0	22.5	0.0	10.0	25.0
M2	27.5	30.0	30.0	27.5	30.0	30.0
Booms	2.5	10.0	20.0	0.0	10.0	22.5
Root Hinges	5.0	10.0	12.5	-2.5	10.0	27.5
M1	5.0	7.5	12.5	0.0	7.5	15.0
PMSS	2.5	10.0	17.5	-22.5	10.0	45.0
IH	0.0	10.0	20.0	-22.5	7.5	40.0

Table 9.6: Temperature results for DST- 4.3 and 4.4, in degrees Celsius.

	DST 4.3			**DST 4.4**		
	Min T	Mean T	Max T	Min T	Mean T	Max T
Baffle Blanket	-87.5	-10.0	127.5	-90.0	-35.0	127.5
Baffle Structure	-100.0	-25.0	85.0	-82.5	-50.0	-2.5
Spider	0.0	12.5	30.0	0.0	10.0	27.5
Top Hinges	0.0	10.0	22.5	-2.5	7.5	20.0
M2	27.5	30.0	30.0	27.5	27.5	30.0
Booms	2.5	10.0	20.0	0.0	5.0	17.5
Root Hinges	2.5	10.0	15.0	-2.5	2.5	7.5
M1	2.5	7.0	12.5	0.0	0.0	5.0
PMSS	0.0	10.0	20.0	-5.0	0.0	12.5
IH	-2.5	7.5	20.0	-5.0	2.5	15.0

9.2.3 Discussion of Results

The temperatures of the telescope are in general not effected when considering a fully internal- or external MLI blanket, apart from the in between configuration (DST 4.2). This because, the baffle structure conducts heat from the outside to the inside or vice versa, due to which the telescope suffers larger ΔT. The in between configuration can therefore be considered undesired.

The exterior baffle (DST 4.3) features the largest ΔT, which is most likely undesired. It is therefore thought that the baffle structure of the external configuration (DST 4.3) should indeed by covered in MLI, as for the DST 4.4 model. Coating the boom structure is not desired since coatings tend to degrade in time, as was concluded in the preceding literature study [8]. Besides, the booms are relatively thin thus a small change in the α/ϵ factor can have large effect.

The DST 4.4 model basically features an entire baffle structure encapsulated in MLI. Considering that the baffle needs to be deployable this is expected to add complexity to the design. Besides, it will most likely be heavier compared to the magic black coating. Currently, there are no requirements provided for the baffle. The desired non-thermal properties are therefore unknown.

Thus to conclude, it is thought that the configurations as used for the DST 2.7 model and the DST 4.4 model are most suitable. Considering that the baffle needs to be deployed and that it should be kept as simple as possible, it is thought that the fully internal baffle structure configuration is the **current best** option.

9.3 Top Closing Analysis

The DST 3.5 model features an additional top closing which seems to decrease the total heat flow to the secondary mirror. Besides, the current baffle designer (A. Korhonen) was curious whether a top closing would be an useful addition or not. Therefore, such an addition will be simulated in this section.

9.3.1 Top Closing Geometries

The top closing will be modelled as a disk with an outer radius equal to the radius of the cylinder, while the inner radius will be adjusted such for it to form a flat ring of MLI. This flat ring will be composed of MLI only without any additional structure. All thermal model variations in this section will be similar to the DST 2.7 model, with the difference in top closing addition. Besides, the blanket has been extended a bit on top for it to cover the top torus of the baffle structure completely from the sides. The thickness of each top closing or flat ring will be considered as the outer radius minus the inner radius. The simulations will be run for three configurations.

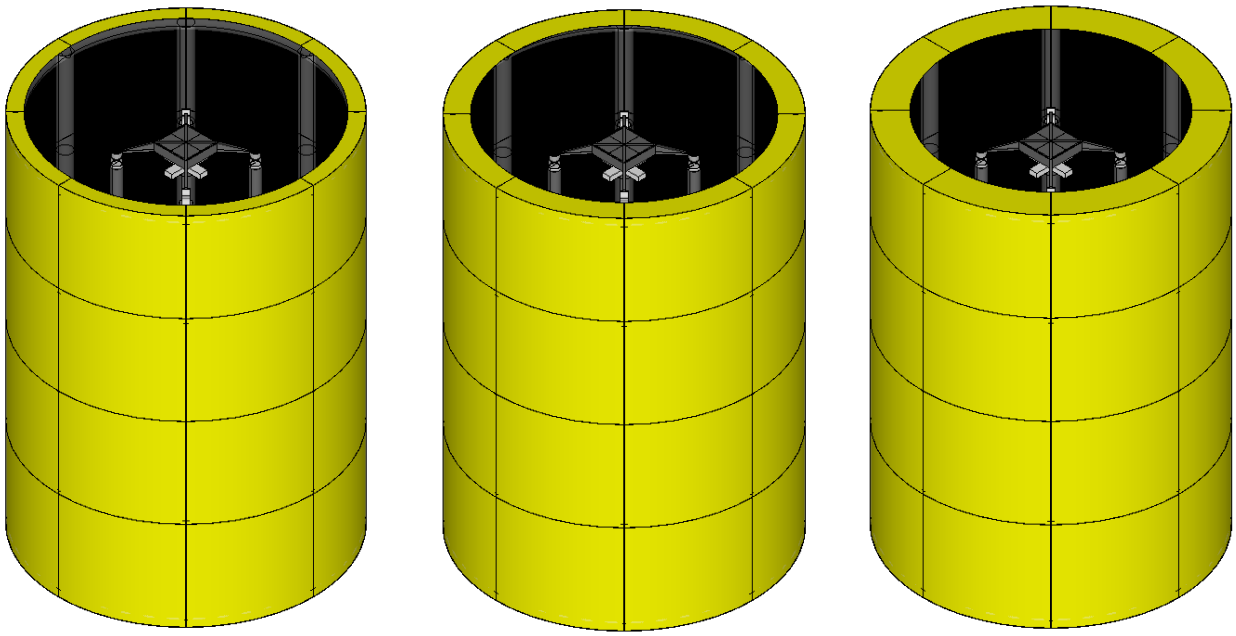

(a) DST 5.1 (b) DST 5.2 (c) DST 5.3

Figure 9.9: Visualisation of the baffle with 10cm closing (a), 15cm closure (b) and 22cm closure (c). As constructed in the ESATAN TMS Workbench.

DST 5.1
The DST 5.1 model has a top closing of 10cm, as shown in Figure 9.9a. This thickness is chosen because the booms of the baffle structure have a diameter of 10cm, thus the top ring covers the entire top torus of the baffle structure when seen from above.

DST 5.2
The DST 5.2 model has a top closing with a inner radius of 0.85cm, as shown in Figure 9.9b. The opening of the baffle would be equal in size when compared to the initial model, which is the reason for choosing this configuration.

DST 5.3
The DST 5.3 model has a top closing of 22cm, as shown in Figure 9.9b. This thickness is chosen such for it to have minimum clearance with respect to the line of sight of the primary mirror segments.

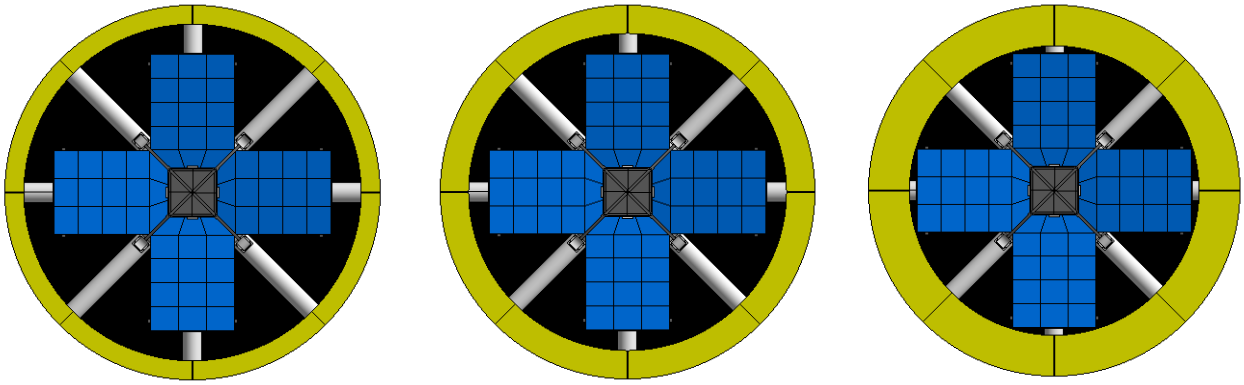

(a) DST 5.1 (b) DST 5.2 (c) DST 5.3

Figure 9.10: Visualisation of the front of the baffle with 10cm closing (a), 15cm closure (b) and 22cm closure (c). As visualised within the ESATAN TMS Workbench.

9.3.2 Temperature Results & Analysis

The 5.x models have been exposed to COLD and HOT thermal conditions. The results of the simulations are depicted in Table 9.7. The difference larger or equal to 10 degrees Celsius are marked in red and green, where green indicates an improvement and red a deterioration.

Table 9.7: Temperature results for DST- 5.1, 5.2 and 5.3 in degrees Celsius, for COLD and HOT conditions.

	DST 5.1				DST 5.2				DST 5.3			
	COLD		HOT		COLD		HOT		COLD		HOT	
	Min	Mean	Mean	Max	Min	Mean	Mean	Max	Min	Mean	Mean	Max
B-B	-125.0	-38.9	0.9	130.0	-122.5	-38.9	0.9	127.5	-122.5	-39.0	0.9	125.0
B-S	-55.0	-39.0	31.2	127.5	-52.5	-38.5	31.4	117.5	-50.0	-38.1	31.7	115.0
Spid.	-52.5	-46.5	37.9	80.0	-50.0	-45.8	37.1	70.0	-50.0	-44.9	35.7	65.0
T-H	-47.5	-43.0	34.5	70.0	-47.5	-42.4	34.0	67.5	-47.5	-41.8	33.2	65.0
M2	-37.5	-36.7	40.3	40.0	-37.5	-36.6	33.8	35.0	-37.5	-36.6	32.4	32.5
Boom	-45.0	-41.5	29.8	50.0	-45.0	-40.9	30.0	47.5	-45.0	-40.2	30.5	45.0
R-H	-43.3	-42.3	27.2	30.0	-42.5	-41.5	27.7	32.5	-42.5	-40.6	28.5	32.5
M1	-42.5	-42.5	26.2	30.0	-42.5	-41.8	26.6	30.0	-42.5	-41.0	27.3	32.5
PMSS	-45.0	-42.3	27.2	37.5	-45.0	-41.5	27.7	35.0	-42.5	-40.6	28.5	35.0
IH	-45.0	-42.4	27.9	37.5	-45.0	-41.6	28.4	37.5	-42.5	-40.8	29.1	37.5

Baffle Temperatures

From the HOT results it can be seen that the maximum temperature of the baffle blanket does decrease for an increase in thickness of the top closing, although the effect is minimal (± 2.5°C for DST 5.3). The top torus of the baffle structure is partly insulated on top, due to the addition of the MLI material for all DST 5.x models, but sadly it does not effect its temperatures. The COLD results showed small changes only, with the largest increase for the baffle structure (+7.5 °C), which seems to be better insulated. The remainder of the COLD results were thought to be irrelevant and will therefore not be further elaborated on.

Telescope Temperatures

The remainder of the telescope geometries are effected to the minimum, apart from the secondary mirror and the spider. A sort of similar effect was seen for the DST 3.5 model, showed in Table 9.3, which included a similar top closing for it to decrease the relatively high opening of the fully parabolic shaped baffle. The closing ring seems to effects the secondary mirror due to which its mean temperature has decreased.

9.3.3 Heat Flow Results & Analysis

In order to allocate the reason for this drop in temperature, additional heat flow results have been generated for the secondary mirror and the spider. These results are shown in Figure 9.11 and 9.12 respectively. The total heat flow results depict the radiative heat flows from the secondary mirror and the spider towards the other geometries and space, for HOT conditions. The Figures do not include the heat flows of the primary mirror, instrument housing, primary mirror support structure and root hinges because their contributions are negligible. The top hinges are kept in there because those are situated nearby, but also since it can be used as the zero line of the graph. The node 99999 is representative of the space environment.

Secondary Mirror

Based on the total heat flow of the secondary mirror, shown in Figure 9.11, it can be seen that the interaction with the baffle blanket (mentioned as baffle shell in the legend of the graph) has shifted upwards for a top closure of 15cm, with an even more upwards effect for the top closure of 22cm. The amplitudes of the graphs are more or less similar for the three models (± 0.2). This means that a larger amount of net heat is rejected compared to what is absorbed. This effect is strongest for the closure of 22cm. Another difference can be found for the heat absorption by the space environment (node 99999). This has decreased for a top closure of 15cm from 0.428W to 0.336W, while it has decreased a bit further for a top closure of 22cm (0.298W).

Thus, it seems that the top closure effects the secondary mirror such that it absorbs less net heat from the space environment and the baffle blanket. Therefore, the temperature of the secondary mirror decreases too. Considering that the contribution of space is constant, it is most likely that its main heat source is OLR.

Spider

The total heat flow of the spider, shown in Figure 9.12, features different behaviour when compared to the secondary mirror. The spider has a minimal amount of heat flow interaction with the top hinges, the secondary mirror and the booms. The major contributors are the baffle structure, the baffle blanket and the space environment (in the respective order). The addition of the top closing does not seem to effect the heat flow interaction with the baffle. However, it does decrease the contribution of the space environment. This effect is almost not noticeable from the graphs, but it is there. Apparently, this is sufficient for decreasing the maximum temperatures as suffered by the spider.

The total heat flow with the space environment is not constant. This is thought to be caused by the influence of sunlight, which is either blocked by the baffle or not. Thus, this would indicate that the spider is effected by the effects of sunlight.

9.3.4 Discussion

The radiative heat flux contributions by the baffle blanket and the space environment are largest, irrespective of the top closing. The secondary mirror receives less heat flow from space and the baffle blanket, for increased thickness of the top closing. The top closing does not seem to be effective in reducing the heat flow to the spider. This is thought to be caused by the orientation of the spider which is situated right in the middle of the opening. The top closing seems to decrease the effects by the sun slightly, which seems to reduce the maximum experienced temperatures. The main OLR contribution is not effected, which is thought to drive the average temperatures. Hence the negligible difference in average temperature of the spider.

Thus to conclude, an additional top closing is effective in reducing the temperatures as experienced by the secondary mirror only. It is not considered effective in reducing the temperatures of any other geometries. Further, an additional top closing is expected to add complexity to the baffle design as well as deployment. Therefore, it is **not** recommended to include an additional top closing to the current design.

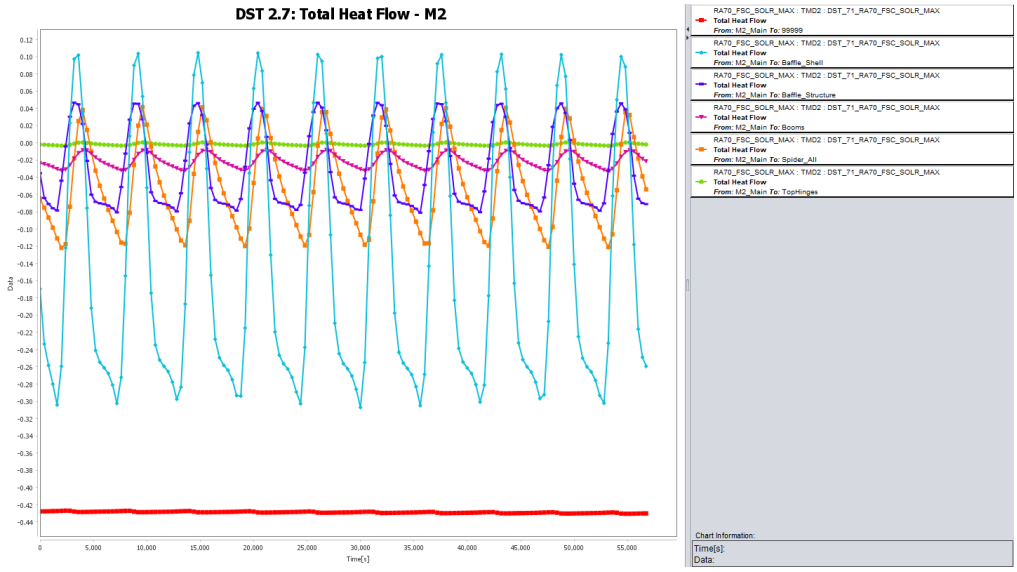

(a)

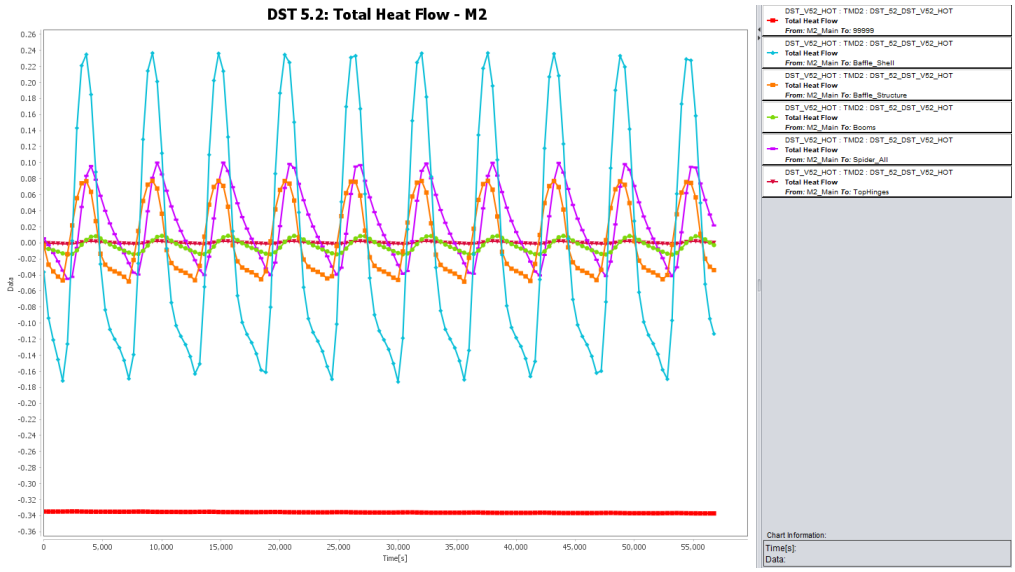

(b)

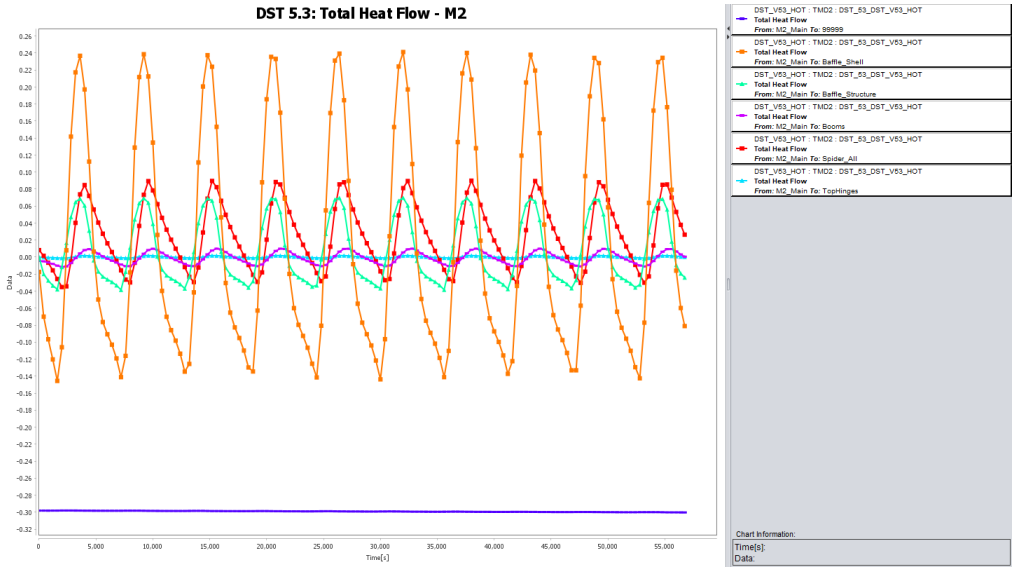

(c)

Figure 9.11: Total heat flow results for the secondary mirror, in Watts. Results visualised using the heat chart function in the ESATAN TMS Workbench.

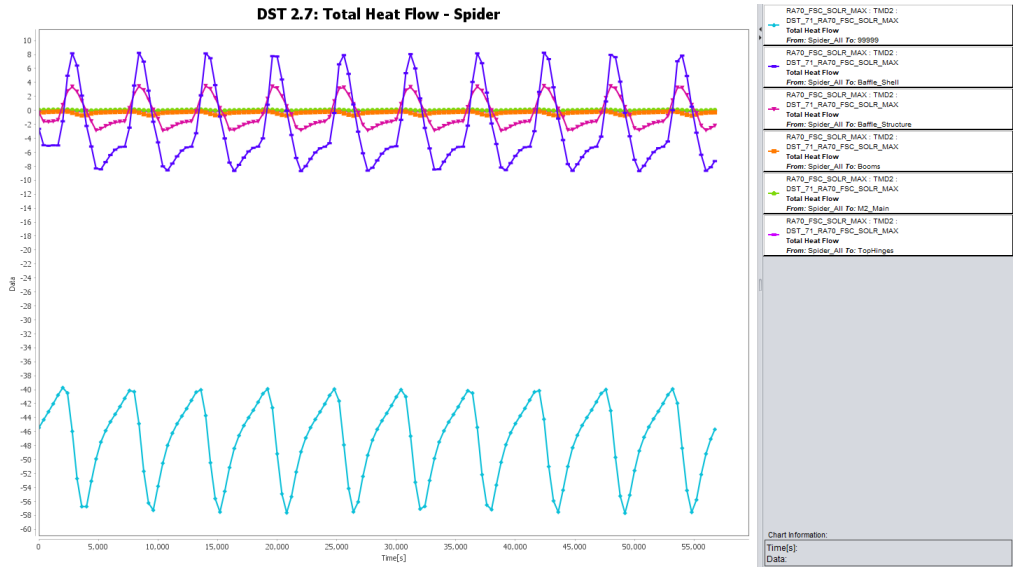

(a)

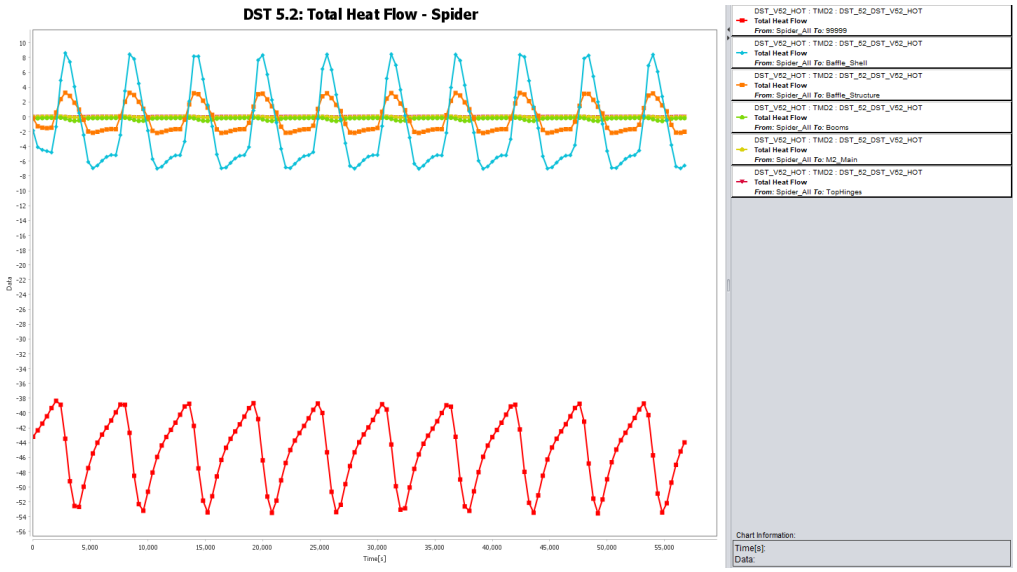

(b)

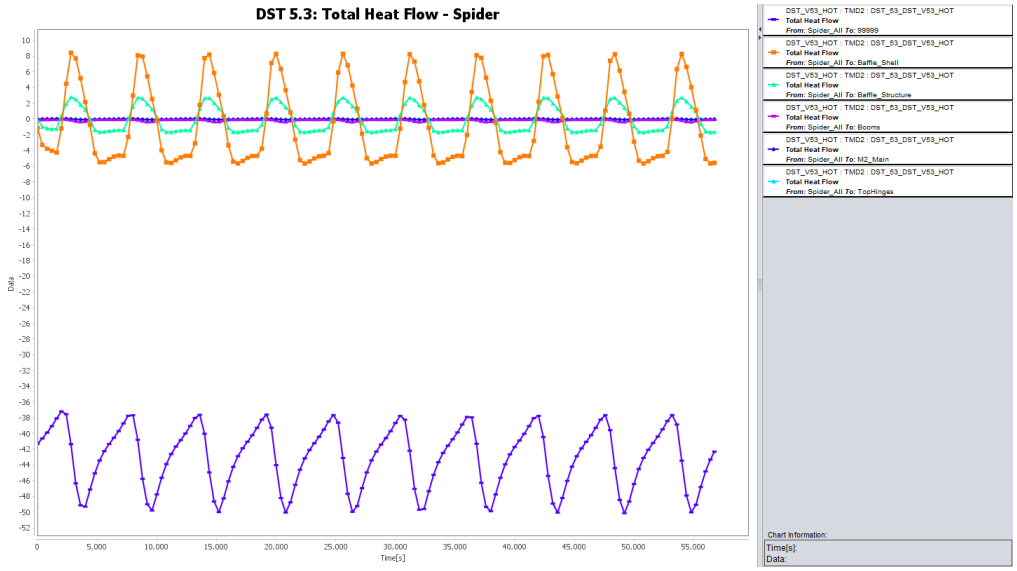

(c)

Figure 9.12: Total heat flow results for the spider, in Watts. Results visualised using the heat chart function in the ESATAN TMS Workbench.

9.4 Dimensional Analysis

The dimensions of the baffle have been determined by its designer providing sufficient clearance with the telescope. The effect of the shape of the baffle has been simulated in previous sections. The effect of its dimensions, thus its diameter and it length, has not been simulated before. Therefore, it is thought that it could be informative to simulate this effect, especially since the baffle is subject to change in the nearby future.

9.4.1 Dimensional Conditions

The difference in dimensions as imposed earlier should be defined such for it to be comparable with control model. Therefore, certain restrictions and boundary conditions are given in between which the baffle dimensions can be adjusted.

Diameter of the Baffle

The diameter of the baffle design is currently fixed at 2m, where the latter denotes the position of the baffle blanket. The primary mirror segments extend ± 75cm in x- and y direction (taken from 2.7 CATIA model), thus the baffle diameter could in theory be reduced down to 1.7m if the baffle structure (10cm per side) would be allowed to touch the segments. Reducing the diameter of the baffle will be majorly interesting since it will also reduce mass.

Length of the Baffle

The total length of the baffle including its structure is currently fixed at 2800mm. The bottom of the baffle attaches to the baffle housing as shown before. The latter setting will remain unchanged but the total length of the baffle can be shortened or lengthened. The baffle housing is thought to have a height no more than 30cm, although the design has not been fixed yet. The amount of material of the baffle which extends the telescope is thus subject to change. It is expected that the length of the baffle should be sufficient for it to prevent sunlight from impinging the telescope directly. The telescope has a length of 2445mm, baffle housing not included, thus the baffle should extend at least the telescope plus some part of the baffle housing.

9.4.2 Dimensional Geometries

The conditions to which the baffle geometry can be adjusted have been mentioned in the previous section. The diameter of the baffle can either be extended or shortened, while the same applies for its length. These two adjustments have been separately initially, after which a preferable combination of the two has been made in the end.

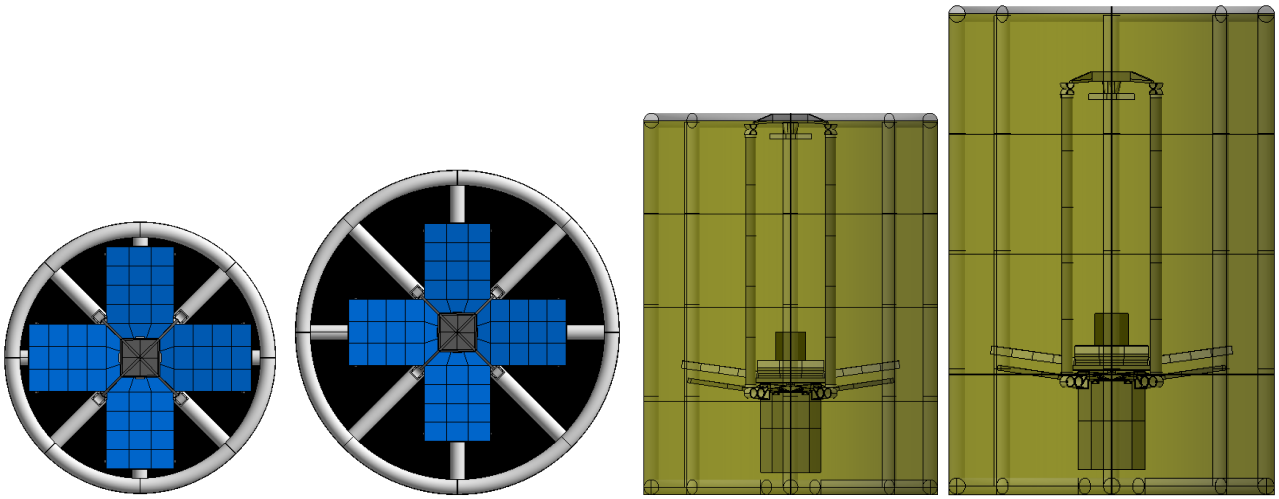

(a) DST 6.1 (b) DST 6.2 (c) DST 6.3 (d) DST 6.4

Figure 9.13: Visualisation of the baffle for configurations narrower (a), wider (b), shorter (c) and longer (d), as opposed to DST 2.7. Figures are scaled to real size. As constructed in the ESATAN TMS Workbench.

DST 6.1

The baffle diameter can be shortened since the baffle structure of the control model (DST 2.7), has around 15cm clearance with the primary mirror segments. A clearance of 5cm is thought to be minimal, hence a decrease of

it diameter with 10cm has been be applied throughout, as visualised in Figure 9.13a.

DST 6.2
Unforeseen factors could be such that the diameter of the baffle has to be extended. For the results to be more or less linearly comparable with the diameter, an increase of the diameter with 10 cm has been found sufficient. The visualisation of this extension is shown in Figure 9.13b.

DST 6.3
The baffle length of this model will be made such for it line up with the telescope in z-direction. This means that the telescope will be completely covered from the sides, although small rotations with respect to the source will expose the telescope. When including the baffle housing and considering that the baffle will be mounted in the middle of this housing, the baffle should extend (2800-2445-150) 205mm from the telescope. The baffle of the DST 6.4 models is therefore shortened with 200mm, as visualised in Figure 9.13c.

DST 6.4
By lengthening the baffle one could potentially decrease the amount of solar flux which would otherwise impinge directly onto the telescope geometries. By means of comparing the effects of baffle length, the baffle has been extended by 200mm of which the result is visualised in Figure 9.13d.

DST 6.5
Finally, a combination of the aforementioned factors has been applied in which the baffle is lengthened and made narrower. The DST 6.5 model can therefore be considered as a combination of DST 6.1 and 6.4.

9.4.3 Results

The DST 6.x models have been subjected to COLD and HOT conditions for which the results are shown in Table 9.8 and 9.9, for which the difference larger or equal to 10 degrees Celsius are marked in red and green, where green indicates an improvement and red a deterioration.

Changing the dimensions of the baffle alters the amount of radiative heat impinging on the satellite geometries, as well as the amount of radiative heat which is distributed among the components. It is therefore thought that it would be interesting to know how the total steady state heat flows from the space environment changes for all DST 6.x models, for HOT conditions. These results are shown in Table 9.10.

Table 9.8: Temperature results for DST- 6.1, 6.2 and 6.3, in degrees Celsius.

	DST 6.1				DST 6.2				DST 6.3			
	COLD		HOT		COLD		HOT		COLD		HOT	
	Min	Mean	Mean	Max	Min	Mean	Mean	Max	Min	Mean	Mean	Max
B-B	-122.5	-37.0	-2.8	117.5	-122.5	-37.1	-2.5	132.5	-122.5	-37.3	-2.6	125.0
B-S	-55.0	-34.5	31.2	110.0	-57.5	-34.8	36.8	122.5	-57.5	-30.2	31.5	112.5
Spid.	-50.0	-43.9	36.7	72.5	-52.5	-46.2	39.5	87.5	-37.5	-23.5	41.6	97.5
TH	-45.0	-40.1	34.0	67.5	-45.0	-41.9	35.1	70.0	-47.5	-35.9	42.9	72.5
M2	-35.0	-34.5	33.4	35.0	-35.0	-35.7	59.1	60.0	-32.5	-31.2	91.6	92.5
Boom	-40.0	-38.8	29.9	47.5	-42.5	-39.6	29.8	50.0	-42.5	-39.8	30.3	60.0
RH	-40.0	-39.6	27.1	30.0	-42.5	-40.5	26.9	30.0	-40.0	-40.5	26.7	30.0
M1	-39.8	-39.8	26.3	30.0	-40.0	-40.7	25.9	30.0	-40.0	-40.6	25.9	92.5
PMSS	-40.0	-39.6	27.1	32.5	-42.5	-40.7	26.9	35.0	-42.5	-40.5	26.7	35.0
IH	-42.5	-39.7	27.6	35.0	-42.5	-40.6	27.9	37.5	-42.5	-40.6	27.6	37.5

9.4.4 Temperature Analysis

The effect of making the baffle narrower, wider, longer or shorter is mainly seen on the baffle itself, and the components near the opening of the baffle. In the previous section it was seen that the secondary mirror decreased in temperature for increasing thickness of the top closing, thus a smaller opening of the baffle led to a decrease in temperature of the secondary mirror.

DST 6.1 & 6.2
By making the baffle narrower one reduces the baffle opening. This alternation seems to decrease the temperatures of the secondary mirror and the spider.
The opposite effect is seen when making the baffle wider. Besides, the maximum temperatures as suffered by the baffle seem to decrease with decreased diameter of the baffle. The opposite is happening for increased diameter of the baffle.

Table 9.9: Temperature results for DST- 6.4 and 6.5, in degrees Celsius.

	DST 6.4				DST 6.5			
	COLD		HOT		COLD		HOT	
	Min	Mean	Mean	Max	Min	Mean	Mean	Max
Baffle Blanket	-122.5	-37.2	-2.5	132.5	-122.5	-37.0	-2.6	125.0
Baffle Structure	-57.5	-35.0	31.7	125.0	-55.0	-34.5	31.5	117.5
Spider	-45.0	-41.7	25.8	45.0	-45.0	-41.0	25.9	42.5
Top Hinges	-42.5	-39.7	28.6	40.0	-42.5	-39.0	29.1	40.0
M2	-37.5	-36.4	29.7	30.0	-37.5	-36.5	29.5	30.0
Booms	-42.5	-39.6	29.4	45.0	-40.0	-39.2	29.4	45.0
Root Hinges	-40.0	-40.3	27.1	30.0	-40.0	-39.8	27.2	30.0
M1	-40.0	-40.6	26.1	30.0	-40.0	-40.0	26.3	30.0
PMSS	-42.5	-40.3	27.0	35.0	-40.0	-39.8	27.2	35.0
IH	-42.5	-40.4	27.9	37.5	-42.5	-39.8	27.8	35.0

Table 9.10: Total heat flow steady state results from the space environment (node: 99999) towards the geometries of the DST 6.x models and the control model (DST 2.7), for HOT conditions in Watts.

	DST 2.7	DST 6.1	DST 6.2	DST 6.3	DST 6.4	DST 6.5
Baffle Blanket	2781.7	2401.0	3181.8	2589.1	2604.2	2560.4
Interior B-B	1008.0	898.0	1097.1	925.0	1070.0	963.2
Baffle Structure	645.2	566.4	728.8	639.8	650.2	571.6
Spider	45.5	43.3	47.3	57.8	31.4	29.2
Top Hinges	10.1	9.3	10.8	14.6	7.0	6.2
M2	0.4	0.3	0.6	1.1	0.2	0.18
Booms	49.3	40.1	59.1	71.9	35.8	28.6
Root Hinges	0.3	0.2	0.4	0.3	0.3	0.2
M1	2.6	2.1	3.3	3.1	2.3	1.8
PMSS	0.8	0.5	1.0	0.9	0.6	0.4
IH	2.2	1.7	2.6	2.5	1.9	1.5

DST 6.3 & 6.4

Shortening the baffle has a positive effect in decreasing the maximum temperature of the baffle although its effect is small (± 2.5°C). Shortening the baffle has a negative effect in the maximum temperatures as suffered by the spider, booms and the secondary- and primary mirror. The average temperatures are only effected by a couples of degrees, which probably indicates that only small areas are effected. The latter property can also indicate a modelling error, which are known to happen to angular geometries when exposed to direct sunlight effects.

Elongation of the baffle has the opposite effect. The maximum baffle temperatures have increased, while the maximum temperatures of the aforementioned telescope components have decreased.

DST 6.5

The last variation features a longer and narrower baffle. This variation was chosen because the longer and narrower baffle both featured desired properties. Regarding the results in Table 9.9 it is indeed shown that DST 6.5 features lower maximum baffle temperatures, opposed to the 6.4 model.

9.4.5 Heat flow Analysis

The total heat flows as shown in Table 9.10 will be compared with the temperatures shown in Table 9.8 and 9.9, in the following analysis.

Baffle

By enlarging the total area of the baffle blanket one increases the total heat flow from space towards the baffle. The baffle blanket can however be considered as an effective insulator and therefore it does not necessarily effect the telescope. The heat flow towards the interior of the baffle seems to be most determinant for the baffle temperature itself. From previous analysis it is known that the baffle interior is in close heat flow relation with the top section components. Therefore, it seems logical that by decreasing the maximum suffered baffle temperature one also decreases temperatures of these respective telescope components.

Telescope

By making the baffle wider and shorter one increases the heat flow from space towards the spider, secondary mirror, top hinges and booms. Thus basically the majority of the SMSS components, due to which they suffer an increase in temperature.
The opposite effect is seen for making the baffle longer or narrower, although lengthening of the baffle seems to be most effective for the telescope components. Lengthening is less effective for the baffle interior since it increases heat flow from space. The latter effect can be further mitigated by making the baffle narrower too.

9.4.6 Discussion

The results as presented in this section have showed that shortening and/or widening of the baffle leads to undesired effects. By lengthening of the baffle one decreases heat flow from space towards the majority of the SMSS components. It does however increases the heat flow from space towards the baffle interior. By narrowing of the baffle one decreases the heat flow from space towards the baffle interior mainly, which is therefore also effective in decreasing the temperature of some SMSS components.

Thus to conclude, lengthening of the baffle reduces heat flow from space to the majority of the SMSS components. Narrowing of the baffle decreases heat flow from space to the baffle interior. Further, the baffle interior radiates heat energy towards the SMSS components and therefore it is beneficial to reduce heat flow towards this interior. Therefore, it is recommended to make the baffle **longer** and **narrower** compared to what it is now, in case possible.

9.5 Attitude Analysis of the Satellite

The baffle shape, the position of the MLI blanket, a potential top closing and the baffle dimensions have been varied in the previous sections. These alternations considered NOM, COLD or HOT thermal conditions but with nominal attitude conditions. The latter property is thought to represent the ideal case during which the satellite is constantly pointed at the centre of Earth, but also where the baffle is deployed completely in line with the telescope. The effect of the satellite not being perfectly pointed at the centre of Earth or a dislocation of the baffle with respect to the telescope is unknown, hence the necessity for this rotation analysis. This analysis will include, the simulation conditions and the considered geometries, for which the results will be analysis and concluded in the end.

9.5.1 Modelling Conditions

The thermal modelling conditions are considered to be composed of the thermal environment, the attitude conditions of the sun, planet and satellite, and the rotation conditions of the spacecraft geometries themselves.

Thermal Conditions

The thermal model in this section will be exposed to NOM conditions. These conditions were thought to be sufficient since the results within this section should be interpreted as informative, rather than actual results or worst case scenario results.

Attitude Conditions

The thermal model will orbit the Earth during the simulations, during which the position of the Sun and Earth will not change. The orbital parameters, apart from the true anomaly, will not change either. Thus, the main relevant simulation parameters will be the attitude of the satellite with respect to the Earth and the Sun.

The attitude of the baffle with respect to the telescope is not guaranteed. Anomalies could occur during deployment or during operation, after which it can be rotated instead of parallel to the telescope. Besides, the satellite pointing direction could deviate from Nadir. Therefore, one will consider two main cases for which either the baffle is rotated with respect to the telescope, or the case where the entire satellite is rotated with respect to the MCS.

Rotation Conditions

The geometric thermal model can be rotated with respect to the MCS by means of the transformation function. After some trial and error it was found that the baffle could be rotated with a maximum of three degrees without interfering the primary mirror field of view. The telescope including baffle, can be rotated to any

degree although a maximum of 45 degrees was found sufficient for indicating the thermal effects.

9.5.2 Attitude Geometries

The two most critical moments for the baffle are found during the samples close after- and before eclipse, during which the sun illuminates the interior of the baffle. By rotation of the baffle towards either x or y, one worsens this effect for either of these two events. Therefore, attitude adjustments have not been made been in the opposite direction. The considered transformations consider rotation of the baffle only, or for the entire spacecraft.

Baffle Rotation Only

The thermal models as considered in this section will be transformed variations of DST 2.7. These variations are depicted in Table 9.11 and visualised in Figure 9.14. These configurations consider baffle rotations of three degrees in either x, y or both.

Table 9.11: Rotated baffle models.

Rotation Axis	Rotation Angle	Label	Figure
[1.0, 0.0, 0.0]	3	x03	9.14a
[0.0, 1.0, 0.0]	3	y03	9.14b
[1.0, 1.0, 0.0]	3	xy03	9.14c
[1.0, -1.0, 0.0]	3	xmy03	9.14d

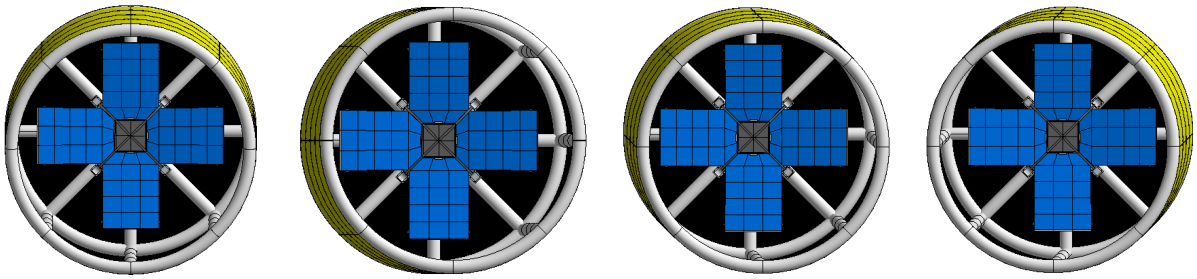

(a) DST 2.7: x03 (b) DST 2.7: y03 (c) DST 2.7: xy03 (d) DST 2.7: xmy03

Figure 9.14: Visualisation of a rotated baffle rotated with 3 degrees in x (a), y (b), x and y (c), and x and minus y (d). As visualised within the ESATAN TMS Workbench.

Satellite Rotation

The results with the baffle rotations only, as presented in the next section, showed that the rotations with respect to the x-axis or the y-axis (inertial axis system of the thermal model) resulted into the coldest and hottest case respectively. Therefore, it is thought that additional research with even larger deflections could be useful. The deflections of 3 degrees will be extended up to 8, 15, 25 and 45 degrees, for which the entire satellite will be rotated. Thus, for the latter four deflections one considers the baffle and telescope to be parallel.

9.5.3 Results & Analysis

The aforementioned variations with rotated baffles have been exposed under NOM conditions for which the results have been shown in Table 9.12. The results have not been included with heat flow results since they were considered irrelevant.

Baffle Rotation Only

The differences from DST 2.7 with a rotated baffle up to three degrees are small. The results show that the local- maximum or minimum temperatures are suffered by y03 and x03 respectively. The remainder of the results, xy3 and xmy3, are less extreme and more or less situated in between. A rotation of three degrees seems to be relatively insignificant, considering that the angle was restricted by the field of view of the primary mirror segments. Still, it has been shown that a small rotation with respect to the Sun will effect the temperature as experienced by the baffle. A larger rotation around the y-axis can therefore have even larger effects on the maximum temperature.

Table 9.12: Main geometry temperatures in degrees Celsius, for DST 2.7 with rotated baffle for different directions, NOM conditions.

	DST 2.7		x03		y03		xy03		xmy03	
	Min T	Max T	Min T	Max T	Min T	Max T	Min T	Max T	Min T	Max T
Baffle Bl.	-90.0	122.5	-92.5	117.5	-92.5	127.5	-92.5	125.0	-92.5	115.0
Baffle Str.	-25.0	110.0	-27.5	105.0	-27.5	117.5	-27.5	112.5	-25.0	110.0
Spider	2.5	30.0	0.0	27.5	0.0	27.5	0.0	25.0	0.0	27.5
Top Hing.	0.0	22.5	0.0	17.5	0.0	20.0	0.0	20.0	0.0	20.0
M2	27.5	30.0	20.0	20.0	30.0	32.5	22.5	22.5	27.5	27.5
Booms	2.5	20.0	2.5	17.5	2.5	20.0	2.5	17.5	2.5	20.0
Root Hing.	5.0	12.5	5.0	12.5	5.0	15.0	5.0	12.5	5.0	12.5
M1	5.0	12.5	5.0	10.0	5.0	12.5	5.0	10.0	5.0	10.0
PMSS	2.5	17.5	2.5	17.5	2.5	20.0	2.5	17.5	2.5	17.5
IH	0.0	20.0	0.0	17.5	0.0	20.0	0.0	20.0	0.0	17.5

Spacecraft Rotations

The results of the rotated satellites are depicted in Table 9.13. The rotations are considered per axis.

Rotations about y
For rotations in y up to 15 degrees, it seems that the baffle is mainly effected. The baffle is rotated towards the Sun for one part of the orbit, while it is rotated towards space for the remainder of the orbit. The effect between 8 and 15 degrees is minor which could indicate that the aforementioned contribution of the Sun is weighted by that of space. For the rotation angles 25 and 45 degrees, large differences are seen for all telescope geometries. The latter is thought to indicate that the baffle looses its function.

Rotations about x
The deflection results around the x-axis show different behaviour since the temperature decreases for all geometries with larger deflections. This is thought to indicate that the telescope is rotated towards space for the majority of the orbit, hence its cold.

Table 9.13: Main geometries minimum and maximum temperatures in degrees Celsius, for DST 2.7 with rotated satellite for two directions and several angles.

	x08	y08	x15	y15	x25	y25	x45	y45
	Min T	Max T	Min T	Max T	Min T	Max T	Min T	Max T
Baffle Blanket	-100.0	135.0	-107.5	135.0	-120.0	127.5	-132.5	130.0
Baffle Structure	-27.5	120.0	-30.0	122.5	-35.0	120.0	-47.5	122.5
Spider	-2.5	27.5	-7.5	22.5	-15.0	42.5	-32.5	60.0
Top Hinges	-2.5	20.0	-7.5	20.0	-15.0	25.0	-30.0	37.5
M2	15.0	32.5	10.0	30.0	2.5	25.0	-15.0	40.0
Booms	0.0	17.5	-5.0	20.0	-12.5	30.0	-30.0	37.5
Root Hinges	2.5	15.0	0.0	17.5	-7.5	20.0	-22.5	30.0
M1	2.5	12.5	0.0	12.5	-7.5	17.5	-22.5	22.5
PMSS	0.0	20.0	-2.5	22.5	-10.0	30.0	-27.5	65.0
IH	-2.5	20.0	-5.0	22.5	-10.0	27.5	-25.0	47.5

9.5.4 Discussion

The results have showed that the thermal effects of a rotated baffle with respect to the telescope up to 3 degrees are small. Spacecraft attitude rotations with respect to Nadir have a relatively small effect up to fifteen degrees, while they can be considered severe for rotations near 25 degrees and larger. This results from the telescope being rotated away from Earth, where the latter is considered as a less severe and uniform thermal environment during simulation. It is therefore recommended to point the telescope such that it is pointed to Earth, rather than towards the Sun or Space.

9.6 Chapter Summary

A total of seven baffle shell variations, including a variation without a baffle, have been simulated under nominal thermal conditions for which its temperature behaviour have been studied in detail. It was found that a baffle with a wide opening and/or a wide bottom, is not desired since both the baffle and the top section suffer largest increase in heat flow from space. Therefore, the effect of the baffle shape itself is found negligible, with the condition that the opening is small and that the baffle is not made unnecessary wide.

Three different MLI configurations have been simulated, namely: externally, in between and internally (which refers to the position of the blanket with respect to the structure). It was found that either the external or the internal configuration can be selected, although the respective configuration would determine the required optical properties of the booms. For simplicity and mass reasons it is thought that the configuration with an internal baffle structure is best.

Three additional baffle variations have been simulated with different top closing thicknesses. This thickness is measured in radial direction, ranging from 10 to 22cm. The results showed that a top closing is not effective in reducing temperature, apart from the secondary mirror. Besides, one should consider that a top closing of 22cm can interfere with the field of view. Therefore, a top closing is **not** considered as an effective addition to the current design.

The baffle dimensions have been altered for which its diameter and length have been increased and/or decreased. The baffle, the spider, the top hinges and the secondary mirror, thus essentially all geometries close to or near the opening of the baffle, are effected most in total heat flow as a result of a change in baffle dimensions.
In terms of reducing the maximum temperatures of the baffle, spider and secondary mirror, it was found beneficial to reduce the diameter of the baffle. In terms of reducing the maximum temperatures of the spider, the top hinges and the secondary mirror temperature, it was found favourable to extend or lengthen the baffle. The last baffle variation, which has been lengthened and made narrower, therefore showed superior performance. Making the baffle a bit narrower with sufficient length can therefore be advisable in case possible. Further, additional measures should be found for the interior of the baffle since its is known to radiate energy towards the telescope.

Small rotations of the baffle with respect to the telescope up to 3 degrees in any direction showed to have small effect on the thermal performance. Therefore, it is thought that the baffle deployment do needs to be perfect but rather close to it. Satellite rotations of 8 and 15 degrees effected the baffle, the spider and the secondary mirror, while rotation of 25 and 45 degrees effected the entire telescope. This is thought to be caused by the baffle, which cannot function properly when rotated towards the Sun or space. Therefore, the telescope should preferably be rotated to the Earth when deployed.

(This page is intentionally left blank.)

10 Thermal System Design

The previous Chapter included a parametric analysis of the baffle. This analysis has been useful for indicating potential improvements for the baffle. This Chapter will present the preliminary thermal system design. Before this design is presented it is thought that the remainder of the system components should be investigated for potential improvements too (10.1). The considered designs will be presented after (10.2). These designs will be investigated for a suitable operational window (H). The thermal results from these windows will be used for the final analysis during which the thermal budgets will be approximated (10.4).

10.1 Additional Research

The following aspect are thought to require additional research: the spider (10.1.1), thermal-optical control coatings (10.1.2), the baffle interior (10.1.3) and the secondary mirror (10.1.4).

10.1.1 Spider Investigation

The current Spider design (Feb. 2019) contains a skeleton design only. An additional top plate made of CFRP has been added to the initial model and has not been alternated after. The additional top plate was found to be required such that it blocks unwanted heat energy impinging on the secondary mirror, as well as other components like the field stop. From the previous Chapter it became clear that the spider is vulnerable for influences of the space environment. It is therefore thought that the spider should be thermally investigated such that it can be improved where possible.

Redefining the Spider Geometry

The investigation required a more refined spider grid, as also the spider top plate had to be redefined for it to not disturb the remainder of the spider. This process has been visualised in Figure 10.1.

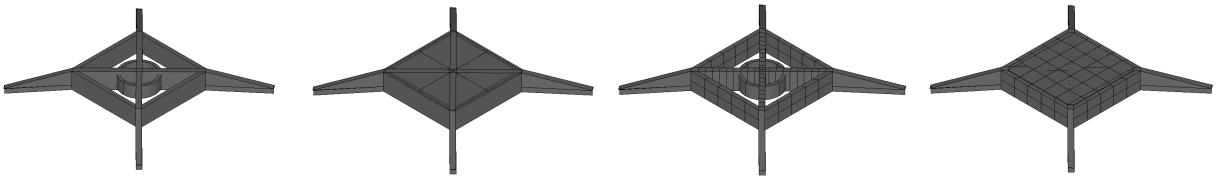

(a) Spider skeleton (b) Addition of the top plate (c) Refined spider grid (d) Refined top plate

Figure 10.1: Visualisation of the spider geometry evolution, as produced within the ESATAN TMS Workbench.

Temperature Visualisation

The spider receives most of its heat energy from the space environment and the baffle. Its maximum temperatures are reached at equal time sample as the baffle does. Figure 10.2 is representative of the DST 7.0 model, which is considered identical to the 2.7 model but with refined- spider grid and top plate as shown in Figure 10.1d. Figure 10.3 is representative of the DST 7.1.0 model. The only difference between these models is the length of the baffle, where the DST 7.1.0 model has a 20 cm extended baffle.
By analyses of these two Figures it is thought that two major differences can be seen. The first difference is the magnitude of temperature as experienced by the spider, while the second difference is found for the main contributors of these temperatures.

Temperature Analysis

In Figure 10.2 it can be seen that the interior of the baffle at the top left of the Figure is hottest, receded by the red colour. From prior analysis it is known that this happens when the orientation of the satellite is such that solar flux can impinge the interior of the baffle. The hottest temperatures of the spider are situated at the other side of the model, seen from the baffle, and therefore it is likely that these are driven by the same source.

For the configuration as shown in Figure 10.3 it is different. This because the nodes of maximum temperature for the spider are situated at the same side of those of the baffle. Prior analysis had shown that the spider is influenced most by the space environment and the baffle. Thus, it is likely that these respective maximum temperatures are driven by the baffle which radiates heat towards the spider.

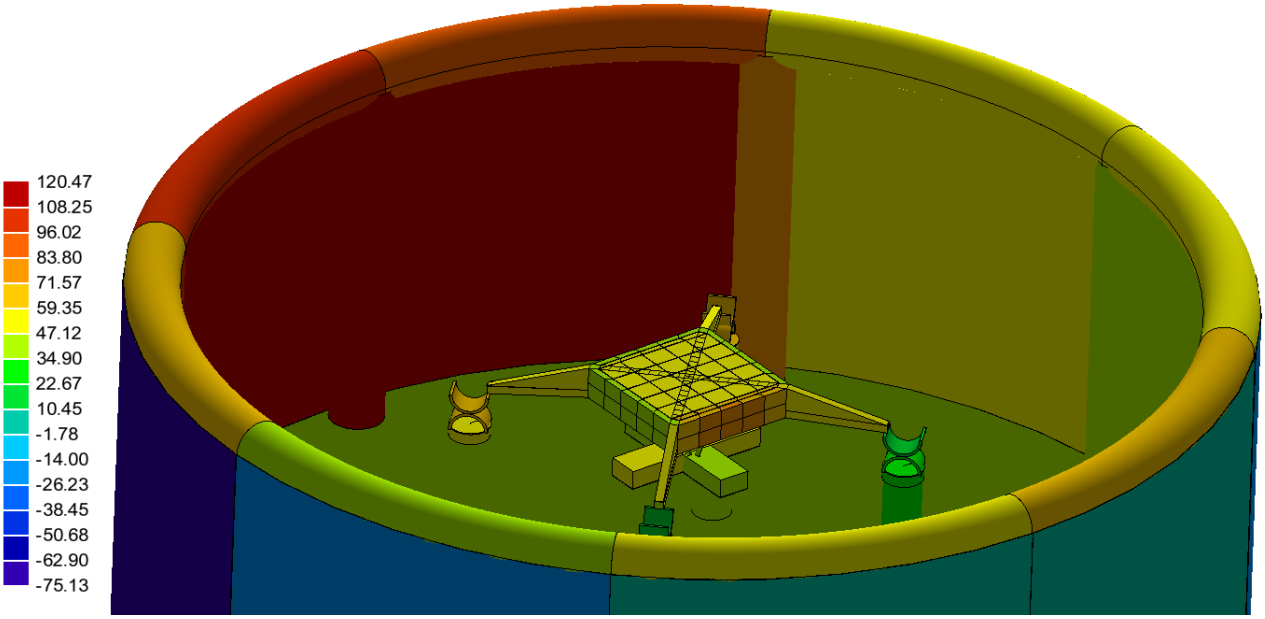

Figure 10.2: Temperature visualisation at t= T_{max} of DST 7.0, with HOT conditions. As visualised within the ESATAN TMS Workbench.

Discussion of Results

The nodes of maximum temperature for the spider are situated at the sides of its the main rectangular structure, for both configurations. Lengthening of the baffle will decrease the total heat flow towards the spider as was seen in the previous Chapter, although its main contribution will be from the baffle instead of space. Further decreasing the heat flow towards the spider therefore requires a change in thermo-optical properties of the spider and/or the baffle.

10.1.2 Thermal Control Coatings

The majority of the satellite geometries have remained uncoated since their desired thermo-optical properties were still unknown. In the previous section it was concluded that the spider and/or the baffle interior are in need for a change in thermo-optical properties for it to reduce the heat flow between the two of them. Therefore, it is thought that the currently uncoated and coated surfaces shall be re-evaluated. These re-evaluation will be considered for the reflective- (10.1.2.a) and absorptive coatings (10.1.2.b). Results will be presented after, included with a corresponding analysis (10.1.2.c). This re-evaluation will be concluded with a discussion (10.1.2.d).

10.1.2.a Application of Reflective Coatings

Highly reflective coatings refer to coatings which have low absorption in both spectra. They consider low solar absorptivity and low emissivity, equivalent to the mirror coatings. Whether a surface can be made highly reflective or not will depend on the stray light analysis. At this moment, it is unknown which component surface will produce stray light in case it will be made reflective. This is because a stray light analysis is not included within this report, as well it is not part of this thesis. The only surface which will probably not produce stray light is the top plate of the spider.

The top plate of the spider has been adjusted in the previous section such that it did not contain any sharp corners. Further, it is designed such for it to provide some clearance with the sides of the rectangular section. This way it can be made reflective. The results of this alternation will be combined with the thermal analysis of the next section, referred to as the DST 7.1.2 model.

Reflective Coating
A proper highly reflective coating has already been selected for the mirror surfaces. Covering it in MLI is not

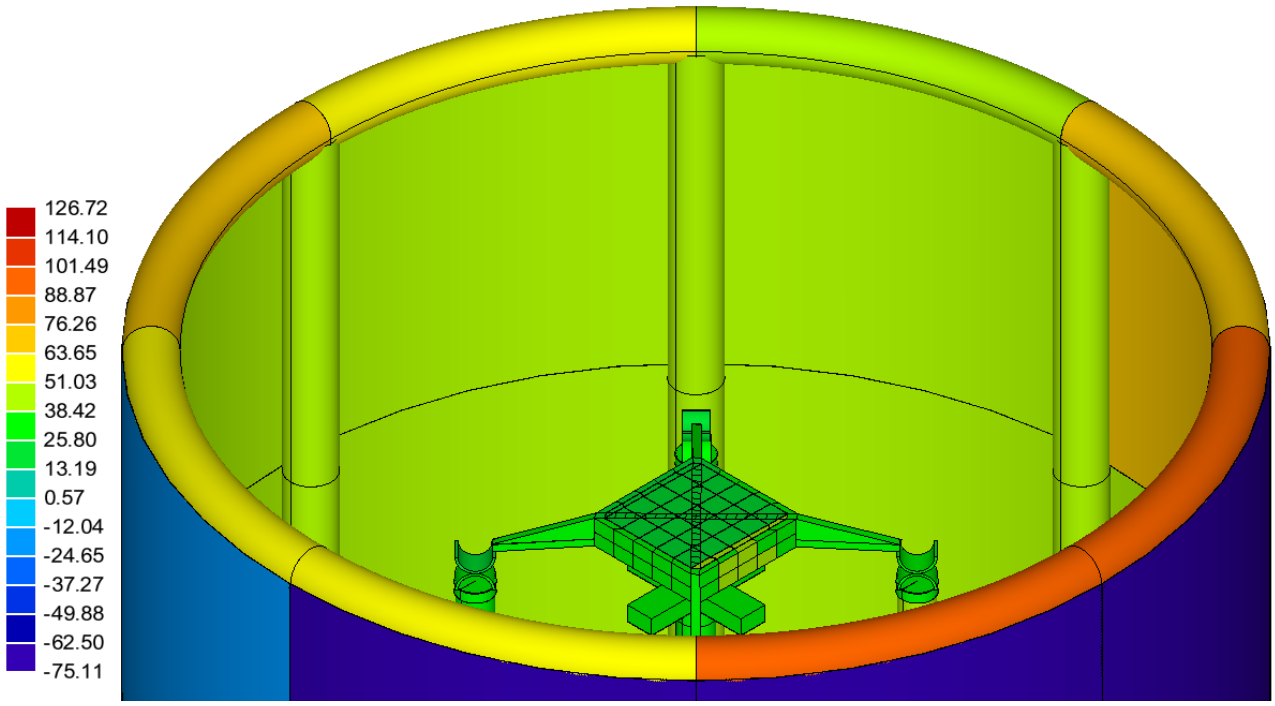

Figure 10.3: Temperature visualisation at t= T_{max} of DST 7.1.0, with HOT conditions. As visualised within the ESATAN TMS Workbench.

considered as a suitable option. This because MLI blankets can wrinkle due to which the reflection of light becomes indeterminable. It is therefore chosen to apply a protected silver coating onto the top plate of the spider.

Coating Definition
This coating is defined as a different geometrical layer on top of the top plate. This because solids feature equal optical properties on all surfaces, while the back of the top plate should not be made as reflective as possible. The thickness of the top plate and the coating are set at 1mm such that it will be clearly distinguishable in the thermal model. The exact thickness of the top plate should be determined by mechanical analysis, while the reflective coating shall be eventually made representative of the coating thickness.

10.1.2.b Application of Absorptive Coatings

This section include the considered absorptive coating, the satellite components onto which it will be applied and the visualisation of these.

Absorptive Coating

A proper absorptive coating, the magic black coating, has already been selected for previous models featuring low- absorptivity and emissivity. The optical properties are depicted in Appendix C *Thermal & Thermo-optical Properties*. This coating is considered to feature excellent non-reflectivity properties, for it to keep stray light to the minimum.

Coating Application

Currently, the magic black coating has been applied to the baffle interior only. The remainder of the structure will be elaborated below. The magic black coated telescope will be referred to as the DST 7.1.1 model.

Secondary Mirror Support Structure
In order to keep stray light to the minimum it is thought that all components in front of the primary mirror should be coated with this coating. This considers the spider, secondary mirror interface, top hinges, booms and root hinges. Thus basically all components of the SMSS. The secondary mirror itself will be considered separately.

Instrument Housing
The top of the instrument housing has already been coated black since it was considered in direct sight of the

secondary mirror. The remainder of the instrument housing has remained uncoated because it is expected that its reflections will not produce stray light for the system.

Primary Mirror Support Structure
The PMSS has eight small ribbon extensions which extend the primary mirror segments on the sides. These need to be coated black in case those will remain as they are. However, at this moment it is unknown whether the construction including ribbons will remain set and therefore they have remained uncoated since the remainder of the structure does not necessarily needs to be coated black.

Visualisation

The effect of these changes are visualised in Figure 10.4 and Figure 10.5, with the DST 7.1.3 representing the magic black coated telescope without the addition of the spider top plate. The latter geometry has been added such that the significance of this plate can be evaluated too. It must be mentioned that the non black coatings and uncoated components depict false colours. The mirror coating for example is chosen to be blue such that it is clearly distinguishable from the remainder of the geometries.

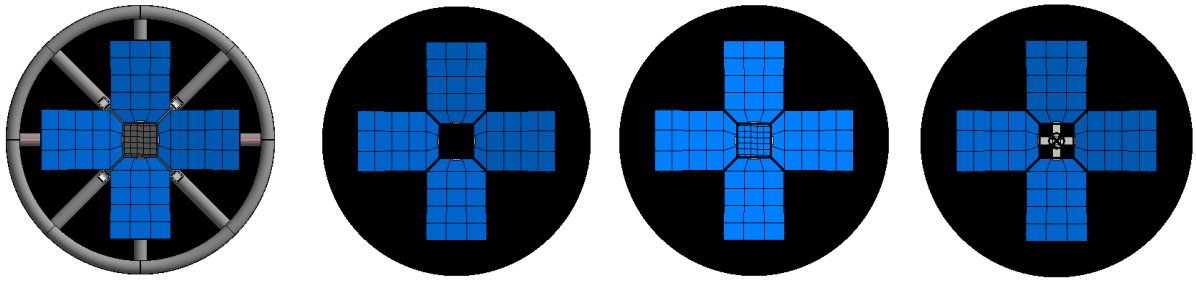

(a) DST 7.1.0 (b) DST 7.1.1 (c) DST 7.1.2 (d) DST 7.1.3

Figure 10.4: Visualisation of the change in optical properties seen from top, as produced in the Workbench of ESATAN TMS.

10.1.2.c Results & Analysis

The DST 7.1.x models have been exposed to HOT conditions for which the results are shown in Table 10.1 and 10.2. They have been exposed to HOT conditions since these are expected to indicate the largest differences in thermal performance. The tables include the global- (Glo.) minimum and maximum, the average- (Av.) minimum, maximum and average (Av.) ΔT temperatures. All DST 7.1.x models feature extended baffles while they are different in optical coatings and/or the application of the top plate on the spider.

First Impression
By analysing the results from the two Tables it become apparent that the differences are small, $\pm 5°$ maximum. The baffle is equal for all models since their coatings and properties are equal, while the colour as visualised in the thermal model has no effect on the results, thus the results are similar.

DST 7.1.1
This model has magic black coated telescope components which seem to affect the global maximum temperature as experienced by the spider (+2.5°C) and the average temperature of the top hinges (+2.8°C). The remainder of the components are negligibly effected which is thought to be caused by the relatively small difference between the uncoated optical- and the magic black properties. Besides, the baffle is effective in minimising the amount of heat which arrives at the majority of these components in the first place.

DST 7.1.2
This model features a highly reflective coated top plate of the spider, which seems to have a positive effect in reducing the average ΔT (1.7°C) as experienced by the spider. The baffle structure global maximum temperature has increased a bit (2.5°C), which is thought to be caused by reflections of the spider.

DST 7.1.3
This model does not include a top plate of the spider, due to which everything underneath is exposed. The secondary mirror is attached by means of an interface to the circular section of the spider. It is therefore thought that these two structures will experience larger ΔT without a top plate, which will most likely degrade performance. Besides, stray light will be generated as heat will impinge on the housing of the field stop. These effects cannot be derived from the depicted results, although it is thought that these are most likely to be a result of not having a spider top plate.

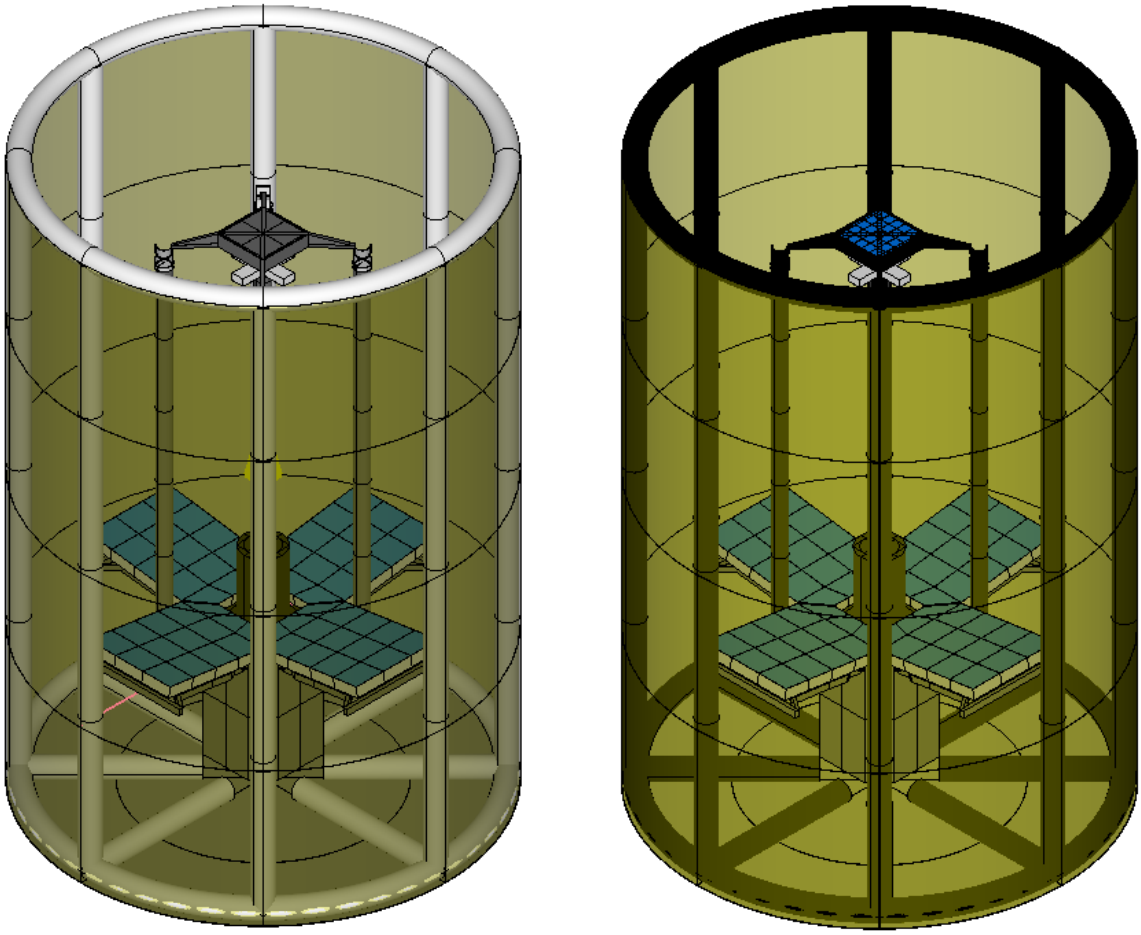

(a) DST 7.1.0 (b) DST 7.1.2

Figure 10.5: Visualisation of the change in optical properties seen from the side, as produced in the Workbench of ESATAN TMS.

10.1.2.d Discussion of Results

The thermal results showed that the protected silver coating is minor effective in reducing the average ΔT as experienced by the spider. The thermal results did not show any significant effects when the top plate was not included, although it is considered to enlarge the amount of stray light in case not present. The thermal model conditions consider constant properties for OLR and solar albedo, while in reality those will vary based on the atmospheric- and surface properties. Therefore, it is thought that the top plate should be made reflective for it to reflect the majority of the heat energy back to the space environment. The exact thickness and size of this plate shall be determined in further research, preferably in a detailed analysis.

The majority of the SMSS components have been coated with the magic black coating for it to keep stray light to the minimum. The results have shown that the temperature differences are small compared to the uncoated SMSS. It is thought this is because the thermo-optical properties of CFRP are close to that of the magic black coating, with a larger difference for the uncoated titanium allow components. The latter would also explain the relatively largest difference as seen for the top hinges.

10.1.3 Baffle Interior Investigation

The interior of the baffle is currently completely covered with the magic black coating. Prior analysis had shown that sunlight is able to impinge the interior of the baffle for certain orientations, by direct and indirect means. Therefore, it absorbs a large amount of heat of which a considerable amount is emitted towards the telescope. Since, generally a good absorber is a good emitter, no coatings exist which feature highly absorptive properties with low emissivity.

Another solution would comprise a reflective baffle, which are known to exist (10.1.3.a). After, such a design will be related to the DST (10.1.3.b). It will be determined how it can be modelled (10.1.3.c). The resultant reflective baffle will be presented (10.1.3.d). Results will be generated and analysed (10.1.3.e). Finally, the results will be discussed (10.1.3.f).

Table 10.1: Temperature results for the DST- 7.1.0 and 7.1.1, for HOT conditions in degrees Celsius.

	DST 7.1.0					DST 7.1.1				
	Glo. Min	Av. Min	Av. ΔT	Av. Max	Glo. Max	Glo. Min	Av. Min	Av. ΔT	Av. Max	Glo. Max
Baffle Bl.	-75.0	-8.9	8.4	-0.5	130.0	-75.0	-9.0	8.2	-0.8	130.0
Baffle Str.	-0.0	19.0	25.0	44.0	125.0	0.0	18.9	24.7	43.6	125.0
Spider	17.5	21.2	7.7	28.9	45.0	17.4	21.2	7.7	28.9	47.5
Top Hinges	20.0	22.2	12.2	34.4	40.0	17.5	21.1	15.1	36.2	42.5
M2	30.0	29.5	0.9	30.4	30.0	30.0	29.4	0.9	30.3	30.0
Booms	20.0	22.5	13.1	35.6	45.0	20.0	22.3	13.3	35.6	45.0
Root Hing.	22.5	24.1	5.5	29.6	30.0	22.5	23.7	6.0	29.7	30.0
M1	22.5	25.6	0.4	26.0	30.0	22.5	25.5	0.4	25.9	30.0
PMSS	22.5	24.2	5.2	29.4	32.5	22.5	24.2	4.8	29.0	32.5
IH	20.0	22.0	11.2	33.2	35.0	20.0	21.9	10.9	32.8	35.0

Table 10.2: Temperature results for the DST- 7.1.2 and 7.1.3, for HOT conditions in degrees Celsius.

	DST 7.1.2					DST 7.1.3				
	Glo. Min	Av. Min	Av. ΔT	Av. Max	Glo. Max	Glo. Min	Av. Min	Av. ΔT	Av. Max	Glo. Max
Baffle Bl.	-75.0	-8.9	8.3	-0.6	130.0	-75.0	-9.2	8.1	-1.1	130.0
Baffle Str.	0.0	19.1	25.0	44.1	127.5	0.0	18.9	24.6	43.5	125.0
Spider	15.0	22.6	6.0	28.6	42.5	20.0	20.7	8.4	29.1	42.5
Top Hinges	17.5	21.3	15.3	36.6	42.5	17.5	21.0	15.1	36.1	42.5
M2	30.0	30.4	0.9	31.3	32.5	30.0	30.0	0.7	30.7	30.0
Booms	20.0	22.6	13.4	36.0	45.0	20.0	22.2	13.2	35.4	45.0
Root Hing.	22.5	24.0	6.1	30.1	32.5	22.5	23.6	5.9	29.5	30.0
M1	25.0	25.9	0.3	26.2	30.0	25.0	25.5	0.3	25.8	30.0
PMSS	20.0	24.5	4.9	29.4	37.5	20.0	24.1	4.7	28.8	35.0
IH	20.0	22.2	11.0	33.2	35.0	20.0	21.8	10.8	32.6	35.0

10.1.3.a Reflective Baffle Measurements

A reflective baffle is considered to be designed such for it to "both reduce straylight to the best possible extent and minimize the heat load to the spacecraft" [39]. The BepiColombo Laser Altimeter (BELA) featured such a design which will be used as main reference in this section [39]. The relevant requirements of this design will be presented first after which the mechanical design will be presented.

Requirements

The most important requirements as presented in [39] are related to the optical performance of the system and the thermal performance of the baffle. Some of these requirements will be elaborated below.

Aspect Angle
"The baffle shall provide an aspect angle of $\leq$35 deg" [39]. This requirements specifies that rays below a certain incident angle should not intersect with the baffle.

Solar Reflectivity
"The reflection efficiency of the baffle in the solar spectrum between 200 nm and 2500 nm shall be >93%" [39]. This basically specifies that only 7% of the visible light-, the near ultraviolet- and the near IR spectrum shall be absorbed. Therefore, it will absorb <7% of the solar flux, either directly or indirectly. The DST will operate within the 450-692nm wavelength range (MIS-REQ-04). Such a design would therefore produce at least <7% stray light.

Infra-red Reflectivity
"The reflection efficiency of the baffle in the thermal IR range between 2.5 μm and 8 μm shall be >98%" [39]. This requirement specifies that <2% of the radiated energy is absorbed by the baffle. It does not specify whether this includes the exterior but for now it will be assumed that it considers the interior only.

Temperature Gradients
"The baffle shall minimize temperature gradients in azimuthal and axial directions that are to be expected due to anisotropic irradiation" [39]. This requirement is formulated for it to prevent baffle distortions. It considers

anisotropic irradiation because the heat majority is expected to impinges one side of the baffle only.

Baffle Mechanical Design

The requirements have been mentioned in the previous section. This section will elaborate the design application of these requirements. Before presenting the actual design one needs to elaborate on the reflective baffle concept, the chosen materials and the required model.

Reflective Baffle Concept
The design concept is shown in Figure 10.6a. The dotted lines represent hyperbolas, the dashed line ellipses and the thick lines the baffle contour. The semi-major axis of these ellipses (y) are situated at the entrance aperture, perpendicular to the optical axis (z). F1 and F2 represent the two focal points. The baffle diameter and the interfocal distance are matched such for the focal points to be situated at the edges of the entrance [39]. The focal points are used to describe the working principle of the reflective baffle, as depicted in Figure 10.6b. The Figure described three types of rays which either passes through one of the two focal points or in between them. Thus, a single ray is reflected twice maximum.

The baffle contour itself is considered to be composed of vanes, referred to as pairs of one hyperbola and one ellipse. The diameter of the baffle is defined by the required aperture while the number of pairs are defined by the required aspect angle.

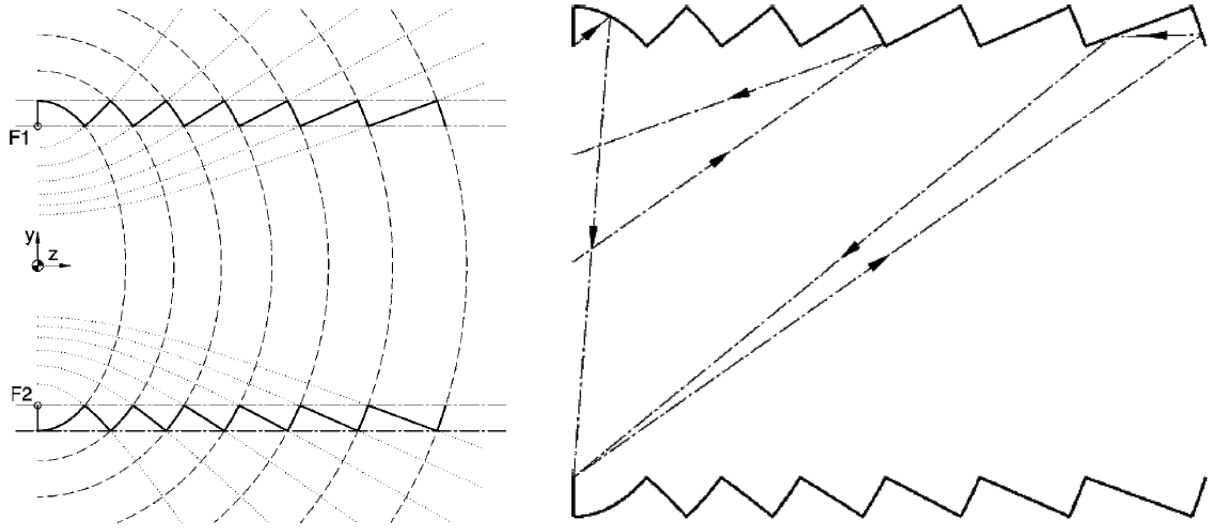

(a) (b)

Figure 10.6: Visualisation of the baffle contour (a) and the working principle (b), of the reflective baffle design as presented in [39].

Chosen Materials
To account for the expected temperature gradients due to anisotropic irradiation it can be chosen to either increase the wall thickness and/or chose a material with high thermal conductivity. Other factors which are taken into account are low density, machinability, mechanical strength, stifness, low cost, outgassing in vacuum and coating suitability [39]. Therefore, aluminium alloy 7075 is chosen as the breadboard material.

Required Model
The baffle geometry consists of a combination of elliptical- and hyperbolic cross sections, which can be computed by their respective equations as described in [39]. These equations will be used to define the baffle contour. This respective model can subsequently by used for a ray-trace simulation in which the aforementioned working principle can be verified.

Detailed Design
The prototype design is shown in Figure 10.7. It is considered to be composed of six vanes (Figure 10.7a) and two end sections, bolted together as shown in Figure 10.7b. The number of pairs have been determined such that rays beyond an incident angle of 38° will be reflected by the baffle. The baffle could also be composed out of one piece, although this is expected to complicate the manufacturing process. The vanes are coated such for it to meet the solar- and IR reflectivity requirements. The chosen material allows for a relatively thin baffle with low mass for it to meet the temperature gradient requirement.

(a) (b)

Figure 10.7: Visualisation of a single polished baffle vane (a) and a fully assembled reflective baffle without coating (b), of the reflective baffle prototype as presented in [39].

10.1.3.b Reflective Baffle Design

The aforementioned baffle design shall be related to the DST after which it can be decided whether it would be feasible for the DST or not.

Relation to the DST

The reflective baffle design will be related to the DST by means of the baffle length, the focal points and the amount of pairs.

Baffle Length
The reflective baffle design as presented in [39] has a inner diameter of 202mm and a length of 296mm. The DST baffle has a diameter of 2000mm and a length of about 2800mm, thus the design can be more or less scaled up by a factor of ten. The major difference is however that the telescope will be situated within the baffle. Making the entire baffle reflective would therefore not work since the majority of the incidence rays will be reflected towards the telescope. Besides, the telescope is most effected by the top section interior of the baffle. Therefore, the reflective design does not need to comprise the entire length of the baffle to start with. The length of the reflective baffle should be made such that the majority of the solar flux which impinges this top section interior, is reflected back into space instead of towards the telescope.

Focal Points
The baffle diameter should equal the interfocal distance. This basically means that the focal points of each subsequent ellipsoid should coincide with the focal point of the previous ellipsoid, as described in [40]. This process is illustrated in 10.8, where the ellipsoid contours H1, H2 and H3 are place such that their focal points coincide in F1,*.

Number of Pairs
The design as presented in [39] features 6 pairs or vanes, thus one vanes will comprise a width of about 50mm. Upscaling this design would result into vanes of 500mm each. The current baffle design extends the telescope by ±205mm only. Applying a single vane reflective design without extending the baffle will most likely not be sufficient for the reflected rays to not interfere with the telescope. The application of one vane is considered sufficient since more vanes will only drive the required total length of the baffle.

Feasibility of the design

Assuming that the aforementioned reflective baffle design of BepiColombo can be upscaled as presented in the previous section, it is thought that a single vane design can be applied to an extended baffle design. The baffle should be lengthened such that reflected rays will not impinge the top section of the telescope.

Further, the design needs to be deployable. Considering that the DST baffle requirements will be similar to those as presented in [39], it is thought that the singular baffle vane cannot be composed of several smaller pieces or segments. Hence, it must be made monolithic and thus it will most likely drive stowed volume. MIS-REQ-09, as

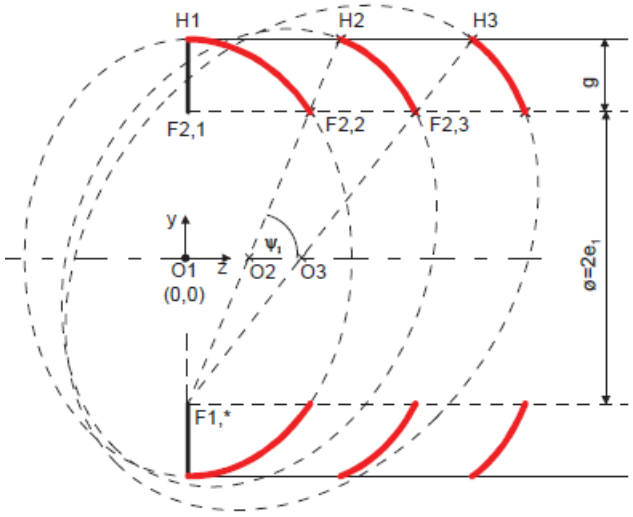

Figure 10.8: Stacked Elliptical sections, as presented in [40].

presented in Appendix A *Mission Requirements*, describes that the volume of the instrument should not exceed 1.5 m^3. This is expected to include the baffle. Therefore, it could well be a killer requirement for this concept.

10.1.3.c Modelling the Reflective Baffle Design

The application of such delicate reflective baffle design requires a detailed geometrical structure for the thermal model, as well as the curvature of the vane should be known for it to be modelled closely in the Workbench of ESATAN TMS. ESATAN TMS does not include a feature where it in which one can alternate the way light is reflected, apart from specifying the hemispherical or normal incidence reflective properties. Therefore, it cannot be modelled by means of a simple flat surface, meaning that it has to include a detailed structure if one wants to demonstrate this measurement properly by means of radiative contribution.

Another option comprises the activity of the respective surface, which as aforementioned can be set to Active, Radiative only, Conductive Only or Inactive. With Active comprising radiation and conduction, while inactive considers neither of them. For the DST thermal model, radiation can be excluded such that the respective surface will be conductively active only. It must be mentioned that it will exclude all radiative contributions of that surface, while in reality it will still absorb and emit some heat energy towards other parts of the satellite.

10.1.3.d Application of the Reflective Baffle Design

The reflective baffle design is considered to include one vane with a height of 500mm. This model will be referred to as the DST 7.2 model and is shown in Figure 10.9b. This model includes an extended baffle of 20 cm, just as the DST 7.1.2 model. This way it will be comparable to this model, as well as it is thought to contain sufficient clearance with the telescope. The baffle structure is depicted in white such that it is distinguishable from the interior blanket.

The baffle structure has been made shorter since the reflective baffle vane is considered to be apart from the remainder of the baffle structure. The interior of the vane is made in-active as discussed before. The exterior of the vanes is considered to be composed of MLI for it to be sufficiently protected from space. This should not necessarily be considered for the final design, although it is thought to be sufficient for prove of concept.

10.1.3.e Results & Analysis

The DST 7.2 model haw been exposed to HOT thermal conditions for which the temperature results are shown in Table 10.3. The DST 7.1.2 functions as the control model. The related total heat flow results are shown in Figure 10.10, 10.11 and 10.12.

Temperature Analysis

From the temperature results it can been seen that the reflective baffle seems to be effective in reducing the suffered average ΔT of all spacecraft component groups. This is mainly because the maximum average temperature have been reduced. The global maximum temperature of all components, apart from the top hinges, have been reduced too. Further, the overall average temperatures have decreased. Although the latter

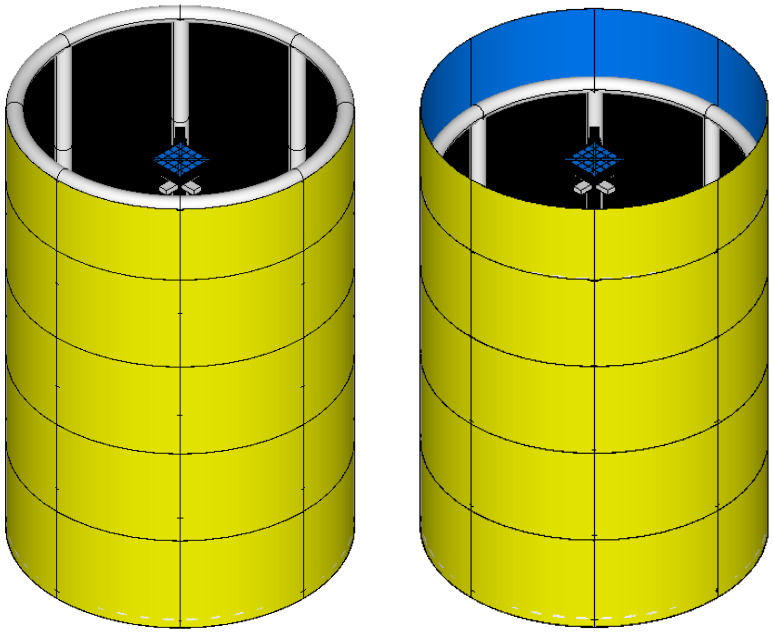

(a) DST 7.1.2 (b) DST 7.2

Figure 10.9: Visualisation of the reflective baffle design as constructed within the Workbench of ESATAN TMS.

Table 10.3: Temperature results for the DST 7.1.2 and 7.2, for HOT conditions in degrees Celsius.

	DST 7.1.2					DST 7.2				
	Glo. Min	Av. Min	Av. ΔT	Av. Max	Glo. Max	Glo. Min	Av. Min	Av. ΔT	Av. Max	Glo. Max
Baffle Bl.	-75.0	-8.9	8.3	-0.6	130.0	-75.0	-8.7	1.7	-7.0	65.0
Baffle Str.	0.0	19.1	25.0	44.1	127.5	7.5	12.5	10.0	22.5	105.0
Spider	15.0	22.6	6.0	28.6	42.5	12.5	16.0	2.3	18.3	37.5
Top Hinges	17.5	21.3	15.3	36.6	42.5	12.5	15.2	6.1	21.3	42.5
M2	30.0	30.4	0.9	31.3	32.5	17.5	19.3	0.1	19.4	20.0
Booms	20.0	22.6	13.4	36.0	45.0	15.0	15.3	2.7	18.0	20.0
Root Hing.	22.5	24.0	6.1	30.1	32.5	15.0	15.3	1.1	16.4	17.5
M1	25.0	25.9	0.4	26.3	30.0	15.0	15.3	0.1	15.4	17.5
PMSS	20.0	24.5	4.9	29.4	37.5	15.0	15.2	1.1	16.3	17.5
IH	20.0	22.2	11.0	33.2	35.0	15.0	14.8	2.2	17.0	17.5

is not necessarily to be considered as an improvement.

Total Heat Flow Analysis

The total heat flow analysis will be elaborated per heat source below.

Space
From Figure 10.10a it can be seen that the heat flows towards the baffle blanket interior (blue) and the baffle structure are largest (pink). The differences between the heat flow towards the entire telescope (orange) and the SMSS (green) are small, which indicates that the majority of heat is absorbed by the SMSS.

When comparing these results with those of Figure 10.10b it becomes clear that there are a couple of differences. The heat flow towards the baffle interior is almost halved, that of the structure is about one third and that of the SMSS is about one tenth of what it was before. The heat flow towards the telescope itself has not changed, thus the majority of heat is absorbed by the remainder of the telescope now. Further, the amplitudes of the heat flows are smaller.

Baffle Blanket Interior
Equal behaviour is seen for the baffle blanket interior (red) in Figure 10.11a and 10.11b. The heat flow between the baffle blanket interior and the baffle structure seems to be similar for both models. The heat flow towards the telescope and the SMMS has decreased significantly for the reflective baffle design, with the largest decrease seen for the SMSS. The latter is probably because the reflective top section of the baffle has largest effect on

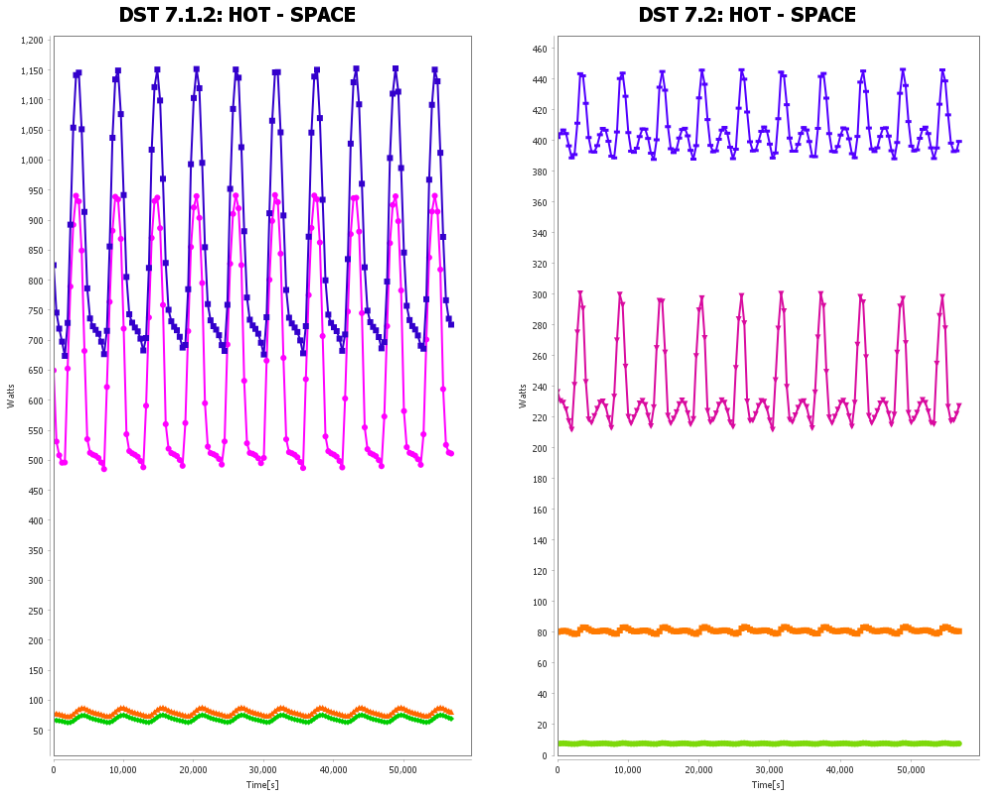

(a) DST 7.1.2 (b) DST 7.2

Figure 10.10: Total heat flow results from space towards the baffle interior (blue), baffle structure (pink), telescope (orange) and SMSS (green). Results are produced with the heat chart function of the ESATAN TMS Workbench.

the top section telescope components.

Secondary Mirror Support structure
By comparison of Figure 10.12a and 10.12b it becomes clear that the largest reduction in heat flow is indeed seen for the SMSS. The heat flow from the baffle interior has been increased the most.

10.1.3.f Discussion

The reflective baffle is effective in reducing the heat flow from space towards the SMSS. It is not effective in reducing the heat flow towards the telescope itself. The entire telescope but in particular the SMSS shows a significant decrease in heat flow with a reflective baffle design. This results into a lower average temperature for all telescope components. Further, the heat flow amplitudes are several degrees smaller such that the suffered ΔT is smaller too. A reflective baffle interior composed of one vane only can therefore be considered as an effective tool in lowering the average- ΔT and temperature for the telescope. Although, it is not known whether the overall decrease in average temperature will be desired. Further, it is effective in reducing the maximum suffered temperatures of the baffle itself.

10.1.4 Secondary Mirror Investigation

The secondary mirror has been remained uncoated, apart from the bottom which faces the primary mirror segments. At this moment it is unknown whether the secondary mirror should remain as it is, be made fully reflective or be coated with a black coating for example. This secondary mirror investigation includes several secondary mirror configurations, which will be exposed to certain thermal conditions. The thermal results will be analysed and discussed after.

10.1.4.a Secondary Mirror Configurations

The considered secondary mirror geometries will consider two additional configurations of which all geometries feature a silver protected reflective mirror coating at the side which faces the primary mirror section directly (considered as the bottom), while the remainder of the surfaces will be coated differently. The DST 7.1.2 model will be considered as the control model. Thus all considered M2 configurations consider a lengthened baffle.

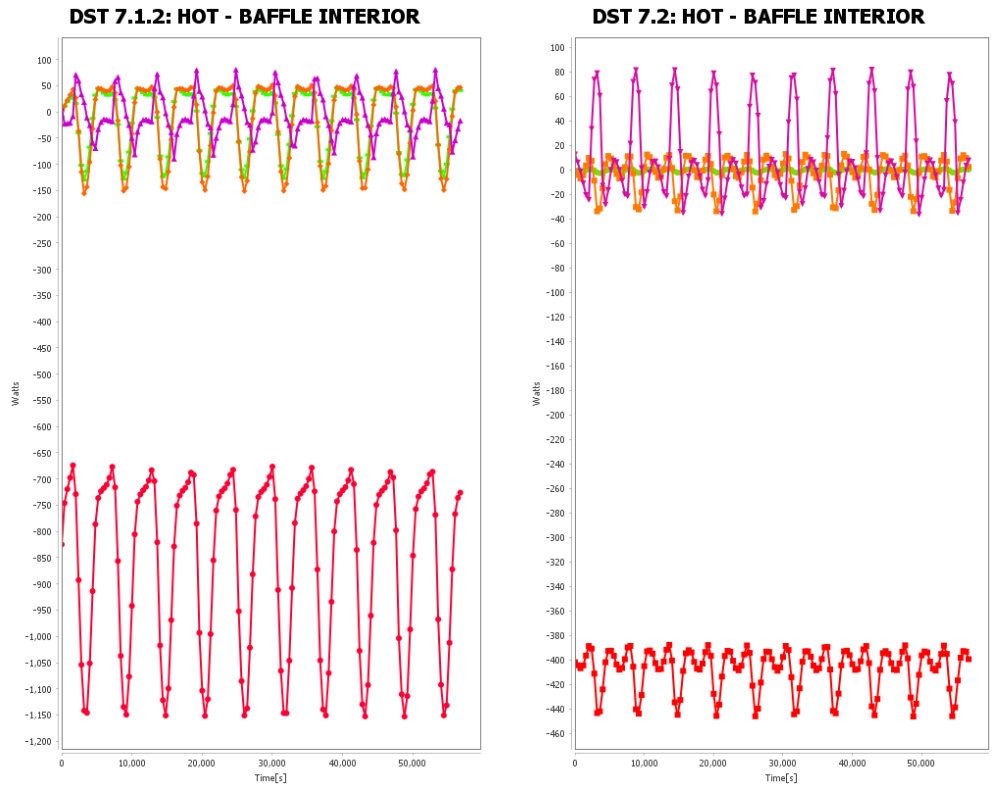

(a) DST 7.1.2 (b) DST 7.2

Figure 10.11: Total heat flow results from the baffle interior towards the baffle structure (pink), telescope (orange), SMSS (green) and space (red). Results are produced with the heat chart function of the ESATAN TMS Workbench.

DST 7.3.1

This model features magic black coated surfaces. Since the mirror is not fully protected by the spider nor the baffle, it is expected that it will suffer larger ΔT.

DST 7.3.2

This model features a fully covered silver protected secondary mirror. Since the uncoated structure already possessed descent reflective properties it is expected that the difference with respect to the control model are small.

10.1.4.b Results & Analysis

The DST 7.3.x models have been exposed to HOT thermal conditions for which the results are shown in Table 10.4. These results will be compared to the 7.1.2 model. The heat flow results for the secondary mirror are shown in Figure 10.13.

Temperature Results
By analysing the results from Table 10.4 it become apparent that the effect of changing the optical properties of the secondary mirror as proposed, does have small effect on the SMSS components and the baffle and negligible effect on the remainder of the satellite components. By applying a black coating on the secondary mirror it can be seen that the average ΔT increases from 0.9- up to 3.2°C, while by making it fully reflective it decreases down to 0.4°C. Further, the average temperature of the secondary mirror is closer to the target temperature for the fully reflective design.

Heat Flow Results
The heat flow results as shown in Figure 10.13 show a large difference for the black coated secondary mirror, while small difference are seen between the uncoated mirror and the fully coated mirror. By coating the mirror black it can be seen that the heat flow with the baffle is encouraged. Further, the amount of heat flow absorbed by space is ten times as much. For the fully coated mirror a small decrease is seen for the heat absorbed by space, which would explain the decrease in average temperature. Further, the amplitudes with the baffle interior have decreased which would explain the decrease in ΔT.

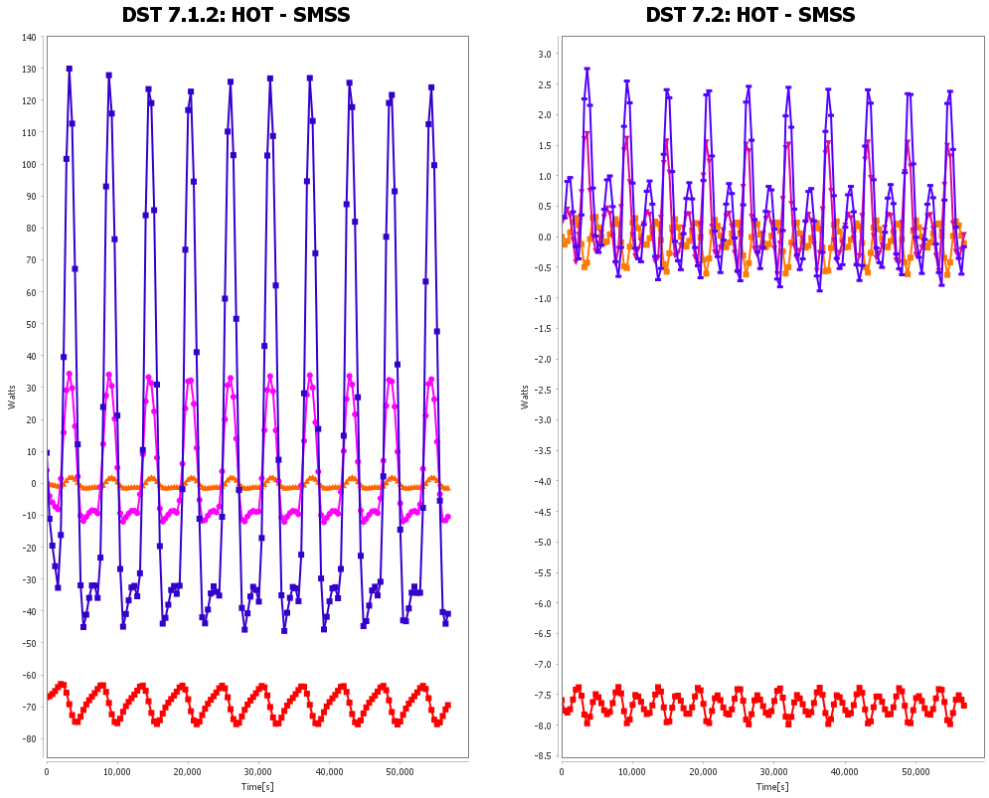

(a) DST 7.1.2 (b) DST 7.2

Figure 10.12: Total heat flow results from the SMSS towards the baffle structure (pink), telescope (orange), baffle interior (blue) and space (red). Results are produced with the heat chart function of the ESATAN TMS Workbench.

10.1.4.c Discussion

It is thought that the secondary mirror should not be coated black since it will encourage heat absorption from space and the baffle. The thermal differences between the fully reflective coated mirror compared to the uncoated mirror was small, as expected beforehand. Nevertheless, by making the mirror fully reflective one decreases the heat flow from space due to which its average temperature decreases. Further, the heat flow with the baffle is discouraged such that the suffered ΔT is smaller.

Since the differences with the uncoated mirror are small, it is thought that a more detailed analysis will be required to determine which configuration is best. Therefore, it will not be included in the final analysis.

10.1.5 Conductive Interfaces

The conductive interfaces have been set in the initial model and have not been altered after, apart from some small adjustments as was mentioned in Chapter 7. Therefore, the current configuration of the conductive interfaces shall be determined first (10.1.5.a). Further, it shall be discussed whether these interfaces should be adjusted or not (10.1.5.b).

10.1.5.a Current Configuration

The current thermal model includes two types of conductive interfaces, namely fused and contact. The conductive interfaces have been visualised in Figure 10.14 and 10.15. The yellow lines represent fused conductive interfaces which consider the geometries to be of one piece of material. The orange lines represent the contact interfaces, for which a contact conductance is be specified by the user. This conduct conductance has not been changed from before. The major locations of interest would most likely be the connections with the hinges, as well as within the hinges themselves. These contact interfaces are currently set at a negligible value of 1 W/m^2K, such that the majority of the analysis is based on the radiative heat flow contribution.

10.1.5.b Discussion

The temperature results as presented within this report consider averaged or global node temperatures of entire component groups. In order to determine the conductive interfaces correctly it is thought that gradient

Table 10.4: Temperature results for the DST 7.3.1 and 7.3.2, for HOT conditions in degrees Celsius.

	DST 7.3.1					DST 7.3.2				
	Glo. Min	Av. Min	Av. ΔT	Av. Max	Glo. Max	Glo. Min	Av. Min	Av. ΔT	Av. Max	Glo. Max
Baffle Bl.	-75.0	-7.0	9.0	2.0	130.0	-75.0	-7.1	9.1	2.0	132.5
Baffle Str.	-2.5	19.2	25.3	44.5	127.5	-2.5	19.2	25.4	44.6	127.5
Spider	15.0	24.7	6.1	30.8	42.5	15.0	24.4	6.5	30.9	42.5
Top Hinges	17.5	21.4	15.1	36.5	42.5	17.5	21.4	15.2	36.6	42.5
M2	27.5	27.2	3.2	30.5	30.0	27.5	27.4	0.4	27.8	27.5
Booms	20.0	22.6	13.4	36.0	42.5	20.0	22.6	13.5	36.1	45.0
Root Hing.	22.5	24.3	5.7	30.0	32.5	22.5	24.3	5.7	30.0	32.5
M1	25.0	25.8	0.4	26.2	30.0	25.0	25.8	0.4	26.2	30.0
PMSS	22.5	24.8	4.5	29.3	37.5	22.5	24.8	4.6	29.4	37.5
IH	20.0	22.5	10.8	33.3	35.0	20.0	22.5	10.8	33.3	35.0

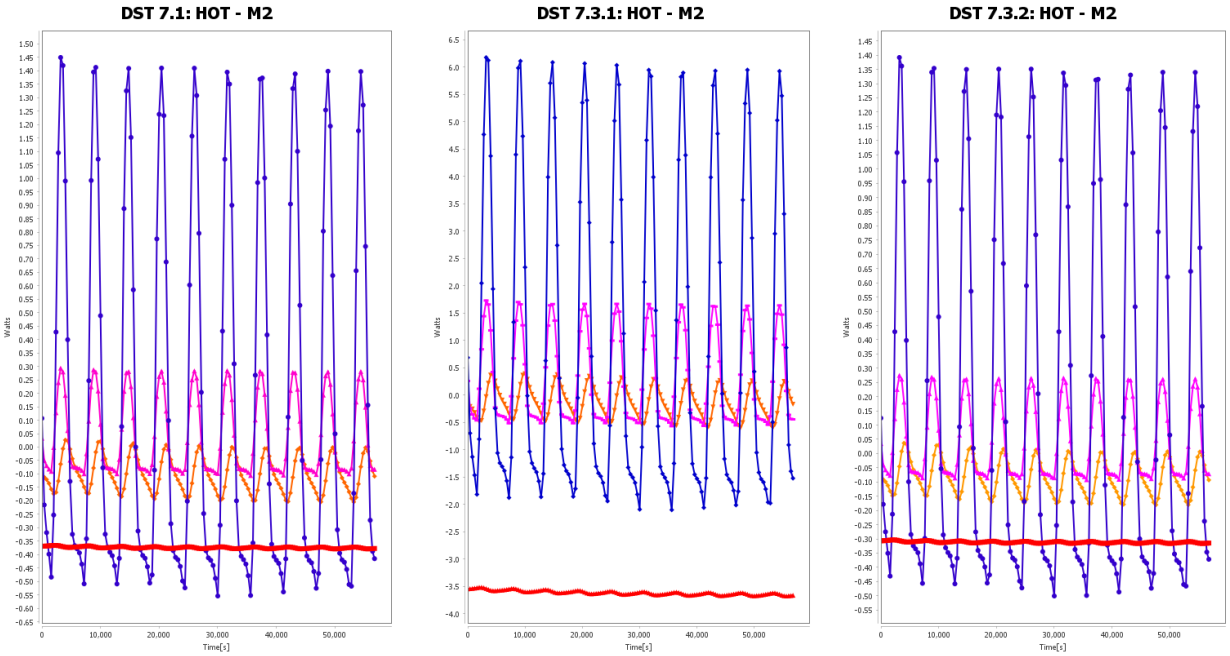

(a) DST 7.1 (b) DST 7.3.1 (c) DST 7.3.2

Figure 10.13: Total heat flow results from the SMSS towards the baffle structure (pink), telescope (orange), baffle interior (blue) and space (red). The results are produced within the Workbench of ESATAN TMS.

temperatures are required per component. Further, the conductive interfaces between the components of the hinges is thought to require a detailed analysis while this report includes the global analysis. Besides, the resulting deformations are not known since the thermomechanical model is not present yet.

Therefore, it is thought that the conductive interfaces should remain as they are. It is recommended to re-evaluate these contact conductive interfaces when gradient temperature data and a thermomechanical model is present.

10.2 Considered Thermal System Designs

The considered thermal system design as will be used for the subsequent budget analysis will not comprise one system only. This is because a comparison will be made with the current system design and the proposed system design. Their differences are depicted in Table 10.5. These differences are based on the previous analysis and have therefore not been further optimised. Neither of these models consider a fully reflective secondary mirror as aforementioned before. The following thermal model design will be considered for the final analysis:

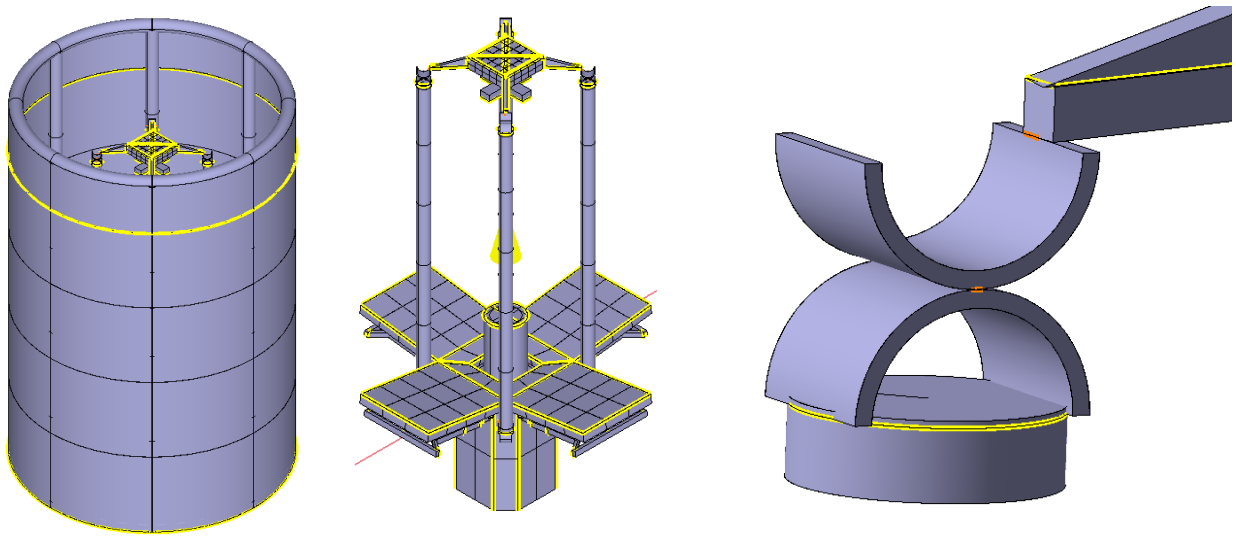

(a) Baffle (b) Telescope (c) Top Hinge

Figure 10.14: Visualisation of the conductive interfaces for several DST components, DST 7.3.2 model. As visualised within the Workbench of ESATAN TMS.

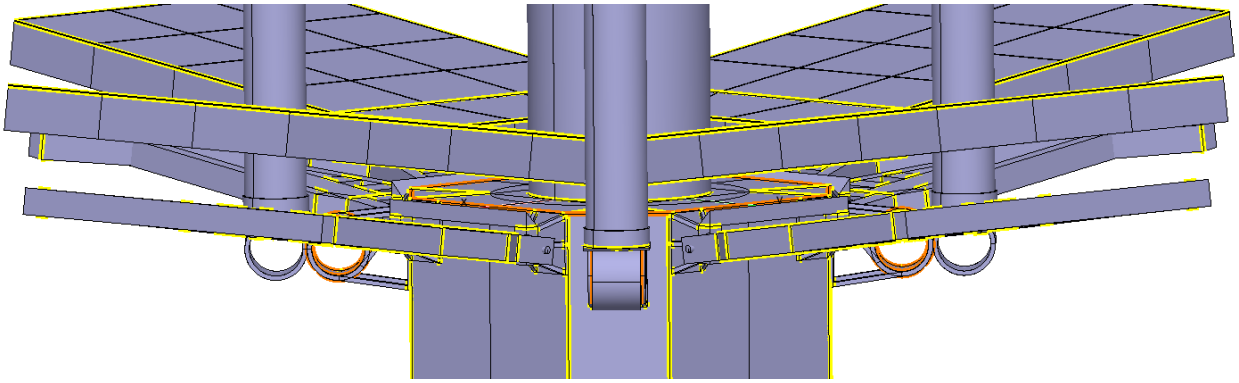

Figure 10.15: Visualisation of the conductive interfaces for the instrument housing and the root hinges, DST 7.3.2 model. As visualised within the Workbench of ESATAN TMS.

DST 2.8

This model is similar to the DST 2.7, which is considered fully representative of the current DST design with nominal baffle, including a spider top plate. Further, the SMSS is considered to be in need of a black coating, hence it will be referred to as the DST 2.8 model.

DST 7.1.2

This model features a 20 cm lengthened baffle with a reflective spider top plate. This configuration is chosen because it is known to reduce heat flow from space towards the telescope. Besides, its feasibility has been confirmed by E. Korhonen.

DST 7.2

This model features a 20 cm lengthened baffle, a reflective spider top plate and a reflective baffle design composed of one vane (50cm). This configuration is expected to feature superior performance although its deployability may be considered as a killer requirement for this design.

Table 10.5: Considered DST thermal models for the final performance.

	Black coated SMSS	Lengthened Baffle	Reflective Baffle Interior
DST 2.8	X	-	-
DST 7.1.2	X	X	-
DST 7.2	X	X	X

10.3 Operational Window Investigation

The aforementioned thermal system designs need to be investigated for a suitable operational window. This investigation will consider thermal results & analysis (10.3.1). This analysis will be concluded with a discussion (10.3.2).

10.3.1 Thermal Results & Analysis

This investigation will consider COLD, HOT and median (MED) conditions as presented in Appendix D *Thermal Modelling Conditions*. The considered system designs have been exposed to these conditions for which results are shown in Appendix H *Operational Window Results*. These results consider the PMSS (red) and the SMSS (yellow) only for the duration of one orbital period, since those are considered to be relevant for choosing a suitable operational window.

Approach

The PMSS is considered to be relevant for the M1 alignment budgets while the SMSS is for M2. These systems are composed of different materials, hence their CTE will not be equal. Nevertheless, an assumption needs to be made thus for now it will considered that their CTE is at least similar. Therefore, the approach will be to select the operational window such that the temperature differences between the two systems are smallest. The duration of this window is set at 1000 seconds which is arbitrary.

Analysis

The analysis will consider each thermal model separately.

Current Design (DST 2.8)
The behaviour of the COLD and MED results seems to be similar. This is not necessarily unexpected since they feature the same orbital parameters, thus the main difference would be found for the intensity of the graphs. The results seem to be most apart between 60000 to 61000 seconds, thus the operational window should not be chosen there. The initial part of this orbit is considered to be most stable, hence the operational window for this model is set at 57000 to 58000 seconds for all three conditions.

Lengthened Baffle (DST 7.1.2)
The temperature behaviour of this model is similar to that of the DST 2.8. The main difference can be found for the PMSS for COLD and MED conditions since it is colder than the SMSS and therefore its operational window is different too. These windows are chosen separately for each condition.

Reflective Baffle Interior (DST 7.2)
The temperature behaviour of this model is completely different from the other models for COLD and MED conditions, although they are similar to themselves. The operational window is therefore chosen separately for the HOT condition.

Operational Window Selection

The determined operational windows are summarised in Table 10.6. The DST 2.8 has equal operation window for all conditions, while the DST 7.1.2 has a different operational window for each condition. The DST 7.2 has equal operational window for COLD and MED condition, but a different one for HOT conditions.

The following budget analysis requires an average ΔT for the selected operational window. In order to do this correctly and fair, one should use each respective window as determined in Table 10.6. Further, one would have to assume that the systems can be aligned at those temperatures.

Table 10.6: Operational window summary as considered for the 11th orbital period, x1000 seconds.

	DST 2.8	DST 7.1.2	DST 7.2
COLD	57-58	60-61	57-58
MED	57-78	59-60	57-58
HOT	57-58	57-58	59-60

10.3.2 Discussion

The desired operational windows are not equal for each model, nor for each set of thermal conditions. Therefore, it would complicate the budget analysis since the ΔT should be determined for each model and conditions separately. This is not considered to add value since the analysis is founded on many assumptions. Besides, the actual operational window is considered to be a function of the desired imaging regions.

The main conclusion which can be drawn from this operational window analysis is that the most suitable window will be a function of the thermal conditions and the eventual baffle configuration. The ideal window is therefore not considered to be constant throughout the lifetime of the satellite.
For the following thermal budget analysis it is chosen to use the average system temperatures for the 11th orbital period, such that the results can be considered converged. These results are depicted in Appendix I *Averaged Temperature Results*. They can be considered as the largest temperature fluctuation for each model and condition, throughout an orbit.

10.4 Thermal Modelling Budgets

The thermal model budgets are considered to be divided into budgets related to the aforementioned imposed thermal requirements (10.4.1), and those related to the optical budgets (10.4.2).

10.4.1 Thermal Budgets

The thermal requirements have been gathered in Chapter 3. These requirements are related to the SMSS and the PMAO system. The majority of the PMAO requirements have been checked for compliance in section 7.4. The PMAO has not been included in any of the following models since it is considered incomplete without the exterior housing design. The remainder of the requirements have also been checked for compliance for which the result are summarised in 10.8. Some of the requirements could not be checked for compliance since the considered thermal model featured a deployed configuration only. The only remaining relevant requirement is discussed below.

M2-THE-02

This requirement states the bulk temperature of the booms shall not exceed 200°C or 175°C including margin. The HOT conditions are most likely to be most critical for which global maximum temperature results are summarised in Table 10.7. The largest boom temperature is seen for the DST 2.8 model. Nevertheless, it is not even close to the 175°C constraint. Therefore, it is given a conditional pass.

Table 10.7: Global maximum temperature of the SMSS booms, for HOT conditions.

	DST 2.8	DST 7.1.2	DST 7.2
Booms	48.4	44.1	21.8

Table 10.8: Thermal requirements verification summary.

ID	Description	Configuration	Verification Reference	Compliance	Comment
Component Bulk Temperature Limits					
M2-THE-01	The bulk temperature of the booms shall not exceed 373K during stowage.	Stowed	-	TBD	Needs a stowed thermal model
M2-THE-02	The bulk temperature of the booms shall not exceed 473K when deployed.	Deployed	Table 10.7	Conditional Pass	Based on simulated HOT conditions
PMAO-THE-01	The bulk temperature of the universal joints shall not deviate more than 2285 K from the assembly temperature (nominally 298 K).	Any	Appendix G	Partial	Based on analogy for deployed state only
PMAO-THE-02	The bulk temperature of the in-plane constraint wire flexures shall not deviate more than 318 K from the assembly temperature (nominally 298 K).	Any	Appendix G	Partial	Based on analogy for deployed state only
PMAO-THE-03	The bulk temperature of the moving frame plate shall not deviate more than 442 K from the assembly temperature (nominally 298 K).	Any	Appendix G	Partial	Based on analogy for deployed state only
Instrumentation Limits					
PMAO-THE-06	The maximum gradient between the actuators in a push/ pull pair (actuators A,C and B,D) shall not exceed 0.01 K.	Any	Appendix G	Fail	Needs a physical exterior housing including thermal control.
PMAO-THE-07	The bulk temperature of the actuators in non-operational phases shall not exceed the range 288 K to 373 K.	Stowed	-	TBD	Needs a stowed thermal model
PMAO-THE-08	The bulk temperature of the actuators in operational phases shall not exceed the range 288 K to 298 K.	Deployed	Appendix G	Fail	Needs thermal control

10.4.2 Optical Budgets

The optical budgets are considered to be a function of the top down system engineering budgets (10.4.2.a). The coarse alignment budgets will be approached using a coarse position calculation method (10.4.2.b). Results will be produced and analysed (10.4.2.c). The analysis will be concluded with a final discussion (10.4.2.d).

10.4.2.a Top Down System Engineering Budgets

The top-down system engineering budgets have been formulated in the work of [7] and relaxed slightly afterwards, shown in Figure 10.16. The budgets consider deployment/coarse alignment budgets, in-orbit drift budgets and stability budgets, with respect to the optical axis frame, as depicted in the thermal model. The idea is that the telescope will be deployed within its deployment budgets such that it can be considered coarse aligned, while a fine actuation system like the PMAO will keep its system within the remaining budgets. These budgets consider translations, rotations, a difference in radius of curvature, and shape error, for the primary-, secondary- and tertiary mirror.

Most of these budgets should be evaluated by means of a thermomechanical model, although a coarse translation analysis is thought to be possible for M1 and M2. The budgets as shown in Figure 10.16 are similar in X and Y, but different from Z. In the upcoming analysis one will consider the position deployment/coarse alignment budgets for M1 and M2 only.

	Position			Orientation			Radius	Shape Error
Element	X [μm]	Y [μm]	Z [μm]	X [μrad]	Y [μrad]	Z [μrad]	[%]	[nm]
Deployment/ Coarse Alignment Budget								
M1	2	2	2	2	4	50	1×10^{-3}	50
M2	15	15	10	100	100	100	1×10^{-2}	25
M3	4	4	4	10	10	50	1×10^{-3}	10
In-Orbit Drift Budget								
M1	2×10^{-2}	2×10^{-2}	2×10^{-2}	1×10^{-2}	2×10^{-2}	5	1×10^{-4}	5
M2	4	4	2	6	6	12	1×10^{-4}	5
M3	1×10^{-1}	1×10^{-1}	1×10^{-1}	1	1	5	1×10^{-4}	5
Stability Budget								
M1	5×10^{-3}	5×10^{-3}	5×10^{-3}	2.5×10^{-3}	1×10^{-2}	5×10^{-1}	n/a	n/a
M2	1	1	5×10^{-1}	1.5	1.5	3	n/a	n/a
M3	2.5×10^{-2}	2.5×10^{-2}	2.5×10^{-2}	2.5×10^{-1}	2.5×10^{-1}	1.25	n/a	n/a

Figure 10.16: Top down system engineering budgets as defined by D. Dolkens, taken from [13].

10.4.2.b Coarse Position Calculation Method

The coarse position alignment budgets will be approximated using a simplified calculation method for both mirrors. These methods consider homogeneous- material properties, temperatures and expansion. Thus, the defined components are considered to be expanding or contraction in equal amount to all sides. Besides, it will be assumed that the system is able to align itself at either of the two temperature extremes. The calculation method will be evaluated per mirror.

Primary Mirror Budget

The primary mirror budgets are considered to depend on: the primary mirror segments, the instrument housing and the primary mirror support structure. The PMAO system is not included in the current thermal model and is therefore excluded here. Each of these components will expand or contract in all direction equally, although some of these systems are constraint due to which they are mounted.

Optical Axis System
A visualisation of the optical Axis system has been given in Figure 10.17a. The $X_O Y_O Z_O$ axis system refers to the optical (O) axis system, while the $X_M Y_M Z_M$ axis system refers to the mechanism axis system. The latter axis system will be used as reference for expressing the expansion of the considered geometries. The system is considered to be symmetric in X and Y and therefore X is not considered.

Directions & Distances of Deformation
The considered directions & distances of deformation of the mirror, the PMSS and the instrument housing are

shown in Figure 10.17b and 10.17c respectively. The primary mirror segments and the instrument housing are in theory not constraint for small temperature increments. However, the support structure is because it cannot deform towards the instrument housing since it is hinged onto it. It says small because these structures are able to expand finitely. The deformation of the instrument housing is parallel to the optical axis, those of the primary mirror segments and the support frame are not. The primary mirror segments are considered to deform in all directions and to be mounted directly onto the primary mirror support structure, thus not considering the PMAO. The primary mirror consists of four segments for which the budgets need to be met by each segment separately. The segments are considered to deform in all directions evenly, thus its segment centre will in theory not deviate from X_O and Y_O, but it will deviate in Z_O.

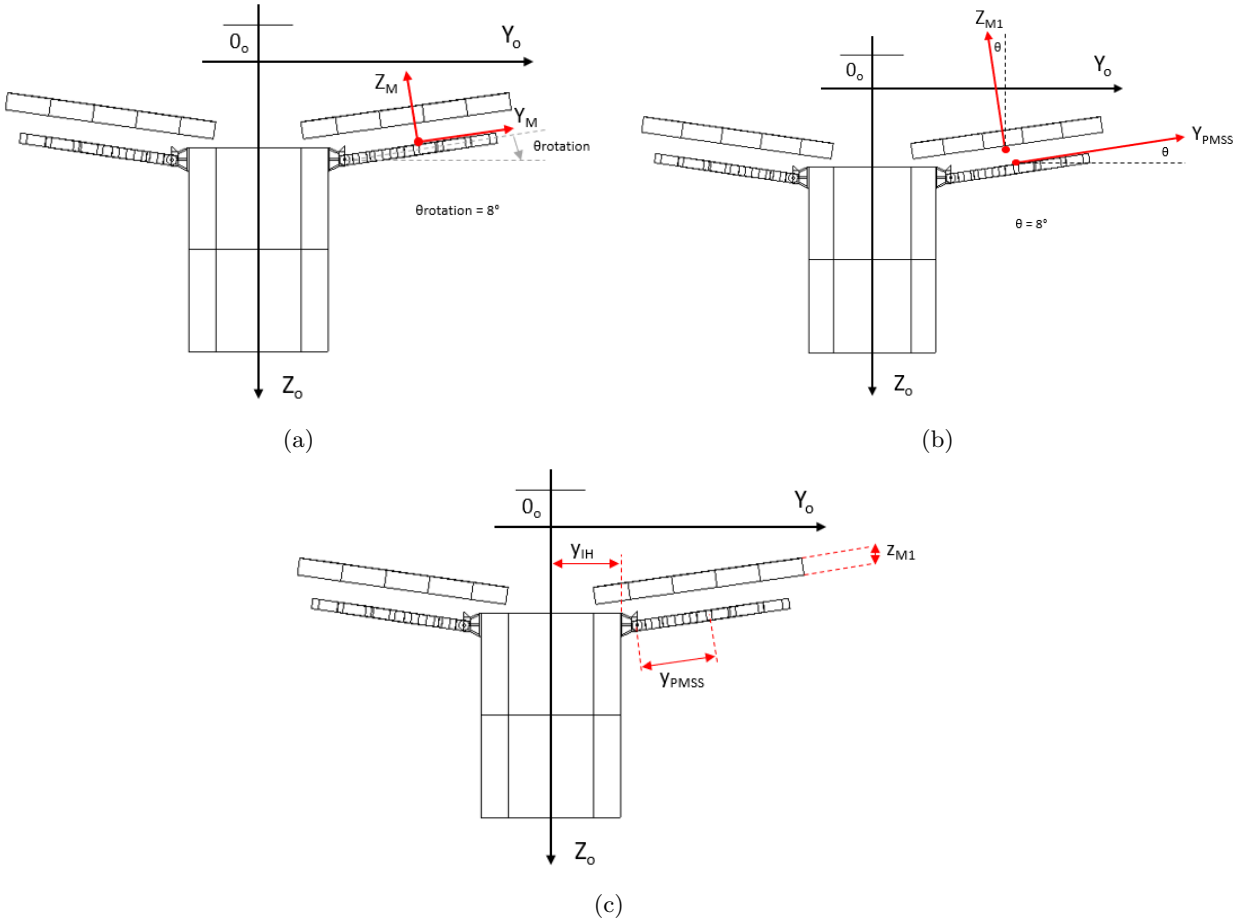

Figure 10.17: Baseline design of M1 mechanism coordinate frame with rotated primary mirror segment (a) (idea taken from [13]), thermal expansion directions (b) and thermal expansion distances (c).

Calculation Method

The considered M1 element translation contributions in Y_M and Z_M are depicted in Table 10.9. The translation distances have been determined using the measurement function in CATIA. The results are depicted in Table 10.10. For the primary mirror this considers the average thickness. In order to calculate deformations one requires to multiply these distances with the respective CTE of the material and the approximated ΔT. The resulting equations are shown in Appendix J *Coarse Translation Calculation*.

Table 10.9: Translation discovery in Y_O and Z_O for M1 alignment.

Translation direction	**M1**	**IH**	**PMSS**
Y_M	-	y_{IH}	$\cos(8°)\cdot\ y_{PMSS}$
Z_M	$\cos(8°)\cdot\ z_{M1}$	-	$\sin(8°)\cdot\ y_{PMSS}$

	z_{M1}	y_{IH}	y_{PMSS}
Distance [m]	0.05	0.410	0.470

Table 10.10: Considered deformation distances for M1 alignment.

Secondary Mirror Budget

The secondary mirror budgets are considered to depend on the thermal performance of the SMSS, consisting of: the booms, the secondary mirror and its interface, the spider, the top hinges, the instrument housing and the root hinges. For the same reasons as for the M1 alignment, the instrument housing will not be considered in Z. The secondary mirror is considered to be centred with the Z_O axis. The DST is considered to be fully symmetric in X and Y. Thus, when considering homogeneous- temperature and expansion, one cannot address a translation in these two directions. Translations in Z can be addressed and will consist of straight contributions only.

Distances of Deformation
The considered deformation distances of the SMSS have been visualised in Figure 10.18. These distances have been adopted from the work of A. Krikken, as presented in Figure 9.10 [12]. The boom distance is included with the height of the spider. Further, the booms are expected to dominate this translation. The calculation method is shown in Appendix J.

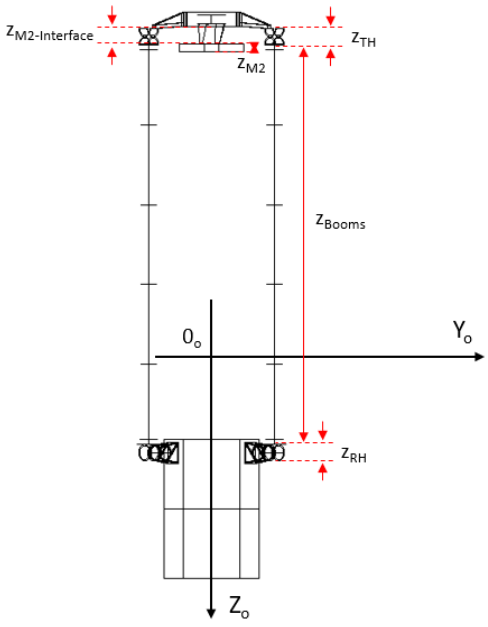

Figure 10.18: Thermal expansion distances as considered for the secondary mirror support structure and M2.

	z_{M2}	$z_{M2-interface}$	z_{TH}	z_{Booms}	z_{RH}
Distance [m]	-0.04	-0.0817	0.04625	1.7657	0.0319

Table 10.11: Considered expansion distances for M1 alignment.

10.4.2.c Results & Analysis

The primary- and secondary mirror budget equations have been combined with the CTE as defined in Appendix C *Thermal & Thermo-Optical Properties* and the average ΔT as depicted in Appendix I *Averaged Temperature Results*. The coarse alignment budget results are summarised in Table 10.12. The violated budgets have been highlighted in red while the non-violated budgets are indicated in green.

Budget Analysis
The COLD alignment budgets seems to be violated by the current design only. The heat inputs are low and thus the experienced Δ are low too. The MED alignment budgets are satisfied for the reflective baffle only. This is mainly caused by the ΔT of the instrument housing (M1) and the SMSS booms (M2). The original baffle is not sufficient in reducing the heat flow to and from these components, while the lengthened baffle is for COLD conditions. The HOT alignment budgets for M1 and M2 are violated for all configurations.

Performance Analysis
The lengthened baffle has more green coloured deformation approximations, although their differences are only about 15 to 50%. The resultant deformations for the reflective baffle are 3 to 6 times as small based on the averaged ΔT. Therefore, it can be concluded that the reflective baffle design is significantly more effective in reducing deformations compared to a lengthened baffle only.

Table 10.12: Summarised translations for the M1 and M2, for COLD and HOT conditions, assuming maximum ΔT, including their respective coarse align position budgets.

		COLD		MED		HOT		Coarse Budget	
		Y [μm]	Z [μm]	Y [μm]	Z [μm]	Y [μm]	Z [μm]	Y [μm]	Z [μm]
Current Design (DST 2.8)	M1	2.11	0.04	2.48	0.06	14.12	0.50	2	2
	M2	-	8.56	-	10.26	-	49.66	5	10
Lengthened Baffle (DST 7.1.2)	M1	1.83	0.03	2.10	0.04	13.61	0.43	2	2
	M2	-	7.54	-	9.21	-	49.01	5	10
Reflective Baffle (DST 7.2)	M1	1.15	0.061	0.51	0.01	2.96	0.09	2	2
	M2	-	2.72	-	2.23	-	12.4	5	10

10.4.2.d Discussion of Results

The calculated alignment budgets consider the maximum average temperature variation throughout one orbit. Further, it considers the system to be aligned at either of two extremes. Besides, it considers the extremes to occur at the same time and approximated deformation distances. Therefore, the magnitude of these budgets are **not** representative of actual deformation calculations.

Nevertheless, it is likely that the current- and lengthened baffle designs are in need of thermal control in order for them to stay within the coarse alignment budgets for M2 in Z direction and for M1 in Y, during operation for HOT conditions. This results into a specific need for thermal control of the SMSS booms since those feature the largest deflections. The SMSS has been made athermal by its designer, although this method is only useful for equal system temperatures at target temperature. Further, the instrument housing has not been designed in detail yet. Therefore, it should be given sufficient thickness for it to expand and/or contract less.

The reflective baffle design has the most constant heat flow from and to the telescope, which result into lowest temperature fluctuation throughout an orbit. Therefore, it features the smallest deformations. However, a downside of this configuration is that the average telescope temperatures are lowest. If this would require even more thermal control for raising these system temperatures, it would not necessarily be considered as an improvement. Therefore, a thermomechanical model shall determine which is worst.

10.5 Chapter Summary

This Chapter has been included with an investigation regarding the desired thermo-optical control coatings for the SMSS and the secondary mirror, a reflective baffle interior and the conductive interfaces. The SMSS has been coated with the magic black coating for it to reduce stray light. The spider has been included with a reflective top plate for it to reduce heat flow and the baffle interior has been made partially reflective for it to reduce heat flow towards the telescope.

The current design (DST 2.8), the lengthened baffle design (DST 7.1.2) and the reflective baffle design (DST 7.2) have been selected for the operational window investigation. Eventually, it was chosen to select the maximum average temperature variation throughout an orbit (ΔT), for COLD, MED and HOT conditions. The coarse position alignment budgets of the top down system engineering budgets have been approximated using these average ΔT. The analysis considered that the system could be aligned at either of the two extremes, from which the budgets have been calculated. The results have shown that the M2 budgets in Z are most likely to be critical due to expansion of the SMSS booms. This can be mitigated by the reflective baffle design, since the lengthened baffle only is just a minor improvement. Further, the M1 budgets showed to be critical in Y due to expansion of the instrument housing. Therefore, the to be designed housing should be given sufficient thickness for it to expand and/or contract less. Finally, it should be mentioned that it is likely that all configurations require additional thermal control for COLD conditions, the least.

11 Thermal Model Discussion

The constructed geometric thermal model can be different from the actual design. These difference are considered to effect their approximated thermal performance (11.1). Some particular thermal results consider simplified conditions or have not been optimised (11.2).

11.1 Discussion of the Thermal Model Geometries

For each of the DST components it will be elaborated below how these relate to their respective geometry as modelled in the fully representative thermal models. The thermal model component performance statements are summarised in a trade-off table, shown in Table 11.1. This Table basically describes how good the thermal model performs in approximating the average-, extreme- and gradient temperatures. The average temperatures are assumed to be a function of the thermal resistance which is considered to be a function of the density and specific heat of the material, and the volume of the geometry. The used material properties are for the majority in line with those of the detailed design, but their volume in the thermal model is not necessarily. The extreme temperatures are usually suffered by geometries with sharp corners, therefore those should have been avoided when possible. Gradient temperatures describe a temperature distribution or difference over distance, which requires a refined grid for it to feature sufficient detail.

Spider

The spider as considered in the initial model has been adjusted accordingly for it to feature no imperfections due to which unrealistic temperature spikes would occur, it has been included with a top plate for it to reduce stray light. The adjustments consider refining of the grid and redefinition of particular geometries with sharp corners. A stray light analysis shall determine whether the top plate can be made reflective or not. A mechanical analysis shall determine the required thickness of the top plate. Apart from these recommendations, it is thought that the spider is a close representative of the actual spider geometry.

Baffle

The baffle is considered to be composed of the baffle structure and the baffle blanket. The cylindrical baffle was relatively easy to model and therefore it is thought that the baffle structure is good representation of its detailed design.

Baffle blanket
The baffle blanket is considered to be of great importance for determining the thermal performance of the telescope. It has been modelled featuring four different layers, composed of an two outer layers, an insulation layer and an inner layer. This structure could most possibly be simplified, for which a professional of ADS (N. van der Pas) can be approached.

Outer Layer
The outer was set at FEP/VDA since it features the smallest fluctuations in temperature of the considered outer layers. This layer is most determinate for the outer layer temperature itself, with negligible effect on the telescope. Therefore, this layer can be chosen differently although it is not expected to improve telescope performance.

Insulation Layer
The insulation layer has been modelled using an average net conductive value, representative of the emissivity and the conductivity. It is thought that this layer is most determinant for the amount of heat which is transported from the outer layer to the inner layer, which eventually is radiated towards the telescope. Since the net conductive value is representative of an actual design and because its respective surface activity is set at conduction only, it is thought to provide reliable results.

Inner Layer
The required highly absorptive and thus highly radiative coating of the inner layer is most determinant for the amount of heat which is radiated toward the telescope. These properties are not considered to change in relation to stray light reduction. The thickness of the inner layer cannot be made thick either since it needs to be foldable. Therefore, it is thought that the reflective baffle design should be thoroughly checked for feasibility.

Booms

The booms exterior dimensions were relatively easy to model. The booms have not been included with the intended cutouts, which is simply because those are quite difficult to model. It is considered to effect the results since those cutouts will restrict the conductive path at those locations, although it will already be limited by its relatively low thermal conductivity in the first place. Since the booms turned out to be a critical component for M2 alignment, it will be recommended to include this feature in a more detailed analysis.

Top Hinges

The top hinges have been modelled by means of two partial cams and the boom attachment. These hinges do not include cutouts are any of the small components, although the housing for the ribbons for example is most likely to be removed. The dimensions are in line with the CATIA model and the orientation and shape of the major components are too. Its thermal resistance and its view factors are expected to be close to the actual values. The conductive couplings between the cams and the boom- and spider attachment need to be determined in detail. These couplings are expected to be most important for the hinge performance itself since it features moving parts. Therefore, it will be recommended to include or determine these in a more detailed analysis.

Root Hinges

The root hinges are modelled in a similar sense to that of the top hinges, while the root hinges are included with a base. Its dimensions are likewise taken from the CATIA model and the conductive couplings between the cams and the base are still to be determined. The recommendation will therefore be identical to that of the top hinges.

The Primary Mirror Segments

The actual primary mirror segments are concave with varying thicknesses, while they are modelled as straight segments of constant thickness and inclination. The cut-offs at the tip are made similar to those of the actual model, but the mass saving cutouts are not. Therefore, it should have been given a smaller thickness such that its thermal resistance would be similar to those of the actual segments. The effect of not featuring the concave shape is considered to be small because the effect of the respective REF of those nodes are expected to be negligible. Therefore, the recommendation will be to adjust the thickness accordingly for it to match the thermal resistance of the actual design.

Secondary Mirror

The actual secondary mirror is monolithic with smaller thickness and round corners at the ends, while it is modelled as two solid rectangles. Since the actual geometry does not feature any cutouts, it is thought that the modelled thermal resistance is similar to the actual design. The secondary mirror interface has been modelled by means of aluminium alloy cylinders and the analysis had shown that the secondary mirror is quite constant in temperature. It is therefore thought that the conductive couplings with the secondary mirror should minimise heat flow for now.

Instrument Housing

The instrument housing has not been designed in detail before. Its outer dimensions are depicted in the CATIA model although its interior, thickness and material are yet to be determined. It has been assumed that it will be made of CFRP with a thickness of 1mm, although this is rather arbitrary. The summarised translation budgets showed that the instrument housing should be given sufficient thickness for to feature sufficient thermal resistance. The interior of the instrument housing has been made inactive, although it will house, among other equipment, M3 and DM. A detailed design will comprise several heat sources and heat sinks, and will plausibly require an insulating interior housing. The housing is expected to be thermally insulated from the mirrors and their support structure. Therefore, it is not considered necessary to be designed after this work.

Primary Mirror Support Structure

The primary mirror support structure can be considered as one of the most complex geometries. It consists of many small components and pieces, although the thermal resistance is thought to be representative of the actual case. Since it is placed under an average angle of 8 degrees, it does include some tiny gaps between certain geometry pieces which is known to effect the global maximum temperatures. The support frame does include

some athermalization measures as described in [15], although those are not included within the thermal model. It is therefore recommended to either adjust some of the pieces such that gaps disappear or ignore those node temperatures during analysis. Besides, athermalization measures can be included in the future in case possible, which could potentially improve its thermal performance.

Field Stop

The field stop has been approximated in accordance with the system designers, although its actual size should be re-evaluated by means of dedicated calculations. The field stop housing is considered to be part of the instrument housing.

Table 11.1: Respective thermal model component temperature approximation performance for average-, extreme- and gradient temperatures.

	Average	**Extreme**	**Gradients**
Spider	Precise geometry modelling, apart from top plate	Sharp corners have been modified	Refined grid
Baffle Structure	Precise geometry modelling	The booms intersect the torus	Descent grid distribution
Baffle Blanket	Approximated interior layer	Approximated interior layer	Descent grid distribution
Booms	Precise geometry modelling, apart from cutouts	Cutouts can effect the behaviour	Cutouts will effect gradients
Top- & Root Hinges	Major components have been modelled coarsely	Sharp corners are kept to the minimum	Conductive couplings need to be determined
Primary Mirror Segments	Mass saving cutouts not considered	Sharp corners have been modified	Mass saving cutouts not considered
Secondary Mirror	Proper representation of detailed design	Sharp corner do not effect extremes	Requires grid refinement
Instrument Housing	Not representative of detailed design	Not representative of detailed design	Not representative of detailed design
PMSS	Proper representation of detailed design	Does include some gaps	Descent grid distribution

Temperature Approximation	**Colour**
Excellent	Blue
Good	Green
Sufficient	Yellow
Unacceptable	Red

11.2 Discussion of Particular Thermal Results

The thermal performance of the thermal model components have been discussed in the previous section. Some of these components have been adjusted for it to improve performance. The coarse position analysis, as provided in Chapter 10, can be considered simplified. The chosen thermal model environment and its worst case conditions are taken globally. All of these aspects shall be discussed below.

Baffle Extension

The baffle has been extended with 20cm since it turned out to reduce the experienced telescope temperature variations throughout an orbit. This research has been useful for demonstrating the potential effects of such a design. The length of the extension itself has **not** been optimised and should therefore be re-evaluated in combination with the proposed reflective top section baffle design.

Reflective Interior Layer Design of the Baffle

The top section interior of the baffle needs to be made reflective. This will allow for heat, which enters the baffle through the opening, to be reflected back to space instead of towards the telescope. The effect of such a design has been simulated optimistically assuming that no heat was radiated towards the telescope, while in reality it will be minor. The detailed design of the proposed vane structure requires a dedicated ray-tracing simulation. Therefore, it is thought that it should be addressed towards the optical team.
Besides, the design should be deployable. This feature should be addressed towards the baffle designer.

Coarse Position Analysis

The coarse position analysis considered homogeneous- distributed component temperatures and CTE in every direction. Further, it considered the group components to have equal temperature. Therefore, the analysis used for determining the optical margin can be considered majorly simplified and non-representative of the complete deformation calculations.
A more extensive analysis is considered to include component temperature differences per group. Further, component gradient temperatures should be considered due to which geometries will suffer local deformations and possibly rotations. Besides, the mirrors are expected to experience radius of curvature- and shape deformations. The totality of these effects can be evaluated by means of a thermomechanical model. This coarse position analysis of this report can therefore be improved and extended by considered group component temperature differences and component gradients. This strengthens the need for a thermomechanical model.

Thermal Environment

The worst case scenarios, cold and hot thermal conditions, have been chosen such for it to result into the global and average minimum- and maximum node temperatures. The selected cold case was indisputably coldest since non of the other minimum thermal input conditions, resulted into similar coldest temperatures. For the hot case a selection had to be made from three potential cases. Eventually, it was decided to select an orbit with highest global temperatures instead of largest average temperature variations throughout an orbit. This choice has been made on basis of the desired thermal conditions, as well as the need for maximum global temperatures for other team members.
Further, the OLR and albedo contributions were considered to remain constant throughout simulation, apart from the satellite facing eclipse. These contributions should be approximated more closely at some point since large variations may occur for nearby polar orbits.

The analysis of this report can therefore be improved by means of incorporating several hot case scenarios, instead of one only. Further, it is known that an orbit including eclipse and non uniform heat inputs, will result into larger temperature variations throughout an orbit, and thus results into larger deformations.

11.3 Chapter Summary

The thermal model is sufficient to good in approximating the average- and extreme temperatures, apart from the primary mirror and the instrument housing. This because the primary mirror segment mass saving cutouts have not been considered and the instrument housing because it lacks a detailed design. The thermal model requires a more refined grid for most of its components, such that it can depict gradients sufficiently. Besides, the booms need to be included with cutouts and the top- and root hinges need to be included with specific conductive couplings.

The proposed lengthening of the baffle should be optimised in accordance with the suggested reflective baffle design. The top level system engineering budgets should be supplemented with a thermomechanical model for it to allow a more- detailed and extensive deformation analysis. The worse case scenario selection should be re-evaluated and extended, including eclipse, non uniform heat inputs.

III

Conclusions & Recommendations

(This page is intentionally left blank.)

12 Final Design & Performance

Several design adjustments have been discussed in the previous Chapters. These adjustments have been analysed regarding their thermal performance, for which a final design shall be presented in this Chapter. The performance of this design shall be presented after, including the performance of potential adjustments.

12.1 Final Design

The goal of this thesis is, among others, to provide a thermal model representative of the Deployable Space Telescope. Therefore, it is chosen to select the fully representative thermal model including the magic black coated SMSS as the final design. The final design is similar to the DST 2.8 model, since it is thought that this respective model is considered to most representative of the current geometric DST design. Its relation to the actual design has been thoroughly discussed in the previous Chapter. It is thus excluded from the PMAO and the baffle housing. The only difference between the final design and the DST 2.8 model is the colouring. The colouring has been changed such for it to match the expected colours of the selected thermo-optical measures. It must be mentioned that the following Figures are therefore included with black and white shades only.

The global final design is visualised in Figure 12.1. This Figure includes a transparent baffle such that the telescope can be seen within the baffle. The interior of the baffle and the SMSS are coated black as shown in Figure 12.2b. In Figure 12.2a it can be seen how the telescope is situated within the baffle for the shown attitude. A front and back view are shown in Figure 12.3a and 12.3b respectively. From these Figures it can be clearly seen how the mirrors are supposed to be reflective while the remainder of the structures are absorptive.

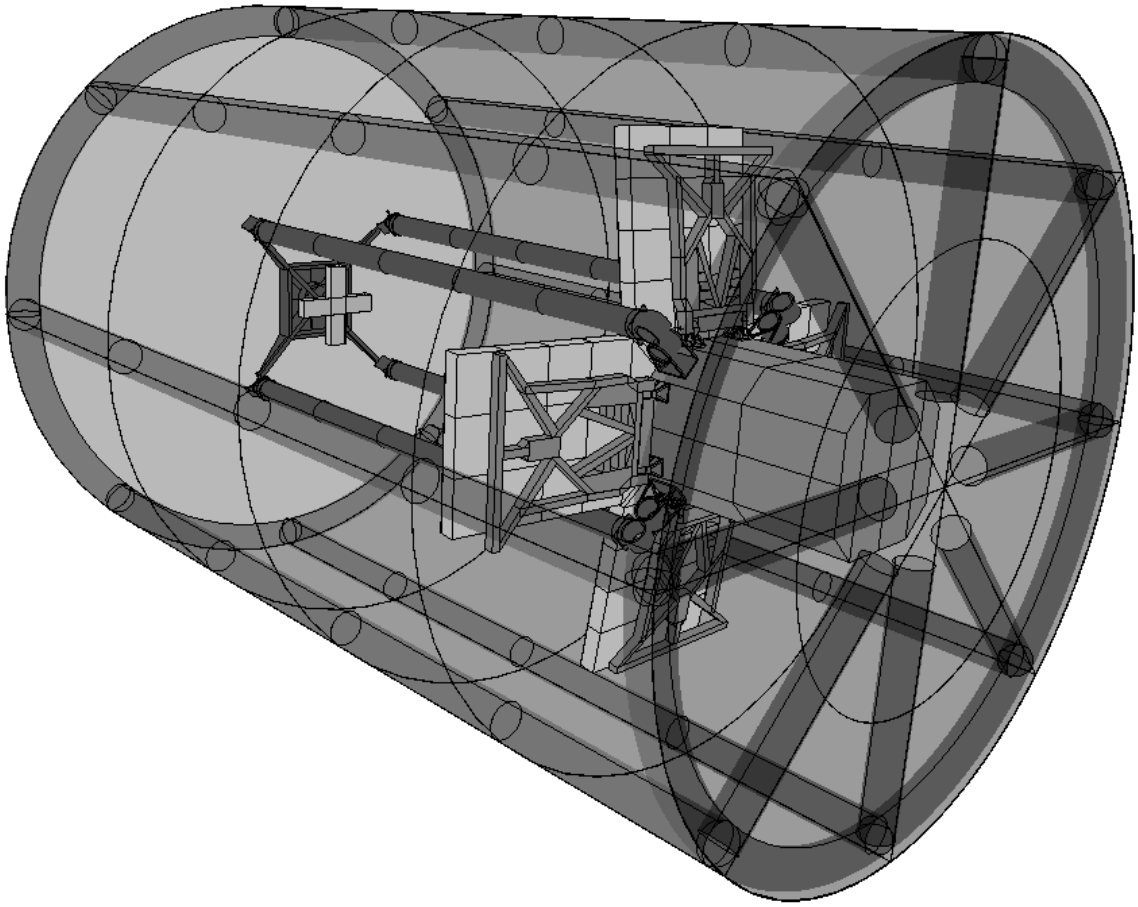

(a)

Figure 12.1: Visualisation of the final global thermal model design, as designed in the Workbench of ESATAN TMS.

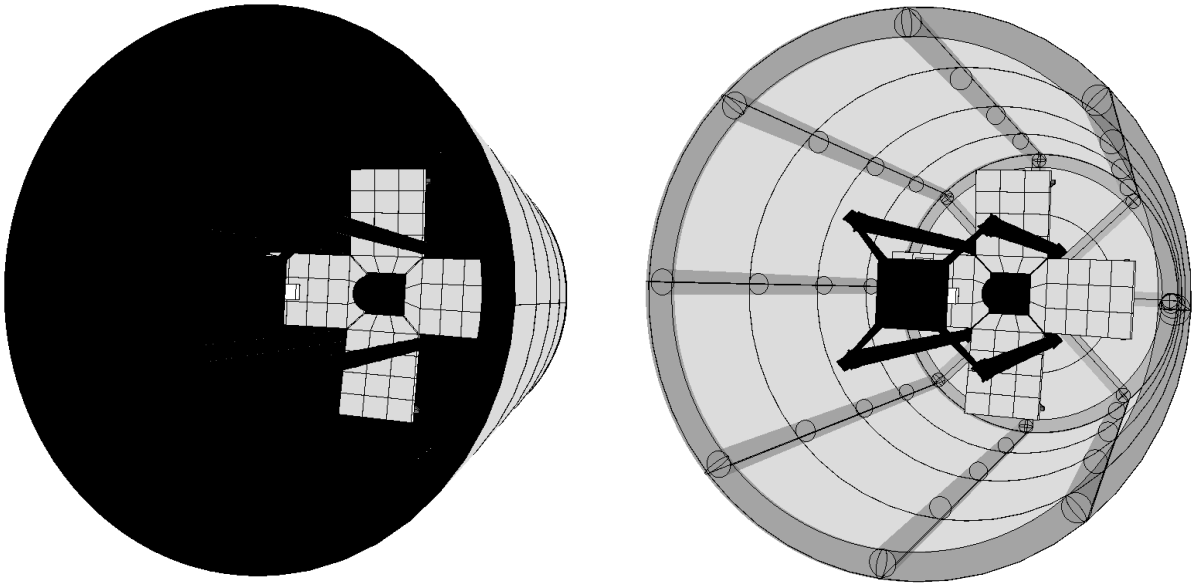

(a) (b)

Figure 12.2: Visualisation of the final thermal model baffle design with opaque baffle (a) and transparent baffle (b), as designed in the Workbench of ESATAN TMS.

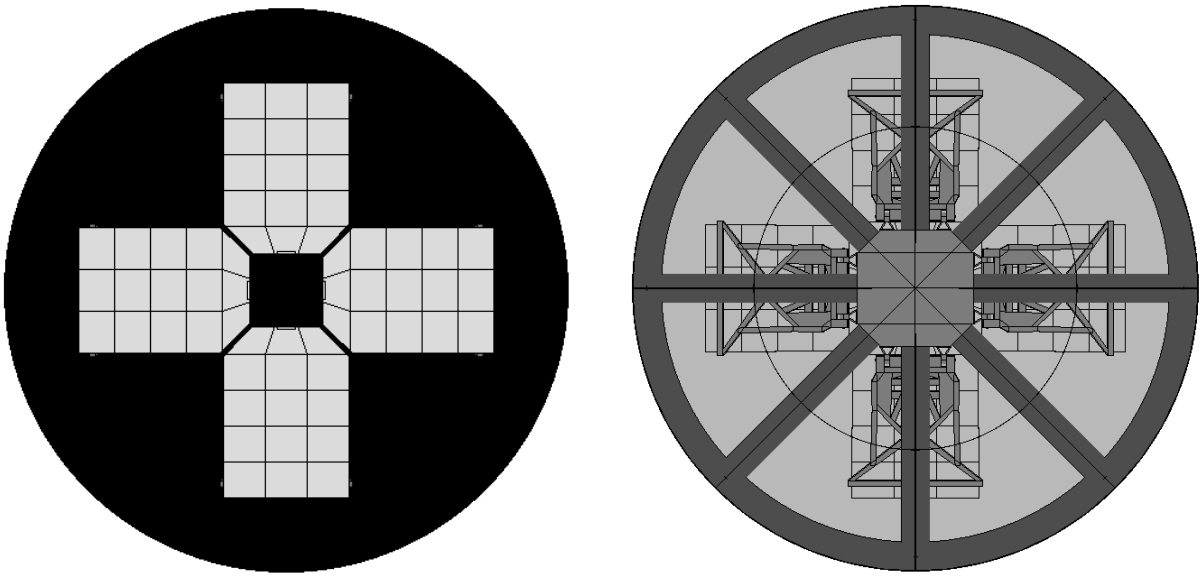

(a) (b)

Figure 12.3: Visualisation of the final thermal model design from the front (a) and the back with transparent baffle blanket (b), as designed in the Workbench of ESATAN TMS.

12.2 Final Performance

The final performance results are representative of coarse translations for M1 and M2. These translations have been determined in Chapter 10 for several configurations. The results are supplemented with those of the DST Without Baffle (WB) for it to indicate the difference with a baffle. The respective temperature results have been included in Appendix K *DST WB Temperature Results*.
A final overview is provided in Table 12.1. The thermal requirements have been checked for compliance in Chapter 10, as was shown in Table 10.8. Further, temperature results are provided for it to provide a clear overview of the expected minimum-, mean average- and maximum temperatures for COLD, MED and HOT conditions respectively. This temperature overview is shown in Table 12.2.

Coarse Alignment Position Budgets

The considered alignment budgets are most likely to be violated completely without the addition of a baffle. The budgets seem similar for COLD and MED conditions, while the M2 budget in Z direction seems to be less critical for HOT conditions. The largest improvements are seen for the M1 budgets by means of including a baffle, for extending it or by making it partly reflective. The M2 budgets are influenced to a lesser degree, which indicates that the baffle is less effective in reducing deformations of the M2 alignment systems. This effect can be best mitigated by making the baffle partly reflective.

Table 12.1: Summarised coarse alignment position budgets for the M1 and M2, for several conditions assuming maximum ΔT.

		COLD		**MED**		**HOT**		**Coarse Budget**	
		Y [μm]	Z [μm]	Y [μm]	Z [μm]	Y [μm]	Z [μm]	Y [μm]	Z [μm]
No Baffle	M1	14.39	0.90	16.09	1.08	32.38	2.91	2	2
(DST WB)	M2	-	28.01	-	29.80	-	5.38	5	10
Current Design	M1	2.11	0.04	2.48	0.06	14.12	0.50	2	2
(DST 2.8)	M2	-	8.56	-	10.26	-	49.66	5	10
Lengthened Baffle	M1	1.83	0.03	2.10	0.04	13.61	0.43	2	2
(DST 7.1.2)	M2	-	7.54	-	9.21	-	49.01	5	10
Reflective Baffle	M1	1.15	0.061	0.51	0.01	2.96	0.09	2	2
(DST 7.2)	M2	-	2.72	-	2.23	-	12.4	5	10

Temperature Results

The foreseen budget estimations assume that the system can be aligned at either of the two average temperature extremes. The final temperature results indicate the mean average temperatures are similar for all considered models with a baffle. The component temperatures of the telescope without a baffle are generally different from each other. Besides, the global temperature differences between minimum and maximum are largest. The global temperature differences between the baffled models are similar, although the reflective baffle design has smallest for the baffle. The latter model is also coldest. Further, the lengthened baffle has smallest global temperature differences for the top section components (spider, top hinge and M2).

Table 12.2: Final temperature results for the fully representative Deployable Space Telescope- with baffle (DST 2.8), without baffle (DST WB), with lengthened baffle (DST 7.1.2) and a reflective baffle design (DST 7.2), in degrees Celsius. The minimum, mean and maximum node temperatures are taken from the COLD, MED and HOT case respectively.

	DST WB			**DST 2.8**			**DST 7.1.2**			**DST 7.2**		
	Min	Mean	Max	Min	Mean	Max	Min	Mean	Max	Min	Mean	Max
B-B	-	-	-	-122.5	-29.3	125.0	-122.5	-20.9	130.0	-122.5	-24.0	65.0
B-S	-	-	-	-57.5	-4.8	115.0	-57.5	-4.6	127.5	-60.0	-15.6	105.0
Spid.	-35.0	8.0	82.5	-50.0	-13.0	82.5	-42.5	-7.8	42.5	-55.0	-15.3	37.5
TH	-2.5	32.0	60.0	-45.0	-9.0	78.5	-42.5	-7.6	42.5	-57.5	-15.4	42.5
M2	97.5	105.3	127.5	-35.0	-6.5	42.5	-37.5	-6.4	32.5	-50.0	-12.3	20.0
Boom	-17.5	30.6	72.5	-42.5	-7.6	47.5	-42.5	-7.8	45.0	-55.0	-15.5	20.0
RH	-97.5	1.4	97.5	-40.0	-7.9	30.0	-40.0	-8.1	32.5	-55.0	-15.3	17.5
M1	-62.5	37.4	275.0	-40.0	-8.5	30.0	-40.0	-8.7	30.0	-55.0	-15.1	17.5
PMSS	-160.0	-26.5	3595.0	-42.5	-7.9	35.0	-42.5	-8.1	37.5	-55.0	-15.3	17.5
IH	-127.5	-3.4	125.0	-42.5	-7.8	35.0	-42.5	-8.0	35.0	-57.5	-15.4	17.5

(This page is intentionally left blank.)

13 Conclusions

The results of the various thermal models developed and applied throughout this thesis are considered to give a good indication of the expected thermal performance of the telescope. However, they cannot serve entirely as a final thermal analysis for the entire structure, since many key parameters are not determined yet. Nevertheless they can be used to answer the initially presented research question:

How can the critical systems of the Deployable Space Telescope be designed such for it to meet the thermal- and/or optical budgets?

Several findings have been presented in this report and are summarised below. Afterwards, the research-objectives and question, stated in Chapter 2, are answered. These findings have been considered for the current baffle design, the proposed baffle design and budget analysis.

13.1 Current Baffle Design

The initial thermal model has been exposed to nominal case simulations conditions. The results showed that the maximum temperatures were reached when the orientation of the satellite was such that sunlight impinged the interior of the baffle and the telescope directly. The largest differences in temperature were seen for the baffle itself, while those of the telescope are smaller. Further, the telescopes respective component temperatures are close to each other. The telescope itself features an average overall temperature of $\pm 10°C$. The components closest to the baffle opening (spider, top hinges and the SMSS booms) featured the largest average temperature variations throughout an orbit.

The baffle design has been alternated to a fully cylindrical design, which simplified the design and therefore facilitated modelling. Besides, the baffle has been included in the model which decreased the total globally experienced temperature variations of the baffle blanket. After exposing the fully representative model to cold conditions it was noticed that the majority of the telescope components cooled down significantly, leading to an overall average temperature of $\pm$-40.0°C. For hot conditions it became evident that the overall average temperatures of $\pm 30.0°C$ were closer to the target temperature of 25.0°C as compared to the average temperature of the cold case. However, the maximum node temperatures of the top section components (spider, top hinges, secondary mirror and SMSS booms) are substantially higher, extending up to 85.0°C. Therefore, the current baffle design proved to be useful for maintaining similar telescope system temperatures, apart from the majority of the SMSS.

13.2 Improvements Investigation

Several aspects of the satellite have been investigated for potential thermal performance improvements. These included lengthening of the baffle, a directional reflective top section baffle interior and a spider top plate. Further, the thermo-optical properties of the baffle interior and the telescope components have been reconsidered.

Extension of the Baffle

Extension of the baffle reduced the amount of solar irradiation experienced by the top section telescope components. It did not affect the heat flow towards the baffle interior. The OLR vector is considered to be parallel to the telescope z-axis (optical axis), while the solar constant and planet albedo are not. The latter is thought to be a function of the Sun-Earth constellation and satellite orientation. Therefore, it was concluded that the top section telescope components are more effectively shielded from solar irradiation effects with an extended baffle, while it does not change the amount of OLR. The length of this extension should be optimised in accordance with a potential reflective interior structure, as will be mentioned next.

Reflective Interior Baffle Structure

Lengthening of the baffle does not decrease the amount of heat energy absorbed, so it also does not decrease the amount of heat radiated by the baffle interior to the telescope. To account for this, two potential solutions were considered: Either a change in thermo-optical coating, or the addition of a reflective interior due to which the majority of heat will be reflected back into space. A change in thermal properties has not been considered

since the internal VDA layer of the blanket should be kept thin, for it to be foldable.

A simple reflective interior coating will definitely not improve the thermal performance, since it results in reflection to all directions. Further, it will generate a considerable amount of stray light. Therefore, the baffle needs a directionally reflective interior which, among others, can be composed of a single vane structure. This enables the majority of the solar irradiation to be reflected back into space, which allows for superior performance in terms of smallest temperature variations throughout an orbit. The shape of this structure can be determined by a dedicated ray-tracing simulation, although the baffles deployability may be considered as a killer requirement for the solid reflective structure.

Spider Top Plate

The spider should be included with a top plate for it to reduce stray light. This plate can be made highly reflective for it to absorb and radiate less heat, in case the stray light analysis will allow for it. The thickness of the plate should be determined by means of a dedicated mechanical analysis.

13.3 Budget Analysis

The budget analysis of this report considered the top-down system budgets and the thermal budgets, as defined by the (thermal) requirements.

Top-down System Budgets

Prior to the coarse position analysis presented within this thesis, it was thought that the primary mirror segments were most likely to be critical in fulfilling the top-down system requirements. This is because they feature the smallest alignment budgets. The coarse position translation analysis has shown that the SMSS booms are critical for M2 alignment in Z-direction, while the instrument housing most affected M1 alignment in Y-direction (as considered for one M1 segment). The latter can be improved by giving the housing structure sufficient thickness.

Critical System Identification
The SMSS is considered to be least protected by the baffle from influences of the space environment. Further, the majority of its components were simulated to be covered with a black coating, in order to reduce stray light. The SMSS booms are relatively long (1.725m) which, in combination with the aforementioned two characteristics, generally results in large deflections in Z-direction for M2. The intended athermal aspect is not useful for varying system temperatures. Further, the analysis did not considered temperature gradients yet. Therefore, it is likely that the booms are in need of further thermal control.
The temperature of the support frames of the primary mirror segments shows little fluctuation in temperature, due to the shielding effect of the baffle and the shielding from the mirror segments. However, the temperature of the instrument housing changes which in relation to its size and orientation, can have a large effect on the relatively small M1 alignment budgets.

Critical System Thermal Performance Improvements
The considered SMSS booms deformations can be partly mitigated by application of a reflective baffle design. However, it is likely that additional thermal control will be required because the temperatures of the booms are not stable enough, even with a more reflective design.
The instrument housing should be given sufficient thickness for it to become less sensitive to temperature variations throughout an orbit. Further, the support structures of the PMSS have been included featuring athermalization measures by M. Corvers [15], which may further allow the design to stay within the M1 alignment budgets.
The reflective baffle design considers that the top section of the baffle (50cm) does not radiate heat towards the telescope. This can be considered an optimistic estimate since a detailed design of the required reflective vane structure will always include radiation of a small amount of heat towards the telescope. These estimates are optimistic, so it is likely that additional measures need to be taken in order to account for the deflections of the SMSS booms. Besides, the orbital conditions did not consider eclipses which are known to increase ΔT, nor did the simulation consider boom temperature differences and surface gradients.
To improve the outcome of the simulation, several additional measures can be taken, such as the actuation of a secondary mirror system, the application of conductive materials or the inclusion of phase change materials. Due to the simplified nature of the simulation, the calculated deformations should be considered as approximations. The outcomes should be treated as temperature indications and yield an understanding of the relations between the temperature of the different telescope components. Still, it is most likely that each configuration is in need of heating under cold conditions.

Finally, a thermomechanical model should be used to determine whether the system can be aligned eventually.

Thermal Budgets

From the thermal budget analysis it became apparent that the deployed phase will most likely **not** be critical when considering bulk temperature limits, based on the currently available thermal requirements. It is concluded that LEOP will be most critical for bulk temperature limits, since the baffle will not yet be deployed in that stage. Furthermore, several detrimental conductive couplings are likely to be present. Nevertheless, it is thought that the thermal requirement list is incomplete. The thermal requirements include, among others, bulk temperature limits, heat flow limits and instrumentation- or component limits. Some of these are written for the PMAO system while the requirements for the remaining systems, apart from the two bulk temperature requirements for the SMSS booms, are simply not formulated yet. However, since the PMAO system and its exterior housing are not fully defined mechanically yet, they have been excluded from the simulation. They can be included as soon as materials and dimensions of the system are fully defined.

13.4 General Conclusions

The goal of this thesis is to answer the research question (3), while the objective is to make recommendations to the DST team about the expected thermal conditions (1) and the critical systems (2). The research question is therefore composed of three elements.

1. The results from the thermal analysis have shown that the average temperature of telescope is furthest away from the target temperature during cold conditions, while the experienced temperature variations throughout an orbit are largest in hot conditions. A thermomechanical model should be used to determine whether the system can be aligned for these conditions, and if not what amount of thermal control will be required for each condition. Furthermore, it has been shown that an orbit featuring eclipse is most likely to feature the largest ΔT and temperature gradients.

2. The baffle is found to be the most critical system regarding its thermal influence on the telescope. By making the baffle longer and/or narrower one decreases the radiative heat flow from space to the telescope, and in particular to the top section telescope components. A downside of the baffle is, that its interior has to be made highly non-reflective for it to reduce stray light. Due to this property it absorbs and radiates a large amount of heat towards the telescope for attitudes where the Sun can impinge the baffle interior. This heat is in particular radiated towards the top section telescope components. The SMSS booms, part of these top section components, are therefore considered most critical for the secondary mirror alignment budgets. This effect can be mitigated with a reflective baffle design, although when considering the average temperature of the telescope it is likely that the majority of the system will require thermal control for cold conditions, no matter what baffle design is applied. Further, the secondary mirror can be included with an actuation system that has not been designed yet, in order to account for the deflection of the SMSS booms.

3. Based on the determined temperature results it is concluded that the baffle should be adjusted such that it reduces direct and indirect heat flow towards the telescope. This requires an extension of the baffle, and a change in anti-reflective interior coating and/or the addition of a directional reflective interior. These aspects are related to each other and can, in combination, help in meeting the intended thermal and/or optical performance. These are considered to be a function of the thermomechanical model, a stray light analysis and deployability. The latter three factors shall determine to which extend the aforementioned critical system aspects can be applied, and whether the thermal- and/or optical budgets can be met or not. Furthermore, it was found that the need for additional thermal control is inevitable. However, it is likely that this need for additional thermal control can be mitigated if the average target temperature of the telescope of 25° is lowered, given that this does not negatively affect system performance otherwise.

The thermal model has been a helpful tool for predicting temperatures. The baffle turned out to be the most critical system for the telescope thermal performance. Nevertheless, a considerable amount of work has to be done to increase the performance of the thermal model. Insights gained from a thermomechanical model and a stray light analysis will aid in performing this work.

(This page is intentionally left blank.)

14 Recommendations

This thesis is useful for providing the initial estimates of the DST thermal performance. In order to improve this work or to give it more significance, recommendations are given. These are structured according to the architecture as shown in Figure 14.1. The numbering schema is representative of the chronological urgency, unless specified otherwise.

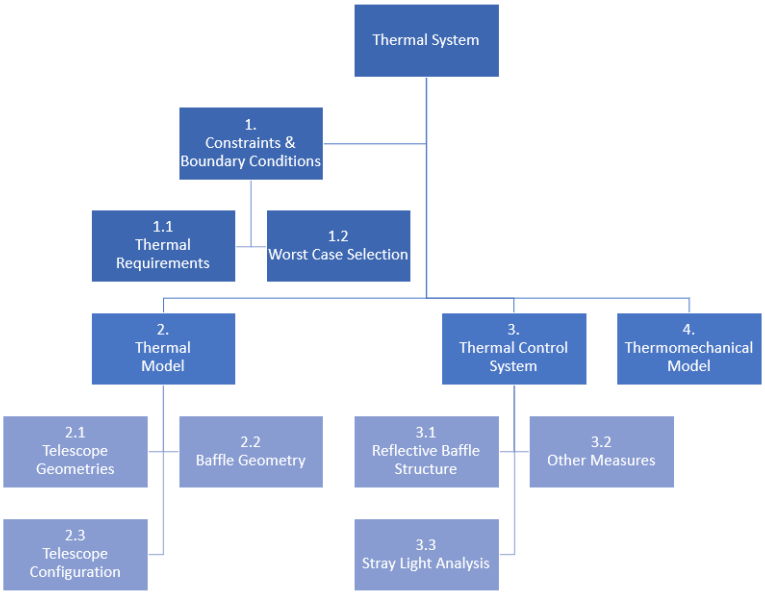

Figure 14.1: Thermal System Recommendation Architecture

1.1 Thermal Requirements

The thermal requirement list is incomplete. The previous designers were majorly interested in the mechanical performance for which mechanical requirements have been generated. Future system designers should also formulate thermal requirements, such that those can be addressed by the thermal model. This will allow the thermal model to be restricted, in terms of bulk temperature-, heat flow-, instrumentation- and gradient limits. These requirements are expected to be a function of the spacecraft- configuration and mode.

The analysis as conducted in this report refers to a target temperature of 25 °C. This is chosen because it is likely that the telescope will be assembled at this temperature. The average temperature results as shown in Appendix I *Averaged Temperature Results*, indicate that the telescope will be colder for all three thermal scenarios (COLD, MED and HOT). Since, the telescope features a deployment mechanism it is expected that the primary- and secondary mirrors can be controlled such for it coarse align at deviating temperatures. Nevertheless, it is unknown to which extend this will be possible. Besides, it does not necessarily make sense to design a telescope for a target temperature which will not be reached during operation. Therefore, it is recommended to lower the operational target temperature if possible.

1.2 Worst Case Scenario Selection

The selected worst case conditions, hot and cold, were selected on basis of their global minimum and maximum temperatures. Furthermore, it considered the satellite to not enter eclipse. However, previous results have shown that when the satellite included eclipse, it experiences the largest temperature fluctuations throughout an orbit.
Therefore, it is recommended to decide whether the telescope is considered to face eclipse regularly or not. At this moment it is known that the telescope will feature a SSO, while the right ascension of the ascending node with respect to the Sun-Earth direction is unknown. It is thought that these parameters should be defined clearly on top-level, since those are considered to be most determinant for the to be expected thermal conditions. The worst case scenarios should be re-selected after.
Following to this, it is not recommended to re-evaluate the worst case scenario selection per component yet.

This is because, the SMSS components and the baffle interior currently feature equal thermo-optical coatings and because those are considered to be critical systems. Therefore, global worst case scenarios are considered to be sufficient.

2.1 Telescope Geometries

The primary mirror segments are considered to be essential for the performance of the system. Therefore, it will be recommended to adjust its average thickness such that its thermal resistance will be similar to that of its detailed design. The instrument housing is considered to be less relevant as long as it is given sufficient thickness, since many other system aspects needs to be determined first. The remainder of the thermal model is thought to be sufficient to good in approximating the average- and extreme temperatures, hence no further adjustments are recommended.

The final model is considered to be insufficient in providing the required temperature gradients, although the majority of the components require grid refinement mainly. Furthermore, the booms should be included with the intended cut-outs halfway its length, the top- and root hinges should be included with their conductive couplings between the cams and/or its support structure, and the primary mirror shall be adjusted to take account for the cut-outs.

2.2 Baffle Geometry

The baffle has proved to be of great influence for the telescope temperatures. The effect of lengthening and a reflective internal structure has been demonstrated. The baffle has been extended by 20cm for it to prove its significance, although this estimate has not been optimised. The same applies for the reflective baffle interior. Therefore, it is recommended to dedicate further research towards these two topics together, for which an optimum shall be chosen based on stowed volume, deployability, mass and thermal performance.

The current baffle structure is thought to be a good representative of the actual design considering the way it is modelled, hence no further adjustments are recommended there. A Commercial Of The Shelf (COTS) MLI configuration has been chosen taken from [22]. The results have shown that the telescope is relatively cold, although the insulation performance of the blanket is considered sufficient. Nevertheless, the required insulation performance can be re-evaluated in accordance with potential internal dissipators and space degradation effects, in case desired.

2.3 Telescope Configuration

The thermal models as presented within this work consider deployed configuration only. The stowed configuration does not feature a deployed baffle, hence it will most likely be critical in terms of bulk temperatures. A stowed configuration will thus be important for determining whether the stowed telescope will survive LEOP. Therefore, it is recommended to construct a stowed configuration in the future with the condition that sufficient thermal requirements regarding this configuration or stage have been formulated, such that the critical interfaces during stowage can be identified accordingly.

3.1 Reflective Baffle Structure

The interior of the baffle is considered to be coated black due to which it radiates a considerable amount of heat towards the telescope. It cannot simply be made reflective, since this will not solve the issue. Therefore, it is thought to be in need of some sort of directional reflective interior design. This report includes the application of a reflective baffle vane structure, which is considered as a potential solution.
The baffle is designed to be deployable and the application of such reflective vanes are considered to be solid. They are not considered to be foldable or composed of smaller pieces. Therefore, it is recommended to verify whether such a design can be made deployable, or to allocate alternative deployable measures with similar thermal performance. This should be followed by a dedicated ray-tracing analysis, after which it is can be implemented in the thermal model. The ray-tracing analysis should be addressed to the optical team.

3.2 Other Measures

The preceding literature study [8] has been useful for identifying several elements of thermal control. Some of these elements may be useful for mitigating the experienced temperature variations of the SMSS booms throughout an orbit, or for increasing temperatures for cold conditions. The passive elements considered MLI, thermo-optical control coatings, thermal- straps and switches, heat pipes and Phase Change Material (PCM). Active elements considered louvers, heaters, thermoelectric devices and heat pumps.

The telescope components cannot be covered in MLI in relation to stray light. It may be covered in different optical coatings although this requires a stray light analysis, as will be mentioned in the next section. Thermal switches can potentially become relevant in combination with the TBD contact conductive interfaces. Heat pipes can be used for distributing heat along a component which would reduce the gradients, but does not decrease the temperature fluctuations. PCM can be used to either release the heat when its cold or to store heat when it warm, such that the maximum- and minimum operating temperatures are limited. Therefore, they could potentially be used for decreasing the temperature variations as experienced by the SMSS booms. The PCM material should be matched with the considered operational temperature range for it to change phase correctly. Further, it can be used such that it constantly changes phase for it to keep the temperature constant or fixed, although this seems rather complex as mentioned in [41].

Louvers in combination with heat pumps can be used to reject or add heat as demanded, although mechanically moving parts are generally not desired. Besides, it will require a complex heat distribution system. Thermo-electric devices have the benefits of featuring no moving parts, although their efficiency decreases for larger temperature ranges. Heaters can be used to increase temperature and require electric currents only. These could potentially become useful for cold conditions. Applications are provided in [42], where heaters can either be attached to or integrated with the structure.

3.3 Stray Light Analysis

It is currently assumed that the coatings of the SMSS and the baffle interior need to be as non-reflective as possible. A stray light analysis regarding the required absorptive properties for these geometries can be useful. This because it basically determines how the system designers will be restricted in the application of thermal control coatings, from which it can potentially be determined that another coating may be used with lower absorptivity and thus lower emissivity. The latter property is considered to effect the need for a reflective baffle vane design as well as other forms of thermal control.

In case the absorptivity can be decreased, one can potentially select other suitable coatings with lower emissivity. This can for example be a variant of the FSFC Dark Mirror Coating or Electrodag, as depicted in Table C.2 of Appendix C. It is unknown how this effects the totality of the performance and therefore it is placed low on the recommendation list. Nevertheless, it is considered a simpler potential solution compared to applying other means of thermal control and/or a reflective baffle design.

4. Thermomechanical Model

The thermal model itself is considered effective in providing temperature estimates but not in providing deformations. The researcher is therefore suggesting that a thermomechanical model should be made eventually such that actual deformations and thus actual performance can be calculated. This would allow for a more accurate approximation of the desired conditions since it is unknown at what temperatures the system is able to align itself, apart from the current target temperature of 25°C.
Furthermore, it can be used to generate additional thermal requirements since the combined system deformations will impose new challenges. Besides, the contact conductive couplings can be re-evaluated and the thermal control system can be provided with more detail.

The suggested thermomechanical model can either be representative of the entire DST structure or just parts of it. The successor can therefore choose to thermomechanically model, among others, the M2 alignment systems only. The European Space Research & Technology Centre (ESTEC) and ESA offer a model package with which one can convert the temperature results as computed in ESATAN into input for a thermo-mechanical or thermo-elastic analysis with MSC.NASTRAN, as described in [43]. This tool is included with support features and is available for students, although it does require the installation and usage of NASTRAN. The recommendation is lowest on the list because the actual performance is not considered relevant yet.

(This page is intentionally left blank.)

Bibliography

[1] Science for a changing world USGS. *What is remote sensing and what is it used for?* Retrieved from `https://www.usgs.gov/faqs/what-remote-sensing-and-what-it-used?qt-news_science_products=7#qt-news_science_products`. (Accessed 2nd November 2018).

[2] National Ocean Service. *What is remote sensing.* Retrieved from `https://oceanservice.noaa.gov/facts/remotesensing.html`. (Accessed 2nd November 2018).

[3] G.P. van Marrewijk. *Deployable Space Telescope Technology Review.* Master's thesis literature study, TU Delft, the Netherlands. 2017.

[4] V. Villalba Corbacho D. Risselada M. Voorn S. Pepper E. Korhonen & S. Leegwater J.M. Kuiper D. Dolkens. "DST SE Document". In: *Department of Aerospace Engineering; Delft University of Technology* (2018).

[5] E Gill. *Identifying stakeholder needs.* Retrieved from https://brightspace.tudelft.nl/d2l/le/content/35328/viewContent/ 2018.

[6] J.J. Sellers L.D. Thomas & D. Verma W.J. Larson D. Kirkpatrick. *Applied Space Systems Engineering. Space Technology Series.* The McGraw-Hill Companies, 2009.

[7] D. Dolkens. *A Deployable Telescope for Sub-Meter Resolutions from MicroSatellite Platforms.* Master's thesis, TU Delft, the Netherlands. 2015.

[8] T.T.D. van Wees. *Deployable Space Telescope, Literature review for thermal modelling & analysis.* Master's thesis literature study, TU Delft, the Netherlands. 2018.

[9] European Cooperation for Space Standardization (ECSS) Secretariat. *Space engineering Thermal control general requirements, ECSS-E-ST-31C.* ESA Requirements and Standards Division, ESTEC, Noordwijk, the Netherlands, 2008.

[10] S.M. Pepper. *Deployable Space Telescope.* Master's thesis literature study, TU Delft, the Netherlands. 2018.

[11] D. Agnolon. *MarcoPolo-R Mission Requirements Document.* European Space Research and Technology Centre (ESTEC), Noordwijk, the Netherlands, 2012.

[12] A. Krikken. *Design of the Secondary Mirror Support Structure for the Deployable Space Telescope.* Master's thesis, TU Delft, the Netherlands. 2018.

[13] S.M. Pepper. *Design of a Primary Mirror Fine Positioning Mechanism for a Deployable Space Telescope.* Master's thesis , TU Delft, the Netherlands. 2018.

[14] B.T. van Putten. *Design of the Deployment Mechanism for the Primary Mirror Elements of a Deployable Space Telescope.* Master's thesis, TU Delft, the Netherlands. 2017.

[15] M. Corvers. *Design of a Primary Mirror Deployment Mechanism for a Deployable Space Telescope.* Master's thesis, TU Delft, the Netherlands. 2018.

[16] J.W. Lopes Barreto. *Deployable Space Telescope: Optimal Boom Design for High Precision Deployment of the Secondary Mirror.* Master's thesis, TU Delft, the Netherlands. 2017.

[17] J.H. Henninger. *Thermal Emittance of Some Common Spacecraft Thermal-Control Coatings.* NASA/Goddard Space Flight Center, Greenbelt, Maryland, 1984.

[18] ITP Engines UK Ltd. *ESATAN-TMS Workbench Getting Started Guide.* ITP Engines UK Ltd., Cambridge Road, Whetstone, Leicester, UK, 2017.

[19] K.F. Wakker. *Fundamentals of Astrodynamics, Lecture Notes AE4874.* Delft: Faculty of Aerospace Engineering, 2015.

[20] P. Yoder & D. Vukobratovich. *Opto-Mechanical Systems Design, Volume 1: Design and Analysis of Opto-Mechanical Assemblies.* Fourth edition. CRC Press, 2015.

[21] R. Joven / R. Das / A. Ahmed / P. Roozbehjavan / B. Minaie. "THERMAL PROPERTIES OF CARBON FIBER-EPOXY COMPOSITES WITH DIFFERENT FABRIC WEAVES". In: *Department of Mechanical Engineering; Wichita State University* (2012).

[22] RUAG Space Products. *Thermal Insulation Products.* Retrieved from `https://www.ruag.com/sites/default/files/media_document/2017-12/140110_Brosch%C3%BCre_Thermal_Nov2017_A4_low_0.pdf`. (Accessed 3rd December 2018).

[23] D.A. Sheikh. "Improved silver mirror coating for ground and space-based astronomy". In: *Proc. SPIE 9912, Advances in Optical and Mechanical Technologies for Telescopes and Instrumentation II, 991239 (22 July 2016); doi: 10.1117/12.2234380* (2016).

[24] Edmund Optics. *Metallic Mirror Coatings*. Retrieved from `https://www.edmundoptics.com/resources/application-notes/optics/metallic-mirror-coatings/`. (Accessed 20th June 2018).

[25] SHELDAHL. *THE RED BOOK*. retrieved via `https://www.sheldahl.com/sites/default/files/2017-09/RedBook.pdf`. 2018.

[26] I. Gouzman G. Lempert E. Grossman D. Katsir R. Cotostiano & T. Minton Y.M. Salomon N.A. Sternberg. *QUALIFICATION OF ACKTAR BLACK COATINGS FOR SPACE APPLICATION*. Retrieved from `http://esmat.esa.int/Materials_News/ISME09/pdf/4-New/S7%20-%20Miron-Salomon.pdf`. (Accessed 6th December 2018).

[27] L. Kauder. *Spacecraft Thermal Control Coatings References*. NASA/Goddard Space Flight Center, Greenbelt, Maryland, 2005.

[28] World Leader in Black Coatings Acktar Advanced Coatings. *Magic Black Coating*. Retrieved from `https://www.acktar.com/product/magic-black/`. (Accessed 23th October 2018).

[29] Yiyu Ou & Haiyan Ou Aikaterini Argyraki. "*Broadband antireflective silicon carbide surface produced by cost-effective method*". In: *Optical Society of America, Vol. 3, No. 8, DOI:10.1364/OME.3.001119* (2013).

[30] Isodoro Martinez. *Properties of solids*. Retrieved from `http://webserver.dmt.upm.es/~isidoro/dat1/eSol.pdf`. (Accessed 14th September 2018).

[31] M. Noorma A.V. Gura & S.N. Mekhontsev C.P. Cagran L.M. Hanssen. "*Temperature-Resolved Infrared Spectral Emissivity of SiC and Pt–10Rh for Temperatures up to 900°C*". In: *International Journal of Thermophysics, Vol. 28, No. 2, DOI:10.1007/s10765-007-0183-1* (2007).

[32] C. MONTE B. GUTSCHWAGER & J. HOLLANDT A. ADIBEKYAN E. KONONOGOVA. "Emissivity, Reflectivity and Transmissivity of Semitransparent Fibre Reinforced Plastic Composites". In: *Thermographie-Kolloquium* (2017).

[33] Material Property Data MatWeb. *Aluminum 1100-O*. Retrieved from `http://www.matweb.com/search/datasheet.aspx?matguid=db0307742df14c8f817bd8d62207368e`. (Accessed 17th October 2018).

[34] C.G. Justus & G.W. Batts B.J. Anderson. *Guidelines for the Selection of Near-Earth Thermal Environment Parameters for Spacecraft Design*. Marshall Space Flight Center, MSFC, Engineering Directoriate, Alabama, 2001.

[35] M.P. Wilkins & C.Bruccoleri D. Mortari. "On Sun-Synchronous Orbits and Associated Constellations". In: *Department of Aerospace Engineering, Texas A&M University, USA* (2004).

[36] Dr. D.R. Williams. *Earth Fact Sheet*. Retrieved from `https://nssdc.gsfc.nasa.gov/planetary/factsheet/earthfact.html`. (Accessed 29th January 2019).

[37] ESA Earthnet Online. *5.5 Geometry Glossary*. Retrieved from `https://earth.esa.int/handbooks/asar/CNTR5-5.html#eph.asar.gloss.geo:NADIR`. (Accessed 4th March 2019).

[38] DU PONT. *DUPONT KAPTON, SUMMARY OF PROPERTIES*. Retrieved from `http://www.dupont.com/content/dam/dupont/products-and-services/membranes-and-films/polyimde-films/documents/DEC-Kapton-summary-of-properties.pdf`. (Accessed 25th February 2019).

[39] K. Gunderson J. Fischer B. Lyuthi D. Piazza M. Rieder M. Sigrist & N. Thomas K. Seiferlin S. Chakraborty. "Design and manufacture of a lightweight reflective baffle for the BepiColombo Laser Altimeter". In: *Optical Engineering 46(4), 043003* (2007).

[40] A. Herren M Domínguez Calvo U. Krähenbühl D. Mouricaud & H. Vayssade E. Rugi-Grond T. Weigel. "REFLECTIVE BAFFLE FOR BEPICOLOMBO MISSION". In: *Proc. 6th Internat. Conf. on Space Optics, ESTEC, Noordwijk, The Netherlands* (2006).

[41] K. Yamada & H. Nagano. "Thermal design and validation of radiation detector for the ChubuSat-2 microsatellite with high-thermal-conductive graphite sheets". In: *K. Yamada, H. Nagano / Applied Thermal Engineering 91 (2015) 894e900* (2015).

[42] R.D. Karam. *Satellite Thermal Control for Space Engineers*. Vol. 181. Reston, Virginia: American Institute of Aeronautics and Astronautics, 1998.

[43] ESTEC/ESA. *SINAS IV: Interpolation of lumped parameter thermal node temperatures (from e.g. ESATAN) to thermo-elastic input data (with MSC.NASTRAN)*. Retrieved from `https://exchange.esa.int/restricted/sinas/`. (Accessed 28th February 2019).

[44] M. Bougoin & J. Lavenac. "From Herschel to Gaia: 3-meter class SiC space optics". In: *In Proc. SPIE, volume 8126* (2011).

[45] Make It From. *Silicon Carbide (SiC)*. Retrieved from `https://www.makeitfrom.com/material-properties/Silicon-Carbide-SiC`. (Accessed 20th June 2018).

[46] Substances & Technologies. *Carbon Fiber Reinforced Polymer Composites*. Retrieved from `http://www.substech.com/dokuwiki/doku.php?id=carbon_fiber_reinforced_polymer_composites`. (Accessed 20th June 2018).

[47] AZO Materials. *Polyethylene Terephthalate Polyester (PET, PETP) - Properties and Applications*. Retrieved from `https://www.azom.com/article.aspx?ArticleID=2047`. (Accessed 5th December 2018).

(This page is intentionally left blank.)

A Mission Requirements

This appendix includes the mission requirements as initially presented in the work of D. Dolkens in [7]. These requirements have been included with a different trace as presented in the DST SE document [4], shown in Table A.1. Some of these requirements are thought to be system requirements rather then mission requirements, since they are thought to describe non-functional properties, which is the reason for presenting them here.

ID	Description	Parent
MIS-REQ-01	The Ground Sampling Distance of the instrument shall be equal to 25 cm in the panchromatic band from an orbital altitude of 500 km	MIS-OBJ-01
MIS-REQ-02	The swath width of the instrument shall be wider than 1 km (threshold) / 5 km (goal).	MIS-OBJ-01
MIS-REQ-03	The system shall have one panchromatic channel from 450 to 650 nm with a 25 cm GSD at an altitude of 500 km.	MIS-OBJ-01
MIS-REQ-04	The system shall have four multispectral bands with the wavelength ranges and GSD indicated (at 500 km): Blue (450 - 510 nm) - 100 cm, Green (518 - 586 nm) - 100 cm, Yellow (590 - 630 nm) - 100 cm, Red (632 - 692 nm) - 100 cm	MIS-OBJ-01
MIS-REQ-05	The Signal-to-Noise Ratio (SNR) of the instrument shall be higher than 100 for a reflectance of 0.30 and a sun Zenith angle of 60°	MIS-OBJ-01
MIS-REQ-06	The nominal Modulation Transfer Function (MTF) at both the Nyquist frequency and half the Nyquist frequency shall be higher than 5% (threshold) / 15% (goal)	MIS-OBJ-01
MIS-REQ-07	After calibration, the residual Strehl ratio of the system shall be higher than 0.80.	MIS-OBJ-01
MIS-REQ-08	The mass of the instrument shall be lower than 100 kg (threshold) / 50 kg (goal).	MIS-OBJ-02
MIS-REQ-09	In the stowed configuration, the volume of the instrument shall not exceed 1.5 m3 (threshold) / 0.75 m3 (goal)	MIS-OBJ-02
SYS-REQ-01	The DST shall not use any ITAR controlled components or technology.	MIS-OBJ-02
SYS-REQ-02	The DST shall be designed for compatibility with the TBD launcher.	MIS-OBJ-02
SYS-REQ-03	The DST shall comply with national (NL) and international regulations during AIT activities, launch, operations and end of life.	MIS-OBJ-01

Table A.1: DST Mission Requirements

B Assumption List

The thermal models as produced within the Workbench of ESATAN TMS consider a certain amount of assumptions which are elaborated below:

- **Homogeneous & Isotropic Materials**: The geometries are considered to be composed of homogeneous materials which dictates that the thermal and thermo-optical properties are identical in all directions.
- **Type of Material**: The geometries are considered to be composed out of one type of material, which is correct for most of the components apart from the support frame. It is assumed that those geometries are composed of the materials which dominate those structures.
- **Constant Material Properties**: The thermal model considers constant thermal and thermo-optical properties. This means that, among others, the thermal conductivity, the specific heat and coefficient of thermal expansion, are not considered to be a function of time nor temperature.
- **Selected Material Properties**: The selected material properties are taken at the target temperature of 25 degrees Celsius.
- **Temperature Results**: The shown maximum- and minimum temperature results are representative of single nodes only as considered for the entire component group. This means that the majority of these nodes do not experience these temperatures, nor does the same node is expected to experience that respective amount of ΔT. The depicted average temperature results are representative of entire components groups.
- **Space Environment**: The thermal environment as considered within this thesis is composed of three factors, namely: solar flux, albedo flux and Earth flux or OLR. The space environment as considered in the thermal network does not consider the three factors to be separate but integrated as node 99999. This includes deep space itself which is considered as a heat sink of about 2.7 Kelvin. The space environment is therefore generally considered as a collective definition within this thesis.
- **Temperature Presentation & Conversion**: The ESATAN TMS Workbench provides temperature results in degrees Celsius. Most of the temperatures as presented in this report are presented in degrees Celsius. The thermal requirements as described in Table 3.3 assume that 273°C equals 0 Kelvin.
- **Geometry Colouring**: The thermal model geometries as visualised in the Workbench of ESATAN TMS have been given a colour which is not necessarily representative of their actual colour, nor is it representative of the applicable optical coatings. The geometries have been coloured such for it to represent the telescope components clearly. This enables the reader to actually notice a geometric difference, or consider certain additions to be apart. Therefore, the visualised colours can be considered false apart from the FINAL model.

C Thermal & Thermo-Optical Material Properties

The thermal and thermo-optical properties of the bulk materials as used in the thermal models are depicted in Table C.1. With ρ being the density, C_p the specific heat capacity, k the thermal conductivity, with CTE being the Coefficient of Thermal Expansion, α the solar absorptivity and ϵ the emissivity. Some materials had varying properties depending on their configuration or working temperature. For those materials it is chosen to use their mid value. The remainder of the applied optical coatings are provided in Table C.2.

Table C.1: Thermal optical properties as applied in the thermal model for uncoated components

	ρ $[kg/m^3]$	C_p $[J/Kg \cdot K]$	**k** $[W/m \cdot K]$	**CTE** [μm/m/K]	α [-]	ϵ [-]	**Reference**
Aluminium 1100-O	2710	904	222	23.6 (20-100°C)	0.14	0.05	[33]
Aluminium 7075	2790	896	142	23.4	0.125	0.05	[13], [30]
BOOSTEC SiC	3150	690	180	2.2	0.254	0.05	[44] at 20°C, [45] hot pressed
CFRP	1800	~820	~7	2.2	0.88	0.88	[46], [21] at 25°C, [12]
Ti-6AI-4V	4400	565	7.2	10.0	0.6	0.6	[13]
PETP or Polyester (FEP)	1350	1300	0.275	-	-	-	[47]

Table C.2: Thermo-optical properties of various thermal control coatings or paints, of which some are applied in the thermal model

	Application	α	ϵ	**Reference**
Magic Black	Black coating	0.99	0.93	[28]
Vel Black	Black coating	0.99	0.95	[27]
Anodize Black	Black coating	0.88	0.88	[27]
Anodized Titanium	Metal Coatings	0.85	0.46	[27]
FEP / VDA	Outer MLI layer	0.14	0.6	[22]
Protected Silver	Reflective mirror coating	0.035	0.035	[23]
GSFC Dark Mirror Coating	Composite coating	0.86	0.04	[27]
Teflon impregnated Anodized Titanium	Composite coating	0.75	0.26	[27]
Electrodag	Conductive paint	0.90	0.68	[27]

D Thermal Modelling Conditions

The thermal models as produced within the Workbench of ESATAN TMS are conducted to several types of thermal conditions, which will consider a common set of Basic conditions (BAS) as depicted in Table D.1. On top of these basic conditions, there are three types of additional case conditions considered throughout this project, namely: Nominal case conditions (NOM), Hot case conditions (HOT) and Cold case conditions (COLD), depicted in Figure D.2, D.3 and D.4, respectively. The median conditions as depicted in Figure D.5 will be used for the final analysis.

Most of the BAS thermal modelling conditions can be considered common, standard or pre-set, in ESATAN TMS and does not require actions by the user. Nevertheless, it is thought useful to elaborate on these parameters in order to understand their purposes. The Earth is set as the celestial body since the satellite is considered to orbit Earth. The planet radius, gravitational acceleration and Sun radius, are considered to be proper approximations and are therefore untouched. The orbital precession, which considers a drift of the rotational axis of the reference system, is thought to be irrelevant at this stage of the project, hence it being equal to zero.

The satellite is supposed to maintain a circular orbit, hence the eccentricity being equal to zero. Due to circular orbit conditions, the semi-major axis equals the orbit radius, which consist of the planet radius plus the orbital height of 500km. The inclination has been calculated as shown in section 6.3.3, required for SSO conditions as function of the orbital height. The argument of periapsis is not relevant for circular orbits, hence it being equal to zero. The number of orbital position is set at 11, as proposed by the ESATAN TMS getting started guide [18]. The eclipse entry exit points is set to true, since this function will set the orbital position such for it to include the eclipse entry and exit points. The eclipse offset describes the angle from the actual eclipse points at which these extra orbital positions are set, as proposed by the same guide.

The solar constant override function allows the user to adjust the solar constant without changing its Sun temperature. The sun rays can either be considered as a point source or as a body of finite size. Throughout this project the Sun will be considered as a point source, thus featuring parallel rays. The Sun distance can be adjusted such that the solar rays effecting the model will change with it, although this function is not considered relevant yet and thus it is set to zero. The planet albedo and temperature are set to uniform, which considers sunlight to reflected uniform irrespective of the Earth's surface properties, and for it to radiate OLR at a uniform temperature. The calculation methods could be set such for it to actually calculate the respective values based on the surfaces properties, thus for example land or sea, although this setting is also not considered relevant yet at this stage of the project. Both uniform method do consider eclipse conditions, during which OLR will be present but albedo will not.

Table D.1: Basic thermal modelling conditions (BAS), applicable for all models

Parameter	**Value**	**Units**
Planet Radius	6371	km
Gravitational Acceleration	9.798	m/s^2
Orbital Precession	0.0	deg/s
Sun Radius	$6.958 \cdot 10^8$	m
Celestial Body	Earth	-
Eccentricity	0	-
Semi-major Axis	6871	km
Inclination	97.4	deg
Argument of Periapsis	0	deg
Number of Positions	11	-
Eclipse Entry Exit Points	True	-
Eclipse Offset	0.5	deg
Solar Constant Override	0	W/m^2
Sun Rays	Parallel Rays	-
Sun Distance Override	0	m
Planet Albedo Method	Uniform	-
Planet Temperature Method	Uniform	-

Table D.2: Nominal case conditions (NOM)

Parameter	Value	Units
Sun Planet Distance	$1.508284754 \cdot 10^{11}$	m
Solar Declination	6.828	deg
Sun's Right Ascension	163.977	deg
Right Ascension	15	deg
Sun Temperature	5778.0	K
Albedo	0.306	-
Planet Temperature	254.3	K

Table D.3: Hot case conditions (HOT), RA70-FSC-SOLR-MAX

Parameter	Value	Units
Sun Planet Distance	$1.5 \cdot 10^{11}$	m
Solar Declination	0	deg
Sun's Right Ascension	0	deg
Right Ascension	70	deg
Sun Temperature	5826.0	K
Albedo	0.22	-
Planet Temperature	276.6	K

Table D.4: Cold case conditions (COLD), RA90-FSC-SOLR-MIN

Parameter	Value	Units
Sun Planet Distance	$1.5 \cdot 10^{11}$	m
Solar Declination	0	deg
Sun's Right Ascension	0	deg
Right Ascension	90	deg
Sun Temperature	5729.0	K
Albedo	0.40	-
Planet Temperature	208.9	K

Table D.5: Median (MED) conditions, RA90-FSC-SAOLR-MED

Parameter	Value	Units
Sun Planet Distance	$1.5 \cdot 10^{11}$	m
Solar Declination	0	deg
Sun's Right Ascension	0	deg
Right Ascension	90	deg
Sun Temperature	5778.0	K
Albedo	0.306	-
Planet Temperature	254.3	K

E Similation Output Frequency

A total simulation time for the duration of ten orbital periods was found to be sufficient for proving mean convergence of most DST components. The time it takes for the analysis case to be fully converged or conduct it calculations, is mainly determined by its output frequency. This output frequency determines at what rate the solutions will be sampled or generated.

The temperature results as shown below are representative of the initial model (DST 1.0), exposed to nominal conditions. The results as shown in Table E.1, are sampled with a rate of 400 seconds. Table E.2, is sampled with a rate of 25 seconds. The latter required a solver time of ± 18 minutes, while the first required ± 3.5 minutes only. Of course this is not even considering the amount of computation time it take to visualise the solutions, for which at most times the program seemed to have stalled at smaller output frequencies. This because the generation of the second Table took more than 1 hour.

The temperature differences between the two simulations are small, with largest differences seen for the baffle (± 10 5°C). Most of the telescope components are similar with maximum differences up to 5°C. The more accurate solution feature largest maximum ΔT which can become important in the more detailed analysis.

Table E.1: Initial thermal model component temperatures, with NOM conditions in degrees Celsius

	Global Min	**Average Min**	**Average ΔT**	**Average Max**	**Global Max**
Baffle	-134.4	-44.7	32.2	-12.4	126.7
Spider	3.5	5.9	13.2	19.1	26.6
Top Hinges	2.9	5.6	11.7	17.3	25.6
M2*	7.1	8.5	1.9	10.4	11.5
Booms	3.8	4.9	11.9	16.8	19.2
Root Hinges*	5.4	2.8	8.2	14.3	15.0
M1*	6.6	6.7	1.1	7.8	8.0
PMSS	1.4	6.2	8.1	14.3	32.7
IH	4.1	4.6	11.7	16.3	17.0

Table E.2: Initial thermal model component temperatures for ten orbital periods, with nominal thermal conditions with 25 seconds sampling in degrees Celsius

	Global Min	**Average Min**	**Average ΔT**	**Average Max**	**Global Max**
Baffle	-138.0	-53.2	40.2	-13.0	123.0
Spider	-1.5	2.8	15.9	18.7	25.1
Top Hinges	2.0	3.6	13.0	16.6	24.6
M2*	7.1	8.5	2.5	11.0	12.9
Booms	1.3	2.3	12.2	14.5	16.3
Root Hinges*	3.3	5.3	6.8	12.1	13.5
M1*	6.6	6.7	0.6	7.3	7.4
PMSS	-4.0	5.2	6.7	11.9	34.0
IH	-0.3	0.6	15.8	16.4	17.1

F Temp. Results MLI Outer Layers

The results of the potential MLI outer layers as presented in this Appendix were used in the outer layer determination process of Chapter 8 *Initial Thermal Model*. These results consider three types of outer layers for which the minimum- and maximum temperatures have been plotted for the duration of five orbital periods, for the inner and outer layer of the MLI blanket. The inner layer considers the insulation layers, while the outer layer is most important for its thermo-optical properties. The results as shown in this Appendix consider the following outer layers:

- **FEP-Silver**: Figure F.1
- **FEP-VDA**: Figure F.2
- **VDA**: Figure F.3

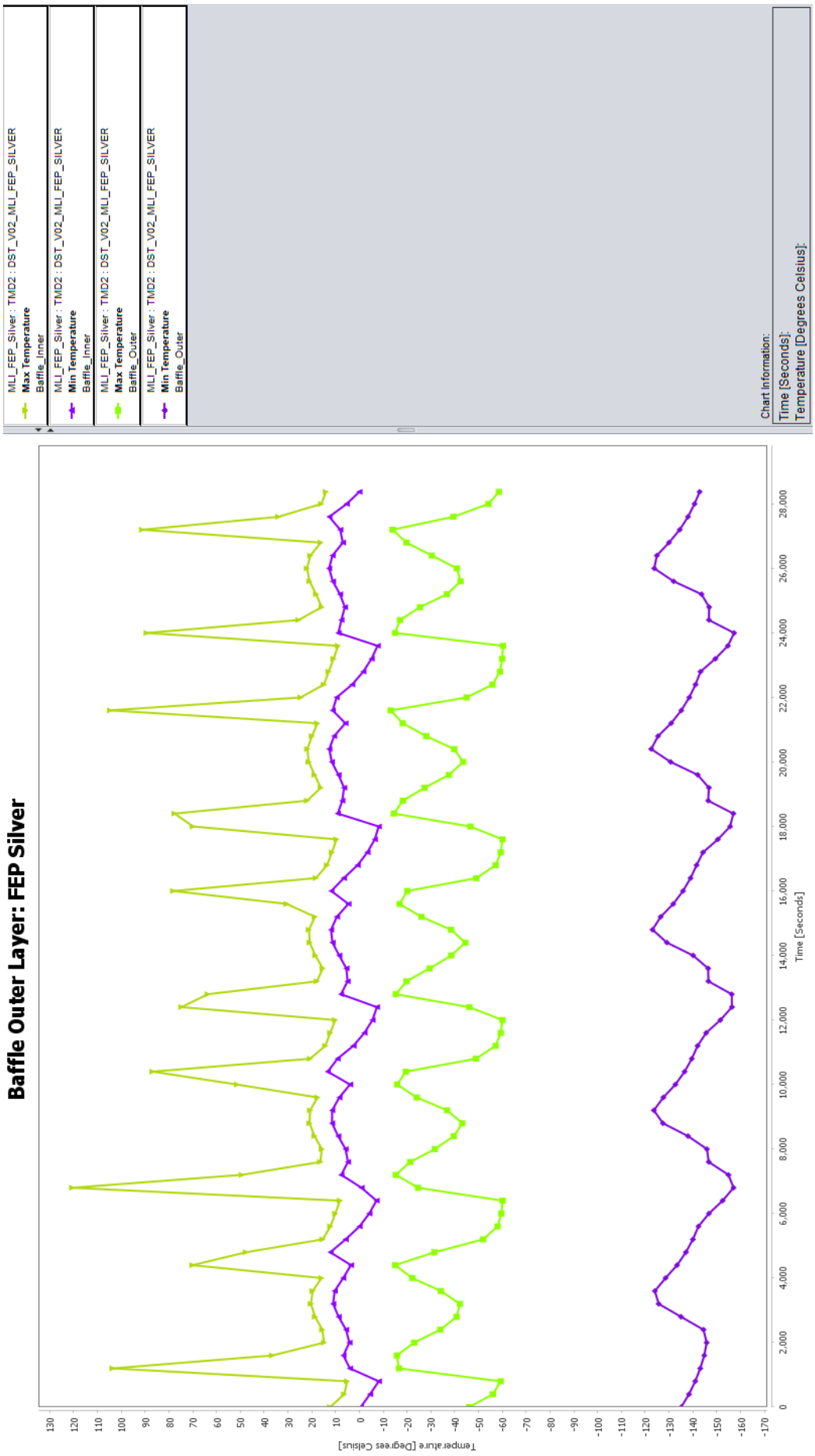

Figure F.1: Initial temperature results of the FEP/Silver MLI outer layer

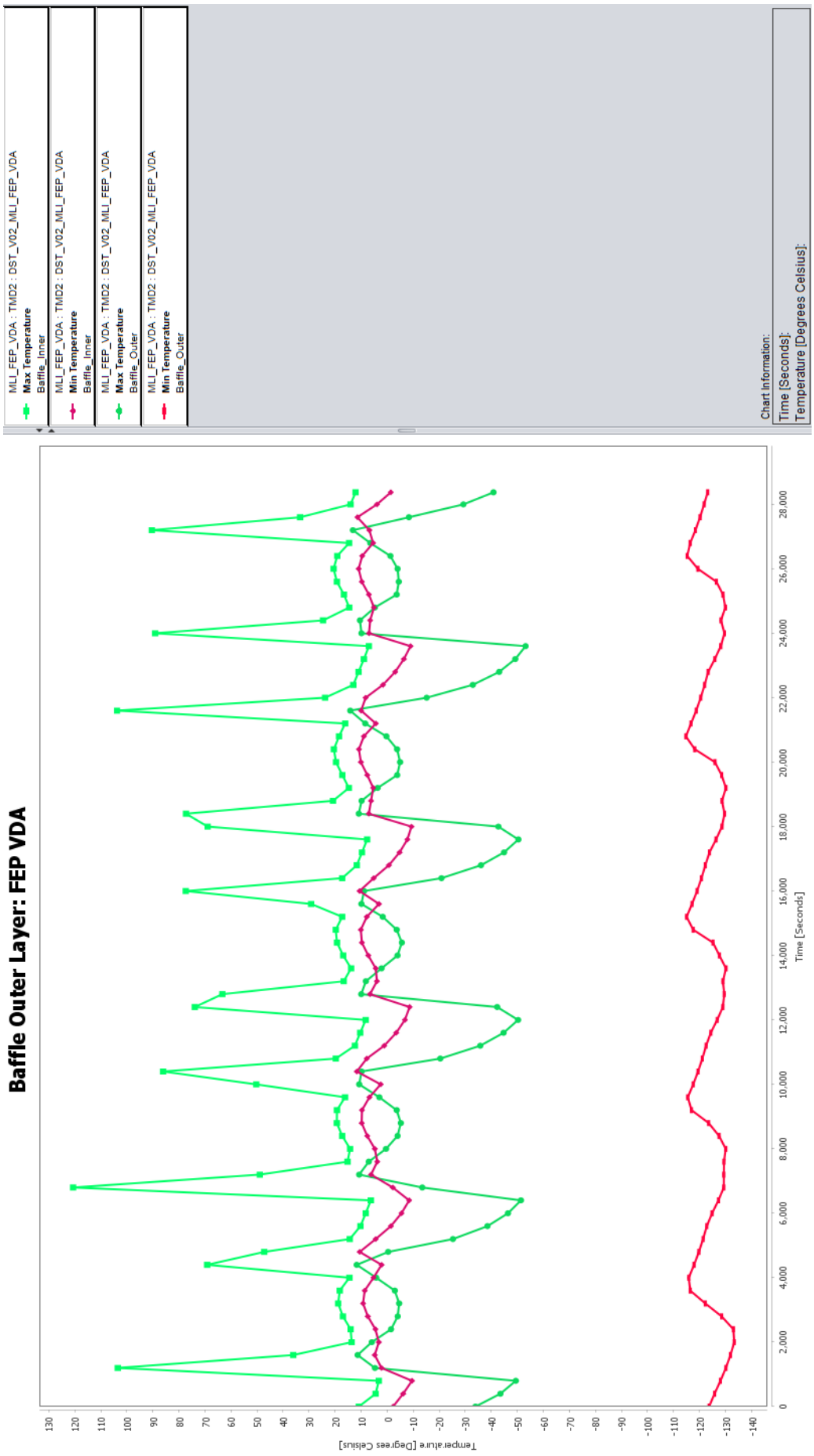

Figure F.2: Initial temperature results of the FEP/VDA MLI outer layer

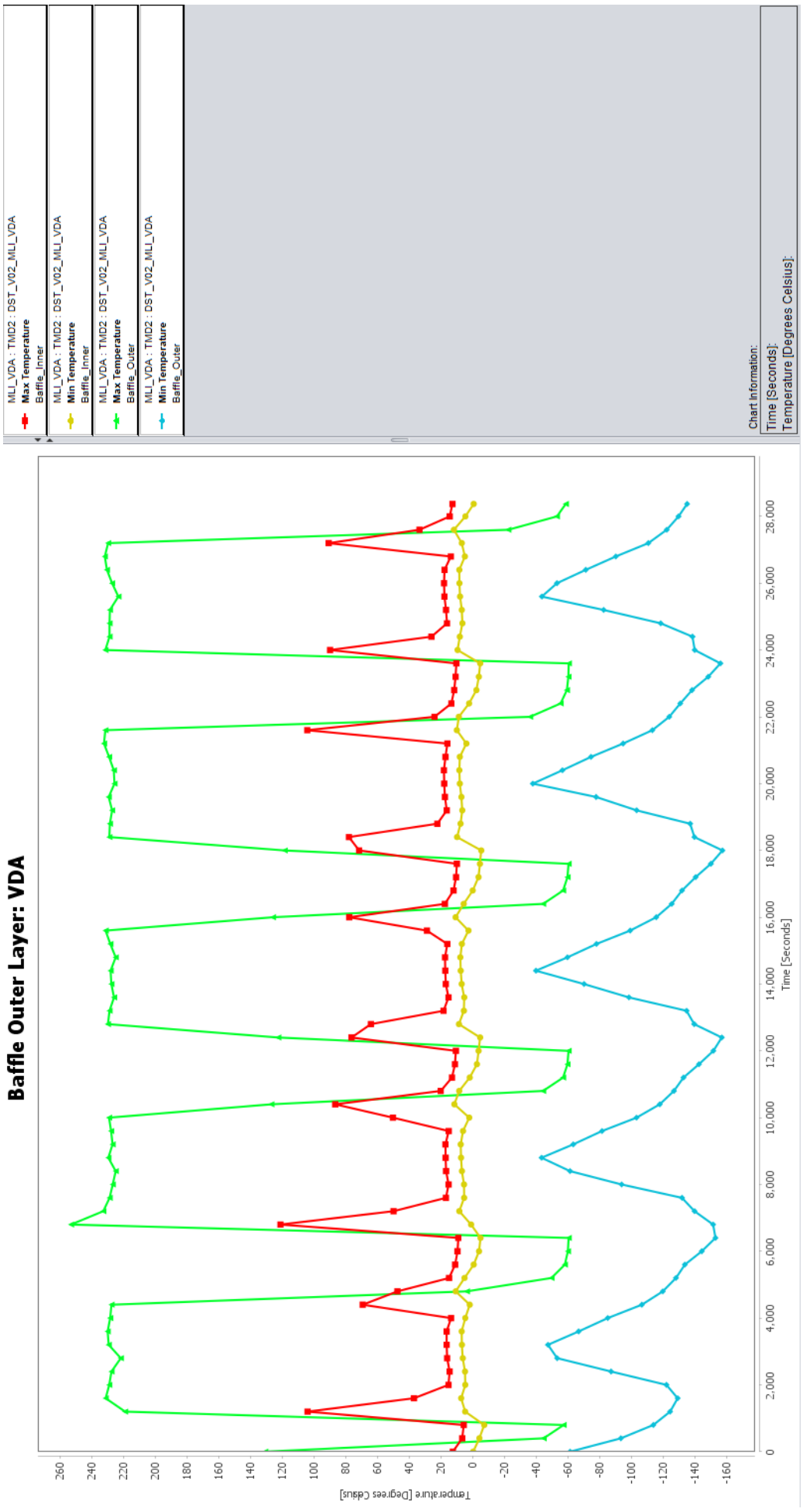

Figure F.3: Initial temperature results of the VDA MLI outer layer

G PMAO Results

The PMAO geometry as defined in Chapter 7 has been exposed to NOM conditions. The corresponding temperature behaviour results are depicted in Figure G.1. These results consider the average temperatures, referred to as Data in the Figures, of the four actuators as configured in the work of [13]. The actuators are considered in pairs of two, for which certain thermal requirements had been imposed which can be addressed coarsely with the use of these results.

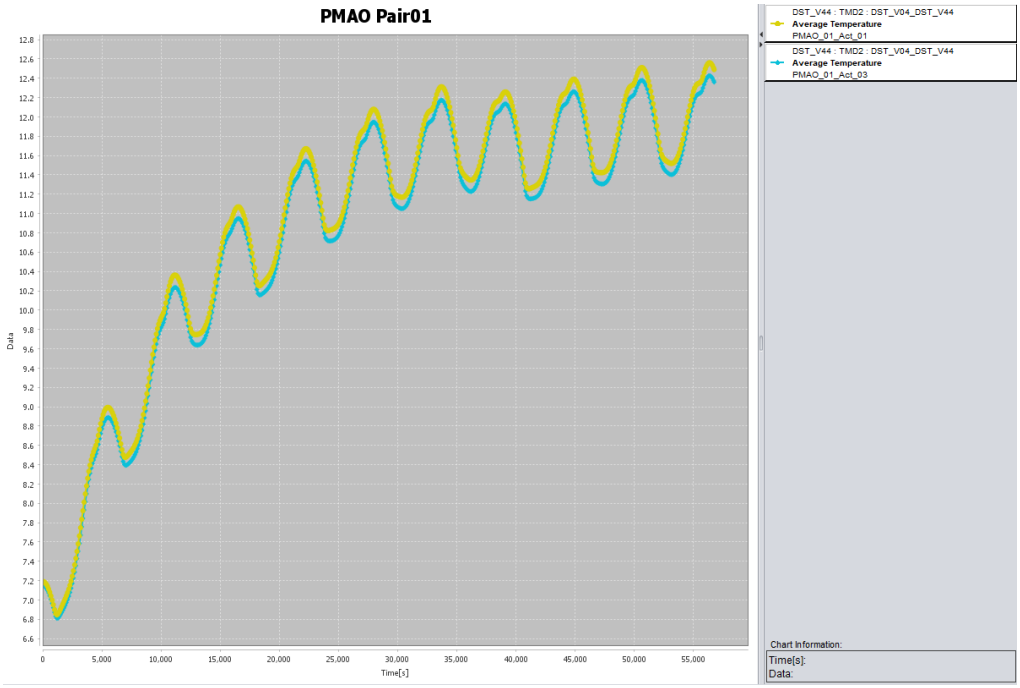

(a)

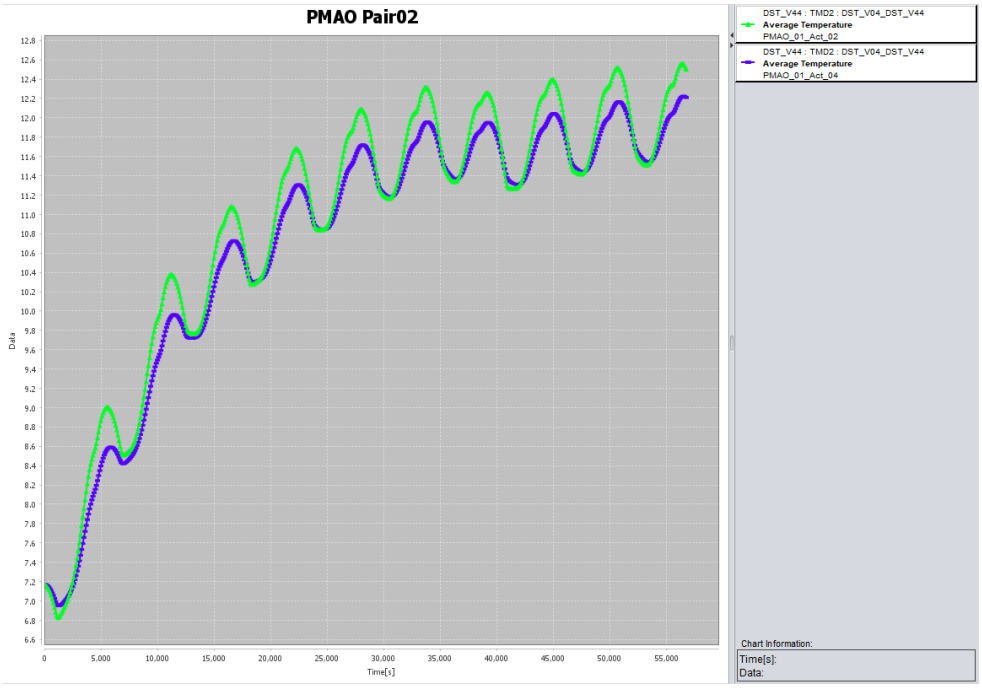

(b)

Figure G.1: Preliminary primary mirror active optics results for the two pairs of actuators

H Operational Window Results

This Appendix is part of the operational window investigation as conducted in Chapter 10 *Preliminary Thermal Control System Design*. The included results consider the 11th orbital period such that averaged results can be considered sufficiently converged, with an output frequency of 40 seconds for it to provide sufficient detail. The results describe the average temperatures of the PMSS and the SMSS considering COLD, MED or HOT conditions.

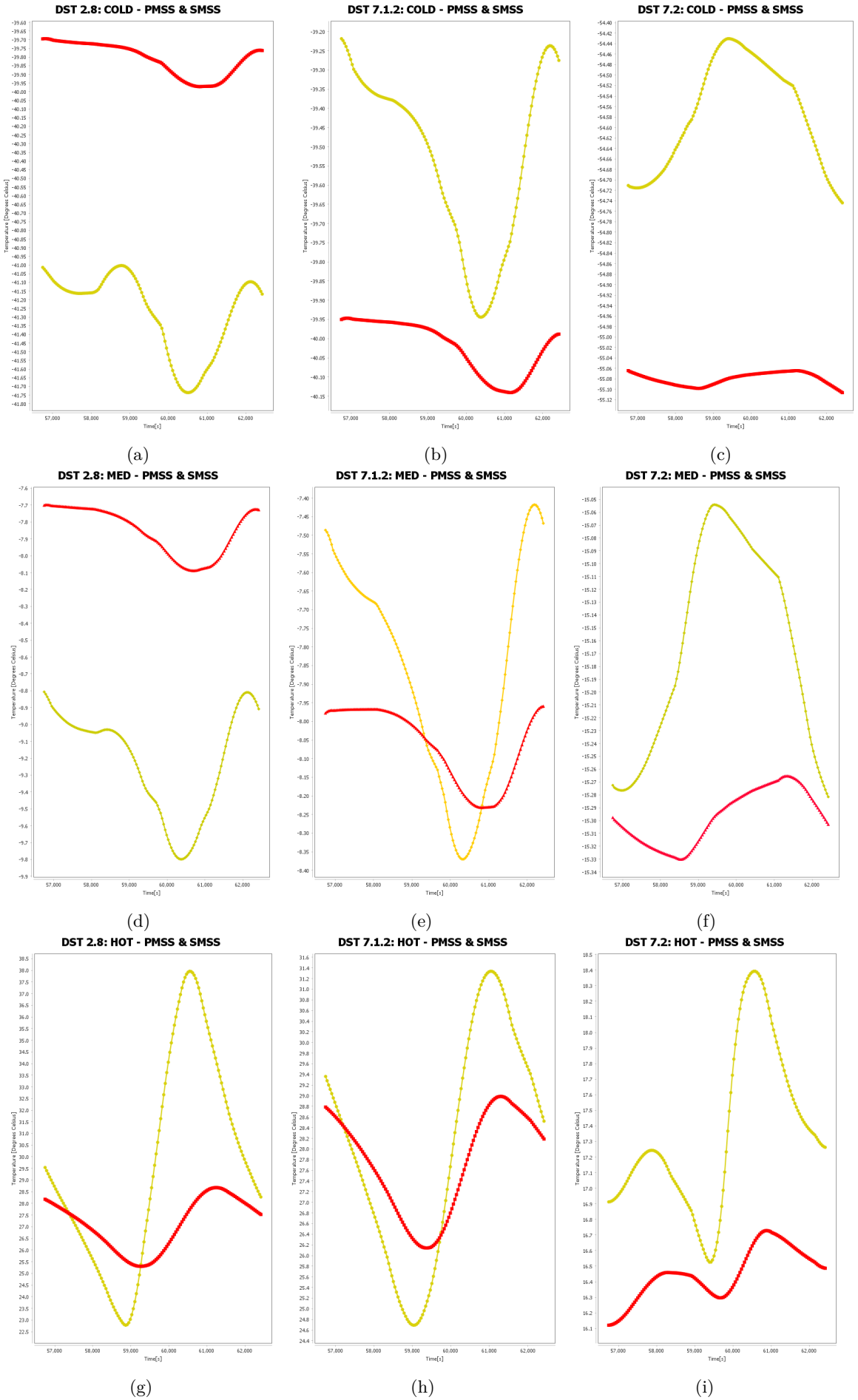

Figure H.1: Average temperatures for the PMSS (red) and SMSS (yellow), for COLD, MED and HOT conditions

I Averaged Temperature Results

This Appendix includes the average temperature results of the considered thermal system designs for the final analysis of this report. These results consider the 11th orbital period such that the simulation results can be considered sufficiently converged. These results consider COLD, HOT and MED conditions as described in Appendix D *Thermal Modelling Conditions*.

Table I.1: Temperature results for the DST 2.8

	COLD			MED			HOT		
	Av. Min	Av. ΔT	Av. Max	Av. Min	Av. ΔT	Av. Max	Av. Min	Av. ΔT	Av. Max
Spider	-46.1	1.4	-44.7	-13.5	1.1	-12.4	20.1	32.6	52.7
Top Hinges	-41.5	1.8	-39.7	-10.2	2.4	-7.8	20.2	30.0	50.2
M2	-35.47	0.01	-35.46	-6.509	0.008	-6.501	43.0	0.4	43.4
M2-Interface	-40.2	0.7	-39.5	-9.6	0.8	-8.8	30.7	10.8	41.5
Booms	-40.0	2.3	-37.7	-8.9	2.7	-6.2	22.0	14.1	36.1
Root Hinges	-40.0	0.4	-39.6	-8.2	0.6	-7.6	24.4	5.3	29.7
M1	-40.48	0.01	-40.47	-8.517	0.016	-8.501	25.8	0.1	25.9
PMSS	-40.0	0.3	-39.7	-8.1	0.4	-7.7	25.3	3.4	28.7
IH	-40.8	2.0	-38.8	-8.9	2.3	-6.6	21.8	11.8	33.6

Table I.2: Temperature results for the DST 7.1.2

	COLD			MED			HOT		
	Av. Min	Av. ΔT	Av. Max	Av. Min	Av. ΔT	Av. Max	Av. Min	Av. ΔT	Av. Max
Spider	-39.7	0.8	-38.9	-8.3	1.0	-7.3	25.1	6.1	31.2
Top Hinges	-40.1	2.2	-37.9	-9.0	2.8	-6.2	20.9	16.0	36.9
M2	-36.2	0.1	-36.1	-6.39	0.04	-6.35	29.9	0.3	30.2
M2-Interface	-37.6	0.7	-36.9	-7.2	0.8	-6.4	28.1	6.2	34.3
Booms	-40.3	2.0	-38.3	-9.0	2.4	-6.6	22.4	13.4	35.8
Root Hinges	-40.2	0.3	-39.9	-8.3	0.4	-7.9	25.3	4.5	29.8
M1	-40.60	0.009	-40.59	-8.7	0.1	-8.6	25.9	0.1	26.0
PMSS	-40.1	0.2	-39.9	-8.2	0.2	-8.0	26.1	2.9	29.0
IH	-40.9	1.8	-39.1	-9.0	2.1	-6.9	22.3	11.8	34.1

Table I.3: Temperature results for the DST 7.2

	COLD			MED			HOT		
	Av. Min	Av. ΔT	Av. Max	Av. Min	Av. ΔT	Av. Max	Av. Min	Av. ΔT	Av. Max
Spider	-54.7	0.5	-54.2	-15.4	0.3	-15.1	16.6	2.3	18.9
Top Hinges	-55.4	1.0	-54.4	-15.7	0.7	-15.0	15.8	6.4	22.2
M2	-48.7	0.1	-48.6	-12.31	0.009	-12.30	19.38	0.05	19.43
M2-Interface	-54.38	0.04	-54.34	-15.26	0.03	-15.23	17.6	1.1	18.7
Booms	-55.5	0.6	-54.9	-15.7	0.5	-15.2	16.0	2.9	18.9
Root Hinges	-55.13	0.05	-55.08	-15.33	0.06	-15.27	16.1	0.9	17.0
M1	-54.36	0.004	-54.35	-15.05	0.003	-15.05	15.44	0.04	15.48
PMSS	-55.11	0.42	-55.06	-15.33	0.06	-15.27	16.1	0.6	16.7
IH	-55.6	0.8	-54.8	-15.6	0.5	-15.1	15.6	2.6	18.2

J Coarse Translation Calculation

The coarse position translation calculations as used for this project are included within this Appendix. The code has been run in MATLAB.

clc, clear all

Parameters
theta = 8*pi/180; [degrees]

PMSS Parameters
(Support Structure (SS), Instrument Housing (IH), Primary Mirror (M1))
(y and z are considered as the deformation distance for the respective)
y_{SS} = 0.470; [m]
y_{IH} = 0.410; [m]
z_{M1} = 0.05; [m]

(Coefficient of Thermal Expansion (CTE))
CTE_{M1} = 2.2E-6; [m/m/K]
CTE_{SS} = 2.2E-6; [m/m/K]
CTE_{IH} = 2.2E-6; [m/m/K]

SMSS Parameters
(Secondary Mirror (M2), M2 Mirror Interface (IF), Top Hinges (TH), SMSS booms (booms), Root Hinges (RH))
z_{M2} = -0.04; [m]
z_{IF} = -0.0817; [m]
z_{TH} = 0.04625; [m]
z_{Booms} = 1.7657; [m]
z_{RH} = 0.0319; [m]

CTE_{M2} = 2.2E-6; [m/m/K]
CTE_{IF} = 23.4E-6; [m/m/K]
CTE_{Spider} = 2.2E-6; [m/m/K]
CTE_{TH} = 10.0E-6; [m/m/K]
CTE_{Booms} = 2.2E-6; [m/m/K]
CTE_{RH} = 10.0E-6; [m/m/K]

Maximum difference in average temperature, or delta T (DT)
($DT_{Component-Condition}$ = [WB, 2.7, 7.1.2, 7.2])
$DT_{TH-COLD}$ = [6.6, 1.8, 2.2, 1.0];
DT_{TH-MED} = [7.1, 2.4, 2.8, 0.7];
DT_{TH-HOT} = [5.9, 30.0, 16.0, 6.4];

$DT_{M2-COLD}$ = [0.1, 0.01, 0.1, 0.1];
DT_{M2-MED} = [0.1, 0.008, 0.04, 0.009];
DT_{M2-HOT} = [0.5, 0.4, 0.3, 0.05];

$DT_{Booms-COLD}$ = [8.0, 2.3, 2.0, 0.6];
$DT_{Booms-MED}$ = [8.6, 2.7, 2.4, 0.5];
$DT_{Booms-HOT}$ = [4.9, 14.1, 13.4, 2.9];

$DT_{RH-COLD}$ = [9.0, 0.4, 0.3, 0.05];
DT_{RH-MED} = [9.0, 0.6, 0.4, 0.06];
DT_{RH-HOT} = [21.9, 5.3, 4.5, 0.9];

$DT_{M1-COLD}$ = [0.9, 0.01, 0.009, 0.004];
DT_{M1-MED} = [0.8, 0.016, 0.1, 0.003];

DT_{M1-HOT} = [1.3, 0.1, 0.1, 0.04];

$DT_{SS-COLD}$ = [5.6, 0.3, 0.2, 0.42];
DT_{SS-MED} = [6.9, 0.4, 0.2, 0.06];
DT_{SS-HOT} = [19.2, 3.4, 2.9, 0.6];

$DT_{IH-COLD}$ = [9.6, 2.0, 1.8, 0.8];
DT_{IH_MED} = [10.0, 2.3, 2.1, 0.5];
DT_{IH-HOT} = [14.1, 11.8, 11.8, 2.6];

$DT_{IF-COLD}$ = [4.7, 0.7, 0.7, 0.04];
DT_{IF-MED} = [5.1, 0.8, 0.8, 0.03];
DT_{IF-HOT} = [12.2, 10.8, 6.2, 1.1];

Temperature Selection
($DT_{Selection}$ = [COLD[WB, 2.7, 7.1.2, 7.2], MED[WB, 2.7, 7.1.2, 7.2],HOT[WB, 2.7, 7.1.2, 7.2]])
$DT_{TH} = [DT_{TH-COLD}, DT_{TH-MED}, DT_{TH-HOT}]$;
$DT_{M2} = [DT_{M2-COLD}, DT_{M2-MED}, DT_{M2-HOT}]$;
$DT_{Booms} = [DT_{Booms-COLD}, DT_{Booms-MED}, DT_{Booms-HOT}]$;
$DT_{RH} = [DT_{RH-COLD}, DT_{RH-MED}, DT_{RH-HOT}]$;
$DT_{M1} = [DT_{M1-COLD}, DT_{M1-MED}, DT_{M1-HOT}]$;
$DT_{SS} = [DT_{SS-COLD}, DT_{SS-MED}, DT_{SS-HOT}]$;
$DT_{IH} = [DT_{IH-COLD}, DT_{IH-MED}, DT_{IH-HOT}]$;
$DT_{IF} = [DT_{IF-COLD}, DT_{IF-MED}, DT_{IF-HOT}]$;

Deformation Calculation
(PMSS)
$Y_{IH} = (y_{IH} * CTE_{IH} * DT_{IH})$;
$Y_{PMSS} = (cos(theta) * (y_{SS} * CTE_{SS} * DT_{SS}))$;
$Y_{M1} = (y_{IH} * CTE_{IH} * DT_{IH}) + (cos(theta) * y_{SS} * CTE_{SS} * DT_{SS})$;
$Z_{M1} = (cos(theta) * z_{M1} * CTE_{M1} * DT_{M1}) + (sin(theta) * y_{SS} * CTE_{SS} * DT_{SS})$;

(SMSS)
$Z_{M2} = (z_{M2} * CTE_{M2} * DT_{M2}) + (z_{IF} * CTE_{IF} * DT_{IF}) + (z_{TH} * CTE_{TH} * DT_{TH}) + (z_{Booms} * CTE_{Booms} * DT_{Booms}) + (z_{RH} * CTE_{RH} * DT_{RH})$;

K DST WB Temperature Results

This Appendix includes the temperature results of the fully representative DST Without Baffle (WB). The results consider the 11th orbital period such that averaged results can be considered sufficiently converged. The results consider COLD, HOT and MED conditions as described in Appendix D *Thermal Modelling Conditions*.

Table K.1: DST WB component temperatures for COLD conditions, in degrees Celsius

	Global Min	**Average Min**	**Average ΔT**	**Average Max**	**Global Max**
Spider	-36.1	-8.6	4.7	-3.9	61.6
Top Hinges	-2.9	19.2	6.6	25.8	45.9
M2	98.3	99.5	0.1	99.6	100.8
Booms	-18.1	17.7	8.0	25.7	53.0
Root Hinges	-98.6	-9.0	9.0	0.0	87.4
M1	-62.4	26.2	0.9	27.1	188.0
PMSS	-159.1	-35.3	5.6	-29.7	3644.6
IH	-127.7	-19.2	9.6	-9.6	121.3

Table K.2: DST WB component temperatures for MED conditions, in degrees Celsius

	Global Min	**Average Min**	**Average ΔT**	**Average Max**	**Global Max**
Spider	-21.8	5.4	5.1	10.5	70.5
Top Hinges	7.1	28.4	7.1	35.5	54.5
M2	104.0	105.3	0.1	105.4	106.7
Booms	-7.4	26.3	8.6	34.9	61.5
Root Hinges	-90.8	-3.1	9.0	6.1	91.8
M1	-43.1	37.0	0.8	37.8	199.7
PMSS	-149.5	-29.9	6.9	-23.0	3740.1
IH	-114.4	-8.4	10.0	1.4	126.1

Table K.3: DST WB component temperatures for HOT conditions, in degrees Celsius

	Global Min	**Average Min**	**Average ΔT**	**Average Max**	**Global Max**
Spider	3.0	26.8	12.2	39.0	81.9
Top Hinges	26.4	43.4	5.9	49.3	59.7
M2	125.6	126.9	0.5	127.4	128.3
Booms	1.5	41.3	4.9	47.2	71.4
Root Hinges	-77.8	-2.8	21.9	19.1	98.1
M1	-16.4	59.9	1.3	61.2	276.2
PMSS	-136.9	-16.2	19.2	3.0	3594.9
IH	-102.4	2.1	14.1	16.3	125.7